INVESTIGATION OF VOLTAGE STABILITY IN THREE-PHASE UNBALANCED DISTRIBUTION SYSTEMS WITH DGS

A Dissertation

by

HUNG-MING CHOU

Submitted to the Office of Graduate and Professional Studies of
Texas A&M University
in partial fulfillment of the requirement for the degree of

DOCTOR OF PHILOSOPHY

Chair of Committee,	Karen L. Butler-Purry
Committee Members,	Garng M. Huang
	Shankar P. Bhattacharyya
	Sergiy Butenko
Head of Department,	Miroslav M. Begovic

May 2016

Major Subject: Electrical Engineering

ABSTRACT

Smart grids draw lots of attention and interests and they are fundamentally changing traditional power grids. One of the key aspects of smart grid is that more distributed generators (DGs) are connected in distribution systems. Distribution systems have changed from passive to active. Stability problems become important issues, one of which is voltage stability problems. To analyze voltage stability problems, many methods are proposed for transmission systems. However, because distribution systems are very different from transmission system, the methods for transmission systems cannot be directly applied to distribution systems. Therefore, effective methods of analyzing voltage stability problems for distribution systems are needed.

The main focus of this dissertation is on three-phase unbalanced distribution systems with DGs. Firstly, improvements were made to an existing three-phase continuation power flow (CPF) method so that the maximum loading factor of distribution systems can be found accurately. Various distribution system components and DGs in PQ mode and PV mode with reactive power were modeled. Comparisons with Matpower software were made to validate the correctness of the implemented three-phase CPF program.

Secondly, to provide more detailed voltage stability analysis and determine the weak buses of distribution systems, a new voltage stability analysis method, the CPF scan method, was proposed. The weak buses found by this method are the buses that have higher impact on the maximum loadability or the maximum total real load power that the system can support. Extensive case studies were performed and the impact of different

distribution components were investigated.

Lastly, to determine whether a distribution will experience voltage stability problems and to determine the weak buses, a measurement-based three-phase voltage stability index was proposed. This voltage stability index provides not only a system-wide index but also an individual index for each bus/phase.

These proposed methods were applied to 8-bus system and a modified IEEE 13-node test feeder with DG to study the performance of the methods and investigate the impact on weak buses of different factors in distribution systems. The case studies showed that the proposed two methods, CPF scan and VSI, can successfully identify the impact of certain distribution system components. For more complicated components, such as untransposed lines and DG in PV mode, more research is needed. Also the CPF scan results shows good applications to distribution system operation and planning.

The applications of the new proposed methods are not limited to identifying the weak buses. These methods have a great potential to be extended to voltage stability preventive and corrective control.

To my lovely wife, Fang-Yu Lin,

who supports me each step of the way.

ACKNOWLEDGMENTS

First and foremost, I would like to thank God for his blessings, strength and wisdom for me.

I would like to thank my advisor, Dr. Karen L. Butler-Purry, for her patience, guidance and support. Even though I made so many mistakes and experienced so many struggles, she still believed in me. I learned from her not only about academics, but also about service, hard working and mentoring. Also, I would like to thank Dr. Garng Huang for giving me his precious time to provide guidance and help. Even though I spent so many hours with him, he was still patient with me and gave me great suggestions and feedback. I would like to thank Dr. Shankar Bhattacharyya and Dr. Sergiy Butenko for their time in serving on my committee.

Moreover, I would like to thank Dr. P. R. Kumar Dr. Le Xie for mentoring me and giving me valuable suggestions and encouragement to initiate the Smart Grid Journal Club and the Energy Club, respectively. I would like to thank the staffs in the electrical and computer engineering department, for making my PhD years at Texas A&M University a great experience.

Thanks to all of my friends and colleagues at the Power System Automation Laboratory: Dr. Fabian Uriarte, Dr. Xianyong Feng, Dr. Milad Falahi, Dr. Salman Mashayekh, Dr. Ebony Mayhorn, Fred Agyekum Ituzaro, Richard Douglin, Bo Chen, Zhengguo Chu, Apoorv Bansal, Lance G. Alpuerto, Ogbonnaya Bassey. I thank them for all of the discussions we had, for all of the problems we solved together, and all of the fun

we had together.

Last but not least, countless thanks to my wife, my parents and my younger sister for their unconditional love, sacrifice and support. My wife always stood by me, scarified for me, and encouraged me any time I struggled during my phD journey. My parents always encouraged me and provided me with anything I needed. Although they are far away in Taiwan, I always felt their warm presence and support. I owe my family everything that I have ever achieved in my life.

TABLE OF CONTENTS

Page

LIST OF FIGURES

FIGURE | Page

LIST OF TABLES

1 INTRODUCTION

The concept of smart grids, as shown in Fig.1.1, has been advocated to improve the operation of power grids. Even though smart grids mean different things to different people, the main features of smart grids include [1]:

- Enabling informed participation by customers
- Accommodating all generation and storage options
- Enabling new products, services, and markets
- Providing the power quality for the range of needs
- Optimizing asset utilization and operating efficiency
- Operating resiliently to disturbances, attacks and natural disasters

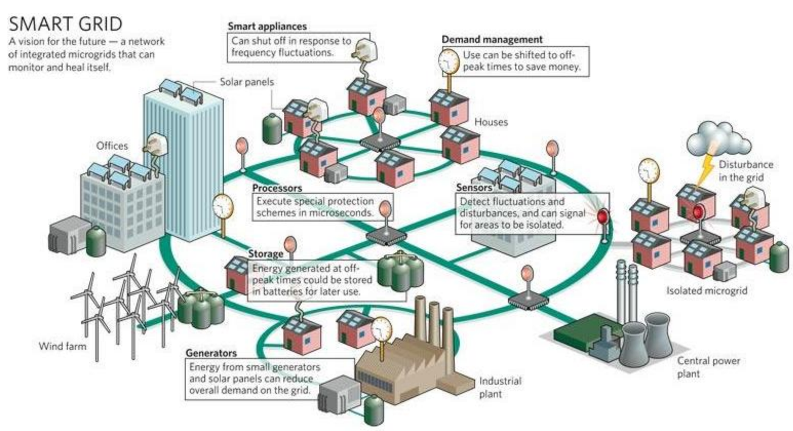

Figure 1.1: Components in smart grids [2]

Some of the key components to implement the smart grid concept is to have better monitoring, analysis and control. More information about the system is available by installing sensors in the grid. However, only information is not enough. Appropriate control actions are required. To determine the appropriated control actions, advanced analysis methods that use information are needed to better understand and better control power systems under various situations.

Since the middle of the twentieth century, transmission systems have progressed more in monitoring, analysis and control than distribution systems. For example, PMU provides synchronized measurements so that the system operator can have a clear view of the system [3]. Several advanced analysis methods are proposed to make use of PMU information, and advanced control strategies are proposed to improve the operation and control of transmission systems [4].

Compared to transmission systems, distribution systems have less monitoring and control. They have sensors installed in substations and primary feeders, but not in secondary feeders. With less information available, monitoring and control of distribution systems are quite limited. Therefore, distribution systems were typically over-designed to ensure distribution systems operate properly under various conditions [5].

However, times have changed. Due to the slow expansion of distribution systems and fast growth in load demand, the systems are operated close to their limits. Several stability and reliability issues may come up. To ensure the system operates reliably, distribution systems require more monitoring, analysis and control. The problem become even critical because distribution systems have more distributed generation (DGs) connected. Distribution systems become from passive to active (Figure 1.2). The power flow in the system is bi-directional: power flow from customers to the grid, leading to a totally different operation from traditional, passive distribution systems. In addition to the problem of protection coordination, stability is becoming a important issue.

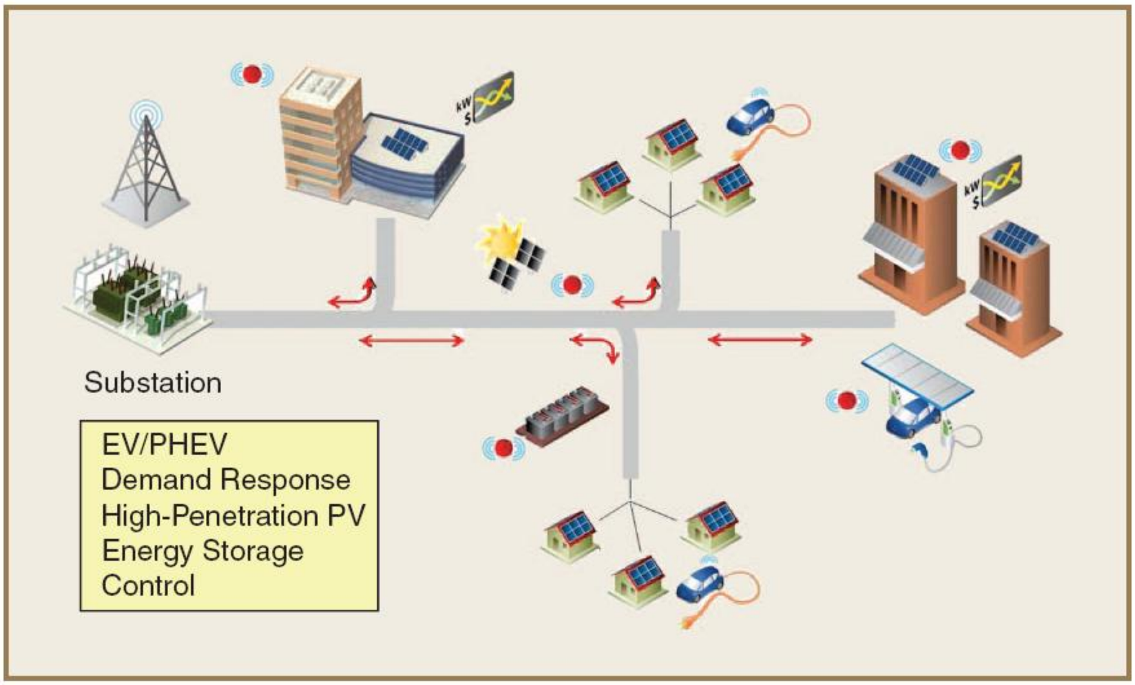

Figure 1.2: Active distribution systems [6]

In this dissertation, voltage stability of distribution systems with DGs will be investigated. Since power systems have gotten stressed recently due to the increase of power consumption and slower expansion of transmission and distribution systems, the voltage stability problem could occur in both systems [7–12]. Because of the concern of voltage instability, the planning and operation of the grid are adjusted accordingly. One way to avoid voltage instability is to reduce the power transfer of the grid. This will under-utilize the capacity of the system, leading to inefficient operation of the system [8]. To fully utilize the capacity of the system, it is important to understand the mechanism of voltage stability, to find methods to avoid voltage stability, and to have information regarding the voltage stability margin: how far the system is from the voltage instability region. With this information, the system operators do not need to operate the system conservatively; they can operate the system closer to the system's capability, which increases the usage of the system. This is important, especially in today's deregulated market.

There have been investigations of the voltage stability problem for transmission systems [13]. However, there have been limited investigations of voltage stability problem for distribution systems, especially for unbalanced distribution systems. The primary reason is that in distribution systems the length of the lines is shorter compared to the transmission line; therefore the loadability is limited not by voltage stability, but by the thermal capacity of the line. Moreover, because many voltage regulation devices and reactive power compensators are installed in distribution systems to maintain the proper voltage profile. Therefore voltage stability issues are not common in distribution systems. However, there are several examples where voltage instability happened in distribution systems. One example is the major blackout in the S/Se Brazilian systems, where a voltage stability problem in a distribution network was widespread to the corresponding transmission system, failing and tripping off a major DC link [14]. Another example is discussed in [15], where in a radial distribution system, voltage collapsed periodically and reactive compensation was needed to avoid voltage collapses.

There has been several literature on the voltage stability of distribution systems. Most of the previous work on voltage stability of distribution systems assumes that distribution systems are balanced. However, in most cases distribution systems are inherently unbalanced. New methods of analyzing voltage stability of three-phase unbalanced distribution systems with DGs are needed.

This work analyzes voltage stability in unbalanced distribution systems. Two types of distribution systems will be investigated: one without DGs and one with DGs. Techniques used for voltage stability in transmission system were adapted for unbalanced distribution systems with DG, including static analysis, bifurcation analysis and dynamic analysis. A new voltage stability index were developed.

The major contributions in this dissertation are in three areas. First, a three-phase CPF method was improved and implemented in Matlab. Improvements were made to an existing three-phase CPF, including the arc length specification and the step size control. Different components in distribution systems and DGs in PQ mode and PV mode with reactive power limit were modeled. The improved three-phase CPF method accurately finds the maximum loadability and the total real power that the system can support.

Second, a new voltage stability analysis method, called CPF scan method, for three-phase unbalanced distribution systems with DGs was proposed. CPF scan method was implemented based on the modified CPF method. This method can analyze the voltage stability in more details. This method simultaneously considers three factors that influence the location of weak buses: network characteristics, base operation point, and load increase direction. Not only does CPF scan method determine the weak bus location of a system, it also determines control actions that might be implemented via demand response to increase its maximum loading factor and maximum total real power.

Third, a new three-phase voltage stability index for three-phase unbalanced distribution systems with DGs was proposed. This new index only requires the network information and the load information. It is measurement based; complicated calculation is not needed. It not only provides the system wide information but also the individual bus information. It can determine the weak buses of the system and determine whether the system is close to voltage collapse point.

1.1 Overview of dissertation

This dissertation consists of six sections. Section 1 provides introduction and organization of the dissertation. Section 2 reviews voltage stability problem, voltage stability analysis method and weak bus identification for transmission and distribution systems. Section 3 describes the improved three-phase CPF method and the implementation. Section 4 presents the proposed voltage stability analysis method, the CPF scan method, and the case study results. Section 5 presents the proposed three-phase voltage stability index and the case study results. The comparison between the results of CPF scan method and VSI is made. Finally, the conclusions and future work are presented in Section 6.

2 BACKGROUND AND LITERATURE REVIEW

2.1 Introduction

In this section, the differences between transmission systems and distribution systems are discussed. The introduction of voltage stability problem is made. The literature review on the existing voltage stability analysis methods for transmission and distribution systems are made. Moreover, the weak bus concept and the ways to identify the weak buses for transmission and distribution systems are reviewed. Lastly, the purpose of the dissertation is presented.

2.2 Transmission and distribution systems

Even though the purpose of transmission systems and distribution systems is to transfer electricity, they are fundamentally different. Transmission systems usually span large geographical areas. The voltage level of transmission systems is high so that the power loss is reduced. The topology of transmission systems usually is networked; there are multiple paths from one bus to another. The ratio of the line resistance to the line reactance (R/X ratio) is small. There are many voltage regulating devices, such as generators in PV mode. These generators in PV mode will adjust their reactive power to regulate the voltage. Therefore, the voltages at different nodes are very close to the nominal value. Lastly, the system is balanced. The voltage, current and power in all of the three phases are approximately the same. The transmission line is transposed, resulting in the same line impedance in all three phases. Because the system is balanced, single-phase analysis can be applied.

On the other hand, distribution systems are quite different. Distribution system usually span a much smaller geographical areas, such as a city. The voltage level is lower because the cost of the equipment of lower voltage is cheaper. The majority of distribution system topologies are radial, meaning that there is only one path from one node to another. The power is flowing from the source to the load unidirectionally. Due to the line conductor design, the R/X ratio of distribution system lines is larger than that of transmission system lines. Compared to transmission systems, distribution systems have fewer voltage regulating devices. Along feeders there are voltage regulators and capacitor banks, but there is no generators in PV mode. Therefore, the voltages at different nodes are not necessarily close to the nominal value. Lastly, distribution systems are unbalanced. Distribution system lines are untransposed because they are much shorter and it is not economical to transpose short lines. Untransposed lines result in different line impedances for each phase. In addition, not all branches are three-phase. Some branches are single- or two-phase. Moreover, three-phase loads may not have the same loading in each phase. Two-phase and single-phase loads also make the system more unbalanced. Because the distribution systems are unbalanced, the single-phase analysis cannot be applied. A three-phase analysis should be used.

2.3 Distribution systems with distributed generators

Recently, increasing numbers of distributed generators (DGs) are connected in distribution systems because of the incentives of installing DGs both for customers and utilities. With high penetration of DGs, distribution systems become from passive to active. In passive systems, the substation is the only source; all the loads are supplied from the substation. On the other hands, in active systems, in addition to substation, DGs are the other sources. If DGs generate more power that are larger than the local loads, these DGs can inject real and reactive power into the system.

There are several benefits that DGs bring to distribution systems [16, 17], such as

- Voltage support and improved power quality
- Loss reduction
- Distribution system capacity release
- Deferments of new or upgraded distribution infrastructure
- Improved utility system reliability

However, high penetration of DGs in distribution system may cause problems, including [17–19]:

- Protection coordination
- Power quality
- Voltage profile
- Voltage stability

DGs may mess up the protection setting of distribution systems. Most distribution systems are designed for unidirectional power flow: power flows from the substation to the load. The protection is based on this assumptions. However, if DGs generate power that is bigger than the load connected on the same bus, this extra power will be injected into the network, resulting in bidirectional power flow. The protection setting that is based on unidirectional power flow is no longer valid under the bidirectional power flow condition. The impact on the protection due to DGs will depends on the size, type and location of DG [20, 21].

In addition to the impact on protection, DGs may affect the power quality of distribution systems, including voltage flickers and harmonics [22]. DGs may cause voltage flicker as a result of starting a machine or of having a step change in the DGs output due to intermittent primary sources such as wind turbine and photovoltaics. DGs may also introduce harmonics into the network. The severity of harmonics depends on the power converter and interconnection configuration.

Moreover, DGs may affect the voltage profile of distribution systems [18]. There is not so many voltage control devices in distribution systems; only LTC in substation, voltage regulators and the capacitor banks along the feeders are available to improve voltage profile. Moreover, these devices are all mechanical devices; they are slow to operate and adjust. On the other hand, the fluctuation of DGs is fast, much faster than these mechanical devices. These voltage control devices cannot deal with the fast fluctuation of DGs. Therefore, DGs can cause over-voltage and under-voltage in a very short period of time, impacting the voltage profile of the system. The impact on the voltage profile may limit the allowable penetration level of DGs. A good coordinated control between voltage control devices and DGs should be done to maintain the proper voltage profile [23, 24].

Even if distribution systems have a good voltage profile, voltage stability problem can occur. For a highly reactive power compensated system, even though the voltage is close to the nominal value, the system is closed to the voltage collapse point [7]. That is because the operating point is close to the knee point of the PV curve, resulting in a small voltage stability margin. The detailed description of voltage stability will be given shortly.

2.4 Introduction of voltage stability

Power system can have different kinds of stability issues, such as rotor angle stability, frequency stability and voltage stability, as shown in Fig.2.1. This work is going to focus on voltage stability, especially small-disturbance, long-term voltage stability.

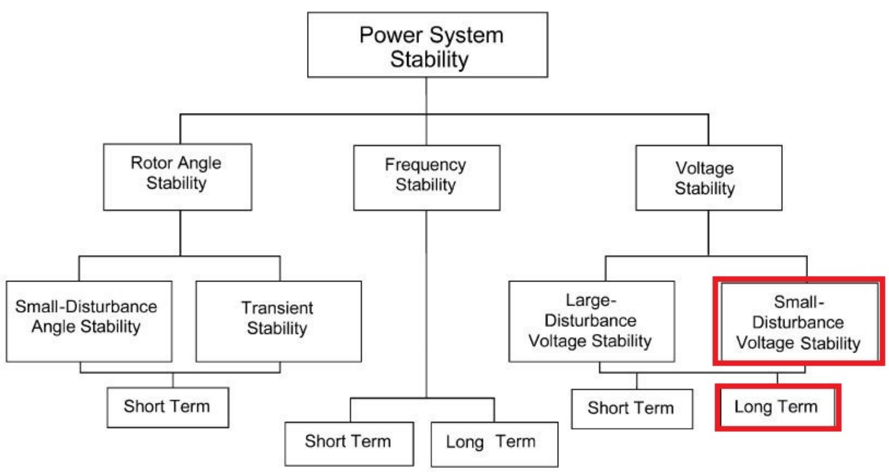

Figure 2.1: Category of power system stability [25]

The definition of voltage stability is "the ability of a power system to maintain acceptable voltages at all buses under normal operating conditions and after being subjected to a disturbance" [8]. Voltage stability problem may occur when the reactive power demand cannot be met [8]. The voltage stability problem is related to the problem of reactive power production, reactive power transmission, and reactive power consumption. For reactive power production, generators and reactive power compensators have their reactive power limits. They cannot generate the amount of reactive power that are behind their limits. Moreover, when voltage decreases due to increased load or other contingencies, the reactive power generated by capacitor banks decreases, which results in less effective reactive power support from the capacitor banks. For reactive power transmission, high reactive power loss occurs when the line is heavily loaded. Also, line outages increase the reactive power loss because the equivalent impedance of the line increases. For reactive power consumption, load increase, load recovery dynamics and motor stalling increase reactive power consumption. Therefore, because of the issues related to reactive power generation, transmission and consumption, the reactive power demand may be more than the amount of reactive power that can be supplied by the system [7, 26].

Two types of disturbances can cause voltage instability: small disturbance and large disturbance [8]. Small disturbance voltage stability is related to the ability of a power system to maintain acceptable voltage following a small disturbance, such as gradual changes in load. This type of stability can be analyzed based on the linear model of the system. Large disturbance voltage stability is related to the ability to maintain acceptable voltage following a large disturbance such as system faults, loss of loads, or loss of generators [7]. Determination of large disturbance voltage stability requires using the dynamic simulation over a period of time that is long enough to capture the interactions of loads and devices such as induction motors, generator excitation limiters, and load tap changers [7]. This work only considers the small disturbance voltage stability.

In terms of time scale, two types of voltage stability can be defined: short-term and long-term voltage stability [7]. This is because power systems have various components of different time scale. For example, exciters, HVDCs, and FACTS belong to shorter time scale dynamics while load tap changers, long term load dynamics, and the limitation of exciters belong to longer time scale. Short-term voltage stability is related to fast dynamics of power systems while long-term voltage stability is related to slow dynamics. The short-term voltage stability is related to the following three phenomena [7]:

- Loss of post-disturbance equilibrium of short-term dynamics
- Lack of attraction towards the stable post-disturbance equilibrium of short-term dynamics
- Oscillatory instability of the post-disturbance equilibrium

The long-term voltage stability is related to the following three phenomena [7]:

- Loss of equilibrium of the long-term dynamics
- Lack of attraction towards the stable long-term equilibrium
- Voltage oscillations with growing magnitude

This work only considers the long-term voltage stability.

2.4.1 Mechanism of voltage stability

Power systems experience voltage instability via two phenomena: voltage collapse and unstable voltage oscillation [8]. The system experiences voltage collapse if a sequence of events leads to saddle node bifurcation (SNB), which results in an unacceptably low voltage profile in a significant part of the power system. Unstable voltage oscillation is related to the interaction of controllers and equipment in power systems [8]. When unstable voltage oscillation occurs, the voltage magnitudes at certain buses begin to oscillate with an increasing magnitude. This work focuses on voltage collapse problem.

Voltage collapse happens when the power system reaches the knee point of the PV curve. This is the operating point where the two power flow solutions converge. The loading of this operating point is the maximum loading point that the system can support. If the loading is further increased, the loading cannot be supplied and there will be no power flow solution.

To describe voltage collapse, a generic codimension one SNB of nonlinear dynamic systems can be used [27]:

$$\dot{x} = f(x, \lambda) \tag{2.1}$$

SNB occurs at equilibrium point (x_0, λ_0) if the corresponding system Jacobian $D_x f|_0 = D_x f(x_0, \lambda_0)$ has a unique zero eigenvalue and the following transversality conditions hold at that particular equilibrium point [28]:

$$\begin{cases} D_x f|_0 v = D_x^T f|_0 w = 0 \\ w^T \frac{\partial f}{\partial \lambda}|_0 \neq 0 \\ w^T [D_x^2 f|_0 v] v \neq 0 \end{cases} \tag{2.2}$$

where v and w are the properly normalized right and left eigenvectors that correspond to the zero eigenvalue of $D_x f|_0$.

When the system experiences voltage collapse, the trajectory of the voltages at different buses can be determined by the one-dimensional center manifold. The center manifold is based on the Taylor series expansion around the bifurcation point (x_0, λ_0):

$$\dot{x_c} = \frac{1}{2} w^T [D_x^2 f\big|_0 v] v x_c^2 + w^T \frac{\partial f}{\partial \lambda}\bigg|_0 (\lambda - \lambda_0) + o(x_c^2, \lambda - \lambda_0) \tag{2.3}$$

where x_c is a scalar variable resulting from a linear transformation of the original state variables x. After voltage collapse occurs, the voltage trajectory of all of the buses can be determined by the eigenvectors corresponding to the zero eigenvalue [28] and [29]. The change of voltage magnitudes at different buses are not the same; it depends on the bus location and the loading at the bus.

2.5 Voltage stability analysis methods

Literature on the voltage stability of transmission system has been published. The current research results are summarized in [7, 13]. This section gives a brief overview of voltage stability analysis techniques for transmission systems. Then the techniques for analyzing voltage stability of balanced and unbalanced distribution systems are reviewed.

2.5.1 Voltage stability analysis methods in transmission systems

Several approaches are available to analyze voltage stability for transmission systems, including static analysis, bifurcation analysis and dynamic analysis. In static analysis, power flow calculation is performed and voltage stability is analyzed based on the power flow results. In bifurcation analysis, the DAE of the system is analyzed with a slowly varying loading factor. In dynamic analysis, time-domain simulation which includes detailed dynamics of the system is performed.

For static analysis, PV/QV curve method and modal analysis are briefly reviewed. PV curves and QV curves are widely used to analyze the static voltage stability problem. Such curves are generated by solving power flow equations at different loading points [8]. Normally, there are two parts in PV curves: the upper part and the lower part. The lower part can be found by using the correct initial condition or by using a continuous power flow method [30]. The stability of upper part and lower part can be determined by investigating the dynamics of the system, including the dynamics of generators and loads [31]. Based on the operating point, the linearization can be performed and the eigenvalues of the linearized equation can be found, which gives the stability information of the system .

Another method that belongs to static method is modal analysis [32]. By linearizing the system around the operating point, the linear state matrix can be derived based on power flow formulation. The eigenvalues, eigenvectors and participation factors of the linear state matrix can be found. The weak points and areas that are prone to voltage stability problem can be determined. Also the proximity to voltage instability can be found.

In addition to static method, bifurcation methods are used to investigate voltage stability in power systems [33,34]. Bifurcation theory deals with the study of the stability of systems that are modeled by ordinary differential equation (ODE) or differential algebraic equation (DAE). The equilibrium points move from one to another as the parameters of the system change. Several types of bifurcation are used to analyze voltage stability: (1) saddle-node bifurcation, (2) Hopf bifurcation, (3) limit-induced bifurcation and (4) singularity-induced bifurcation.

Saddle-node bifurcation can be identified by a couple of equilibrium points converging at the bifurcation point and then disappearing as the slow varying parameters changes. Many cases of actual voltage collapse in power system are related to saddle-node bifurcation [7]. At the bifurcation point, the state matrix has a unique zero eigenvalue and the transversality conditions are met. Hopf bifurcation happens when a complex conjugate pair of eigenvalues crosses the imaginary axis of the complex plane from left to right as the slow varying parameters changes. This bifurcation is associated with various oscillatory phenomena in power systems [7]. Another kind of bifurcation, limit-induced bifurcation, occurs when system control limits are reached and the eigenvalues instantaneously change, affecting the stability status of the system. Of particular interest are those bifurcation points where two equilibria merge and vanish, similar to a saddle-node bifurcation but without the state matrix becoming singular [7]. Singularity induced bifurcation happens if the Jacobian matrix of the algebraic equations of DAE is singular, In this case, it is not easy to compute and analyze the stability of the system. To analyze the singularity induced bifurcation, a more detailed model of the system is needed [7].

In addition to static analysis and bifurcation methods, dynamic analysis is used to simulate the detailed time-domain system response. Several commercially available software, such as PSCAD/EMTDC can perform transient time-domain simulation. In addition to the steady-state response, time domain simulation can simulate the transient response. Because various components in the system are modeled, the interaction among different components in the system can be observed.

Even though dynamic analysis can provide detailed time-domain system responses, it is time consuming, especially when the system is large. The most effective approach for studying voltage stability is to make complementary use of QSS and dynamic simulations [35]. Power flow solution with QSS assumption approximately finds the trajectory. The time-domain dynamic simulation models components in detail; therefore the detailed trajectory between the equilibrium points derived from QSS analysis can be found. Also, dynamic simulations are useful when QSS assumption is invalid, which could happen if the fast dynamics of the system become unstable following a disturbance.

2.5.2 Voltage stability analysis methods in distribution systems

Compared to the voltage stability analysis of transmission systems, analysis of distribution systems has not made as much progress as transmission systems [36]. Even though there have been many methodologies for voltage stability analysis for transmission systems, these methodologies cannot be applied directly to distribution systems. Distribution systems have several characteristics that are different from that of transmission systems [5, 37].

Firstly, distribution systems are unbalanced due to the unbalanced loads and single- or two-phase laterals. Moreover, unlike the lines in transmission systems, the lines in the distribution systems are untransposed. The couplings between phases are different. Therefore, we can no longer use single-phase analysis which assumes that the system is balanced. Three-phase analysis that takes all three phases into account is necessary.

Secondly, the coupling between buses is stronger in distribution systems than that in transmission systems because the distance between the buses are shorter. The voltages of neighboring buses tend to move together. Moreover, the higher line R/X ratio in distribution systems makes several useful assumptions of transmission systems invalid. For example, in transmission systems the real power transferred is primarily related to bus angle while the reactive power transferred is related to bus voltage. But in distribution systems both real and reactive power are related to bus angle and magnitude. No decoupling exists.

Lastly, radial topology of distribution system may make some power flow program diverge because the initial condition of power flow solution may be outside the region of convergence. Several techniques are required to help the power flow program converge. Moreover, radial topology causes the Jacobian matrix of power flow not diagonally dominant. Diagonally dominance of Jacobian matrix is one of the assumption that is used in transmission system analysis method, such as modal analysis.

In the following we will discuss the existing voltage stability analysis approaches used for distribution systems, balanced and unbalanced.

For balanced distribution systems with and without DG

There is more literature on the voltage stability for balanced distribution systems than that for unbalanced distribution systems. Some of techniques for the transmission systems are directly applied in balanced distribution systems. Here we just briefly review three major analysis methods: time-domain simulation, real-root condition and monitoring of reduced Jacobian matrix.

Time domain simulation is used to show voltage stability problem in radial distribution system in [15]. The simulation shows that when the voltages on industrial loads falls below 0.9 pu, voltage collapse is likely. When motors stall, these motors will reduce the voltage at nearby nodes and cause additional motors to stall in a cascading fashion. The stalling motor will cause voltage to drop to 0.6 pu or less within 1 second.

Several papers investigate the voltage stability and derive a voltage stability index by checking the condition of real number solution of voltage [9–12]. They derive the voltage closed form solution of the equivalent two-bus system, and find the condition under which the voltage solution is a real number. Different formulations of voltage give different conditions. By using these voltage indices, the voltage stability margin of the system can be determined.

Reduced Jacobian matrix is used in [14, 38]. By calculating the determinant of the reduced Jacobian matrix, the condition of voltage instability can be found. If the determinant is closed to zero, the system is close to voltage collapse. Synchronous type DGs is modeled as negative PQ load in [39]. It is found that DGs can increase the voltage stability based on the observation of PV curve of the balanced distribution system. Depending on the connection points, the influences of DGs on the voltage stability are different. DGs support the voltage stability strongly at nearby nodes and has less impact on distant ones. If DGs are modeled as the induction generator, the improvement is not clear since induction generators consume reactive power.

DGs are assumed to generate only real power in [22]. After the power flow program of the balanced distribution was solved, a voltage index was calculated to investigate the impact of DGs on voltage stability. It is found that DGs can improve the voltage stability of the system, and it is better to distribute the amount of DGs power than to allocate the whole DGs at a certain bus.

For unbalanced distribution systems with and without DG

Several literature investigates voltage stability in unbalanced distribution systems. Most literature discusses the static voltage stability by using methods such as PV curve methods, optimization methods, analysis of Jacobian and voltage stability index methods.

A three-phase power flow program is used to investigate the impact of different static loads, including constant power load, constant impedance load and constant current load [40]. By observing the result from the power flow program performed on IEEE 34 bus test feeder with different static load modeling, it was found a constant power load is suitable modeling to study the voltage stability. The author argued that if the power flow program does not converge for certain levels of loading, voltage stability occurs in the system.

To avoid the divergence of power flow at critical loading, a three-phase continuation power flow program is proposed to find the PV curve for each of the three phases [41]. In [37] three-phase continuation power flow is applied to IEEE 37 bus test feeder to investigate the impact of DGs on voltage stability. It is found that DGs in PQ mode can increase the voltage stability of unbalanced distribution system. The location of DGs can impact how much improvement DGs make to the system. Moreover, the PV curves of phase a and b are anticlockwise and the higher part of PV curve is unstable. The PV curves of phase c are clockwise and the lower part of PV curve is unstable.

The PV curve method is also used in [42]. A simple 2-bus system is analyzed. A closed-form terminal voltage is derived for two cases: loads are constant impedance loads and constant power loads. For constant impedance loads, there is one pair of solutions. However, for constant power loads, there are two pairs of solution. In the latter case, there is a point where two out of the four solutions converge. This point is proportional to the degree of the unbalance of the system. Once this point is identified, the two pair solutions can be combined to find two PV curves. This paper propose a criteria to determine which PV curves matches the PV curve of constant impedance loads. This criteria is related to the complex power in each of the three phases.

Saddle node bifurcation theory is used to investigate voltage stability in [43]. The singularity of the Jacobian matrix from the three-phase power flow is analyzed by calculating the eigenvalues. It is found that both the unbalance factor and power factor of the load can affect the bifurcation point. The maximum loading can be increased by increasing the power factor of the load and by decreasing the degree of load unbalance.

Moreover, DGs are modeled as negative PQ loads, meaning that DGs not only provide active power, but also reactive power. From a simple two-bus system case study, it is shown that DGs can improve the voltage stability and increase the loadability of the system.

Optimization method is used in [44]. The objective function is to maximize the load at certain bus, either single-, two- and three-phase bus. The constraints are the three-phase power flow and the inequality constrains on system components, including reactive power limit, rotor field thermal limit and the under-excitation limit. Unlike the PV curve method, this optimization method can directly calculate the voltage stability limits without having to calculate the solution path between the base case and the limit point. The paper uses IEEE 13-bus test feeder as an example. From the case studies, it is found that the maximum loadability is reduced by the degree of unbalance.

A more theoretical work is done in [45]. It is found that a three-phase power flow solution with feasible voltage magnitude for radial three-phase distribution with nonlinear load modeling always exists. The power flow solution is unique under the condition that the voltage is in a feasible range. Also, there is monotonic properties of the voltage magnitude at each bus with respect to load increases. This statement implies if the voltage is feasible, there is no voltage stability issues in passive radial distribution system, where there is no active component, such as load tap changer, distributed generator, etc. However, as the penetration of DGs is increasing, distribution systems are no longer passive. The voltage stability issues may occur.

2.6 Weak buses concept and methods

In the voltage stability analysis, how to identify the weak buses is an important issue. Generally speaking, the weak buses are the buses that cause the system to experience the voltage collapse problem. If the weak buses can be identified, the appropriate actions can be taken to strengthen the weak buses such that the system is more stable and is away from the voltage collapse point.

There are many definitions of weak buses in the literature. For different methods the weak bus definition will be different. In the following, different methods of finding weak buses will be described. Most of the methods are for transmission systems, while some are for distribution systems. These methods can be divided into three categories: voltage variation, sensitivity, and index method.

2.6.1 Voltage variation

For a given loading change, if the voltage magnitude at the bus reduces significantly, this bus could be a weak bus. This concept comes from the notion of electrical distance. Based on Kirchoff voltage law:

$$V_L = V_S - ZI \tag{2.4}$$

If the impedance Z between the voltage source and the load is larger, for a given load increase ΔI, the change of voltage magnitude ΔV_L will be larger [46].

If the voltage variation of a bus between the initial loading and the critical loading is larger than other buses, this bus is a weak bus compared to other buses [47]. The voltage variation of bus i is defined as

$$VC_i = \frac{V_i^{init} - V_i^{limit}}{V_i^{limit}} \tag{2.5}$$

where V_i^{init} is the voltage magnitude of the initial loading while V_i^{limit} is the voltage magnitude of the loading at the maximum loadability. A similar concept is proposed in [48]. The weak buses have the highest voltage drop when the loads are increased to the maximum loading point. Continuation power flow (CPF) is used to find the maximum loading point and defines a voltage stability margin (VSM) as the change of a loading factor between the current operating point and the maximum loading point.

Several methods are also based on this voltage variation concept. One method is to use the tangent vector found in CPF [49], as discussed in section 3. The weak buses are determined to be the buses that have higher voltage magnitude change in the tangent vector.

Another method, modal analysis, uses a similar concept [32]. Instead of looking only at voltage variation, modal analysis uses the relative voltage change and relative reactive power change. The bus participation factor of bus i determines the relationship between ΔV_i and ΔQ_i, where ΔV_i is the incremental voltage change while ΔQ_i is the incremental reactive power injection change at bus i. The weak buses are the buses that have a higher bus participation factor. Similar to modal analysis, the right eigenvectors of the reduced Jacobian matrix, which can be found from the Jacobian matrix, are used to determine the weak bus in [50]. The weak buses are the buses that have the higher magnitude in the corresponding element of the right eigenvector.

For unbalanced distribution systems, the index in (2.6) is proposed in [51] and [52]. The index for bus i is based on the positive sequence voltage of bus i:

$$\mathrm{PVR}_i = \frac{V^{+}_{i,collapse}}{V^{+}_{i,no-load}} \tag{2.6}$$

where $V^{+}_{i,no-load}$ is the positive sequence voltage of bus i in the no load condition while $V^{+}_{i,collapse}$ is that in the maximum loading condition. These positive sequence voltages are found based on the three-phase power flow solution. The weak buses are the buses with higher PVR_i. However, because this method only considers the positive sequence voltage, the impacts of negative and zero sequence voltage are not considered. This should be fine if the unbalance degree is small, but when the unbalance degree is large, this method may be inaccurate. Moreover, the positive sequence voltage is only defined for three-phase buses. For two- or single-phase buses, the positive sequence voltage is not defined. Therefore, the method proposed by [51] and [52] cannot be applied to the system where some of the buses are two- or single-phase.

Another method for unbalanced distribution systems is three-phase CPF. It is used to determine the PV curves for the three phases in [53]. This work claims that the weak location is phase-wised; the weak phases and weak buses are the ones that have a higher voltage drop at the knee point of PV curve. The proposed CPF method also considers the DG in PV mode with reactive power limit.

2.6.2 Sensitivity method

Sensitivity of total MVA load with respect to the load increment at bus i, defined in (2.7), is used to determine the weak buses [47].

$$SI_i = \frac{\partial S^T}{\partial \beta_i} \tag{2.7}$$

where S^T is the total MVA load demand and β_i is a per unit value representing the relative increase in the load at bus i with respect to the corresponding system total MVA load increase. This index SI_i is dependent on the strength of bus i.

An explicit equation of the sensitivity between generated reactive power and the load increment at a specific bus is derived in [54]. For a given load increment at bus i, if the total reactive power generation increases more than the case at other buses, bus i is a weaker bus. This is because the given load increment at bus i causes more reactive power loss in the system than other buses.

A similar concept is used in modal analysis [32]. The branch participation factor determines which branches have the highest reactive power loss given that the reactive power load increase direction is along with the right eigenvector that corresponds to the smallest eigenvalue. However, branch participation factor is related to the branches, not directly related to the weak buses. One example in [8] shows that the two buses at the end of the weak branch are not necessarily the weak buses.

Instead of finding the sensitivity of generated reactive power, the sensitivity of maximum loadability with respect to any system parameters is proposed in [55]. This sensitivity can be used to determine the weak buses. The increase of the load on the weak buses will reduce the maximum loadability more than the increase of the load on the other buses. Assuming that the maximum loadability is λ^*, the load at bus i is increased by ΔP_i, and the corresponding change of the maximum loadability is $\Delta\lambda_i^*$. The sensitivity between ΔP_i and $\Delta\lambda_i^*$ can be found. This information can be used to determine the weak buses.

2.6.3 Index method

The third type of method is based on the voltage stability index. Some indices are applied to overall system while others are applied to buses. A voltage stability index in two-bus system and based on the real power flow condition to determine the voltage stability index is proposed in [56] and [57]. This index is extended to multiple-bus system and is defined for all load buses in the system. The weak bus is the bus with the highest index value. However, these two methods do not describe how to deal with the case with generator in PV mode and the change into PQ mode when reactive power limit is hit. Only the current operating point is considered.

There are other indices that use the condition of real solution of power flow equation [58] and [59]. The equivalent effect of other buses is not considered in [60] because it claims that the equivalent circuit is valid only at a specific operating point. The equivalent circuit cannot be used for the case where the load is changing, especially due to the nonlinear behavior of a system near the maximum loadability. Moreover, only balanced systems are considered in [60] even though this paper is related to radial distribution systems.

2.6.4 Summary

Table 2.1 summarizes the methods of identifying weak buses for distribution systems. It can be found that all the stability indices are only for single-phase case. Even though the method proposed by [52] can find the weak buses for unbalanced system, the major limitation is that this method uses positive sequence voltage. For single- or two-phase buses, positive sequence voltage is not defined. Therefore, this method can be applied only to the unbalanced system where all the buses are three-phase. The method proposed by [53] uses three-phase CPF to identify the weak buses. The weak buses are the buses with a high voltage drop. However, the voltage is not a good voltage stability indicator [7].

Table 2.1: Summary of weak bus identification for distribution systems

Index methods	3P	Bal.	DG
[60]	N	Y	Y
[9]	N	Y	N
[12]	N	Y	N
[38]	N	Y	N
[61]	N	Y	N
Voltage variation	3P	Bal.	DG
[52]	Y	N	Y
[53]	Y	N	Y

2.7 Purpose statement

This work has three major purposes. The first purpose is to improve and implement the three-phase CPF method so that the maximum loadability of the system can be found accurately. The second purpose is to propose a new voltage stability analysis method, the CPF scan method. This method will identify weak buses by considering the three important factors that impact the weak bus location. The third purpose is to propose a new three-phase voltage stability index that not only monitors whether the system is close to collapse point but also identifies the weak buses of the system.

3 THREE-PHASE CONTINUATION POWER FLOW FOR UNBALANCED DISTRIBUTION SYSTEMS WITH DGS*

3.1 Introduction

To investigate voltage stability, the information about the maximum system loadability is important because it can be used to determine the voltage stability margin of the current operating point.

The maximum system loadability is due to saddle node bifurcation, where the conditions in (2.2) are satisfied. Several methods have been proposed to find this maximum loadability [62–64]. The PV curve is widely used because it not only finds the system maximum loadability, $P_{\max}$, but also finds the corresponding voltage. Fig.3.1 shows an example PV curve of a bus in a system. The X-axis is the total real power of the system while the Y-axis is the voltage magnitude of a particular bus. The point where the maximum total real power is located is the knee point, or nose point of the PV curve.

PV curves are found by running a power flow program multiple times with load increased by a loading factor λ [8]. However, the Jacobian matrix of the power flow tends to become singular even when the total real power is less than $P_{\max}$. In other words, the power flow diverges at $P = P_{\text{div}}$, where P_{div} is smaller than $P_{\max}$, as shown in Fig. 3.2. To avoid this singularity problem, continuation power flow program (CPF) has been proposed

*Part of this section is used with permission from ”Investigation of Voltage Stability in Unbalanced Distribution Systems with DG using Three-Phase Current Injection Based CPF” by H. M Chou, K. L. Bulter-Purry, 2014 IEEE PES General Meeting | Conference & Exposition, National Harbor, MD, 2014, pp. 1-5, ©2011 IEEE to accurately find the maximum loadability of a system [30] .

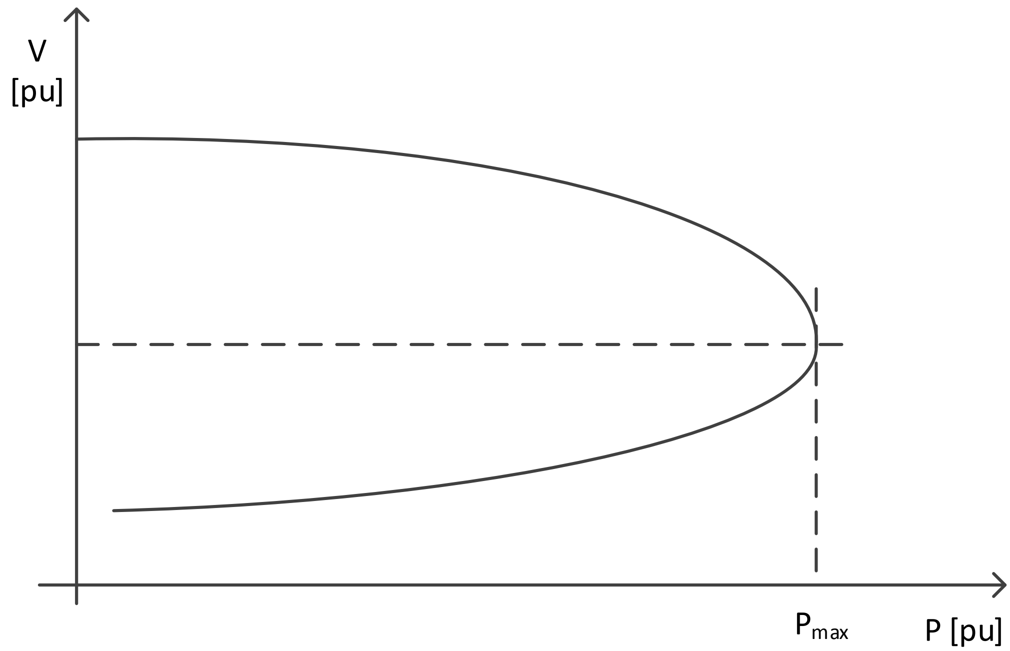

Figure 3.1: PV curve of a bus

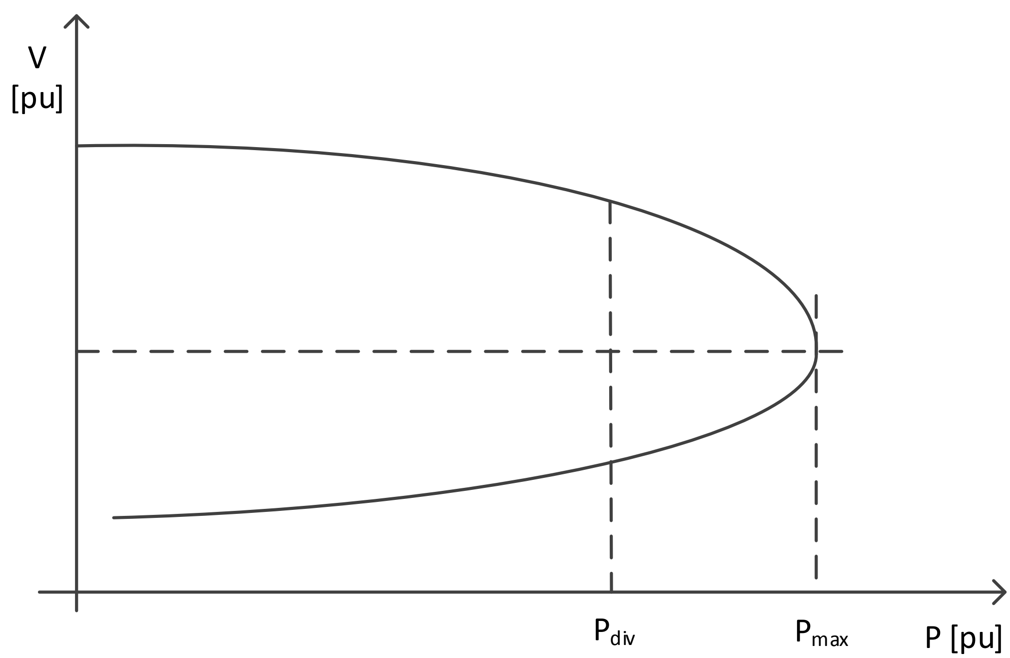

Figure 3.2: Diverge before maximum loading point

To find the maximum loadability of a three-phase unbalanced distribution system, three-phase CPF can be used. A three-phase CPF was proposed in [41] which uses local parameterization to avoid singularity issues. The same technique was applied to distribution systems with DGs in [37]. However, DGs were modeled as constant negative power loads while DGs in PV mode with reactive power limit were not modeled [37]. Another three-phase CPF approach was proposed in [53] which uses arc length parameterization to avoid singularity issues . DG in PV mode with reactive power limits were modeled.

In this dissertation work two improvements were made to the existing three-phase CPF method proposed by [53]. Firstly, the specified arc length is determined automatically, instead of being found by trial and error as done in [53]. If the specified arc length is not selected carefully, the CPF method may not trace the PV curve successfully. Secondly, a new approach for adjusting the step size for the CPF prediction stage is proposed. Instead of using the iteration number in CPF correction stage as proposed in [53], the change of loading factor, λ, is used to adjust the step size.

In this section, based on the existing three-phase CPF method proposed by [53], an improved three-phase CPF method will be presented. This method was implemented in Matlab. The important component in the three-phase CPF method, which is a three-phase power flow using the power injection method, will be described. Then the theory, implementation and improvement of the three-phase CPF method will be presented Results of a comparison with Matpower [65] will be presented. Lastly, the three-phase CPF method was applied to the modified IEEE 13-node test feeder with DG and some observation of the results will be discussed.

3.2 Three-phase power flow for unbalanced distribution systems with DGs

The fundamental part of CPF is a three-phase power flow because in one of the steps of CPF, the three-phase power flow is solved. The power flow equations can be expressed as

$$\mathbf{f}(\mathbf{x}) = \mathbf{0} \tag{3.1}$$

where $\mathbf{x}$ represents the state variables, such as the bus voltage and angle. The vector of function $\mathbf{f}$ represents the power balance equations at each bus/phase except the slack bus.

There are many ways to solve three-phase power flow. The Newton-Raphson method is used in this work because it can easily solve mesh network with multiple generators, either in PQ or PV mode. Two representations are available for the Newton-Raphson method. The first one is to use the current injection method with rectangular representation [66]. The second one is to use the power injection method with polar representation [67]. In this work, the second method is used. The formulation assumes the neutral nodes at all buses are solidly grounded, which is a common practice in North American distribution systems [5]. Therefore, the voltage of the neutral nodes is zero.

The injected power flow at bus k in phase s is represented as shown in (3.2) [41]

$$\vec{S}_k^s = \vec{V}_k^s(\vec{I}_k^s)^* = \vec{V}_k^s[\sum_{i=1}^{N}\sum_{t=1}^{3}\vec{Y}_{ki}^{st}\vec{V}_i^t]^* \tag{3.2}$$
$$= V_k^s\sum_{i=1}^{N}\sum_{t=1}^{3}V_i^tY_{ki}^{st}\cos(\theta_k^s-\theta_i^t-\delta_{ki}^{st})$$
$$+ jV_k^s\sum_{i=1}^{N}\sum_{t=1}^{3}V_i^tY_{ki}^{st}\sin(\theta_k^s-\theta_i^t-\delta_{ki}^{st}) = P_k^s + jQ_k^s$$

where

$$P_k^s = V_k^s\sum_{i=1}^{N}\sum_{t=1}^{3}V_i^tY_{ki}^{st}\cos(\theta_k^s-\theta_i^t-\delta_{ki}^{st}) \tag{3.3}$$
$$Q_k^s = V_k^s\sum_{i=1}^{N}\sum_{t=1}^{3}V_i^tY_{ki}^{st}\sin(\theta_k^s-\theta_i^t-\delta_{ki}^{st} \tag{3.4}$$

N is the number of buses of the network, $\vec{V}_k^s = V_k^s\angle\theta_s^s$ is the phase-to-neutral voltage phasor, $\vec{S}_k^s = P_k^s + jQ_k^s$ is the injected complex power at bus k in phase s. $\vec{Y}_{ki}^{st} = Y_{ki}^{st}\angle\delta_{ki}^{st}$ is the network admittance matrix element.

The injected complex power at bus k in phase s is

$$P_k^s = P_{gk}^s - P_{lk}^s \tag{3.5}$$

$$Q_k^s = Q_{gk}^s - Q_{lk}^s \tag{3.6}$$

where P_{gk}^s and Q_{gk}^s are the generated active and reactive power while P_{lk}^s and Q_{lk}^s are the active and reactive load at bus k in phase s.

Therefore, the elements that corresponds to bus k phase s in the power balance equation, $\mathbf{f}(\mathbf{x}) = \mathbf{0}$ are

$$\left[P_{gk}^s - P_{lk}^s\right] - \left[V_k^s\sum_{i=1}^{N}\sum_{t=1}^{3}V_i^tY_{ki}^{st}\cos(\theta_k^s-\theta_i^t-\delta_{ki}^{st})\right] = 0 \tag{3.7}$$
$$\left[Q_{gk}^s - Q_{lk}^s\right] - \left[V_k^s\sum_{i=1}^{N}\sum_{t=1}^{3}V_i^tY_{ki}^{st}\sin(\theta_k^s-\theta_i^t-\delta_{ki}^{st}\right] = 0 \tag{3.8}$$

3.2.1 Component models

Distribution line model

Distribution lines are modeled with series impedance matrix **Z** and shunt admittance matrix **B** [5]. **Z** and **B** have the format shown in (3.9) and (3.10). The detailed equations of the elements in these matrices are described in [5].

$$\mathbf{Z} = \begin{bmatrix} \vec{z}^{aa} & \vec{z}^{ab} & \vec{z}^{ac} \\ \vec{z}^{ba} & \vec{z}^{bb} & \vec{z}^{bc} \\ \vec{z}^{ca} & \vec{z}^{cb} & \vec{z}^{cc} \end{bmatrix} \tag{3.9}$$

$$\mathbf{B} = \begin{bmatrix} \vec{b}^{aa} & \vec{b}^{ab} & \vec{b}^{ac} \\ \vec{b}^{ba} & \vec{b}^{bb} & \vec{b}^{bc} \\ \vec{b}^{ca} & \vec{b}^{cb} & \vec{b}^{cc} \end{bmatrix} \tag{3.10}$$

If the line is two-phase or single-phase, the corresponding elements in these matrices are zero for missing phases. For example, if the line only has phases a and b, then the elements of Z: $\vec{z}^{ac}$, $\vec{z}^{bc}$, $\vec{z}^{ca}$, $\vec{z}^{cb}$, and $\vec{z}^{cc}$ are all zero, and the elements of B: $\vec{b}^{ac}$, $\vec{b}^{bc}$, $\vec{b}^{ca}$, $\vec{b}^{cb}$, and $\vec{b}^{cc}$ are zero. Because of these zero elements, the **Z** and **B** can be reduced to another matrix of a smaller dimension, which only have nonzero elements. Two-phase lines will have two by two while single-phase lines will have one by one **Z** and **B** matrix.

Load model

There are two types of load connections: Y and Delta connection. Y-connected loads are connected between line and neutral conductors while Delta-connected loads are connected between two line conductors. Because of different connections, the load power equations are different. For Y-connected loads at bus k in phase s, the active and reactive power can be expressed as (3.11) and (3.12) [41].

$$P_{lk}^{s} = P_{0k}^{s} + P_{1k}^{s} V_k^s + P_{2k}^{s} (V_k^s)^2 \tag{3.11}$$

$$Q_{lk}^{s} = Q_{0k}^{s} + Q_{1k}^{s} V_k^s + Q_{2k}^{s} (V_k^s)^2 \tag{3.12}$$

where P_{0k}^s models a constant power load, P_{1k}^s models a constant current load and P_{2k}^s models a constant impedance load. V_k^s represents the line to neutral voltage magnitude of bus k in phase s.

For Delta-connected loads shown in Fig.3.3, the active and reactive power can be expressed as (3.13) to (3.18) [5].

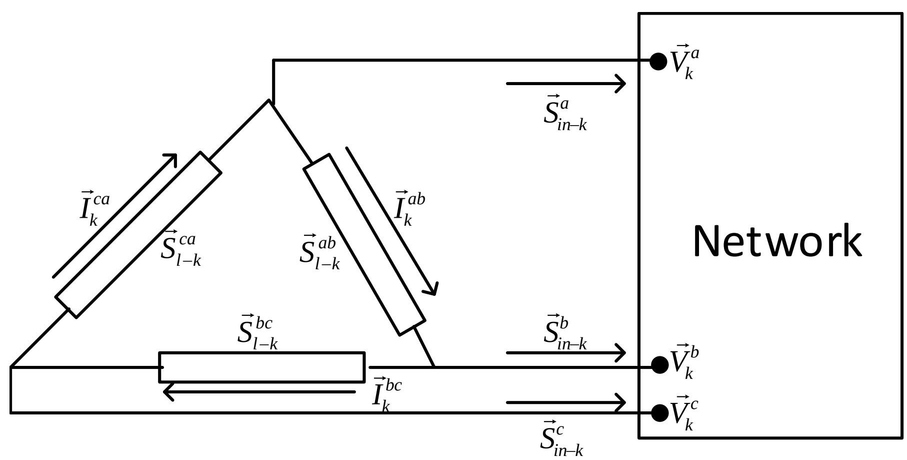

Figure 3.3: Delta-connected Load

$$P_{lk}^{ab} = P_{0k}^{a} + P_{1k}^{a}\sqrt{(V_k^a \cos\theta_k^a - V_k^b \cos\theta_k^b)^2 + (V_k^a \sin\theta_k^a - V_k^b \sin\theta_k^b)^2} \tag{3.13}$$

$$+ P_{2k}^{a}[(V_k^a \cos\theta_k^a - V_k^b \cos\theta_k^b)^2 + (V_k^a \sin\theta_k^a - V_k^b \sin\theta_k^b)^2]$$

$$Q_{lk}^{ab} = Q_{0k}^{a} + Q_{1k}^{a}\sqrt{(V_k^a \cos\theta_k^a - V_k^b \cos\theta_k^b)^2 + (V_k^a \sin\theta_k^a - V_k^b \sin\theta_k^b)^2} \tag{3.14}$$

$$+ Q_{2k}^{a}[(V_k^a \cos\theta_k^a - V_k^b \cos\theta_k^b)^2 + (V_k^a \sin\theta_k^a - V_k^b \sin\theta_k^b)^2]$$

$$P_{lk}^{bc} = P_{0k}^{b} + P_{1k}^{b}\sqrt{(V_k^b \cos\theta_k^b - V_k^c \cos\theta_k^c)^2 + (V_k^b \sin\theta_k^b - V_k^c \sin\theta_k^c)^2} \tag{3.15}$$

$$+ P_{2k}^{b}[(V_k^b \cos\theta_k^b - V_k^c \cos\theta_k^c)^2 + (V_k^b \sin\theta_k^b - V_k^c \sin\theta_k^c)^2]$$

$$Q_{lk}^{bc} = Q_{0k}^{b} + Q_{1k}^{b}\sqrt{(V_k^b \cos\theta_k^b - V_k^c \cos\theta_k^c)^2 + (V_k^b \sin\theta_k^b - V_k^c \sin\theta_k^c)^2} \tag{3.16}$$

$$+ Q_{2k}^{b}[(V_k^b \cos\theta_k^b - V_k^c \cos\theta_k^c)^2 + (V_k^b \sin\theta_k^b - V_k^c \sin\theta_k^c)^2]$$

$$P_{lk}^{ca} = P_{0k}^{c} + P_{1k}^{c}\sqrt{(V_k^c \cos\theta_k^c - V_k^a \cos\theta_k^a)^2 + (V_k^c \sin\theta_k^c - V_k^a \sin\theta_k^a)^2} \tag{3.17}$$

$$+ P_{2k}^{c}[(V_k^c \cos\theta_k^c - V_k^a \cos\theta_k^a)^2 + (V_k^c \sin\theta_k^c - V_k^a \sin\theta_k^a)^2]$$

$$Q_{lk}^{ca} = Q_{0k}^{c} + Q_{1k}^{c}\sqrt{(V_k^c \cos\theta_k^c - V_k^a \cos\theta_k^a)^2 + (V_k^c \sin\theta_k^c - V_k^a \sin\theta_k^a)^2} \tag{3.18}$$

$$+ Q_{2k}^{c}[(V_k^c \cos\theta_k^c - V_k^a \cos\theta_k^a)^2 + (V_k^c \sin\theta_k^c - V_k^a \sin\theta_k^a)^2]$$

To model Delta-connected loads, the load power should be converted into phase to neutral. As shown in Fig.3.3, the relationship between the load and phase current for each phase is

$$\vec{S}_{lk}^{ab} = P_{lk}^{ab} + jQ_{lk}^{ab} = (\vec{V}_k^a - \vec{V}_k^b)(\vec{I}_k^{ab})^* \tag{3.19}$$

$$\vec{S}_{lk}^{bc} = P_{lk}^{bc} + jQ_{lk}^{bc} = (\vec{V}_k^b - \vec{V}_k^c)(\vec{I}_k^{bc})^* \tag{3.20}$$

$$\vec{S}_{lk}^{ca} = P_{lk}^{ca} + jQ_{lk}^{ca} = (\vec{V}_k^c - \vec{V}_k^a)(\vec{I}_k^{ca})^* \tag{3.21}$$

while the relationship between the phase current and line current is

$$\vec{I}^{a}_{in-k} = \vec{I}^{ca}_{k} - \vec{I}^{ab}_{k} \tag{3.22}$$

$$\vec{I}^{b}_{in-k} = \vec{I}^{ab}_{k} - \vec{I}^{bc}_{k} \tag{3.23}$$

$$\vec{I}^{c}_{in-k} = \vec{I}^{bc}_{k} - \vec{I}^{ca}_{k} \tag{3.24}$$

The power injection at each phase for Delta-connected load is

$$\vec{S}^{a}_{in-k} = \vec{V}^{a}_{k}(\vec{I}^{a}_{in-k})^{*} = \vec{V}^{a}_{k}\left[\frac{\vec{S}^{ca}_{l-k}}{\vec{V}^{c}_{k} - \vec{V}^{a}_{k}} - \frac{\vec{S}^{ab}_{l-k}}{\vec{V}^{a}_{k} - \vec{V}^{b}_{k}}\right]^{*} \tag{3.25}$$

$$\vec{S}^{b}_{in-k} = \vec{V}^{b}_{k}(\vec{I}^{b}_{in-k})^{*} = \vec{V}^{b}_{k}\left[\frac{\vec{S}^{ab}_{l-k}}{\vec{V}^{a}_{k} - \vec{V}^{b}_{k}} - \frac{\vec{S}^{bc}_{l-k}}{\vec{V}^{b}_{k} - \vec{V}^{c}_{k}}\right]^{*} \tag{3.26}$$

$$\vec{S}^{c}_{in-k} = \vec{V}^{c}_{k}(\vec{I}^{c}_{in-k})^{*} = \vec{V}^{c}_{k}\left[\frac{\vec{S}^{bc}_{l-k}}{\vec{V}^{b}_{k} - \vec{V}^{c}_{k}} - \frac{\vec{S}^{ca}_{l-k}}{\vec{V}^{c}_{k} - \vec{V}^{a}_{k}}\right]^{*} \tag{3.27}$$

The specified injected P and Q for each phase are

$$P^{s}_{sp,k} = P^{s}_{gk} + \mathrm{Re}[\vec{S}^{s}_{in-k}] \tag{3.28}$$

$$Q^{s}_{sp,k} = Q^{s}_{gk} + \mathrm{Im}[\vec{S}^{s}_{in-k}] \tag{3.29}$$

Capacitor bank model

Capacitor banks are modeled as a constant shunt impedance. This impedance is taken into account when the system admittance matrix is developed. Suppose that Q_c is the reactive power provided by a single-phase capacitor bank in phase a, and the magnitude of line-to-neutral voltage is V^a. The capacitance for each phase can be calculated as

$$X^{a}_{\mathrm{cap}} = \frac{(V^{a})^{2}}{Q_c} \tag{3.30}$$

A similar method is applied to three-phase capacitor banks.

Voltage regulator model

Voltage regulators play an important role in maintaining a good voltage profile in feeders [5]. They can adjust their tap positions a_k^s (the tap position of the voltage regulator at bus k in phase s) to regulate the voltage at a specific location. To accurately perform voltage stability analysis on distribution systems, voltage regulators must be modeled in the power flow program.

In this work, the tap position a_k^s is found by using an iterative method [68]. In the program, in addition to the loop for the Newton-Raphson method to solve power flow equations, there is another loop. This second loop is for control purpose. The tap position is adjusted by one tap if the voltage is not within the V_{reg}. If one tap position change is not enough, this second loop will iterate again to change the tap position such that the voltage can be regulated. This method is used in OpenDSS [69]. In this work, this method is adopted.

In the overall program structure, the power flow procedure is executed first. Then the regulated voltage is checked to see whether it is within V_{reg}. If not, tap is changed by one position and the power flow procedure is rerun. Note that since the voltage regulators already change their tap, their admittance matrix and the corresponding system admittance matrix are changed. Therefore, before the power flow procedure is rerun, the system admittance matrix needs to be rebuilt.

Suppose a voltage regulator is between bus i and bus j. The line admittance of the branch between bus i and bus j is:

$$\begin{bmatrix} \vec{y}^{aa} & \vec{y}^{ab} & \vec{y}^{ca} \\ \vec{y}^{ba} & \vec{y}^{bb} & \vec{y}^{bc} \\ \vec{y}^{ca} & \vec{y}^{cb} & \vec{y}^{cc} \end{bmatrix} \tag{3.31}$$

As a starting point, the turn ratio of the voltage regulator is 1 initially. The system admittance matrix that corresponds to bus i and j is shown in (3.32) [70].

$$\mathbf{Y_{ij}} = \begin{bmatrix} \vec{y}^{aa} & \vec{y}^{ab} & \vec{y}^{ca} & -\vec{y}^{aa} & -\vec{y}^{ab} & -\vec{y}^{ac} \\ \vec{y}^{ab} & \vec{y}^{bb} & \vec{y}^{bc} & -\vec{y}^{ab} & -\vec{y}^{bb} & -\vec{y}^{bc} \\ \vec{y}^{ca} & \vec{y}^{bc} & \vec{y}^{cc} & -\vec{y}^{ca} & -\vec{y}^{bc} & -\vec{y}^{cc} \\ -\vec{y}^{aa} & -\vec{y}^{ab} & -\vec{y}^{ac} & \vec{y}^{aa} & \vec{y}^{ab} & \vec{y}^{ca} \\ -\vec{y}^{ab} & -\vec{y}^{bb} & -\vec{y}^{bc} & \vec{y}^{ab} & \vec{y}^{bb} & \vec{y}^{bc} \\ -\vec{y}^{ca} & -\vec{y}^{bc} & -\vec{y}^{cc} & \vec{y}^{ca} & \vec{y}^{bc} & \vec{y}^{cc} \end{bmatrix} \tag{3.32}$$

The admittance matrix for the voltage regulator with turn ratio A^a, A^b and A^c for phase a, b,c respectively, is shown in (3.33) [70].

$$\mathbf{Y_{ij}} = \begin{bmatrix} \frac{y^{aa}}{(A^a)^2} & \frac{y^{ab}}{A^aA^b} & \frac{y^{ca}}{A^aA^c} & -\frac{y^{aa}}{A^a} & -\frac{y^{ab}}{A^a} & -\frac{y^{ac}}{A^a} \\ \frac{y^{ab}}{A^aA^b} & \frac{y^{bb}}{(A^b)^2} & \frac{y^{bc}}{A^bA^c} & -\frac{y^{ab}}{A^b} & -\frac{y^{bb}}{A^b} & -\frac{y^{bc}}{A^b} \\ \frac{y^{ca}}{A^aA^c} & \frac{y^{bc}}{A^bA^c} & \frac{y^{cc}}{(A^c)^2} & -\frac{y^{ca}}{A^c} & -\frac{y^{bc}}{A^c} & -\frac{y^{cc}}{A^c} \\ -\frac{y^{aa}}{A^a} & -\frac{y^{ab}}{A^b} & -\frac{y^{ac}}{A^c} & y^{aa} & y^{ab} & y^{ca} \\ -\frac{y^{ab}}{A^a} & -\frac{y^{bb}}{A^b} & -\frac{y^{bc}}{A^c} & y^{ab} & y^{bb} & y^{bc} \\ -\frac{y^{ca}}{A^a} & -\frac{y^{bc}}{A^b} & -\frac{y^{cc}}{A^c} & y^{ca} & y^{bc} & y^{cc} \end{bmatrix} \tag{3.33}$$

Sometimes a voltage regulator is controlled such that the voltage of a bus that downstream of the voltage regulator is regulated. Because the voltage regulator only has local voltage measurements and does not have voltage information on the bus being regulated, line compensator is used [5]. Based on the local voltage measurement of the voltage regulator, the line compensator can calculate the voltage at a certain location that is being regulated. Fig.3.4 shows the components of a line compensator. X and R will depend on X_{line} and R_{line}. X_{line} and R_{line} depends on the distance between the voltage regulator and the bus that is being regulated, as well as the line parameters.

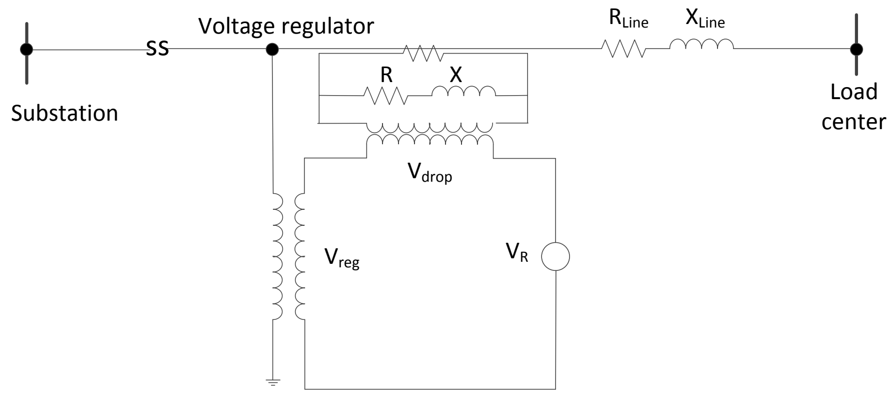

Figure 3.4: Line compensator of voltage regulators [5]

The secondary voltage and current based on local measurements are calculated first. The voltage across the relay V_R can be found. Based on V_R, the voltage regulator controller adjusts the tap position. Once the tap adjustment is made, the system admittance matrix is rebuilt and the power flow equation is solved. The control loop will check whether the voltage at the regulated location is within the range. If not in the range, the control loop will adjust the tap position again till the voltage is within the range.

In each control loop, the tap positions of each of the three phases are adjusted at the same time but independently. The tap position of each phase will be adjusted according to the voltage and current in the corresponding phase.

Because tap position has a maximum and minimum whether the voltage regulator hits the tap position limit needs to be checked. If the voltage regulator hits the limit, the tap position is no longer changed, unless the tap position change is such that the voltage regulator does not hit the limit. For example, if the tap position is already at maximum and the tap position change is positive, then the tap position is kept at maximum tap. However, if the tap position change is negative, then the tap position is reduced by the tap position change.

Distributed generator (DG) modeling

DGs can operate in two modes: PQ and PV mode. DGs in PQ mode generate the specified real and reactive power while DGs in PV mode generate the specified real power and adjust their reactive power to regulate the bus voltage.

The modelings of DGs in these two different modes are different. It is easier to model DGs in PQ mode because the generated real and reactive power are already specified. Two methods are available to model the DG in PV mode. In [71] and [66], the generated reactive power of the DG is regarded as an unknown variables and the terminal voltage as the known variables. One major problem of this method is that the reactive power mismatch is needed even for PV bus. However, PV bus has no specified reactive power. We can only guess the specified reactive power. If the guess is far away from the true value, the power flow will not converge.

In this work, we use the other way, a more robust way [67]. Because DG in PV mode regulates its terminal voltage, the corresponding voltage magnitude is known value fixed at the specified voltage. The DG in PV mode does not have the corresponding ΔV term in the $[\Delta V \Delta\theta]$ vector. Similarly, because the generated reactive power is not specified, but is adjusted to regulate the terminal voltage, this generated reactive power is an unknown value. DG in PV mode does not have the corresponding reactive power mismatch term ΔQ in the power mismatch vector $[\Delta P \Delta Q]$.

The reactive power limit of DGs in PV mode should be considered. Once the power flow equation is solved, the reactive power outputs of the DGs in PV mode are calculated. The reactive power output of a DG connected at bus k phase s, Q^s_{gk}, can be found as $Q^s_{k-in} + Q^s_{k-load}$. If the sum of Q^s_{gk} for each phase is larger than $Q_{gk\lim}$, then this DG hits the reactive power limit. Q^s_{gk} is adjusted so that the total generated reactive power of the DG is equal to the reactive power limit $Q_{gk\lim}$:

$$Q^s_{gk\mathrm{mod}} = \frac{Q_{gk\lim}}{Q^a_{gk} + Q^b_{gk} + Q^c_{gk}} Q^s_{gk} \tag{3.34}$$

After the reactive power output adjustment, the power flow needs to be resolved with this DG changed from PV mode into PQ mode. Because this DG is in PQ mode, the number of state variables will be increased: there will be ΔV and ΔQ terms corresponding to this DG.

Sometimes there are oscillations between PV mode and PQ mode in different iterations. The calculated Q^s_{gk} of DG in PV mode could be larger than the limit value in this iteration, and smaller than the limit value in the next iteration. To avoid the complexity of the program, the step size for the updated reactive power ΔQ^s_{gk} of DG is reduced much smaller than the step size for the updated voltage ΔV_{rk}^{s} and ΔV_{mk}^{s}. In this way, if the updated Q_{gk}^{s} is greater than the limit in this iteration, Q_{gk}^{s} is likely to be larger than the limit in the next iteration and this DG is changed into PQ mode. The oscillation between PV and PQ mode during the iterations can be avoided.

3.2.2 Building system admittance matrix

The system admittance matrix **Y** plays an important role in three-phase power flow program. **Y** can be found in the way that is similar to single-phase systems [67].

- $\mathbf{Y}_{ii}$ is equal to the sum of the primitive admittances of all the components connected to the ith node
- $\mathbf{Y}_{ij}$ is equal to the negative of the primitive admittance of all components connected between node i and j

In the following section, two simple examples will be used to explain the way of building system admittance matrix for three-phase distribution systems.

Firstly, a two-bus system is used, shown in Fig.3.5. These two buses are three-phase. The relationship between line current and bus voltage can be expressed as

$$\begin{bmatrix} \vec{I}^{a} \\ \vec{I}^{b} \\ \vec{I}^{c} \end{bmatrix}_{line} = \begin{bmatrix} \vec{Z}_1^{aa} & \vec{Z}_1^{ab} & \vec{Z}_1^{ac} \\ \vec{Z}_1^{ba} & \vec{Z}_1^{bb} & \vec{Z}_1^{bc} \\ \vec{Z}_1^{ca} & \vec{Z}_1^{cb} & \vec{Z}_1^{cc} \end{bmatrix}^{-1} \left(\begin{bmatrix} \vec{V}_1^{a} \\ \vec{V}_1^{b} \\ \vec{V}_1^{c} \end{bmatrix} - \begin{bmatrix} \vec{V}_2^{a} \\ \vec{V}_2^{b} \\ \vec{V}_2^{c} \end{bmatrix} \right) \tag{3.35}$$

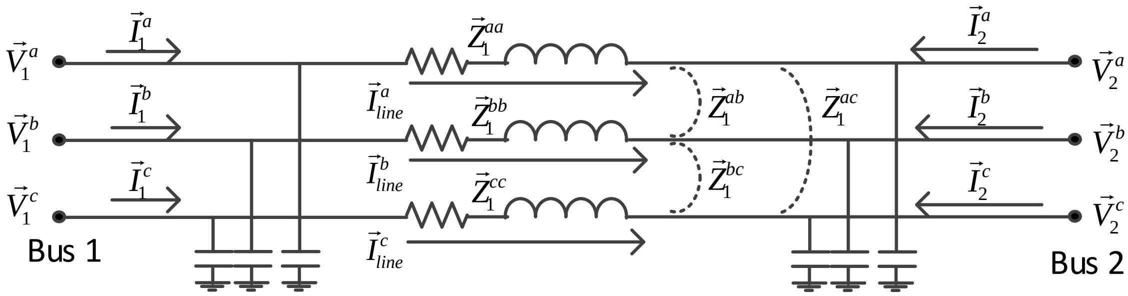

Figure 3.5: Three-phase line segment model

The injection current at Bus 1 is

$$\begin{bmatrix} \vec{I}_1^a \\ \vec{I}_1^b \\ \vec{I}_1^c \end{bmatrix} = \begin{bmatrix} \vec{I}^a \\ \vec{I}^b \\ \vec{I}^c \end{bmatrix}_{line} + \frac{1}{2}\mathbf{Y_{abc}} \begin{bmatrix} \vec{V}_1^a \\ \vec{V}_1^b \\ \vec{V}_1^c \end{bmatrix} = (\mathbf{Z_{abc}}^{-1} + \frac{\mathbf{Y_{abc}}}{2}) \begin{bmatrix} \vec{V}_1^a \\ \vec{V}_1^b \\ \vec{V}_1^c \end{bmatrix} - \mathbf{Z_{abc}}^{-1} \begin{bmatrix} \vec{V}_2^a \\ \vec{V}_2^b \\ \vec{V}_2^c \end{bmatrix} \tag{3.36}$$

Similarly, the injection current at Bus 2 is

$$\begin{bmatrix} \vec{I}_2^a \\ \vec{I}_2^b \\ \vec{I}_2^c \end{bmatrix} = - \begin{bmatrix} \vec{I}_a \\ \vec{I}_b \\ \vec{I}_c \end{bmatrix}_{line} + \frac{1}{2}\mathbf{Y_{abc}} \begin{bmatrix} \vec{V}_2^a \\ \vec{V}_2^b \\ \vec{V}_2^c \end{bmatrix} = -Z_{abc}^{-1} \begin{bmatrix} \vec{V}_1^a \\ \vec{V}_1^b \\ \vec{V}_1^c \end{bmatrix} + (\mathbf{Z_{abc}}^{-1} + \frac{\mathbf{Y_{abc}}}{2}) \begin{bmatrix} \vec{V}_2^a \\ \vec{V}_2^b \\ \vec{V}_2^c \end{bmatrix} \tag{3.37}$$

Therefore, the injection current vector can be expressed as (3.38). The system admittance matrix for a three-phase system can be found with the same method as for a single-phase system.

$$\begin{bmatrix} \mathbf{I_1^{abc}} \\ \mathbf{I_2^{abc}} \end{bmatrix} = \begin{bmatrix} \mathbf{Z_{abc}}^{-1} + \frac{\mathbf{Y_{abc}}}{2} & -\mathbf{Z_{abc}}^{-1} \\ -\mathbf{Z_{abc}}^{-1} & \mathbf{Z_{abc}}^{-1} + \frac{\mathbf{Y_{abc}}}{2} \end{bmatrix} \begin{bmatrix} \mathbf{V_1^{abc}} \\ \mathbf{V_2^{abc}} \end{bmatrix} \tag{3.38}$$

Secondly, a three-bus system is used, where one line is three-phase while the other line is two-phase, shown in Fig. 3.6 to illustrate how to build Y matrix for a system with buses with different phase configurations. For simplicity the shunt admittance is not considered here. The line impedance matrix between Bus 1 and Bus 2 is $\mathbf{Z_1}$ and between

Bus 1 and Bus 3 is $\mathbf{Z_2}$.

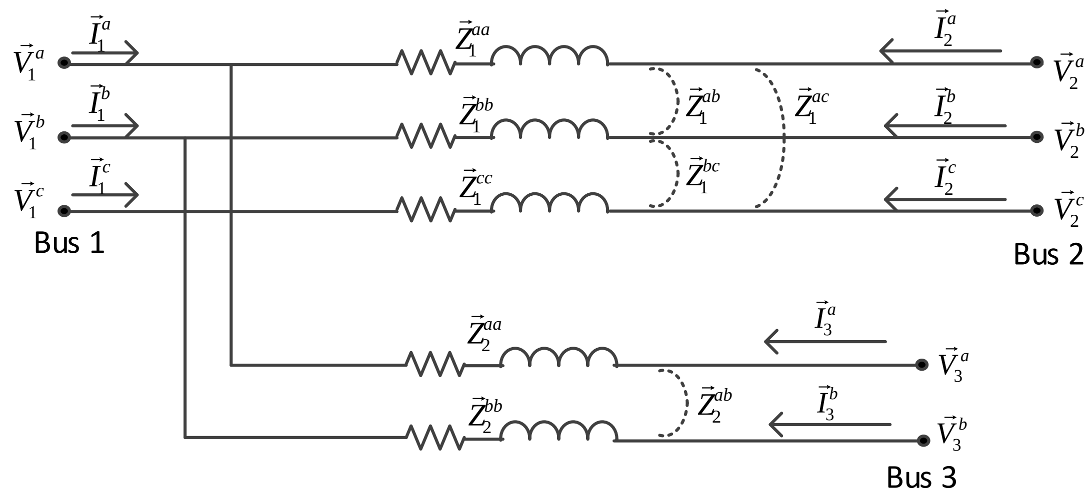

Figure 3.6: Three-bus system with mixed phases

$$\tilde{\mathbf{Z}}_\mathbf{1} = \begin{bmatrix} \vec{Z}_1^{aa} & \vec{Z}_1^{ab} & \vec{Z}_1^{ac} \\ \vec{Z}_1^{ba} & \vec{Z}_1^{bb} & \vec{Z}_1^{bc} \\ \vec{Z}_1^{ca} & \vec{Z}_1^{cb} & \vec{Z}_1^{cc} \end{bmatrix} \tag{3.39}$$

$$\tilde{\mathbf{Z}}_\mathbf{2} = \begin{bmatrix} \vec{Z}_2^{aa} & \vec{Z}_2^{ab} \\ \vec{Z}_2^{ba} & \vec{Z}_2^{bb} \end{bmatrix} \tag{3.40}$$

Now we write the current injection equation at Bus 1:

$$\begin{bmatrix} \vec{I}_1^a \\ \vec{I}_1^b \\ \vec{I}_1^c \end{bmatrix} = \begin{bmatrix} \vec{Z}_1^{aa} & \vec{Z}_1^{ab} & \vec{Z}_1^{ac} \\ \vec{Z}_1^{ba} & \vec{Z}_1^{bb} & \vec{Z}_1^{bc} \\ \vec{Z}_1^{ca} & \vec{Z}_1^{cb} & \vec{Z}_1^{cc} \end{bmatrix}^{-1} \left(\begin{bmatrix} \vec{V}_1^a \\ \vec{V}_1^b \\ \vec{V}_1^c \end{bmatrix} - \begin{bmatrix} \vec{V}_2^a \\ \vec{V}_2^b \\ \vec{V}_2^c \end{bmatrix} \right) + \begin{bmatrix} \vec{Z}_2^{aa} & \vec{Z}_2^{ab} \\ \vec{Z}_2^{ba} & \vec{Z}_2^{bb} \end{bmatrix}^{-1} \left(\begin{bmatrix} \vec{V}_1^a \\ \vec{V}_1^b \end{bmatrix} - \begin{bmatrix} \vec{V}_3^a \\ \vec{V}_3^b \end{bmatrix} \right) \tag{3.41}$$

$$= \begin{bmatrix} \vec{Y}_1^{aa} & \vec{Y}_1^{ab} & \vec{Y}_1^{ac} \\ \vec{Y}_1^{ba} & \vec{Y}_1^{bb} & \vec{Y}_1^{bc} \\ \vec{Y}_1^{ca} & \vec{Y}_1^{cb} & \vec{Y}_1^{cc} \end{bmatrix} \left(\begin{bmatrix} \vec{V}_1^a \\ \vec{V}_1^b \\ \vec{V}_1^c \end{bmatrix} - \begin{bmatrix} \vec{V}_2^a \\ \vec{V}_2^b \\ \vec{V}_2^c \end{bmatrix} \right) + \begin{bmatrix} \vec{Y}_2^{aa} & \vec{Y}_2^{ab} \\ \vec{Y}_2^{ba} & \vec{Y}_2^{bb} \end{bmatrix} \left(\begin{bmatrix} \vec{V}_1^a \\ \vec{V}_1^b \end{bmatrix} - \begin{bmatrix} \vec{V}_3^a \\ \vec{V}_3^b \end{bmatrix} \right) \tag{3.42}$$

$$= \begin{bmatrix} \vec{Y}_1^{aa} + \vec{Y}_2^{aa} & \vec{Y}_1^{ab} + \vec{Y}_2^{ab} & \vec{Y}_1^{ac} \\ \vec{Y}_1^{ba} + \vec{Y}_2^{ba} & \vec{Y}_1^{bb} + \vec{Y}_2^{bb} & \vec{Y}_1^{bc} \\ \vec{Y}_1^{ca} & \vec{Y}_1^{cb} & \vec{Y}_1^{cc} \end{bmatrix} \begin{bmatrix} \vec{V}_1^a \\ \vec{V}_1^b \\ \vec{V}_1^c \end{bmatrix} - \begin{bmatrix} \vec{Y}_1^{aa} & \vec{Y}_1^{ab} & \vec{Y}_1^{ac} \\ \vec{Y}_1^{ba} & \vec{Y}_1^{bb} & \vec{Y}_1^{bc} \\ \vec{Y}_1^{ca} & \vec{Y}_1^{cb} & \vec{Y}_1^{cc} \end{bmatrix} \begin{bmatrix} \vec{V}_2^a \\ \vec{V}_2^b \\ \vec{V}_2^c \end{bmatrix} \tag{3.43}$$

$$- \begin{bmatrix} \vec{Y}_2^{aa} & \vec{Y}_2^{ab} \\ \vec{Y}_2^{ba} & \vec{Y}_2^{bb} \\ 0 & 0 \end{bmatrix} \begin{bmatrix} \vec{V}_3^a \\ \vec{V}_3^b \end{bmatrix} \tag{3.44}$$

$$= \mathbf{Y_{11}} \begin{bmatrix} \vec{V}_1^a \\ \vec{V}_1^b \\ \vec{V}_1^c \end{bmatrix} + \mathbf{Y_{12}} \begin{bmatrix} \vec{V}_2^a \\ \vec{V}_2^b \\ \vec{V}_2^c \end{bmatrix} + \mathbf{Y_{13}} \begin{bmatrix} \vec{V}_3^a \\ \vec{V}_3^b \end{bmatrix} \tag{3.45}$$

Similar equations can be derived for Bus 2 and Bus 3.

$$\begin{bmatrix} \vec{I}_2^a \\ \vec{I}_2^b \\ \vec{I}_2^c \end{bmatrix} = \begin{bmatrix} \vec{Y}_1^{aa} & \vec{Y}_1^{ab} & \vec{Y}_1^{ac} \\ \vec{Y}_1^{ba} & \vec{Y}_1^{bb} & \vec{Y}_1^{bc} \\ \vec{Y}_1^{ca} & \vec{Y}_1^{cb} & \vec{Y}_1^{cc} \end{bmatrix} \left(\begin{bmatrix} \vec{V}_2^a \\ \vec{V}_2^b \\ \vec{V}_2^c \end{bmatrix} - \begin{bmatrix} \vec{V}_1^a \\ \vec{V}_1^b \\ \vec{V}_1^c \end{bmatrix} \right)$$

$$= \begin{bmatrix} -\vec{Y}_1^{aa} & -\vec{Y}_1^{ab} & -\vec{Y}_1^{ac} \\ -\vec{Y}_1^{ba} & -\vec{Y}_1^{bb} & -\vec{Y}_1^{bc} \\ -\vec{Y}_1^{ca} & -\vec{Y}_1^{cb} & -\vec{Y}_1^{cc} \end{bmatrix} \begin{bmatrix} \vec{V}_1^a \\ \vec{V}_1^b \\ \vec{V}_1^c \end{bmatrix} + \begin{bmatrix} \vec{Y}_1^{aa} & \vec{Y}_1^{ab} & \vec{Y}_1^{ac} \\ \vec{Y}_1^{ba} & \vec{Y}_1^{bb} & \vec{Y}_1^{bc} \\ \vec{Y}_1^{ca} & \vec{Y}_1^{cb} & \vec{Y}_1^{cc} \end{bmatrix} \begin{bmatrix} \vec{V}_2^a \\ \vec{V}_2^b \\ \vec{V}_2^c \end{bmatrix}$$

$$= \mathbf{Y_{21}} \begin{bmatrix} \vec{V}_1^a \\ \vec{V}_1^b \\ \vec{V}_1^c \end{bmatrix} + \mathbf{Y_{22}} \begin{bmatrix} \vec{V}_2^a \\ \vec{V}_2^b \\ \vec{V}_2^c \end{bmatrix} + \mathbf{Y_{23}} \begin{bmatrix} \vec{V}_3^a \\ \vec{V}_3^b \end{bmatrix} \tag{3.46}$$

$$\begin{bmatrix} \vec{I}_3^a \\ \vec{I}_3^b \end{bmatrix} = \begin{bmatrix} \vec{Y}_2^{aa} & \vec{Y}_2^{ab} \\ \vec{Y}_2^{ba} & \vec{Y}_2^{bb} \end{bmatrix} \left(\begin{bmatrix} \vec{V}_3^a \\ \vec{V}_3^b \end{bmatrix} - \begin{bmatrix} \vec{V}_1^a \\ \vec{V}_1^b \end{bmatrix} \right)$$

$$= \begin{bmatrix} -\vec{Y}_2^{aa} & -\vec{Y}_2^{ab} \\ -\vec{Y}_2^{ba} & -\vec{Y}_2^{bb} \end{bmatrix} \begin{bmatrix} \vec{V}_1^a \\ \vec{V}_1^b \end{bmatrix} + \begin{bmatrix} \vec{Y}_2^{aa} & \vec{Y}_2^{ab} \\ \vec{Y}_2^{ba} & \vec{Y}_2^{bb} \end{bmatrix} \begin{bmatrix} \vec{V}_3^a \\ \vec{V}_3^b \end{bmatrix}$$

$$= \mathbf{Y_{31}} \begin{bmatrix} \vec{V}_1^a \\ \vec{V}_1^b \end{bmatrix} + \mathbf{Y_{32}} \begin{bmatrix} \vec{V}_2^a \\ \vec{V}_2^b \end{bmatrix} + \mathbf{Y_{33}} \begin{bmatrix} \vec{V}_3^a \\ \vec{V}_3^b \end{bmatrix} \tag{3.47}$$

If we put all the current and voltage in vectors, the injection current vector can be expressed as (3.48). Therefore, the procedure of building system admittance matrix for three-phase case is similar to the single-phase case.

$$
\begin{bmatrix} \vec{I}_1^a \\ \vec{I}_1^b \\ \vec{I}_1^c \\ \vec{I}_2^a \\ \vec{I}_2^b \\ \vec{I}_2^c \\ \vec{I}_3^a \\ \vec{I}_3^b \end{bmatrix} = \begin{bmatrix} \vec{Y}_1^{aa}+\vec{Y}_2^{aa} & \vec{Y}_1^{ab}+\vec{Y}_2^{ab} & \vec{Y}_1^{ac} & -\vec{Y}_1^{aa} & -\vec{Y}_1^{ab} & -\vec{Y}_1^{ac} & \vec{Y}_2^{aa} & \vec{Y}_2^{ab} \\ \vec{Y}_1^{ba}+\vec{Y}_2^{ba} & \vec{Y}_1^{bb}+\vec{Y}_2^{bb} & \vec{Y}_1^{bc} & -\vec{Y}_1^{ba} & -\vec{Y}_1^{bb} & -\vec{Y}_1^{bc} & \vec{Y}_2^{ba} & \vec{Y}_2^{bb} \\ \vec{Y}_1^{ca} & \vec{Y}_1^{cb} & \vec{Y}_1^{cc} & -\vec{Y}_1^{ca} & -\vec{Y}_1^{cb} & -\vec{Y}_1^{cc} & 0 & 0 \\ -\vec{Y}_1^{aa} & -\vec{Y}_1^{ab} & -\vec{Y}_1^{ac} & \vec{Y}_1^{aa} & \vec{Y}_1^{ab} & \vec{Y}_1^{ac} & 0 & 0 \\ -\vec{Y}_1^{ba} & -\vec{Y}_1^{bb} & -\vec{Y}_1^{bc} & \vec{Y}_1^{ba} & \vec{Y}_1^{bb} & \vec{Y}_1^{bc} & 0 & 0 \\ -\vec{Y}_1^{ca} & -\vec{Y}_1^{cb} & -\vec{Y}_1^{cc} & \vec{Y}_1^{ca} & \vec{Y}_1^{cb} & \vec{Y}_1^{cc} & 0 & 0 \\ -\vec{Y}_2^{aa} & -\vec{Y}_2^{ab} & 0 & 0 & 0 & 0 & \vec{Y}_2^{aa} & \vec{Y}_2^{ab} \\ -\vec{Y}_2^{ba} & -\vec{Y}_2^{bb} & 0 & 0 & 0 & 0 & \vec{Y}_2^{ba} & \vec{Y}_2^{bb} \end{bmatrix} \begin{bmatrix} \vec{V}_1^a \\ \vec{V}_1^b \\ \vec{V}_1^c \\ \vec{V}_2^a \\ \vec{V}_2^b \\ \vec{V}_2^c \\ \vec{V}_3^a \\ \vec{V}_3^b \end{bmatrix} \tag{3.48}
$$

3.2.3 The Netwon-Raphson method to solve power flow equation

The Newton-Raphson method is used to solve three-phase power flow equations. The detailed theory and implementation about the Netwon-Raphson method can be found in [67]. The power flow solutions are ($\mathbf{V}$, θ) for PQ buses and ($\mathbf{Q}$, θ) for PV buses.

Newton-Raphson is an iterative method. Take a PQ bus as an example. Newton-Raphson updates the state variables ($\mathbf{V}$, θ) during each iteration by the updating vector: ($\Delta\mathbf{V}$, $\Delta\theta$). This updating vector can be found based on the power mismatch ($\Delta\mathbf{P}$, $\Delta\mathbf{Q}$), which is the difference between the specified PQ value and the calculated PQ value.

The relationship between the power mismatch and update vector is shown in (3.49), assuming that n^{th} bus is the slack bus which corresponds to the substation bus. The voltage of the substation is a balanced three-phase voltage with magnitude 1 pu and 120 degree apart among phases.

$$\begin{bmatrix} \Delta\mathbf{P}_1^{abc} \\ \vdots \\ \Delta\mathbf{P}_{n-1}^{abc} \\ \Delta\mathbf{Q}_1^{abc} \\ \vdots \\ \Delta\mathbf{Q}_{n-1}^{abc} \end{bmatrix} = \begin{bmatrix} \mathbf{J_{PV}} & \mathbf{J_{P\theta}} \\ \mathbf{J_{QV}} & \mathbf{J_{Q\theta}} \end{bmatrix} \begin{bmatrix} \Delta\mathbf{V}_1^{abc} \\ \vdots \\ \Delta\mathbf{V}_{n-1}^{abc} \\ \Delta\theta_1^{abc} \\ \vdots \\ \Delta\theta_{n-1}^{abc} \end{bmatrix} = \mathbf{J} \begin{bmatrix} \Delta\mathbf{V}_1^{abc} \\ \vdots \\ \Delta\mathbf{V}_{n-1}^{abc} \\ \Delta\theta_1^{abc} \\ \vdots \\ \Delta\theta_{n-1}^{abc} \end{bmatrix} \tag{3.49}$$

The Jacobian matrix $\mathbf{J}$ has submatrices: $\mathbf{J_{PV}}$, $\mathbf{J_{P\theta}}$, $\mathbf{J_{QV}}$ and $\mathbf{J_{Q\theta}}$. These submatrices can be expressed in (3.50), (3.51), (3.52) and (3.53), respectively. In these above equations, all buses are assumed to be three-phases. In most of distribution systems, buses may not be three-phase. For buses that are not three-phase, the appropriate changes are needed for the elements of the matrices. For buses that only have one or two phases, these submatrices have no elements in the missing phases. For example, if Bus 1 only has phase A, then these submatrices will have no elements that are related to ΔP_1^b, ΔP_1^c, ΔQ_1^b, ΔQ_1^c, V_1^b, V_1^c, θ_1^b, and θ_1^c. Therefore, the dimension of these matrices is reduced and depends on the phase information of the buses in the system.

$$\mathbf{J_{PV}} = \begin{bmatrix} \frac{\partial \Delta P_1^a}{\partial V_1^a} & \frac{\partial \Delta P_1^a}{\partial V_1^b} & \frac{\partial \Delta P_1^a}{\partial V_1^c} & \dots & \frac{\partial \Delta P_1^a}{\partial V_{n-1}^a} & \frac{\partial \Delta P_1^a}{\partial V_{n-1}^b} & \frac{\partial \Delta P_1^a}{\partial V_{n-1}^c} \\ \frac{\partial \Delta P_1^b}{\partial V_1^a} & \frac{\partial \Delta P_1^b}{\partial V_1^b} & \frac{\partial \Delta P_1^b}{\partial V_1^c} & \dots & \frac{\partial \Delta P_1^b}{\partial V_{n-1}^a} & \frac{\partial \Delta P_1^b}{\partial V_{n-1}^b} & \frac{\partial \Delta P_1^b}{\partial V_{n-1}^c} \\ \frac{\partial \Delta P_1^c}{\partial V_1^a} & \frac{\partial \Delta P_1^c}{\partial V_1^b} & \frac{\partial \Delta P_1^c}{\partial V_1^c} & \dots & \frac{\partial \Delta P_1^c}{\partial V_{n-1}^a} & \frac{\partial \Delta P_1^c}{\partial V_{n-1}^b} & \frac{\partial \Delta P_1^c}{\partial V_{n-1}^c} \\ \vdots & \vdots & \vdots & \dots & \vdots & \vdots & \vdots \\ \frac{\partial \Delta P_{n-1}^a}{\partial V_1^a} & \frac{\partial \Delta P_{n-1}^a}{\partial V_1^b} & \frac{\partial \Delta P_{n-1}^a}{\partial V_1^c} & \dots & \frac{\partial \Delta P_{n-1}^a}{\partial V_{n-1}^a} & \frac{\partial \Delta P_{n-1}^a}{\partial V_{n-1}^b} & \frac{\partial \Delta P_{n-1}^a}{\partial V_{n-1}^c} \\ \frac{\partial \Delta P_{n-1}^b}{\partial V_1^a} & \frac{\partial \Delta P_{n-1}^b}{\partial V_1^b} & \frac{\partial \Delta P_{n-1}^b}{\partial V_1^c} & \dots & \frac{\partial \Delta P_{n-1}^b}{\partial V_{n-1}^a} & \frac{\partial \Delta P_{n-1}^b}{\partial V_{n-1}^b} & \frac{\partial \Delta P_{n-1}^b}{\partial V_{n-1}^c} \\ \frac{\partial \Delta P_{n-1}^c}{\partial V_1^a} & \frac{\partial \Delta P_{n-1}^c}{\partial V_1^b} & \frac{\partial \Delta P_{n-1}^c}{\partial V_1^c} & \dots & \frac{\partial \Delta P_{n-1}^c}{\partial V_{n-1}^a} & \frac{\partial \Delta P_{n-1}^c}{\partial V_{n-1}^b} & \frac{\partial \Delta P_{n-1}^c}{\partial V_{n-1}^c} \end{bmatrix} \tag{3.50}$$

$$\mathbf{J_{P\theta}} = \begin{bmatrix} \frac{\partial \Delta P_1^a}{\partial \theta_1^a} & \frac{\partial \Delta P_1^a}{\partial V_1^b} & \frac{\partial \Delta P_1^a}{\partial \theta_1^c} & \dots & \frac{\partial \Delta P_1^a}{\partial \theta_{n-1}^a} & \frac{\partial \Delta P_1^a}{\partial \theta_{n-1}^b} & \frac{\partial \Delta P_1^a}{\partial \theta_{n-1}^c} \\ \frac{\partial \Delta P_1^b}{\partial \theta_1^a} & \frac{\partial \Delta P_1^b}{\partial \theta_1^b} & \frac{\partial \Delta P_1^b}{\partial \theta_1^c} & \dots & \frac{\partial \Delta P_1^b}{\partial \theta_{n-1}^a} & \frac{\partial \Delta P_1^b}{\partial \theta_{n-1}^b} & \frac{\partial \Delta P_1^b}{\partial \theta_{n-1}^c} \\ \frac{\partial \Delta P_1^c}{\partial \theta_1^a} & \frac{\partial \Delta P_1^c}{\partial \theta_1^b} & \frac{\partial \Delta P_1^c}{\partial \theta_1^c} & \dots & \frac{\partial \Delta P_1^c}{\partial \theta_{n-1}^a} & \frac{\partial \Delta P_1^c}{\partial \theta_{n-1}^b} & \frac{\partial \Delta P_1^c}{\partial \theta_{n-1}^c} \\ \vdots & \vdots & \vdots & \dots & \vdots & \vdots & \vdots \\ \frac{\partial \Delta P_{n-1}^a}{\partial \theta_1^a} & \frac{\partial \Delta P_{n-1}^a}{\partial \theta_1^b} & \frac{\partial \Delta P_{n-1}^a}{\partial \theta_1^c} & \dots & \frac{\partial \Delta P_{n-1}^a}{\partial \theta_{n-1}^a} & \frac{\partial \Delta P_{n-1}^a}{\partial \theta_{n-1}^b} & \frac{\partial \Delta P_{n-1}^a}{\partial \theta_{n-1}^c} \\ \frac{\partial \Delta P_{n-1}^b}{\partial \theta_1^a} & \frac{\partial \Delta P_{n-1}^b}{\partial \theta_1^b} & \frac{\partial \Delta P_{n-1}^b}{\partial \theta_1^c} & \dots & \frac{\partial \Delta P_{n-1}^b}{\partial \theta_{n-1}^a} & \frac{\partial \Delta P_{n-1}^b}{\partial \theta_{n-1}^b} & \frac{\partial \Delta P_{n-1}^b}{\partial \theta_{n-1}^c} \\ \frac{\partial \Delta P_{n-1}^c}{\partial \theta_1^a} & \frac{\partial \Delta P_{n-1}^c}{\partial \theta_1^b} & \frac{\partial \Delta P_{n-1}^c}{\partial \theta_1^c} & \dots & \frac{\partial \Delta P_{n-1}^c}{\partial \theta_{n-1}^a} & \frac{\partial \Delta P_{n-1}^c}{\partial \theta_{n-1}^b} & \frac{\partial \Delta P_{n-1}^c}{\partial \theta_{n-1}^c} \end{bmatrix} \tag{3.51}$$

$$
\mathbf{J_{QV}} = \begin{bmatrix}
\frac{\partial \Delta Q_1^a}{\partial V_1^a} & \frac{\partial \Delta Q_1^a}{\partial V_1^b} & \frac{\partial \Delta Q_1^a}{\partial V_1^c} & \cdots & \frac{\partial \Delta Q_1^a}{\partial V_{n-1}^a} & \frac{\partial \Delta Q_1^a}{\partial V_{n-1}^b} & \frac{\partial \Delta Q_1^a}{\partial V_{n-1}^c} \\
\frac{\partial \Delta Q_1^b}{\partial V_1^a} & \frac{\partial \Delta Q_1^b}{\partial V_1^b} & \frac{\partial \Delta Q_1^b}{\partial V_1^c} & \cdots & \frac{\partial \Delta Q_1^b}{\partial V_{n-1}^a} & \frac{\partial \Delta Q_1^b}{\partial V_{n-1}^b} & \frac{\partial \Delta Q_1^b}{\partial V_{n-1}^c} \\
\frac{\partial \Delta Q_1^c}{\partial V_1^a} & \frac{\partial \Delta Q_1^c}{\partial V_1^b} & \frac{\partial \Delta Q_1^c}{\partial V_1^c} & \cdots & \frac{\partial \Delta Q_1^c}{\partial V_{n-1}^a} & \frac{\partial \Delta Q_1^c}{\partial V_{n-1}^b} & \frac{\partial \Delta Q_1^c}{\partial V_{n-1}^c} \\
\vdots & \vdots & \vdots & \cdots & \vdots & \vdots & \vdots \\
\frac{\partial \Delta Q_{n-1}^a}{\partial V_1^a} & \frac{\partial \Delta Q_{n-1}^a}{\partial V_1^b} & \frac{\partial \Delta Q_{n-1}^a}{\partial V_1^c} & \cdots & \frac{\partial \Delta Q_{n-1}^a}{\partial V_{n-1}^a} & \frac{\partial \Delta Q_{n-1}^a}{\partial V_{n-1}^b} & \frac{\partial \Delta Q_{n-1}^a}{\partial V_{n-1}^c} \\
\frac{\partial \Delta Q_{n-1}^b}{\partial V_1^a} & \frac{\partial \Delta Q_{n-1}^b}{\partial V_1^b} & \frac{\partial \Delta Q_{n-1}^b}{\partial V_1^c} & \cdots & \frac{\partial \Delta Q_{n-1}^b}{\partial V_{n-1}^a} & \frac{\partial \Delta Q_{n-1}^b}{\partial V_{n-1}^b} & \frac{\partial \Delta Q_{n-1}^b}{\partial V_{n-1}^c} \\
\frac{\partial \Delta Q_{n-1}^c}{\partial V_1^a} & \frac{\partial \Delta Q_{n-1}^c}{\partial V_1^b} & \frac{\partial \Delta Q_{n-1}^c}{\partial V_1^c} & \cdots & \frac{\partial \Delta Q_{n-1}^c}{\partial V_{n-1}^a} & \frac{\partial \Delta Q_{n-1}^c}{\partial V_{n-1}^b} & \frac{\partial \Delta Q_{n-1}^c}{\partial V_{n-1}^c}
\end{bmatrix} \tag{3.52}
$$

$$
\mathbf{J_{Q\theta}} = \begin{bmatrix}
\frac{\partial \Delta Q_1^a}{\partial \theta_1^a} & \frac{\partial \Delta Q_1^a}{\partial V_1^b} & \frac{\partial \Delta Q_1^a}{\partial \theta_1^c} & \cdots & \frac{\partial \Delta Q_1^a}{\partial \theta_{n-1}^a} & \frac{\partial \Delta Q_1^a}{\partial \theta_{n-1}^b} & \frac{\partial \Delta Q_1^a}{\partial \theta_{n-1}^c} \\
\frac{\partial \Delta Q_1^b}{\partial \theta_1^a} & \frac{\partial \Delta Q_1^b}{\partial \theta_1^b} & \frac{\partial \Delta Q_1^b}{\partial \theta_1^c} & \cdots & \frac{\partial \Delta Q_1^b}{\partial \theta_{n-1}^a} & \frac{\partial \Delta Q_1^b}{\partial \theta_{n-1}^b} & \frac{\partial \Delta Q_1^b}{\partial \theta_{n-1}^c} \\
\frac{\partial \Delta Q_1^c}{\partial \theta_1^a} & \frac{\partial \Delta Q_1^c}{\partial \theta_1^b} & \frac{\partial \Delta Q_1^c}{\partial \theta_1^c} & \cdots & \frac{\partial \Delta Q_1^c}{\partial \theta_{n-1}^a} & \frac{\partial \Delta Q_1^c}{\partial \theta_{n-1}^b} & \frac{\partial \Delta Q_1^c}{\partial \theta_{n-1}^c} \\
\vdots & \vdots & \vdots & \cdots & \vdots & \vdots & \vdots \\
\frac{\partial \Delta Q_{n-1}^a}{\partial \theta_1^a} & \frac{\partial \Delta Q_{n-1}^a}{\partial \theta_1^b} & \frac{\partial \Delta Q_{n-1}^a}{\partial \theta_1^c} & \cdots & \frac{\partial \Delta Q_{n-1}^a}{\partial \theta_{n-1}^a} & \frac{\partial \Delta Q_{n-1}^a}{\partial \theta_{n-1}^b} & \frac{\partial \Delta Q_{n-1}^a}{\partial \theta_{n-1}^c} \\
\frac{\partial \Delta Q_{n-1}^b}{\partial \theta_1^a} & \frac{\partial \Delta Q_{n-1}^b}{\partial \theta_1^b} & \frac{\partial \Delta Q_{n-1}^b}{\partial \theta_1^c} & \cdots & \frac{\partial \Delta Q_{n-1}^b}{\partial \theta_{n-1}^a} & \frac{\partial \Delta Q_{n-1}^b}{\partial \theta_{n-1}^b} & \frac{\partial \Delta Q_{n-1}^b}{\partial \theta_{n-1}^c} \\
\frac{\partial \Delta Q_{n-1}^c}{\partial \theta_1^a} & \frac{\partial \Delta Q_{n-1}^c}{\partial \theta_1^b} & \frac{\partial \Delta Q_{n-1}^c}{\partial \theta_1^c} & \cdots & \frac{\partial \Delta Q_{n-1}^c}{\partial \theta_{n-1}^a} & \frac{\partial \Delta Q_{n-1}^c}{\partial \theta_{n-1}^b} & \frac{\partial \Delta Q_{n-1}^c}{\partial \theta_{n-1}^c}
\end{bmatrix} \tag{3.53}
$$

Because the specified PQ values for Y-connected loads and Delta-connected loads are different, as seen in Section 3.2.1, the Jacobian matrix elements will be different for each connection. In the following section, the Jacobian matrix elements for these two load connection configurations will be discussed. The elements of phase A will be presented. For Phase B and C, the way to derive the Jacobian submatrices is similar.

Notice that for buses that have both Y-connected loads and Delta-connected loads, the

Jacobian elements for the buses are the summation of the Jacobian matrix of Y-connected loads and that of Delta-connected loads.

Jacobian submatrices for buses with Y-connected loads

Y-connected loads are modeled as ZIP loads:

$$P_{lk}^{s} = P_{0k}^{s} + P_{1k}^{s} V_k^s + P_{2k}^{s} (V_k^s)^2 \tag{3.54}$$

$$Q_{lk}^{s} = Q_{0k}^{s} + Q_{1k}^{s} V_k^s + Q_{2k}^{s} (V_k^s)^2 \tag{3.55}$$

The specified injected P and Q are:

$$P_{sp,k}^{s} = P_{gk}^{s} - [P_{0k}^{s} + P_{1k}^{s} V_k^s + P_{2k}^{s} (V_k^s)^2] \tag{3.56}$$

$$Q_{sp,k}^{s} = Q_{gk}^{s} - [Q_{0k}^{s} + Q_{1k}^{s} V_k^s + Q_{2k}^{s} (V_k^s)^2] \tag{3.57}$$

where P_{gk}^{s} and Q_{gk}^{s} are the real and reactive power generated by the DG in PQ mode connected at bus k in phase s. (DG in PQ mode produces a specified amount of real and reactive power)

The real and reactive power mismatches at bus k in phase s are:

$$\begin{aligned} \Delta P_k^s = {} & [P_{gk}^{s} - P_{0k}^{s} - P_{1k}^{s} V_k^s - P_{2k}^{s} (V_k^s)^2] \\ & - V_k^s \sum_{i=1}^{N} \sum_{t=1}^{3} V_i^t Y_{ki}^{st} \cos(\theta_k^s - \theta_i^t - \delta_{ki}^{st}) \end{aligned} \tag{3.58}$$

$$\begin{aligned} \Delta Q_k^s = {} & [Q_{gk}^{s} - Q_{0k}^{s} - Q_{1k}^{s} V_k^s - Q_{2k}^{s} (V_k^s)^2] \\ & - V_k^s \sum_{i=1}^{N} \sum_{t=1}^{3} V_i^t Y_{ki}^{st} \sin(\theta_k^s - \theta_i^t - \delta_{ki}^{st}) \end{aligned} \tag{3.59}$$

Based on the power mismatches, the Jacobian matrix for Newton-Raphson technique can be found by doing the partial derivative of (3.58) and (3.59) with respect to V_m^t and θ_b^t, where $m = 1, \ldots, N-1$, and $t = a, b, c$. The Jacobian matrix consists of different diagonal and off-diagonal elements.

Here are the diagonal elements of the Jacobian matrix ($m = k$):

$$\frac{\partial \Delta P_k^s}{\partial V_k^s} = -P_{1k}^s - 2P_{2k}^s V_k^s - V_k^s Y_{kk}^{ss} \cos(-\delta_{kk}^{ss})$$
$$-[\sum_{i=1}^{N}\sum_{t=1}^{3} V_i^t Y_{ki}^{st} \cos(\theta_k^s - \theta_i^t - \delta_{ki}^{st})] \tag{3.60}$$

$$\frac{\partial \Delta P_k^s}{\partial V_k^t} = -V_k^s Y_{kk}^{st} \cos(\theta_k^s - \theta_k^t - \delta_{kk}^{st}) \tag{3.61}$$

$$\frac{\partial \Delta P_k^s}{\partial \theta_k^s} = -V_k^s\{[\sum_{i=1}^{N}\sum_{t=1}^{3} -V_i^t Y_{ki}^{st} \sin(\theta_k^s - \theta_i^t - \delta_{ki}^{st})]$$
$$+V_k^s Y_{kk}^{ss} \sin(-\delta_{kk}^{ss})\} \tag{3.62}$$

$$\frac{\partial \Delta P_k^s}{\partial \theta_k^t} = -V_k^s V_k^t Y_{kk}^{st} \sin(\theta_k^s - \theta_k^t - \delta_{kk}^{st}) \tag{3.63}$$

$$\frac{\partial \Delta Q_k^s}{\partial V_k^s} = -Q_{1k}^s - 2Q_{2k}^s V_k^s - V_k^s Y_{kk}^{ss} \sin(-\delta_{kk}^{ss})$$
$$-[\sum_{i=1}^{N}\sum_{t=1}^{3} V_i^t Y_{ki}^{st} \sin(\theta_k^s - \theta_i^t - \delta_{ki}^{st})] \tag{3.64}$$

$$\frac{\partial \Delta Q_k^s}{\partial V_k^t} = -V_k^s Y_{kk}^{st} \sin(\theta_k^s - \theta_k^t - \delta_{kk}^{st}) \tag{3.65}$$

$$\frac{\partial \Delta Q_k^s}{\partial \theta_k^s} = -V_k^s\{[\sum_{i=1}^{N}\sum_{t=1}^{3} V_i^t Y_{ki}^{st} \cos(\theta_k^s - \theta_i^t - \delta_{ki}^{st})]$$
$$-V_k^s Y_{kk}^{ss} \cos(-\delta_{kk}^{ss})\} \tag{3.66}$$

$$\frac{\partial \Delta Q_k^s}{\partial \theta_k^t} = V_k^s V_k^t Y_{kk}^{st} \cos(\theta_k^s - \theta_k^t - \delta_{kk}^{st}) \tag{3.67}$$

Here are the off-diagonal elements of the Jacobian matrix ($m \neq k$):

$$\frac{\partial \Delta P_k^s}{\partial V_m^s} = -V_k^s Y_{km}^{ss} \cos(\theta_k^s - \theta_m^s - \delta_{km}^{ss}) \tag{3.68}$$

$$\frac{\partial \Delta P_k^s}{\partial V_m^t} = -V_k^s Y_{km}^{st} \cos(\theta_k^s - \theta_m^t - \delta_{km}^{st}) \tag{3.69}$$

$$\frac{\partial \Delta P_k^s}{\partial \theta_m^s} = -V_k^s V_m^s Y_{km}^{ss} \sin(\theta_k^s - \theta_m^s - \delta_{km}^{ss}) \tag{3.70}$$

$$\frac{\partial \Delta P_k^s}{\partial \theta_m^t} = -V_k^s V_m^t Y_{km}^{st} \sin(\theta_k^s - \theta_m^t - \delta_{km}^{st}) \tag{3.71}$$

$$\frac{\partial \Delta Q_k^s}{\partial V_m^s} = -V_k^s Y_{km}^{ss} \sin(\theta_k^s - \theta_m^s - \delta_{km}^{ss}) \tag{3.72}$$

$$\frac{\partial \Delta Q_k^s}{\partial V_m^t} = -V_k^s Y_{km}^{st} \sin(\theta_k^s - \theta_m^t - \delta_{km}^{st}) \tag{3.73}$$

$$\frac{\partial \Delta Q_k^s}{\partial \theta_m^s} = V_k^s V_m^s Y_{km}^{ss} \cos(\theta_k^s - \theta_m^s - \delta_{km}^{ss}) \tag{3.74}$$

$$\frac{\partial \Delta Q_k^s}{\partial \theta_m^t} = V_k^s V_m^t Y_{km}^{st} \cos(\theta_k^s - \theta_m^t - \delta_{km}^{st}) \tag{3.75}$$

Jacobian submatrices for buses with Delta-connected loads

The Delta-connected loads are modeled as ZIP loads:

$$P_{lk}^{st} = P_{0k}^s + P_{1k}^s V_k^{st} + P_{2k}^s (V_k^{st})^2 \tag{3.76}$$

$$Q_{lk}^{st} = Q_{0k}^s + Q_{1k}^s V_k^{st} + Q_{2k}^s (V_k^{st})^2 \tag{3.77}$$

where $V_k^{st} = V_k^s - V_k^t$ is the phase-to-phase voltage between phase s and t at bus k.

As shown previously Fig.3.3, the relationship between the load and phase current for each phase is

$$S^{ab}_{l-k} = P^{ab}_{l-k} + jQ^{ab}_{l-k} = (V^a_k - V^b_k)(I^{ab}_k)^* \tag{3.78}$$

$$S^{bc}_{l-k} = P^{bc}_{l-k} + jQ^{bc}_{l-k} = (V^b_k - V^c_k)(I^{bc}_k)^* \tag{3.79}$$

$$S^{ca}_{l-k} = P^{ca}_{l-k} + jQ^{ca}_{l-k} = (V^c_k - V^a_k)(I^{ca}_k)^* \tag{3.80}$$

while the relationship between the phase current and line current is

$$I^a_{in-k} = I^{ca}_k - I^{ab}_k \tag{3.81}$$

$$I^b_{in-k} = I^{ab}_k - I^{bc}_k \tag{3.82}$$

$$I^c_{in-k} = I^{bc}_k - I^{ca}_k \tag{3.83}$$

If no generator is connected at this bus, the power injection at each phase for delta connected load is

$$S^a_{in-k} = V^a_k(I^a_{in-k})^* = V^a_k[\frac{S^{ca}_{l-k}}{V^c_k - V^a_k} - \frac{S^{ab}_{l-k}}{V^a_k - V^b_k}] \tag{3.84}$$

$$S^b_{in-k} = V^b_k(I^b_{in-k})^* = V^b_k[\frac{S^{ab}_{l-k}}{V^a_k - V^b_k} - \frac{S^{bc}_{l-k}}{V^b_k - V^c_k}] \tag{3.85}$$

$$S^c_{in-k} = V^c_k(I^c_{in-k})^* = V^c_k[\frac{S^{bc}_{l-k}}{V^b_k - V^c_k} - \frac{S^{ca}_{l-k}}{V^c_k - V^a_k}] \tag{3.86}$$

If one generator in Y-connection is connected at this bus, the specified power injection at each phase from the load for this bus are:

$$S^a_{in-k} = V^a_k(I^a_{in-k})^* = S^a_{gk} + V^a_k[\frac{S^{ca}_{lk}}{V^c_k - V^a_k} - \frac{S^{ab}_{lk}}{V^a_k - V^b_k}] \tag{3.87}$$

$$S^b_{in-k} = V^b_k(I^b_{in-k})^* = S^b_{gk} + V^b_k[\frac{S^{ab}_{lk}}{V^a_k - V^b_k} - \frac{S^{bc}_{lk}}{V^b_k - V^c_k}] \tag{3.88}$$

$$S^c_{in-k} = V^c_k(I^c_{in-k})^* = S^c_{gk} + V^c_k[\frac{S^{bc}_{lk}}{V^b_k - V^c_k} - \frac{S^{ca}_{lk}}{V^c_k - V^a_k}] \tag{3.89}$$

The specified injected P and Q for each phase are

$$P^s_{sp,k} = P^s_g + \mathrm{Re}[S^s_{in-k}] \tag{3.90}$$

$$Q^s_{sp,k} = Q^s_g + \mathrm{Im}[S^s_{in-k}] \tag{3.91}$$

The real and reactive power mismatches at bus k in phase s are the same as

$$\Delta P^s_k = P^s_{sp,k} - V^s_k \sum_{i=1}^{n} \sum_{t=1}^{3} V^t_i Y^{st}_{ki} \cos(\theta^s_k - \theta^t_i - \delta^{st}_{ki}) \tag{3.92}$$

$$\Delta Q^s_k = Q^s_{sp,k} - V^s_k \sum_{i=1}^{n} \sum_{t=1}^{3} V^t_i Y^{st}_{ki} \sin(\theta^s_k - \theta^t_i - \delta^{st}_{ki}) \tag{3.93}$$

Jacobian matrix elements for Delta-connected loads can be found similarly as Y-connected loads. To derive the Jacobean matrix elements in a manageable way, the load is assumed to be a constant power load. Therefore, we do not need to do the partial derivative on P^{st}_{lk} and Q^{st}_{lk} when finding the Jacobian matrix elements. But in the Newton-Raphson algorithm, the power mismatch calculation uses the exact load model. Because the Jacobian matrix elements are approximated due to the constant power load assumption, it may take more iterations to find the three-phase power flow solutions.

For Phase A:

$$S_{in}^{a} = (V_a \cos\theta_a + jV_a \sin\theta_a)[(\frac{P_c + jQ_c}{(V_c \cos\theta_c - V_a \cos\theta_a) + j(V_c \sin\theta_c - V_a \sin\theta_a)}) \tag{3.94}$$
$$-(\frac{P_a + jQ_a}{(V_a \cos\theta_a - V_b \cos\theta_b) + j(V_a \sin\theta_a - V_b \sin\theta_b)})]$$
$$= (V_a \cos\theta_a + jV_a \sin\theta_a)[\frac{(P_c + jQ_c)[(V_c \cos\theta_c - V_a \cos\theta_a)] - j(V_c \sin\theta_c - V_a \sin\theta_a)}{(V_c \cos\theta_c - V_a \cos\theta_a)^2 + (V_c \sin\theta_c - V_a \sin\theta_a)^2}$$
$$-\frac{(P_a + jQ_a)[(V_a \cos\theta_a - V_b \cos\theta_b)] - j(V_a \sin\theta_a - V_b \sin\theta_b)}{(V_a \cos\theta_a - V_b \cos\theta_b)^2 + (V_a \sin\theta_a - V_b \sin\theta_b)^2}]$$
$$= \{\frac{(V_a \cos\theta_a)(P_cA + Q_cB) - (V_a \sin\theta_a)(Q_cA - P_cB)}{(V_c \cos\theta_c - V_a \cos\theta_a)^2 + (V_c \sin\theta_c - V_a \sin\theta_a)^2}$$
$$-\frac{(V_a \cos\theta_a)(P_aC + Q_aD) - (V_a \sin\theta_a)(Q_aC - P_aD)}{(V_a \cos\theta_a - V_b \cos\theta_b)^2 + (V_a \sin\theta_a - V_b \sin\theta_b)^2}\}$$
$$+ j\{\frac{(V_a \sin\theta_a)(P_cA + Q_cB) + (V_a \cos\theta_a)(Q_cA - P_cB)}{(V_c \cos\theta_c - V_a \cos\theta_a)^2 + (V_c \sin\theta_c - V_a \sin\theta_a)^2}$$
$$-\frac{(V_a \sin\theta_a)(P_aC + Q_aD) + (V_a \cos\theta_a)(Q_aC - P_aD)}{(V_a \cos\theta_a - V_b \cos\theta_b)^2 + (V_a \sin\theta_a - V_b \sin\theta_b)^2}\}$$

where

$$A = V_c \cos\theta_c - V_a \cos\theta_a \tag{3.95}$$

$$B = V_c \sin\theta_c - V_a \sin\theta_a \tag{3.96}$$

$$C = V_a \cos\theta_a - V_b \cos\theta_b \tag{3.97}$$

$$D = V_a \sin\theta_a - V_b \sin\theta_b \tag{3.98}$$

P_{in}^{a} can be express as:

$$P_{in}^{a} = \frac{f_1}{g_1} - \frac{f_2}{g_2} \tag{3.99}$$

where

$$f_1 = (V_a \cos\theta_a)[P_c(V_c \cos\theta_c - V_a \cos\theta_a) + Q_c(V_c \sin\theta_c - V_a \sin\theta_a)] \tag{3.100}$$

$$- (V_a \sin\theta_a)[Q_c(V_c \cos\theta_c - V_a \cos\theta_a) - P_c(V_c \sin\theta_c - V_a \sin\theta_a)]$$

$$= V_a \cos\theta_a)[AA] - (V_a \sin\theta_a)[BB]$$

$$g_1 = (V_c \cos\theta_c - V_a \cos\theta_a)^2 + (V_c \sin\theta_c - V_a \sin\theta_a)^2 \tag{3.101}$$

$$f_2 = (V_a \cos\theta_a)[P_a(V_a \cos\theta_a - V_b \cos\theta_b) + Q_a(V_a \sin\theta_a - V_b \sin\theta_b)] \tag{3.102}$$

$$- (V_a \sin\theta_a)[Q_a(V_a \cos\theta_a - V_b \cos\theta_b) - P_a(V_a \sin\theta_a - V_b \sin\theta_b)]$$

$$= (V_a \cos\theta_a)[CC] - (V_a \sin\theta_a)[DD]$$

$$g_2 = (V_a \cos\theta_a - V_b \cos\theta_b)^2 + (V_a \sin\theta_a - V_b \sin\theta_b)^2 \tag{3.103}$$

$$\tag{3.104}$$

Since P_{in}^a is the specified value, the following derived items are only part of the Jacobian matrix elements. The other part of Jacobian matrix elements comes from the calculated values, which can be computed same as the Y-connected load. The Jacobian element can be found by subtracting the items corresponding to the specified value from the items corresponding to the calculated value.

For the specified P value, the partial derivative with respect to x can be expressed as:

$$\frac{\partial P_{in}}{\partial x} = \frac{\partial \frac{f_1}{g_1} - \frac{f_2}{g_2}}{\partial x} = \frac{f_1' g_1 - f_1 g_1'}{g_1^2} - \frac{f_2' g_2 - f_2 g_2'}{g_2^2} \tag{3.105}$$

here x can be V_a, V_b, V_c, θ_a, θ_b and θ_c.

The element of $\frac{\partial P_{in}^{a}}{\partial V_a}$ can be found by:

$$\frac{\partial f_1}{\partial V_a} = \cos\theta_a[AA] + V_a\cos\theta_a[-P_c\cos\theta_a - Q_c\sin\theta_a] - \sin\theta_a[BB] \tag{3.106}$$

$$- V_a\sin\theta_a[-Q_c\cos\theta_a + P_c\sin\theta_a]$$

$$\frac{\partial f_2}{\partial V_a} = \cos\theta_a[CC] + V_a\cos\theta_a[P_a\cos\theta_a + Q_a\sin\theta_a] - \sin\theta_a[DD] \tag{3.107}$$

$$- V_a\sin\theta_a[Q_a\cos\theta_a - P_a\sin\theta_a]$$

$$\frac{\partial g_1}{\partial V_a} = 2(V_c\cos\theta_c - V_a\cos\theta_a)(-\cos\theta_a) + 2(V_c\sin\theta_c - V_a\sin\theta_a)(-\sin\theta_a) \tag{3.108}$$

$$\frac{\partial g_2}{\partial V_a} = 2(V_a\cos\theta_a - V_b\cos\theta_b)(\cos\theta_a) + 2(V_a\sin\theta_a - V_b\sin\theta_b)(\sin\theta_a) \tag{3.109}$$

The element of $\frac{\partial P_{in}^{a}}{\partial V_b}$ can be found by:

$$\frac{\partial f_1}{\partial V_b} = 0 \tag{3.110}$$

$$\frac{\partial f_2}{\partial V_b} = V_a\cos\theta_a[-P_a\cos\theta_b - Q_a\sin\theta_b] - V_a\sin\theta_a[-Q_a\cos\theta_b + P_a\sin\theta_b] \tag{3.111}$$

$$\frac{\partial g_1}{\partial V_b} = 0 \tag{3.112}$$

$$\frac{\partial g_2}{\partial V_b} = 2(V_a\cos\theta_a - V_b\cos\theta_b)(-\cos\theta_b) + 2(V_a\sin\theta_a - V_b\sin\theta_b)(-\sin\theta_b) \tag{3.113}$$

The element of $\frac{\partial P_{in}^{a}}{\partial V_c}$ can be found by:

$$\frac{\partial f_1}{\partial V_c} = V_a\cos\theta_a[P_c\cos\theta_c + Q_c\sin\theta_c] - V_a\sin\theta_a[Q_c\cos\theta_c - P_c\sin\theta_c] \tag{3.114}$$

$$\frac{\partial f_2}{\partial V_c} = 0 \tag{3.115}$$

$$\frac{\partial g_1}{\partial V_c} = 2(V_c\cos\theta_c - V_a\cos\theta_a)(\cos\theta_c) + 2(V_c\sin\theta_c - V_a\sin\theta_a)(\sin\theta_c) \tag{3.116}$$

$$\frac{\partial g_2}{\partial V_c} = 0 \tag{3.117}$$

The element of $\frac{\partial P_{in}^{a}}{\partial \theta_a}$ can be found by:

$$\frac{\partial f_1}{\partial \theta_a} = -V_a \sin\theta_a[AA] + V_a \cos\theta_a[P_c V_a \sin\theta_a - Q_c V_a \cos\theta_a] \tag{3.118}$$

$$- V_a \cos\theta_a[BB] - V_a \sin\theta_a[Q_c V_a \sin\theta_a + P_c V_a \cos\theta_a]$$

$$\frac{\partial f_2}{\partial \theta_a} = -V_a \sin\theta_a[CC] + V_a \cos\theta_a[-P_a V_a \sin\theta_a + Q_a V_a \cos\theta_a] \tag{3.119}$$

$$- V_a \cos\theta_a[DD] - V_a \sin\theta_a[-Q_a V_a \sin\theta_a - P_a V_a \cos\theta_a]$$

$$\frac{\partial g_1}{\partial \theta_a} = 2(V_c \cos\theta_c - V_a \cos\theta_a)(V_a \sin\theta_a) + 2(V_c \sin\theta_c - V_a \sin\theta_a)(-V_a \cos\theta_a) \tag{3.120}$$

$$\frac{\partial g_2}{\partial \theta_a} = 2(V_a \cos\theta_a - V_b \cos\theta_b)(-V_a \sin\theta_a) + 2(V_a \sin\theta_a - V_b \sin\theta_b)(V_a \cos\theta_a) \tag{3.121}$$

The element of $\frac{\partial P_{in}^{a}}{\partial \theta_b}$ can be found by:

$$\frac{\partial f_1}{\partial \theta_b} = 0 \tag{3.122}$$

$$\frac{\partial f_2}{\partial \theta_b} = V_a \cos\theta_a[P_a V_b \sin\theta_b - Q_a V_b \cos\theta_b] - V_a \sin\theta_a[Q_a V_b \sin\theta_b + P_a V_b \cos\theta_b] \tag{3.123}$$

$$\frac{\partial g_1}{\partial \theta_b} = 0 \tag{3.124}$$

$$\frac{\partial g_2}{\partial \theta_b} = 2(V_a \cos\theta_a - V_b \cos\theta_b)(V_b \sin\theta_b) + 2(V_a \sin\theta_a - V_b \sin\theta_b)(-V_b \cos\theta_b) \tag{3.125}$$

The element of $\frac{\partial P_{in}^{a}}{\partial \theta_c}$ can be found by:

$$\frac{\partial f_1}{\partial \theta_c} = V_a \cos\theta_a[-P_c V_c \sin\theta_c + Q_c V_c \cos\theta_c] - V_a \sin\theta_a[-Q_c V_c \sin\theta_c - P_c V_c \cos\theta_c] \tag{3.126}$$

$$\frac{\partial f_2}{\partial \theta_c} = 0 \tag{3.127}$$

$$\frac{\partial g_1}{\partial \theta_c} = 2(V_c \cos\theta_c - V_a \cos\theta_a)(-V_c \sin\theta_c) + 2(V_c \sin\theta_c - V_a \sin\theta_a)(V_c \cos\theta_c) \tag{3.128}$$

$$\frac{\partial g_2}{\partial \theta_c} = 0 \tag{3.129}$$

Similarly, Q_{in}^{a} can be express as:

$$Q_{in}^{a} = \frac{f_1}{g_1} - \frac{f_2}{g_2} \tag{3.130}$$

where

$$f_1 = (V_a \sin\theta_a)[P_c(V_c\cos\theta_c - V_a\cos\theta_a) + Q_c(V_c\sin\theta_c - V_a\sin\theta_a)] \tag{3.131}$$

$$+ (V_a\cos\theta_a)[Q_c(V_c\cos\theta_c - V_a\cos\theta_a) - P_c(V_c\sin\theta_c - V_a\sin\theta_a)]$$

$$= (V_a\sin\theta_a)[AA] + (V_a\cos\theta_a)[BB]$$

$$g_1 = (V_c\cos\theta_c - V_a\cos\theta_a)^2 + (V_c\sin\theta_c - V_a\sin\theta_a)^2 \tag{3.132}$$

$$f_2 = (V_a\sin\theta_a)[P_a(V_a\cos\theta_a - V_b\cos\theta_b) + Q_a(V_a\sin\theta_a - V_b\sin\theta_b)] \tag{3.133}$$

$$+ (V_a\cos\theta_a)[Q_a(V_a\cos\theta_a - V_b\cos\theta_b) - P_a(V_a\sin\theta_a - V_b\sin\theta_b)]$$

$$= (V_a\sin\theta_a)[CC] + (V_a\cos\theta_a)[DD]$$

$$g_2 = (V_a\cos\theta_a - V_b\cos\theta_b)^2 + (V_a\sin\theta_a - V_b\sin\theta_b)^2 \tag{3.134}$$

$$\tag{3.135}$$

The element of $\frac{\partial Q_{in}^{a}}{\partial V_a}$ can be found by:

$$\frac{\partial f_1}{\partial V_a} = \sin\theta_a[AA] + V_a\sin\theta_a[-P_c\cos\theta_a - Q_c\sin\theta_a] + \cos\theta_a[BB] \tag{3.136}$$

$$+ V_a\cos\theta_a[-Q_c\cos\theta_a + P_c\sin\theta_a]$$

$$\frac{\partial f_2}{\partial V_a} = \sin\theta_a[CC] + V_a\sin\theta_a[P_a\cos\theta_a + Q_a\sin\theta_a] + \cos\theta_a[DD] \tag{3.137}$$

$$+ V_a\cos\theta_a[Q_a\cos\theta_a - P_a\sin\theta_a]$$

$$\frac{\partial g_1}{\partial V_a} = 2(V_c\cos\theta_c - V_a\cos\theta_a)(-\cos\theta_a) + 2(V_c\sin\theta_c - V_a\sin\theta_a)(-\sin\theta_a) \tag{3.138}$$

$$\frac{\partial g_2}{\partial V_a} = 2(V_a\cos\theta_a - V_b\cos\theta_b)(\cos\theta_a) + 2(V_a\sin\theta_a - V_b\sin\theta_b)(\sin\theta_a) \tag{3.139}$$

The element of $\frac{\partial Q_{in}^a}{\partial V_b}$ can be found by:

$$\frac{\partial f_1}{\partial V_b} = 0 \tag{3.140}$$

$$\frac{\partial f_2}{\partial V_b} = V_a \sin\theta_a[-P_a\cos\theta_b - Q_a\sin\theta_b] + V_a\cos\theta_a[-Q_a\cos\theta_b + P_a\sin\theta_b] \tag{3.141}$$

$$\frac{\partial g_1}{\partial V_b} = 0 \tag{3.142}$$

$$\frac{\partial g_2}{\partial V_b} = 2(V_a\cos\theta_a - V_b\cos\theta_b)(-\cos\theta_a) + 2(V_a\sin\theta_a - V_b\sin\theta_b)(-\sin\theta_b) \tag{3.143}$$

The element of $\frac{\partial Q_{in}^a}{\partial V_c}$ can be found by:

$$\frac{\partial f_1}{\partial V_c} = V_a\sin\theta_a[P_c\cos\theta_c + Q_c\sin\theta_c] + V_a\cos\theta_a[Q_c\cos\theta_c - P_c\sin\theta_c] \tag{3.144}$$

$$\frac{\partial f_2}{\partial V_c} = 0 \tag{3.145}$$

$$\frac{\partial g_1}{\partial V_c} = 2(V_c\cos\theta_c - V_a\cos\theta_a)(\cos\theta_c) + 2(V_c\sin\theta_c - V_a\sin\theta_a)(\sin\theta_c) \tag{3.146}$$

$$\frac{\partial g_2}{\partial V_c} = 0 \tag{3.147}$$

The element of $\frac{\partial Q_{in}^a}{\partial \theta_a}$ can be found by:

$$\frac{\partial f_1}{\partial \theta_a} = V_a\cos\theta_a[AA] + V_a\sin\theta_a[P_cV_a\sin\theta_a - Q_cV_a\cos\theta_a] \tag{3.148}$$

$$- V_a\sin\theta_a[BB] + V_a\cos\theta_a[Q_cV_a\sin\theta_a + P_cV_a\cos\theta_a]$$

$$\frac{\partial f_2}{\partial \theta_a} = V_a\cos\theta_a[CC] + V_a\sin\theta_a[-P_aV_a\sin\theta_a + Q_aV_a\cos\theta_a] \tag{3.149}$$

$$- V_a\sin\theta_a[DD] + V_a\cos\theta_a[-Q_aV_a\sin\theta_a - P_aV_a\cos\theta_a]$$

$$\frac{\partial g_1}{\partial \theta_a} = 2(V_c\cos\theta_c - V_a\cos\theta_a)(V_a\sin\theta_a) + 2(V_c\sin\theta_c - V_a\sin\theta_a)(-V_a\cos\theta_a) \tag{3.150}$$

$$\frac{\partial g_2}{\partial \theta_a} = 2(V_a\cos\theta_a - V_b\cos\theta_b)(-V_a\sin\theta_a) + 2(V_a\sin\theta_a - V_b\sin\theta_b)(V_a\cos\theta_a) \tag{3.151}$$

The element of $\frac{\partial Q_{in}^a}{\partial \theta_b}$ can be found by:

$$\frac{\partial f_1}{\partial \theta_b} = 0 \tag{3.152}$$

$$\frac{\partial f_2}{\partial \theta_b} = V_a \sin\theta_a[P_a V_b \sin\theta_b - Q_a V_b \cos\theta_b] + V_a \cos\theta_a[Q_a V_b \sin\theta_b + P_a V_b \cos\theta_b] \tag{3.153}$$

$$\frac{\partial g_1}{\partial \theta_b} = 0 \tag{3.154}$$

$$\frac{\partial g_2}{\partial \theta_b} = 2(V_a \cos\theta_a - V_b \cos\theta_b)(V_b \sin\theta_b) + 2(V_a \sin\theta_a - V_b \sin\theta_b)(-V_b \cos\theta_b) \tag{3.155}$$

The element of $\frac{\partial Q_{in}^a}{\partial \theta_c}$ can be found by:

$$\frac{\partial f_1}{\partial \theta_c} = V_a \sin\theta_a[-P_c V_c \sin\theta_c + Q_c V_c \cos\theta_c] + V_a \cos\theta_a[-Q_c V_c \sin\theta_c - P_c V_c \cos\theta_c] \tag{3.156}$$

$$\frac{\partial f_2}{\partial \theta_c} = 0 \tag{3.157}$$

$$\frac{\partial g_1}{\partial \theta_c} = 2(V_c \cos\theta_c - V_a \cos\theta_a)(-V_c \sin\theta_c) + 2(V_c \sin\theta_c - V_a \sin\theta_a)(V_c \cos\theta_c) \tag{3.158}$$

$$\frac{\partial g_2}{\partial \theta_c} = 0 \tag{3.159}$$

3.3 Three-phase continuation power flow

The purpose of continuation power flow is to be trace the whole PV curve and find the maximum loading factor, λ. For this dissertation work, the improved three-phase CPF method is based on the work of [53]. The power flow equations for three-phase CPF for loads and DGs are expressed as follows. For PQ type buses,

$$(P_{Gi}^{\phi} - P_{Li}^{\phi}) - V_i^{\phi} \sum_{j=1}^{N} \sum_{k=1}^{M} V_j^k (G_{ij}^{\phi k} \cos\theta_{ij}^{\phi k} + B_{ij}^{\phi k} \sin\theta_{ij}^{\phi k}) + \lambda(\Delta P_{Gi}^{\phi} - \Delta P_{Li}^{\phi}) = 0 \tag{3.160}$$

$$(Q_{Gi}^{\phi} - Q_{Li}^{\phi}) - V_i^{\phi} \sum_{j=1}^{N} \sum_{k=1}^{M} V_j^k (G_{ij}^{\phi k} \sin\theta_{ij}^{\phi k} - B_{ij}^{\phi k} \cos\theta_{ij}^{\phi k}) + \lambda(-\Delta Q_{Li}^{\phi}) = 0 \tag{3.161}$$

For PV type buses,

$$(P_{Gi}^{\phi}-P_{Li}^{\phi})-V_i^{\phi}\sum_{j=1}^{N}\sum_{k=1}^{M}V_j^k(G_{ij}^{\phi k}\cos\theta_{ij}^{\phi k}+B_{ij}^{\phi k}\sin\theta_{ij}^{\phi k})+\lambda(\Delta P_{Gi}^{\phi}-\Delta P_{Li}^{\phi})=0 \quad (3.162)$$

$$(Q_{Gi}^{\phi}-Q_{Li}^{\phi})-V_i^{\phi}\sum_{j=1}^{N}\sum_{k=1}^{M}V_j^k(G_{ij}^{\phi k}\sin\theta_{ij}^{\phi k}-B_{ij}^{\phi k}\cos\theta_{ij}^{\phi k})+\lambda(-\Delta Q_{Li}^{\phi})=0 \quad (3.163)$$

$$V_i^{\phi}=V_{i0} \quad (3.164)$$

$$Q_{\min,i}\leq Q_{Gi}^{\phi}\leq Q_{\max,i} \quad (3.165)$$

where λ is the loading factor of the system, ΔP_{Gi}^{ϕ} is the proposed active generation variation at bus i phase ϕ, ΔP_{Li}^{ϕ} and ΔQ_{Li}^{ϕ} are the proposed real and reactive load variations at bus i phase ϕ.

(3.160) and (3.162) can be reorganized as (3.166), while (3.161) and (3.163) can be reorganized as (3.167).

$$(P_{Gi}^{\phi}+\lambda\Delta P_{Gi}^{\phi})-(P_{Li}^{\phi}+\lambda\Delta P_{Li}^{\phi})-V_i^{\phi}\sum_{j=1}^{N}\sum_{k=1}^{M}V_j^k(G_{ij}^{\phi k}\cos\theta_{ij}^{\phi k}+B_{ij}^{\phi k}\sin\theta_{ij}^{\phi k})=0 \quad (3.166)$$

$$Q_{Gi}^{\phi}-(Q_{Li}^{\phi}+\lambda\Delta Q_{Li}^{\phi})-V_i^{\phi}\sum_{j=1}^{N}\sum_{k=1}^{M}V_j^k(G_{ij}^{\phi k}\sin\theta_{ij}^{\phi k}-B_{ij}^{\phi k}\cos\theta_{ij}^{\phi k})=0 \quad (3.167)$$

The load model is represented as

$$P_{Li}^{\phi}+jQ_{Li}^{\phi}=\alpha_i\vec{S}_{Li0}^{\phi}|\vec{V}_i^{\phi}|^2+\beta_i\vec{S}_{Li0}^{\phi}\frac{\vec{V}_i^{\phi}}{\vec{V}_{i0}^{\phi}}+\gamma_i\vec{S}_{Li0}^{\phi} \quad (3.168)$$

The CPF algorithm implemented in this work is exactly the same as in [53], except some improvements were made, as will be discussed in Section 3.3.2 and Section 3.3.3. Also, the notations in [53] are changed to match the purpose of this work. Table 3.1 summarizes the notation changes. We use the polar representation in the power flow equations. The real and reactive load, P_{Li}^{ϕ} and Q_{Li}^{ϕ} are renamed as the base loading point with the corresponding notations $P^s_{\text{base},k}$ and $Q^s_{\text{base},k}$, respectively. The real and reactive load variations, ΔP^{ϕ}_{Li} and ΔQ^{ϕ}_{Li} are renamed as load increase direction, LID. The corresponding notations are $P^s_{\text{LID},k}$ and $Q^s_{\text{LID},k}$. The active generation variation, ΔP^{ϕ}_{Gi} is renamed as generator increase direction, GID. The corresponding notation is $P^s_{\text{base}-\text{g},k}$.

Table 3.1: Modification from [53] to this work

From [53]	This work
ϕ	s
i	k
$P^{\phi}_{Li}+\lambda\Delta P^{\phi}_{Li}$	$P^s_{\text{base},k}+\lambda P^s_{\text{LID},k}$
$Q^{\phi}_{Li}+\lambda\Delta Q^{\phi}_{Li}$	$Q^s_{\text{base},k}+\lambda Q^s_{\text{LID},k}$
$P^{\phi}_{Gi}+\lambda\Delta P^{\phi}_{Gi}$	$P^s_{\text{base}-\text{g},k}+\lambda P^s_{\text{GID},k}$

Therefore, for PQ buses, the corresponding CPF power flow equations, (3.160) and (3.161) , are changed into (3.169) and (3.170), respectively. Similarly, for PV buses, the corresponding CPF power flow equations, (3.162) and (3.163) , are changed into (3.169) and (3.170), respectively.

$$\left[(P^s_{\text{base}-\text{g},k}+\lambda P^s_{\text{GID},k})-(P^s_{\text{base},k}+\lambda P^s_{\text{LID},k})\right]-\left[V^s_k\sum_{i=1}^{N}\sum_{t=1}^{3}V^t_iY^{st}_{ki}\cos(\theta^s_k-\theta^t_i-\delta^{st}_{ki})\right]=0 \tag{3.169}$$

$$\left[Q^s_{gk}-(Q^s_{\text{base},k}+\lambda Q^s_{\text{LID},k})\right]-\left[V^s_k\sum_{i=1}^{N}\sum_{t=1}^{3}V^t_iY^{st}_{ki}\sin(\theta^s_k-\theta^t_i-\delta^{st}_{ki}\right]=0 \tag{3.170}$$

where $P^s_{\text{base},k}+\lambda P^s_{\text{LID},k}$ and $Q^s_{\text{base},k}+\lambda Q^s_{\text{LID},k}$ are the real power and reactive power load at bus k phase s at the loading factor λ. When $\lambda=0$, the real and reactive power load at bus k phase s are $P^s_{\text{base},k}$ and $Q^s_{\text{base},k}$, respectivey. When λ increases, the real and reactive power load increases with λ. How real and reactive power load increase depend on $P^s_{\text{LID},k}$

and $Q^s_{\mathrm{LID},k}$. This is why we call $P^s_{\mathrm{LID},k}$ and $Q^s_{\mathrm{LID},k}$ to be the load increase direction that corresponds to bus k phase s.

Note that in the previous three-phase power flow discussed in Section 3.2, the load at each bus are fixed. In the CPF formulation, the load at each bus can be changed with loading factor λ.

When the loading factor, λ, is increased to a certain value, the power flow program may diverge. This is because the Jacobian matrix of power flow equation almost become singular. Some literature determines the maximum loadability based on whether the power flow program diverges or not [40]. However, the power flow program divergence may be caused by numerical issues [30]. The maximum loadability found based on whether the power flow program diverges may not be correct.

To find correct and precise values of maximum loading factor, the CPF method was proposed [30]. The CPF method introduces a continuation parameter λ, which is the loading factor of the system, and an extra equation (3.172). Because of this extra equation, the Jacobian matrix remains non-singular even near the maximum loadability. Note that in power flow equation shown in (3.1), λ is given. But in the CPF method, λ is a state variable to be solved, as shown in (3.171).

$$\mathbf{f}(\mathbf{x},\lambda) = \mathbf{0} \tag{3.171}$$

$$g(\mathbf{x},\lambda) = 0 \tag{3.172}$$

where $\mathbf{f}(\mathbf{x},\lambda)$ is the vector of power flow equations of all buses/phases. The elements of $\mathbf{f}(\mathbf{x},\lambda)$ can be expressed by (3.169) and (3.170) for PQ buses and by (3.169) for

PV buses. Note that (3.164) and (3.164) are not included in this vector. These two equations are not solved directly in the power flow program. On the other hand, (3.172) represents the continuation parameter equation. It can be derived based on two different methods. One is based on local parameterization [30] while the other one is based on arc length parameterization [72], [53]. Local parameterization is more intuitive and easier to implement, but its performance and accuracy is not as good as the arc length parameterization. The arc length parameterization takes less iterations to trace the whole PV curve [72], [53]. In this work, the arc length parameterization was adopted.

Fig.3.7 shows the relationship between arc length, Δs, and state variables change between two CPF iteration of i and $i-1$. The X-axis is the loading factor, λ, while the Y-axis is the voltage of a bus, V. The arc length Δs in Fig.3.7 can be expressed as

$$\Delta s^2 = \Delta V^2 + \Delta\lambda^2 \tag{3.173}$$

where

$$\Delta V = V^i - V^{i-1} \tag{3.174}$$

$$\Delta\lambda = \lambda^i - \lambda^{i-1} \tag{3.175}$$

Note that Fig.3.7 is only used for explanation purpose. In reality, the figure should be multi-dimensional. The arc length for CPF iteration i can be calculated as (3.176) [53].

$$\Delta s^i = \sum_{k=1}^{n} (x_k^i - x_k^{i-1})^2 + (\lambda^i - \lambda^{i-1})^2 \tag{3.176}$$

where x^{i-1} is the state variables, such as voltage and angle of each bus, of power flow equation found in the (i-1)th CPF correction result while λ is the loading factor.

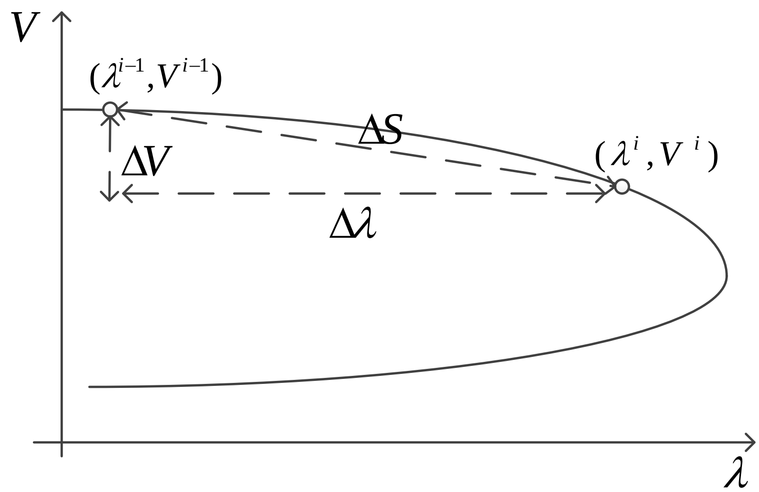

Figure 3.7: Arc length parameterization

In the arc length parameterization, the arc length, Δs^i in (3.176) should be equal to Δs_{spec}, the specified arc length. Therefore, the extra equation (3.172) can be expressed as

$$\sum_{k=1}^{n}(x_k^i - x_k^{i-1})^2 + (\lambda^i - \lambda^{i-1})^2 = (\Delta s_{\text{spec}})^2 \tag{3.177}$$

3.3.1 CPF prediction and correction

The CPF method has two steps: CPF prediction and CPF correction. CPF prediction is used to predict the solution of the next iteration, while CPF correction finds the corrected solution to (3.171) and (3.172). For CPF prediction, two methods are proposed in [72] and [53]: the tangent and the secant method. In the first CPF iteration, the tangent method is used. The tangent vector has $n+1$ elements:

$$\frac{dx_i}{ds} \qquad i = 1, 2, \ldots n, n+1 \tag{3.178}$$

where n is the number of state variables while the extra one is the loading factor λ ($x_{n+1} = \lambda$)

This tangent vector $\mathbf{dx}/\mathbf{ds}$ is found by solving (3.179) [72]

$$\begin{cases} 0 = \mathbf{f_x}\frac{d\mathbf{x}}{ds} \\ (\frac{dx_1}{ds})^2 + \ldots + (\frac{dx_n}{ds})^2 + (\frac{dx_{n+1}}{ds})^2 = 1 \end{cases} \tag{3.179}$$

Once the tangent vector is found, the state variables of next iteration can be found as

$$\mathbf{x}^i_{\text{pre}} = \mathbf{x}^{i-1}_{\text{cor}} + h(\mathbf{dx}/\mathbf{ds}) \tag{3.180}$$

where h is the step size used in CPF prediction, $\mathbf{x}^{i-1}_{\text{cor}}$ is the state variables found by CPF correction in $i-1$th iteration, and $\mathbf{x}^i_{\text{pre}}$ is the state variable found by CPF prediction in ith iteration.

Because the tangent method requires more computation to solve this set of equations, after the first CPF iteration, another method, the secant method, is used. This method uses the results from the previous two CPF iterations (i and $i-1$) to predict the result of current CPF iteration ($i+1$) [72]

$$\mathbf{x}^i_{\text{pre}} = \mathbf{x}^{i-1}_{\text{cor}} + h(\mathbf{x}^i - \mathbf{x}^{i-1}, \lambda^i - \lambda^{i-1}) \tag{3.181}$$

For CPF correction, all state variables are adjusted to satisfy (3.182). The Newton-Raphson method is used to find the solution. The initial condition for the Newton-Raphson method is $\mathbf{x}^i_{\text{pre}}$. The solution of CPF correction is denoted as $\mathbf{x}^i_{\text{cor}}$.

Notice that the Jacobian matrix to solve (3.182) is shown in (3.183). Because of the continuation parameter equation, the Jacobian matrix has extra elements shown in red color. These extra elements in the Jacobian matrix make the Jacobian matrix nonsingular even if the loading factor is close to the maximum value.

$$\begin{cases} \mathbf{f}(\mathbf{x},\lambda) = \mathbf{0} \\ \sum_{k=1}^{n} (x_k^i - x_k^{i-1})^2 + (\lambda^i - \lambda^{i-1})^2 = (\Delta s_{\text{spec}})^2 \end{cases} \tag{3.182}$$

$$\begin{bmatrix} \Delta\mathbf{P}_1^{abc} \\ \vdots \\ \Delta\mathbf{P}_{n-1}^{abc} \\ \Delta\mathbf{Q}_1^{abc} \\ \vdots \\ \Delta\mathbf{Q}_{n-1}^{abc} \\ \Delta s \end{bmatrix} = \begin{bmatrix} \mathbf{J_{PV}} & \mathbf{J_{P\theta}} & \mathbf{J_{P\lambda}} \\ \mathbf{J_{QV}} & \mathbf{J_{Q\theta}} & \mathbf{J_{Q\lambda}} \\ \mathbf{J_{sV}} & \mathbf{J_{s\theta}} & \mathbf{J_{s\lambda}} \end{bmatrix} \begin{bmatrix} \Delta\mathbf{V}_1^{abc} \\ \vdots \\ \Delta\mathbf{V}_{n-1}^{abc} \\ \Delta\theta_1^{abc} \\ \vdots \\ \Delta\theta_{n-1}^{abc} \\ \Delta\lambda \end{bmatrix} \tag{3.183}$$

Fig.3.8 shows the CPF prediction and correction for the arc parameterization approach. The red points represent the predicted state variables, $\mathbf{x}_{\text{pre}}$, while the blue points represent the corrected state variables, $\mathbf{x}_{\text{cor}}$. CPF correction adjusts the state variables in a circle whose center is the current solution and the radius is the specified arc length [72] and [53].

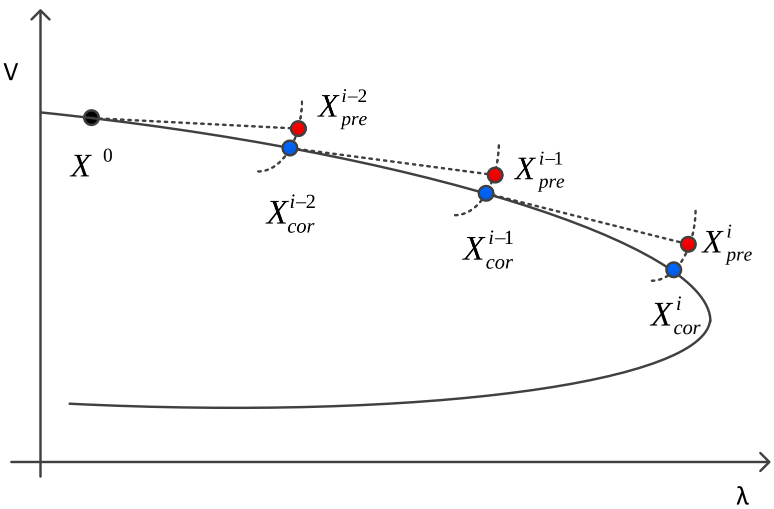

Figure 3.8: CPF prediction and correction for arc parameterization

Fig. 3.9 shows the flowchart of the CPF method. It can be seen that there is a loop that continuously does the prediction and correction such that λ is changed and the corresponding state variables are found. When λ passes the maximum value of λ, the loop is terminated. The whole PV curve are traced and the knee point of the PV curve is found.

3.3.2 Improvement for arc-length parameterization CPF

The specified arc length, Δs_{spec}, is found by trial and error in [53]. However, Δs_{spec} should be found very carefully so that the CPF method can successfully trance the whole PV curve. Δs_{spec} is related to the step size, h, used in CPF prediction. There is a certain relationship between Δs_{spec} and h, as seen from (3.177), (3.180) and (3.181). Therefore, Δs_{spec} cannot be chosen randomly. For example, if h is big, then Δs_{spec} should be big. If Δs_{spec} is too small, the CPF correction tends to diverge.

This is because with big h, the distance between state variables of the precious CPF

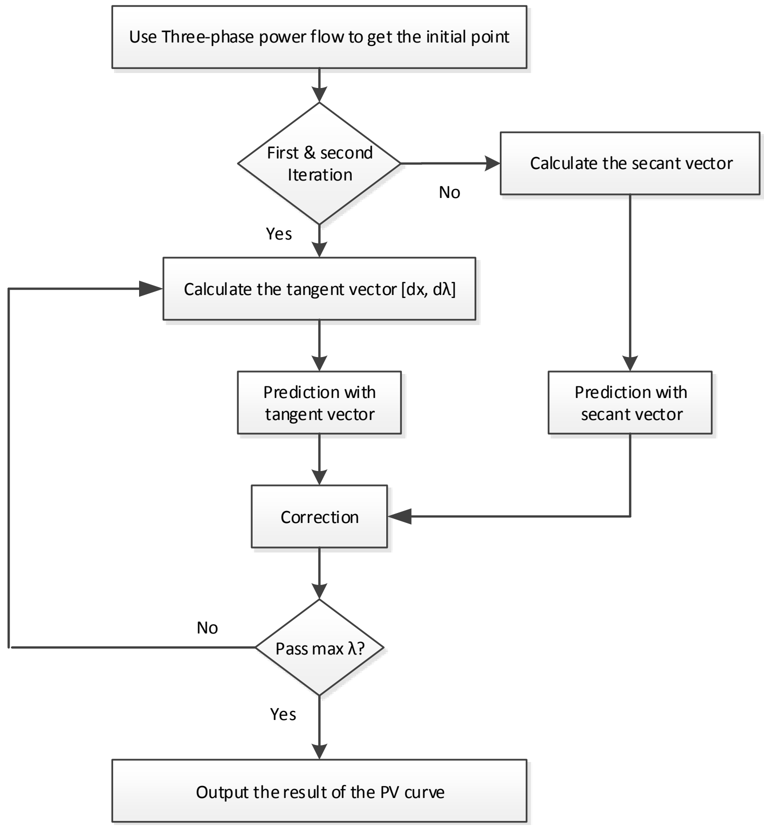

Figure 3.9: Flowchart of the CPF method

iteration and that of the current CPF iteration will be big, resulting in bigger calculated arc length. If Δs_{spec} is too small, the difference between the calculated arc length from (3.176) and the specified arc length, Δs_{spec}, will be big. This difference may be outside the region of convergence of CPF correction and cause CPF correction to diverge. Therefore, it is important to choose carefully Δs_{spec} and h so that CPF correction can converge.

To address this problem, a way to calculate Δs_{spec} directly is proposed. Suppose that we are at CPF iteration i. We have predicted state variables $\mathbf{x}^{i}_{\text{pre}}$ of CPF iteration i and the corrected state variables $\mathbf{x}^{i-2}_{\text{cor}}$ and $\mathbf{x}^{i-1}_{\text{cor}}$ of CPF iteration $i-2$ and $i-1$, respectively. The CPF correction will find $\mathbf{x}^{i}_{\text{cor}}$ by solving (3.182). Δs_{spec} is calculated based on the state variable of previous two CPF iteration results with (3.184).

$$\Delta s_{\text{spec}} = \sum_{j=1}^{\text{n}} (x_{\text{cor},j}^{i-1} - x_{\text{cor},j}^{i-2})^2 + (\lambda_{\text{cor}}^{i-1} - \lambda_{\text{cor}}^{i-2})^2 \tag{3.184}$$

Notice that Δs_{spec} also depends on the number of state variables n.

3.3.3 Improvement of step size variation

The step size h used in CPF Prediction, (3.180) and (3.181), can be varied to speed up the simulation. If the step size is larger, the CPF iteration number required to trace the whole PV curve will be smaller. However, if the step size is too large, the predicted state variables will be outside the convergence region of CPF Correction and CPF Correction may diverge. Therefore, it is important to select the step size appropriately.

A method is proposed to change the step size in in [72] and [53]. This method is based on the actual Newton-Raphson iterations, N_{Actual}^i, to solve the CPF correction equations shwon in (3.182). If N_{Actual}^i is larger, the step size is too big and the predicted state variable is far away from the correct value. The step size needs to be reduced. The equation of adjusting the step size is (3.185) [53].

$$\begin{cases} h_{i+1} = h_i[1 + \alpha(\frac{N_{\text{Desired}} - N_{\text{Actual}}^i}{N_{\text{Desired}} - N_{\text{Actual}}^i})] \\ h_{\min} \leq h_{i+1} \leq h_{\max} \end{cases} \tag{3.185}$$

where N_{Desired} is the desired number of iteration to solve the CPF correction shown in (3.182), $h_{\min}$ and $h_{\max}$ are the minimum and maximum step size, respectively.

However, the number of iterations required in CPF correction, N_{Actual}^i, does not have large enough change. This is because the Newton Raphson converges very fast. The difference of iteration required may be just one or two iterations. Therefore, the step size adjustment based on (3.185) may be very small.

Another way to adjust the step size, h, is proposed in this work. The key idea is shown in Fig.3.10. Between the previous two CPF iterations, the change of λ, $\Delta\lambda$, is calculated. If $\Delta\lambda$ is bigger than $\Delta\lambda_{\text{threshold,upper}}$, meaning that the curve is on the flat part of the PV curve, the step size is increased by Δh. That is,

$$h := h + \Delta h \quad \text{If } \Delta\lambda \geq \Delta\lambda_{\text{threshold,upper}} \tag{3.186}$$

If $\Delta\lambda$ is smaller than $\Delta\lambda_{\text{threshold,lower}}$, meaning that the curve is close to the knee point of the PV curve, the step size is reduced by Δh. That is,

$$h := h - \Delta h \quad \text{If } \Delta\lambda \geq \Delta\lambda_{\text{threshold,upper}} \tag{3.187}$$

If the change is between $\Delta\lambda_{\text{threshold,upper}}$ and $\Delta\lambda_{\text{threshold,lower}}$, the step size remains the same. Also h remains within the range of $h_{\max}$ and $h_{\min}$. Note that the value of Δh is predetermined. For different systems, the best Δh is different. In this work, $\Delta h = 0.01$.

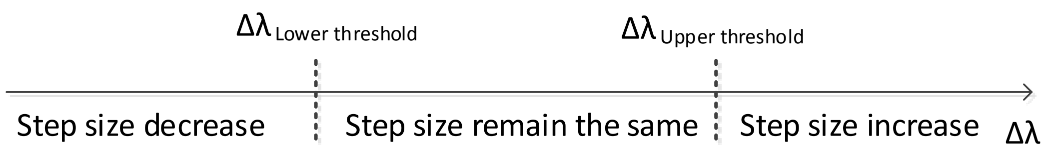

Figure 3.10: Proposed method to adjust the step size

Because the step size h and the specified arc length Δs are related, if h is changed, Δs should be changed accordingly. Assuming that in the previous two CPF iterations, the step size is h_{old} while at the current CPF iteration, the step size is h_{new} and the specified arc length is calculated as Δs_{old}. The adjust specified arc length of current CPF iteration with new step size should be

$$\Delta s_{\text{new}} = \Delta s_{\text{old}} \sqrt{\frac{h_{\text{new}}}{h_{\text{old}}}} \tag{3.188}$$

If we have no such adjustment, the change of h will have no effect.

3.3.4 CPF mathematical formulation

The purpose of the CPF method is to find the maximum loading factor, λ^*, of the system accurately. By using the continuation parameter and adding an extra equation (3.172), the Jacobian matrix remains nonsingular even when the system is close to the maximum loading point.

CPF is using an iterative method to trace the whole PV curve, as shown in Fig. 3.9. At each CPF iteration, CPF prediction and CPF correction are performed. CPF prediction is achieved by using the tangent method or the secant method, shown in (3.180) and (3.181), respectively. CPF correction is achieved by solving (3.182). The equations solved for each iteration include two types of equation. The first is the power flow equations. For PQ buses, the power flow equations are (3.160) and (3.161). For PV buses, the power flow equations are (3.164) and (3.165). The second is (3.177), which is related to the continuation parameter.

We denote the maximum loading factor as λ^*. At this maximum loading factor, the maximum total real power, $\sum P^*$, can be found as (3.189).

$$\sum P^* = \sum_{k=1}^{N-1} \sum_{s=a,b,c} \left[P^s_{\text{base},k} + \lambda^* \cdot \text{PLID}(k,s) \right] \tag{3.189}$$

The reason why the summation is from 1 to N-1 is that the bus N is the slack bus. The load at bus k phase s at the maximum loading factor is $P^s_{\text{base},k} + \lambda^* \cdot \text{PLID}(k,s)$.

Notice that CPF method not only provides the maximum loading point, λ^*, and the corresponding state variables, $\mathbf{V}^*$, θ^*, it also traces the whole PV curve. In other words, CPF method calculates $\mathbf{V}$, θ for any loading factor λ that is smaller than λ^*.

3.4 Verification of three-phase CPF with MatPower results

To verify the proposed CPF program, the simulation results were compared with the Matpower program [65], which has the CPF function. However, because Matpower can only model single-phase balanced systems, the IEEE 13 node test feeder was modified so that the test feeder is balanced and has a DG connected.

Fig. 3.11 shows the one-line diagram of the 13 Bus system. This 13 bus system was modified from the one described in [73]. All buses were modified as three-phase and all the loads were three-phase. All lines were transposed and of the same line configuration. The line impedance matrix used for all lines is given in (3.190). The load information is shown in Table 3.2.

$$\mathbf{Z} = \begin{bmatrix} 0.347+1.018i & 0.1560+0.502i & 0.1560+0.502i \\ 0.1560+0.502i & 0.347+1.018i & 0.1560+0.502i \\ 0.1560+0.502i & 0.1560+0.502i & 0.347+1.018i \end{bmatrix} \quad \Omega/\text{mile} \tag{3.190}$$

In the following sections, we will first show how we converted a three-phase balanced system into a single-phase system. Then we will compare the results of three-phase power flow and CPF from our proposed program and that from Matpower.

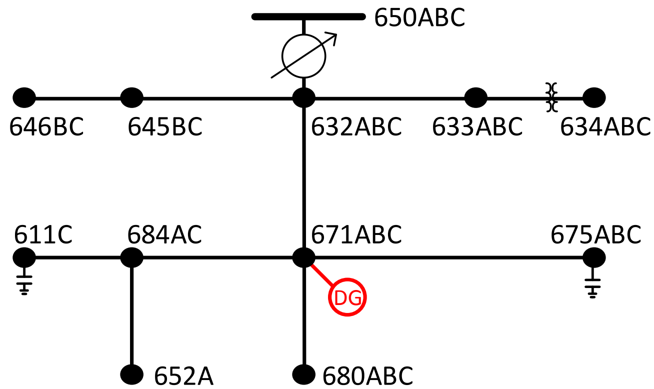

Figure 3.11: Modified IEEE 13-node test feeder with DG [73]

Table 3.2: Balanced loads for the IEEE 13-node test feeder

Node	Load Model	Ph-1 kW	Ph-1 kVAr	Ph-2 kW	Ph-2 kVAr	Ph-3 kW	Ph-3 kVAr
645	Y-PQ	170	125	170	125	170	125
671	Y-PQ	385	220	385	220	385	220
634	Y-PQ	160	110	160	110	160	110
646	Y-PQ	230	132	230	132	230	132
652	Y-PQ	128	86	128	86	128	86
611	Y-PQ	170	80	170	80	170	80
675	Y-PQ	485	190	485	190	485	190

3.4.1 Conversion from three-phase to single-phase systems

Because Matpower can only model single-phase balanced systems, the IEEE 13 node test feeder was modified so that the test feeder is balanced and has a DG connected. To convert the three-phase balanced system into single phase, we need to convert the three-phase impedance matrix into one-phase impedance matrix. We have to find the relationship between three-phase impedance matrix and single-phase impedance matrix [67].

In a balanced system, zero sequence current is zero: $\vec{I}_a + \vec{I}_b + \vec{I}_c = 0$. The relationship between voltage drop and current is:

$$\begin{bmatrix} \vec{V}_1^a - \vec{V}_2^a \\ \\ \vec{V}_1^b - \vec{V}_2^b \\ \\ \vec{V}_1^c - \vec{V}_2^c \end{bmatrix} = \begin{bmatrix} \vec{Z}_s & \vec{Z}_m & \vec{Z}_m \\ \\ \vec{Z}_m & \vec{Z}_s & \vec{Z}_m \\ \\ \vec{Z}_m & \vec{Z}_m & \vec{Z}_s \end{bmatrix} \begin{bmatrix} \vec{I}_a \\ \\ \vec{I}_b \\ \\ \vec{I}_c \end{bmatrix} \tag{3.191}$$

where $\vec{V}_k^s$ is the voltage phasor at Bus k phase s, $\vec{Z}_s$ is the self impedance, $\vec{Z}_m$ is the mutal impedance, and $\vec{I}_k^s$ is the current phasor at Bus k phase s.

Therefore, we can express the voltage drop in each phase as:

$$\vec{V}_1^a - \vec{V}_2^a = \vec{Z}_s\vec{I}_a + \vec{Z}_m(\vec{I}_b + \vec{I}_c) = (\vec{Z}_s - \vec{Z}_m)\vec{I}_a \tag{3.192}$$

$$\vec{V}_1^b - \vec{V}_2^b = \vec{Z}_s\vec{I}_b + \vec{Z}_m(\vec{I}_a + \vec{I}_c) = (\vec{Z}_s - \vec{Z}_m)\vec{I}_b \tag{3.193}$$

$$\vec{V}_1^c - \vec{V}_2^c = \vec{Z}_s\vec{I}_c + \vec{Z}_m(\vec{I}_a + \vec{I}_b) = (\vec{Z}_s - \vec{Z}_m)\vec{I}_c \tag{3.194}$$

To find the impedance, $\vec{Z}_{s,single}$, for the single-phase power flow , we can have:

$$\vec{Z}_{s,single} = \vec{Z}_{s,three-phase} - \vec{Z}_{m,three-phase} \tag{3.195}$$

where $\vec{Z}_{s,single}$ is the self impedance for single-phase power flow, $\vec{Z}_{s,three-phase}$ is the self impedance and $\vec{Z}_{m,three-phase}$ is the mutal impedance from the three-phase power flow. $\vec{Z}_{s,single}$ is going to be used in Matpower.

The relationship shown in (3.195) can also be derived by using the symmetrical component transformation. The relationship between The sequence impedance matrix $\mathbf{Z}_{012}$ and the phase impedance matrix $\mathbf{Z}_{abc}$ are related by (3.196).

$$\mathbf{Z}_{012} = \begin{bmatrix} \vec{Z}_0 & 0 & 0 \\ \\ 0 & \vec{Z}_1 & 0 \\ \\ 0 & 0 & \vec{Z}_2 \end{bmatrix} = \mathbf{A}^{-1}\mathbf{Z}_{abc}\mathbf{A} \tag{3.196}$$

where

$$\mathbf{A} = \begin{bmatrix} 1 & 1 & 1 \\ 1 & a^2 & a \\ a & a & a^2 \end{bmatrix}, \mathbf{Z}_{abc} = \begin{bmatrix} \vec{Z}_s & \vec{Z}_m & \vec{Z}_m \\ \vec{Z}_m & \vec{Z}_s & \vec{Z}_m \\ \vec{Z}_m & \vec{Z}_m & \vec{Z}_s \end{bmatrix} \tag{3.197}$$

Therefore,

$$\vec{Z}_0 = \vec{Z}_s + 2\vec{Z}_m \tag{3.198}$$

$$\vec{Z}_1 = \vec{Z}_2 = \vec{Z}_s - \vec{Z}_m \tag{3.199}$$

The single-phase power flow program, Matpower, will use $\vec{Z}_1$, the positive sequence impedance, as the impedance value of the line. Note that the system is a perfectly balanced system.

3.4.2 Power flow result comparison

Three case studies were made: no DG, DG in PV mode, and DG in PQ mode. The operating point was at the base operating point. The power flow solution results from the CPF program were compared with the result from Matpower. The error was calculated by (3.200).

$$Error = 100 \times \frac{Result_{\text{CPFprogram}} - Result_{\text{Matpower}}}{Result_{\text{Matpower}}} \tag{3.200}$$

The first case study did not have any DG. The comparison results of voltage and branch flow are shown in Table 3.3 and 3.4. It can be found that the error was quite small. The largest error for voltage was 0.0008% while the larger error for branch flow was 0.0003%. Therefore, the power flow results from the CPF program were quite accurate.

In the second case, a three-phase DG in PV mode was connected at Bus 671. The

Table 3.3: Bus voltage comparison of 13 bus without DG

Bus	$|V|$ [pu]			Angle [rad]		
	Matpower	CPF	Error	Matpower	CPF	Error
632	0.9384	0.9384	-0.0001	-2.8540	-2.8540	0.0006
633	0.9368	0.9368	-0.0001	-2.9199	-2.9199	0.0006
645	0.9347	0.9347	-0.0001	-3.0227	-3.0227	0.0006
671	0.8995	0.8995	-0.0001	-5.0505	-5.0505	0.0007
634	0.9353	0.9353	-0.0001	-2.9859	-2.9859	0.0006
646	0.9335	0.9335	-0.0001	-3.0832	-3.0831	0.0006
684	0.8980	0.8980	-0.0001	-5.1358	-5.1358	0.0007
680	0.8995	0.8995	-0.0001	-5.0505	-5.0505	0.0007
652	0.8959	0.8959	-0.0001	-5.2286	-5.2286	0.0008
611	0.8971	0.8971	-0.0001	-5.1866	-5.1865	0.0008
675	0.8960	0.8960	-0.0001	-5.3002	-5.3002	0.0008
650	1.0000	1.0000	0.0000	0.0000	0.0000	0

Table 3.4: Branch power flow comparison of 13 bus without DG

From Bus	To Bus	P [pu]			Q [pu]		
		Matpower	CPF	Error	Matpower	CPF	Error
650	632	1.8161	1.8161	0.0001	1.1809	1.1809	0.0003
632	633	0.1603	0.1603	0.0001	0.1107	0.1107	0.0000
633	634	0.1601	0.1601	0.0001	0.1104	0.1104	0.0000
632	645	0.4010	0.4010	0.0001	0.2596	0.2596	0.0000
645	646	0.2302	0.2302	0.0001	0.1324	0.1324	0.0000
632	671	1.1960	1.1960	0.0002	0.6516	0.6516	0.0002
671	675	0.4861	0.4861	0.0002	0.1929	0.1929	-0.0001
671	684	0.2985	0.2985	0.0002	0.1674	0.1674	-0.0001
684	611	0.1701	0.1701	0.0002	0.0802	0.0802	-0.0001
684	652	0.1281	0.1281	0.0002	0.0864	0.0864	0.0000

reactive power limit was large enough so that the DG was in PV mode for the base operating point. In this particular case, the DG in PV mode only generated reactive power. No real power was generated. This DG adjusted its reactive power output such that the voltage at Bus 671 was regulated at 1 pu. Note that the load is at the base operating point. The comparison results of voltage and branch flow are shown in Table 3.5 and 3.6. It can be found that the error was quite small. The largest error for voltage was 0.0006% while the larger error for branch flow was 0.00021%. Therefore, the power flow result from the CPF program when there is a DG in PV mode was quite accurate.

Table 3.5: Bus voltage comparison of 13 bus with DG in PV mode

Bus	$\|V\|$ [pu]			Angle [rad]		
	Matpower	CPF	Error	Matpower	CPF	Error
632	0.98841	0.98841	-0.00001	-3.72262	-3.72260	0.00060
633	0.98695	0.98695	-0.00001	-3.78197	-3.78195	0.00060
645	0.98492	0.98492	-0.00001	-3.87462	-3.87459	0.00060
671	1.00000	1.00000	0.00000	-6.61076	-6.61072	0.00060
634	0.98550	0.98550	-0.00001	-3.84149	-3.84147	0.00060
646	0.98379	0.98380	-0.00001	-3.92905	-3.92903	0.00060
684	0.99859	0.99859	0.00000	-6.67974	-6.67970	0.00060
680	1.00000	1.00000	0.00000	-6.61076	-6.61072	0.00060
652	0.99678	0.99678	0.00000	-6.75477	-6.75473	0.00060
611	0.99786	0.99786	0.00000	-6.72077	-6.72073	0.00060
675	0.99685	0.99685	0.00000	-6.81265	-6.81261	0.00060
650	1.00000	1.00000	0.00000	0.00000	0.00000	0.00000

Table 3.6: Branch power flow comparison of 13 bus with DG in PV mode

From Bus	To Bus	P [pu]			Q [pu]		
		Matpower	CPF	Error	Matpower	CPF	Error
650	632	1.79716	1.79716	0.00002	-0.26156	-0.26156	-0.00021
632	633	0.16024	0.16024	0.00000	0.11066	0.11066	0.00000
633	634	0.16012	0.16012	0.00000	0.11033	0.11033	0.00000
632	645	0.40087	0.40087	0.00000	0.25935	0.25935	0.00001
645	646	0.23014	0.23014	0.00000	0.13237	0.13237	0.00000
632	671	1.19468	1.19468	0.00001	-0.74332	-0.74332	0.00002
671	675	0.48586	0.48586	0.00000	0.19231	0.19231	0.00001
671	684	0.29841	0.29841	0.00000	0.16710	0.16710	0.00000
684	611	0.17007	0.17007	0.00000	0.08018	0.08018	0.00000
684	652	0.12812	0.12812	0.00000	0.08632	0.08632	0.00000

In the third case, a three-phase DG in PQ mode was connected at Bus 671. The DG injected 100 kVar reactive power while injected 0 kW real power. The comparison results of voltage and branch flow are shown in Tables 3.7 and 3.8. It can be found that the error was quite small. The largest error for voltage was 0.00008% while the larger error for branch flow was 0.00025%. Therefore, the power flow result from the CPF program when there was a DG in PQ mode was quite accurate.

Table 3.7: Bus voltage comparison of 13 bus with DG in PQ mode

Bus	$\lvert V \rvert$ [pu]			Angle [rad]		
	Matpower	CPF	Error	Matpower	CPF	Error
632	0.94240	0.94241	-0.00005	-2.91814	-2.91813	0.00063
633	0.94088	0.94088	-0.00005	-2.98343	-2.98342	0.00063
645	0.93874	0.93874	-0.00005	-3.08540	-3.08538	0.00064
671	0.90759	0.90759	-0.00008	-5.16988	-5.16984	0.00071
634	0.93935	0.93935	-0.00005	-3.04894	-3.04892	0.00064
646	0.93756	0.93756	-0.00005	-3.14533	-3.14531	0.00064
684	0.90603	0.90604	-0.00008	-5.25365	-5.25361	0.00071
680	0.90759	0.90759	-0.00008	-5.16988	-5.16984	0.00071
652	0.90403	0.90403	-0.00008	-5.34482	-5.34478	0.00072
611	0.90523	0.90523	-0.00008	-5.30349	-5.30346	0.00071
675	0.90412	0.90412	-0.00008	-5.41514	-5.41510	0.00072
650	1.00000	1.00000	0.00000	0.00000	0.00000	0.00000

Table 3.8: Branch power flow comparison of 13 bus with DG in PQ mode

From Bus	To Bus	P [pu]			Q [pu]		
		Matpower	CPF	Error	Matpower	CPF	Error
650	632	1.81045	1.81045	0.00006	1.06575	1.06574	0.00025
632	633	0.16027	0.16027	0.00004	0.11072	0.11072	0.00000
633	634	0.16013	0.16013	0.00004	0.11036	0.11036	0.00000
632	645	0.40096	0.40096	0.00004	0.25958	0.25958	0.00000
645	646	0.23015	0.23015	0.00004	0.13241	0.13241	-0.00001
632	671	1.19387	1.19387	0.00012	0.54589	0.54589	0.00016
671	675	0.48604	0.48604	0.00017	0.19281	0.19281	-0.00006
671	684	0.29849	0.29849	0.00015	0.16734	0.16734	-0.00003
684	611	0.17008	0.17008	0.00016	0.08022	0.08022	-0.00006
684	652	0.12815	0.12815	0.00015	0.08639	0.08639	-0.00003

3.4.3 CPF results comparison

We performed several case studies for the CPF results comparison: No DG, DG in PV mode, DG in PQ mode, and different load increase directions. It can be found that the differences of the maximum loading factor λ_{max} between Matpower and the program were very small.

The first case did not have any DG. The comparison results are shown in Table 3.9. λ_{max} error was about 0.24 %. Because λ_{max} was not exactly the same, the node voltage at this maximum operating point from the CPF program and Matpower had relative larger difference; the maximum error is about 3.52%. Especially the downstream node, such as Bus 675, Bus 611, and Bus 652, had higher error than the upstream node, such as Bus 632 and Bus 671. Notice that this difference between voltages were not the error of the program. This difference came from the fact that λ_{max} from the program and the Matpower were slightly different.

Table 3.9: 13 bus CPF comparison with No DG

	Matpower	CPF	Error
V632	0.7016	0.7108	-1.3222
V633	0.6963	0.7056	-1.3415
V645	0.6888	0.6982	-1.3695
V671	0.5036	0.5202	-3.2890
V634	0.6910	0.7004	-1.3609
V646	0.6847	0.6942	-1.3851
V684	0.4963	0.5131	-3.3867
V680	0.5036	0.5202	-3.2890
V652	0.4868	0.5039	-3.5163
V611	0.4925	0.5094	-3.4369
V675	0.4870	0.5041	-3.5164
V650	1.0000	1.0000	0.0000
λ_{max}	1.5328	1.5365	-0.2395

In the second case, there was one DG in PV mode connected at Bus 671. The reactive power limit of the DG was 60 MVar. The reactive power was adjusted so that the voltage at Bus 671 was regulated at 1 pu. No real power was generated by this DG. The comparison results are shown in Table 3.10. The error for λ_{max} was about 0.0022 % and the maximum error for the voltage was 0.4155%. Therefore, the CPF results were almost the same as Matpower results.

The third case had one DG in PQ mode connected at Bus 671. The reactive power output of the DG was 100 Kvar while no real power was generated by this DG. The comparison results are shown in Table 3.11. The error for λ_{max} was about 0.0021 % and the maximum error for the voltage was 0.3257%. Therefore, the CPF results were almost the same as Matpower results.

Table 3.10: 13 bus CPF comparison with DG in PV

	Matpower	CPF	Error
V632	0.7669	0.7698	-0.3780
V633	0.7562	0.7591	-0.3892
V645	0.7408	0.7438	-0.4061
V671	1.0000	1.0000	0.0000
V634	0.7455	0.7485	-0.4005
V646	0.7324	0.7355	-0.4155
V684	0.9921	0.9921	0.0000
V680	1.0000	1.0000	0.0000
V652	0.9819	0.9819	0.0000
V611	0.9880	0.9880	0.0000
V675	0.9822	0.9822	0.0000
V650	1.0000	1.0000	0.0000
$\lambda_{\max}$	4.5292	4.5293	-0.0022

Table 3.11: 13 bus CPF comparison with DG in PQ

	Matpower	CPF	Error
V632	0.7123	0.7114	0.1278
V633	0.7070	0.7060	0.1297
V645	0.6995	0.6985	0.1326
V671	0.5258	0.5242	0.3052
V634	0.7017	0.7008	0.1317
V646	0.6954	0.6944	0.1342
V684	0.5186	0.5170	0.3140
V680	0.5258	0.5242	0.3052
V652	0.5094	0.5078	0.3257
V611	0.5150	0.5133	0.3186
V675	0.5096	0.5080	0.3257
V650	1.0000	1.0000	0.0000
$\lambda_{\max}$	1.5854	1.5854	0.0021

3.5 IEEE 13-node test feeder case studies

In this section, the modified IEEE 13-node test feeder with DG described in [73] was used. This test feeder had different line configurations for each branch, each bus could be single, two or three phase node and the loads were unbalanced. The detailed information can be found in [73].

The improved and implemented three-phase CPF method with arc parameterization was used to compute the PV curves and investigate the maximum loadability of this modified IEEE 13-node test feeder with DG. In the PV curve, the x-axis is the loading factor λ while the y-axis is the voltage of the bus. From the PV curve, the maximum loading factor, λ_{max}, can be found and the impact of several factors on λ_{max} were investigated.

There are many ways to increase the loads in the system: the load at all buses can be increased at the same time with the loading factor λ, or only the loads at certain sets of buses or at one specific bus can be increased. λ_{max} depends on how the load is increased. λ_{max} for one way of increasing load cannot be directly compared with that for other ways. However, by comparing λ_{max} of different cases where the loads are increased in the same way, the impact of several factors on voltage stability can be investigated.

Table 3.12 shows different ways the loads were increased and the resulting λ_{max}. In this case, no DG was connected in the system. The loads that were not increased in the CPF remained constant. From the results it can be seen that λ_{max} was minimum when the loads in the system were increased simultaneously. If only load at a certain bus was increased, λ_{max} was larger. However, there is no clear pattern about the relationship between λ_{max}

and the bus where the loads were increased.

Table 3.12: Maximum loading factor for different ways of increasing the loads

Description	λ_{max}
All loads increased at same loading factor	1.0761
Only load at Bus 611 increased	6.0655
Only load at Bus 634 increased	4.7693
Only load at Bus 645 increased	10.4208
Only load at Bus 646 increased	7.2864
Only load at Bus 652 increased	6.1697
Only load at Bus 671 increased	3.4462
Only load at Bus 675 increased	2.5316

Next, the impact of the type of load model on λ_{max} was investigated. The load model at a specified bus was varied while the load model of the other buses remained the same. The loads whose models were not changed were kept constant while the load whose model was changed to the specified type was increased with the loading factor λ in CPF. Table 3.13 shows the λ_{max} for each load model. The column shows the corresponding maximum loading factor of the cases where the model of the specified bus was changed into three different load models. From the results, it can be seen that when the load was modeled as constant power load, λ_{max} was the smallest. When the load was modeled as constant impedance load, λ_{max} was the largest. This is because if the voltage across the constant power load decreased, the current flowing into the load increased. Higher current would have higher reactive power loss, resulting in lower λ_{max}. Therefore, constant power load models are the worst case scenario for voltage stability studies.

Next, the impact of unbalance on λ_{max} was also investigated. The unbalance degree φ at Bus 671 was varied, where the phase B load was $\varphi\%$ less than the phase A load, and

Table 3.13: $\lambda_{\max}$ for different load models

	Bus Number					
Load Model	634	646	652	671	675	611
Constant PQ	6.3	18.85	8.75	5.5	4.53	8.05
Constant Z	13.39	27.31	17.09	10.2	6.19	22.1
Constant I	10.81	25.92	16.21	7.3	5.94	15.49

the phase C load was φ% more than the phase A load. The phase A load of this specified bus and the load at other buses were specified in [73]. In this case study, all the loads were increased at the same time in CPF. Table 3.14 shows the $\lambda_{\max}$ for each scenario. $\lambda_{\max}$ was different for different unbalanced degree φ at Bus 671. Also, the results show that if the load at Bus 671 is more unbalanced, the corresponding $\lambda_{\max}$ is smaller. However, this conclusion may not be accurate because the degree of unbalance for the overall system may become less if the load at the 671 is more unbalanced.

Table 3.14: Unbalanced degree at 671

Description (unbalance degree:φ)	$\lambda_{\max}$
671 was balanced	1.0761
671 was 10% unbalanced locally	1.0676
671 was 20% unbalanced locally	1.0596
671 was 30% unbalanced locally	1.0523
671 was 40% unbalanced locally	1.0454

The impact of DG in PQ mode on $\lambda_{\max}$ was investigated next. A three-phase DG was connected at either Bus 671 or Bus 675. In both cases, DG generated different amounts of real power and reactive power. The amounts of real and reactive power are specified in Table 3.15 and Table 3.16, respectively. In these case studies, all the loads were increased at the same loading factor, λ, in CPF. Table 3.15 and Table 3.16 show that when the DG generated higher amount of real power, $\lambda_{\max}$ was increased.

Table 3.15: DG in PQ mode at 671

Description	$\lambda_{\max}$
DG in PQ at 671 (P_g = 50 kW, Q_g = 10 kVar)	1.107
DG in PQ at 671 (P_g = 100 kW, Q_g = 20 kVar)	1.1369
DG in PQ at 671 (P_g = 150 kW , Q_g = 30 kVar)	1.1677
DG in PQ at 671 (P_g = 200 kW, Q_g = 40 kVar)	1.1978

Table 3.16: DG in PQ mode at 675

Description	$\lambda_{\max}$
DG in PQ at 675 (P_g = 50 kW, Q_g = 10 kVar)	1.1109
DG in PQ at 675 (P_g = 100 kW, Q_g = 20 kVar)	1.1451
DG in PQ at 675 (P_g = 150 kW, Q_g = 30 kVar)	1.1791
DG in PQ at 675 (P_g = 200 kW, Q_g = 40 kVar)	1.2137

Next the impact of DG in PV mode was investigated. DG in PV mode was connected at 671 or 675. Table 3.17 and Table 3.18 show the impacts of different reactive power limits on $\lambda_{\max}$ for DG in PV mode. In this case study, all the loads were increased at the same loading factor, λ, in CPF. In these two cases, it can be found that when the reactive power limit was increased, $\lambda_{\max}$ was increased. This is because the DG could provide more reactive power support for the system. When reactive power limit was 20 MVar and 30 MVar, the corresponding $\lambda_{\max}$ was the same. This is because in both cases, the DG in PV mode did not hit its reactive power limit.

Table 3.17: DG in PV mode at 671

Q limit of DG	P_g	Q_g	Hitting Q limit?	$\lambda_{\max}$
5 Mvar	0	5 Mvar	Y	1.9247
10 Mvar	0	10 Mvar	Y	2.6042
20 Mvar	0	16.73 Mvar	N	3.6262
30 Mvar	0	16.73 Mvar	N	3.6262

Table 3.18: DG in PV mode at 675

Q limit of DG	P_g	Q_g	Hitting Q limit?	$\lambda_{\max}$
5 Mvar	0	5 Mvar	Y	1.9118
10 Mvar	0	10 Mvar	Y	2.5081
20 Mvar	0	14.32 Mvar	N	3.0792
30 Mvar	0	14.32 Mvar	N	3.0792

The impact of different step sizes k used in arc-parameterization CPF was investigated. In this case study, all the loads were increased at the same loading factor, λ, in CPF. The step size k was adjusted to different values. From Table 3.19, the following observations can be made. When k was too large, the program failed to converge, because the predicted value was already outside the region of convergence of CPF correction. When k was too small, the program was trapped in one local solution, not able to trace the whole PV curve. This is because with a very small step size, the change of predicted value was very close to the original value. The CPF correction would bring this predicted value back to the corrected value of the previous CPF iteration. When k was between 0.02 to 0.5, the CPF program was able to trace the whole PV curve and find the $\lambda_{\max}$. Within this range, smaller k yielded larger $\lambda_{\max}$, because smaller step size allowed the program to trace the knee point of the PV curve more precisely.

Table 3.19: Impact of different step sizes of CPF

Step size k	$\lambda_{\max}$
0.8	Failure (Divergence)
0.5	1.0575
0.2	1.0729
0.1	1.0755
0.04	1.0761
0.03	1.0762
0.02	1.0762
0.01	Failure (trapped at a single solution)
0.005	Failure (trapped at a single solution)

3.6 Summary

In this section, the theory and the implementation of a modified three-phase CPF using arc length parameterization were described in detail. The model of various components, including DG in PQ and PV mode with reactive power limit, was presented. Improvements to an existing three-phase CPF algorithm were presented. Two improves are the calculation of specified arc length and the step size variation. Matpower program results were used to verify the CPF program result. The results of these two programs were fairly consistent. Some case studies were performed to investigate the impact of different factors, such as load model and degree of unbalance, on the maximum loadability result. In the next section, a new voltage analysis method is presented which uses the CPF algorithm to determine the weak buses of an unbalanced distribution system with DGs.

4 NEW VOLTAGE STABILITY ANALYSIS METHOD: CPF SCAN

4.1 Introduction

The modified CPF method discussed in the previous section can find the maximum loading point very accurately. The maximum loading point is system-wide information. However, system-wide information cannot determine which buses are weak. The purpose of the section is to discuss a new method, called CPF scan method, which uses the CPF method to identify the weak buses of an unbalanced distribution system with DGs.

In the literature, the sensitivity methods, such as dV/dQ [32] and dQg/dQ [47], are widely use to identify the weak buses. However, these methods cannot identify the weak buses accurately for three reasons. Firstly, these methods only investigate linear phenomena. For example, one of the sensitivity methods, dV/dQ, investigates the incremental change of voltage given the incremental change of reactive power injection, which is related to linear phenomena. However, voltage stability problems involve nonlinear phenomena [7]. For example, the maximum loading point is related to the saddle node bifurcation, which is a nonlinear phenomenon. More detailed description of saddle node bifurcation is discussed in Section 2.4.1. Therefore, these methods that only investigate linear phenomena cannot analyze voltage stability problem accurately. Secondly, if these sensitivity methods are applied at the maximum loading point of a system, the result would be inaccurate, because at this operating point, the Jacobian matrix is close to being singular. Any calculation based on the inverse of this Jacobian matrix is numerically unstable. Lastly, these methods only investigate the voltage stability problem at a specific operating point. As a result, they do not consider the impact of 1) load increase direction (LID) and 2) DG transition from PV to PQ mode, which play an important role in the mechanism of voltage stability. Because of these three reasons, the sensitivity type of analysis cannot identify the weak buses very accurately.

On the other hand, the three-phase CPF [53] was used to find the weak buses. The authors in [53] identify the weak buses as the buses with the lowest voltage magnitude at the maximum loading point. However, voltage magnitude alone is not a good indicator for voltage stability [7]. Generally speaking, for highly reactive power compensated bus, even if the bus is weak bus, the voltage magnitude can be of nominal value [8].

To identify the weak buses of a system more accurately, a new method, called CPF scan method, is proposed in this work. The CPF scan method addresses the problems mentioned earlier. It is based on the CPF method which investigates nonlinear phenomenon. Moreover, it avoids the singularity issues of the Jacobian matrix and considers the impact of LID and DG transition from PV to PQ mode.

In the following sections, the motivation behind the CPF scan method are explained. Then the application of the CPF scan method to single-phase transmission systems and three-phase distribution systems is described. Furthermore, the properties of the CPF scan method are discussed. Moreover, a comparison with one similar method proposed in [55] is made. Lastly, case studies on an 8-bus, the case studies on the modified IEEE 13-node test feeder with DG, and the application of CPF scan method to planning and operation of distribution systems are presented.

4.2 Motivations behind CPF scan

The motivations behind the CPF scan method come from the observation of weak buses. There are many definitions of weak buses as discussed in section 2. For example, the weakest bus has been defined as the bus with the highest value of dQg/dQ [47], the bus with the highest value of dV/dQ [32], the bus that corresponds to the largest element in the tangent vector of CPF [49], and the bus/phase that has the largest voltage drop at the maximum loading point [53]. In this work, we propose a new definition of the weak bus. The weak buses are the buses that have high impact on the maximum loading factor, λ^*, and on the maximum total real power , $\sum P^*$ that a system can have. A similar concept was proposed in [74]. λ^* and $\sum P^*$ are important for the system operation. Voltage stability margin can be defined as the difference between the current loading factor λ and λ^* , or as the difference between the current total real power, $\sum P$, and $\sum P^*$ [75]. It is desirable to have higher λ^* and $\sum P^*$ so that the system can have higher voltage stability margin. If the voltage stability margin is too small, the system is close to voltage collapse point. Therefore, it is important to know which buses have high impact on λ^* and $\sum P^*$.

Based on the proposed definition of weak buses, three factors can influence the location of weak buses in the system: network characteristics, base operating point, and load increase direction (LID). We will use a simple 3-bus transmission system, shown in Fig.4.1, to illustrate these three factors. In this system, a voltage source is connected at

Bus 0 and the voltage is V_0. The loads at Bus 1 and Bus 2 are P_1 and P_2, respectively. The length of branch 1, which is between Bus 0 and Bus 1, is shorter than the length of branch 2, which is between Bus 0 and Bus 2.

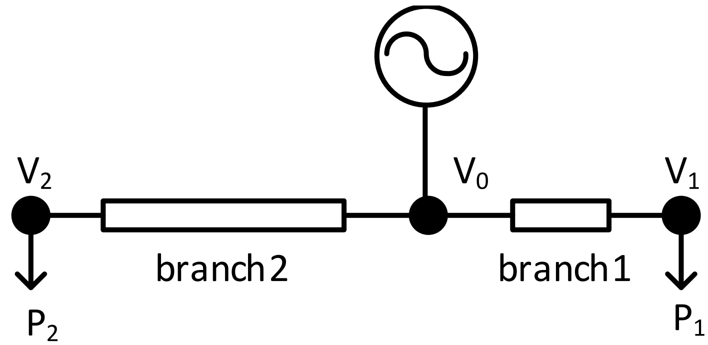

Figure 4.1: One line diagram for a 3-bus single-phase system

All the saddle node bifurcation points compose the SNB surface in the parameter space of the system [76]. Suppose that the SNB surface of the system is known, which is shown in Fig. 4.2. Even thought the shape of the SNB surface is simple, in reality the shape of the SNB surface is extremely complicated [77]. The simple shape of the SNB surface is only for explanation purposes.

Fig. 4.2 shows the hypothetical SNB surface of this simple 3-bus transmission system. The X-axis represents the load at Bus 1, P_1, while the Y-axis represents the load at Bus 2, P_2. The physical meaning of the SNB surface are as follows. The system can support any P_1 and P_2 that lie inside the SNB surface. The system will experience voltage collapse if P_1 or P_2 is outside the SNB surface [75].

Because branch 1 is shorter than branch 2 as shown in Fig. 4.1, the line impedance of branch 1 is smaller than that of branch 2, making P_{1max} larger than P_{2max}, as shown in

Fig. 4.2. Therefore, network characteristics, including the impedance of the lines and the network topology, influence the shape of the SNB surface.

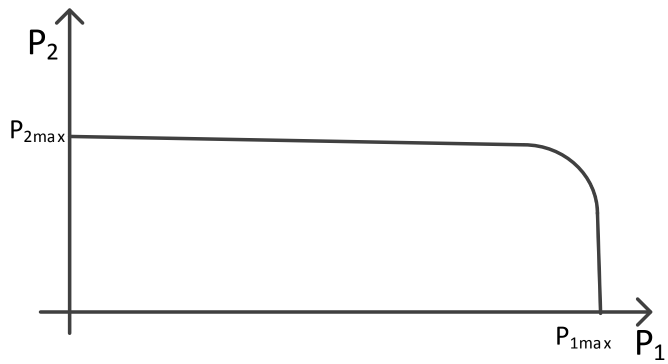

Figure 4.2: Hypothetical SNB surface of the system

In addition to the network characteristics, the base operating point also influences the locations of the weak buses. Fig.4.3 shows two base operating points, Op1 and Op2, with the same LID. For the base operating point Op1, the load at Bus 2 is much larger than the load at Bus 1. In this case, if Bus 2 is strengthened, meaning that the SNB surface is moved upward (red line), the resulting maximum loading factor is increased. Therefore, for Op1, Bus 2 limits the value of the maximum loading factor, which makes Bus 2 the weaker bus. On the other hand, for the base operating point Op2, the load at Bus 1 is much larger than the load at Bus 2. If Bus 1 is strengthened, meaning that the SNB surface is moved to the right side (blue line), the maximum loading factor is increased. Bus 1 limits the value of the maximum loading factor. Therefore, for base operating point Op2, even though branch1 is shorter than branch2, the weaker bus is Bus 1.

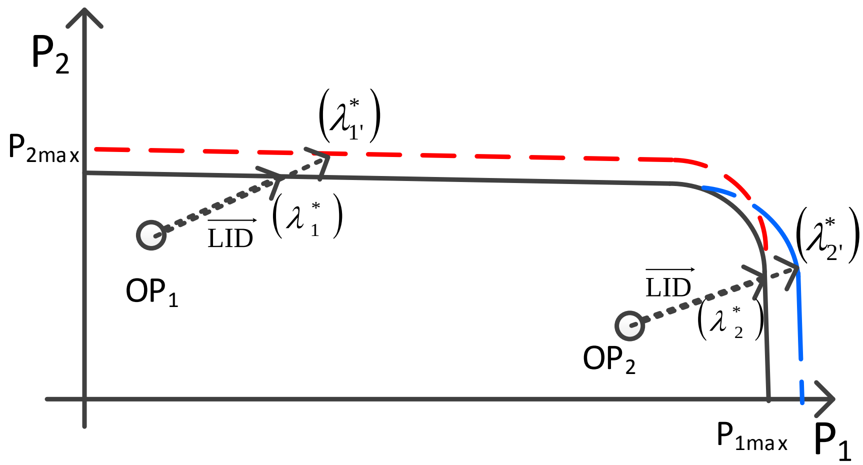

Figure 4.3: Different base operating points have different weak buses

In addition to network characteristics and base operating point, the load increase direction (LID) also influences the location of weak buses. As shown in Fig.4.4, the base operating point is $(P_{1,\text{base}}, P_{2,\text{base}})$ and there are two LIDs: LID_1 and LID_2. For different LIDs, the bus that limits how much the load can be increased is different. For LID_1, the original maximum loading factor is λ_1^*. If Bus 1 is strengthened, meaning that the SNB surface is expanded to the right, the corresponding maximum loading factor is increased to $\lambda_1^{*'}$ and the total load of the system can be increased. In this case, Bus 1 is the weaker bus. For LID_2, the original maximum loading factor is λ_2^*. If Bus 2 is strengthened, the corresponding maximum loading factor is increased to $\lambda_2^{*'}$ and the total load of the system can be increased. Therefore, in this case, Bus 2 is the weaker bus.

In conclusion, we can argue that the weak buses depend on three factors: the network characteristics, the base operating point and the load increase direction. Similar arguments can be applied in the three-phase unbalanced distribution systems. To consider

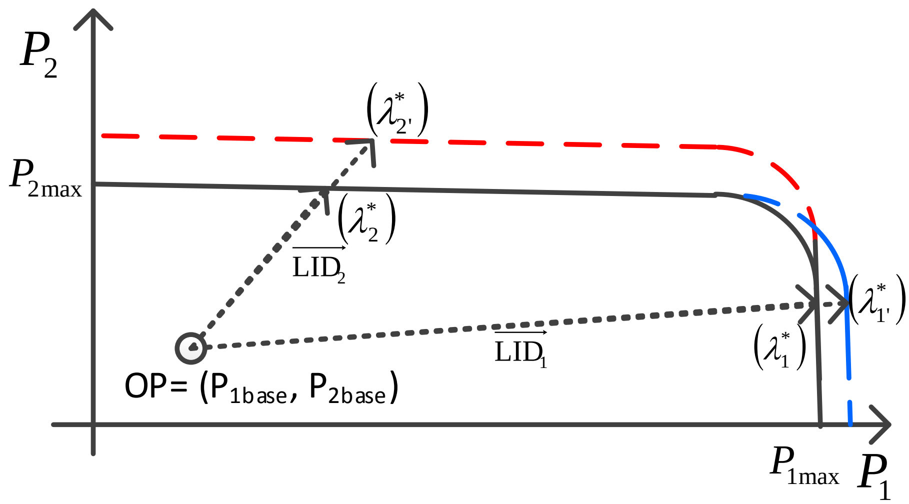

Figure 4.4: Limiting factors for different LIDs

simultaneously these three factors that influence the weak bus location, the CPF scan method is proposed.

4.3 Description of CPF scan method

To illustrate the CPF scan method, a single phase transmission system is used first. Then the illustration is extended to three-phase unbalanced distribution systems.

The CPF scan method needs the following three pieces of information: 1) network characteristics, 2) base operating point, $(\mathbf{P}_{\text{base}}, \mathbf{Q}_{\text{base}})$, and 3) load increase direction, $\overrightarrow{\mathrm{LID}}$, which can be determined using the load forecast information. The kth element of $\overrightarrow{\mathbf{LID}}$, $\mathbf{LID}(k)$, has two components: $\mathrm{PLID}(k)$ and $\mathrm{QLID}(k)$. The real and reactive power at bus k can be expressed as:

$$P_k = P_{\text{base},k} + \lambda \cdot \mathrm{PLID}(k) \tag{4.1}$$

$$Q_k = Q_{\text{base},k} + \lambda \cdot \mathrm{QLID}(k) \tag{4.2}$$

There are three steps in the CPF scan method. The first step is to find the maximum loading factor, λ^*, and the maximum total real power, $\sum P^*$, which is the summation of real power at all buses in the system, that is,

$$\sum P^* = \sum_{k=1}^{N} P_{\text{base},k} + \lambda^* \cdot \text{PLID}(k) \tag{4.3}$$

The maximum loading factor, λ^*, and the maximum total real power, $\sum P^*$, can be found by using the CPF method shown in Section 3.3.4.

The second step is to perturb $\overrightarrow{\text{LID}}$ along different buses. The motivation is that we are trying to identify the weak buses that have large impacts on the maximum loading factor and the maximum total real power. Therefore, each time $\overrightarrow{\text{LID}}$ is perturbed along one specific bus. After one specific bus is done, the perturbation is moved to another bus. The concept is similar to the one used in dQg/dQ [47], where the impact of the reactive power injection of a specific bus is calculated. In [47], the same amount of incremental change of reactive power is injected at different buses and the corresponding changes of the generated reactive power are calculated. The weaker buses are defined as the ones that have the higher changes of generated reactive power . The key idea is that the same amount of perturbation of injected reactive power is applied to different buses. The corresponding change in generated reactive power is used to identify the weak buses. Similarly, in this dissertation work, the same amount of perturbation along different buses are applied to $\overrightarrow{\text{LID}}$. The amount of perturbation needs to be selected carefully. As will be shown in Section 4.6.3, different amounts of perturbation will have different CPF scan results.

Denote the perturbation of $\overrightarrow{\mathbf{LID}}$ along bus k as $\overrightarrow{\mathbf{LID}_{(k)}}$. The meaning of perturbing

$\overrightarrow{\mathbf{LID}}$ along bus k can be define as follows. The ith element of the vector $\overrightarrow{\mathbf{LID}_{(k)}}$ is

$$\mathbf{LID}_{(k)}(i) = \begin{cases} \mathbf{LID}(i) - \Delta\mathbf{LID}(k) & \text{for } i = k \\ \\ \mathbf{LID}(i) & \text{otherwise} \end{cases} \tag{4.4}$$

where $\mathbf{LID}(i)$ is the ith element of the unperturbed $\overrightarrow{\mathbf{LID}}$. In (4.4), $\overrightarrow{\mathbf{LID}}$ is perturbed in a way that the LID element that corresponds to bus k is changed by $\Delta\mathbf{LID}(k)$, while the other LID elements remain the same.

With this perturbed LID along bus k, $\overrightarrow{\mathbf{LID}_{(k)}}$ and the base operating point, the CPF method is used to find the corresponding maximum loading factor $\lambda^*_{(k)}$ and the total real power $\sum P^*_{(k)}$ by using CPF method shown in Section 3.3.4. After solving $\lambda^*_{(k)}$ and $\sum P^*_{(k)}$, two differences are calculated. The first difference is the difference between λ^* and $\lambda^*_{(k)}$, denoted as $\Delta\lambda^*_{(k)}$ as shown in (4.5) The second difference is the difference between $\sum P^*$ and $\sum P^*_{(k)}$ and denoted as $\Delta \sum P^*_{(k)}$ as shown in (4.6).

$$\Delta\lambda^*_{(k)} = \lambda^*_{(k)} - \lambda^* \tag{4.5}$$

$$\Delta \sum P^*_{(k)} = \sum P^*_{(k)} - \sum P^* \tag{4.6}$$

This step is repeat to perturb the original LID along different buses so that the impact of the perturbation of LID along different buses can be found.

In the third step, the buses are ranked based on the absolute values of $\Delta\lambda^*_{(k)}$ and $\Delta \sum P^*_{(k)}$ at each bus. The larger the absolute value of $\Delta\lambda^*_{(k)}$ and $\Delta \sum P^*_{(k)}$, the weaker the corresponding bus. The physical meaning of the weak bus is that the weak buses have a high impact on the maximum loading factor, λ^*, or on the maximum total real power, $\sum P^*$, that the system can support. In other words, for the same amount of LID perturbation, the perturbation direction that is along the weak bus results in larger change of the maximum loading factor or larger change of the maximum total real power.

4.3.1 Extension to three-phase unbalanced distribution systems

The CPF scan method can be extended from single-phase transmission systems into three-phase unbalanced distribution systems. The idea is the same. The input of CPF scan method is the base operating point($\mathbf{P}_{\text{base}}$, $\mathbf{Q}_{\text{base}}$) and LID, $\overrightarrow{\mathbf{LID}}$. The element of $\overrightarrow{\mathbf{LID}}$ corresponding to bus kth in phase s, $\mathbf{LID}(k,s)$, has two components: $\text{PLID}(k,s)$ and $\text{QLID}(k,s)$. The real and reactive power at bus k in phase s can be expressed as:

$$P_k^s = P_{\text{base},k}^s + \lambda \cdot \text{PLID}(k,s) \tag{4.7}$$

$$Q_k^s = Q_{\text{base},k}^s + \lambda \cdot \text{QLID}(k,s) \tag{4.8}$$

There are also three steps in the CPF scan method. The first step is to find the maximum loading factor, λ^*, and the maximum total real power, $\sum P^*$ for the given $\overrightarrow{\mathbf{LID}}$. They can be found by using the CPF method shown in Section 3.3.4.

The second step in the CPF scan method is to perturb the original LID along different buses and phases. Suppose we perturb $\overrightarrow{\mathbf{LID}}$ along the direction of bus k in phase s and denote this perturbed LID as $\overrightarrow{\mathbf{LID}_{(k,s)}}$. The ith element in phase t of the vector $\overrightarrow{\mathbf{LID}_{(k)}}$ can be expressed as:

$$\mathbf{LID}_{(k,s)}(i,t) = \begin{cases} \mathbf{LID}(i,t) - \Delta\mathbf{LID}(k,s) & \text{for } i = k, t = s \\ \mathbf{LID}(i,t) & \text{otherwise} \end{cases} \tag{4.9}$$

where $\mathbf{LID}(i,t)$ is the ith element in phase t of the unperturbed $\overrightarrow{\mathbf{LID}}$. In (4.9), $\overrightarrow{\mathbf{LID}}$ is perturbed in a way that the LID element that corresponds to bus k in phase s is changed by $\Delta\mathbf{LID}(k,s)$, while the rest of the LID element of remains the same.

With this perturbed LID along bus k in phase s, $\overrightarrow{\mathbf{LID}_{(k,s)}}$, the CPF method is used to find the corresponding maximum loading factor $\lambda^*_{k,s}$ and the total real power $\sum P^*_{k,s}$. Two differences are calculated. The first difference is the difference between λ^* and $\lambda^*_{k,s}$, denoted as $\Delta\lambda^*_{k,s}$. The second difference is the difference between $\sum P^*$ and $\sum P^*_{k,s}$ and denoted as $\Delta\sum P^*_{k,s}$. That is,

$$\Delta\lambda^*_{(k,s)} = \lambda^*_{(k,s)} - \lambda^* \tag{4.10}$$

$$\Delta\sum P^*_{(k,s)} = \sum P^*_{(k,s)} - \sum P^* \tag{4.11}$$

Repeat this step to perturb the original LID along all of the buses and phases so that the impact of the perturbation of LID along different buses and phases can be found.

In the third step, the buses are ranked based on the absolute values of $\Delta\lambda^*_{(k,s)}$ and $\Delta\sum P^*_{(k,s)}$ at each bus. The larger the absolute value of $\Delta\lambda^*_{(k,s)}$ and $\Delta\sum P^*_{(k,s)}$, the weaker the corresponding bus. The physical meaning of the weak bus is that the weak buses/phases have the high impact on the maximum loading factor, λ^*, and on the maximum total real power, $\sum P^*$, that the system can support. In other words, for the same amount of LID perturbation, the direction of the perturbation that is along the weak buses/phases will result in the larger change of maximum loading factor and large change of maximum total real power.

Fig. 4.5 shows the flowchart of CPF scan for three-phase cases It can be seen that the CPF scan method uses the CPF method as the fundamental block. The input of the

CPF scan method is network information, base operating point and LID. Using the CPF method, the maximum loading factor, λ^*, and the maximum total real power, $\sum P^*$, are found. Then LID is perturbed along each bus k and phase s. Using the CPF method, the corresponding loading factor $\lambda^*_{(k,s)}$ and $\sum P^*_{(k,s)}$ are found. By comparing with λ^* and $\sum P^*$, the difference between the base and the perturbed case are found as $\Delta\lambda^*_{(k,s)}$ and $\Delta\sum P^*_{(k,s)}$, respectively. After LID is perturbed along all buses and phases, the ranking of each bus and phase are performed based on the absolute value of $\Delta\lambda^*_{(k,s)}$ and $\Delta\sum P^*_{(k,s)}$.

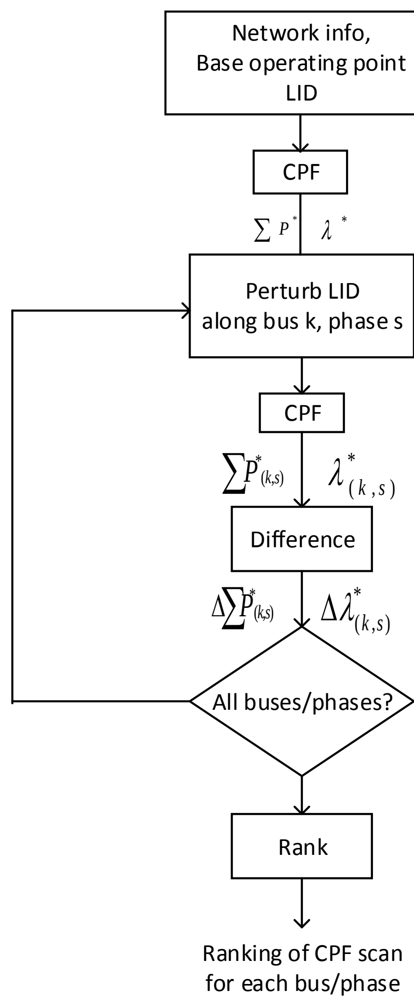

Figure 4.5: Flow chart of the three-phase CPF scan method

4.3.2 Single-phase two-bus example

To illustrate the CPF scan method, a single-phase two-bus example, shown in Fig.4.1 is used. Suppose that the base operating point and the load increase direction are:

$$\mathrm{OP} = \begin{bmatrix} P_{\mathrm{base},1} & Q_{\mathrm{base},1} & P_{\mathrm{base},2} & P_{\mathrm{base},2} \end{bmatrix} \tag{4.12}$$

$$\overrightarrow{\mathbf{LID}} = \begin{bmatrix} \mathrm{PLID}(1) & \mathrm{QLID}(1) & \mathrm{PLID}(2) & \mathrm{QLID}(2) \end{bmatrix} \tag{4.13}$$

Therefore, the load at Bus 1 and Bus 2 are:

$$P_1 = P_{\mathrm{base},1} + \lambda \cdot \mathrm{PLID}(1) \tag{4.14}$$

$$Q_1 = Q_{\mathrm{base},1} + \lambda \cdot \mathrm{QLID}(1) \tag{4.15}$$

$$P_2 = P_{\mathrm{base},2} + \lambda \cdot \mathrm{PLID}(2) \tag{4.16}$$

$$Q_2 = Q_{\mathrm{base},2} + \lambda \cdot \mathrm{QLID}(2) \tag{4.17}$$

By using CPF method, the maximum loading factor and maximum total real power can be found. Denote maximum λ as λ^* and total maximum real power is $\sum P^*$:

$$\sum P^* = P_{\mathrm{base},1} + P_{\mathrm{base},2} + \lambda^* \cdot (\mathrm{PLID}(1) + \mathrm{PLID}(2)) \tag{4.18}$$

Fig. 4.6 shows that the base operating point is OP while the LID is $\overrightarrow{\mathbf{LID}}$. The CPF method finds the maximum loading factor λ^*.

In the second step of CPF scan method, the LID is perturbed along different buses. First, the LID is perturbed along Bus 1 by ΔLID, which is defined as ΔLID =

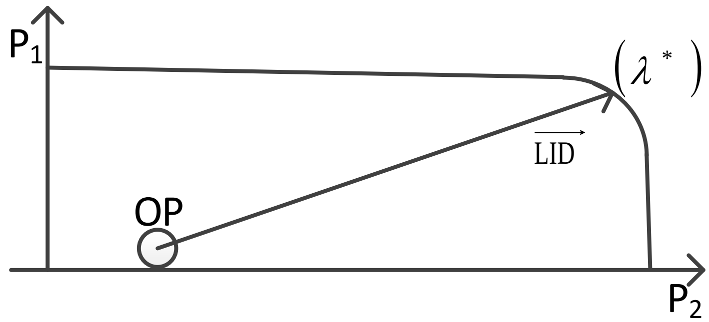

Figure 4.6: CPF scan - no perturbation

$[\Delta\text{LIDP}, \Delta\text{LIDQ}]$. Therefore,

$$\text{OP} = \begin{bmatrix} P_{\text{base},1} & Q_{\text{base},1} & P_{\text{base},2} & P_{\text{base},2} \end{bmatrix} \tag{4.19}$$

$$\overrightarrow{\textbf{LID}}_{(1)} = \begin{bmatrix} \text{PLID}(1) - \Delta\text{LIDP} & \text{QLID}(1) - \Delta\text{LIDQ} & \text{PLID}(2) & \text{QLID}(2) \end{bmatrix} \tag{4.20}$$

The loads at Bus 1 and Bus 2 are:

$$P_1 = P_{\text{base},1} + \lambda \cdot (\text{PLID}(1) - \Delta\text{LIDP}) \tag{4.21}$$

$$Q_1 = Q_{\text{base},1} + \lambda \cdot (\text{QLID}(1) - \Delta\text{LIDQ}) \tag{4.22}$$

$$P_2 = P_{\text{base},2} + \lambda \cdot \text{PLID}(2) \tag{4.23}$$

$$Q_2 = Q_{\text{base},2} + \lambda \cdot \text{QLID}(2) \tag{4.24}$$

Use the CPF method to solve for the maximum loading factor and total maximum real power. Denote the maximum loading factor as $\lambda^*_{(1)}$ and total maximum real power as $\sum P^*_{(1)}$.

Fig. 4.7 shows that the base operating point is OP while the LID is $\overrightarrow{\textbf{LID}}_{(1)}$. The CPF method finds the maximum loading factor $\lambda^*_{(1)}$.

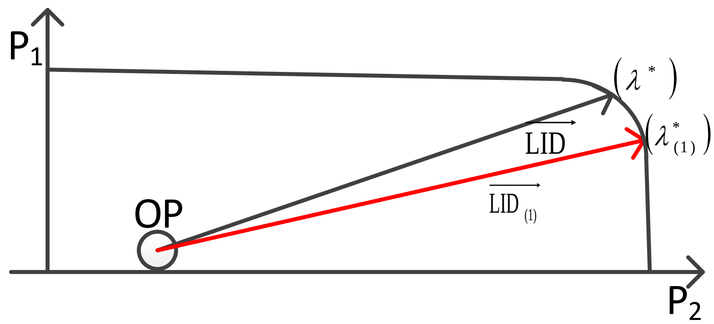

Figure 4.7: CPF scan - perturb along Bus 1

Then, the LID is perturbed along Bus 2 by ΔLID,

$$\text{OP} = \begin{bmatrix} P_{\text{base},1} & Q_{\text{base},1} & P_{\text{base},2} & P_{\text{base},2} \end{bmatrix} \tag{4.25}$$

$$\overrightarrow{\textbf{LID}}_{(2)} = \begin{bmatrix} \text{PLID}(1) & \text{QLID}(1) & \text{PLID}(2) - \Delta\text{LIDP} & \text{QLID}(2) - \Delta\text{LIDQ} \end{bmatrix} \tag{4.26}$$

The load at Bus 1 and Bus 2 are:

$$P_1 = P_{\text{base},1} + \lambda \cdot \text{PLID}(1) \tag{4.27}$$

$$Q_1 = Q_{\text{base},1} + \lambda \cdot \text{QLID}(1) \tag{4.28}$$

$$P_2 = P_{\text{base},2} + \lambda \cdot (\text{PLID}(2) - \Delta\text{LIDP}) \tag{4.29}$$

$$Q_2 = Q_{\text{base},2} + \lambda \cdot (\text{QLID}(2) - \Delta\text{LIDQ}) \tag{4.30}$$

Use the CPF method to solve for the maximum loading factor and total maximum real power. Denote the maximum loading factor as $\lambda^*_{(2)}$ and total maximum real power as $\sum P^*_{(2)}$.

Fig. 4.8 shows that the base operating point is OP while the LID is $\overrightarrow{\textbf{LID}}_{(2)}$. The CPF method finds the maximum loading factor $\lambda^*_{(2)}$.

After these two perturbations of load increase direction, we can calculate $\Delta\lambda^*_{(1)}$ and

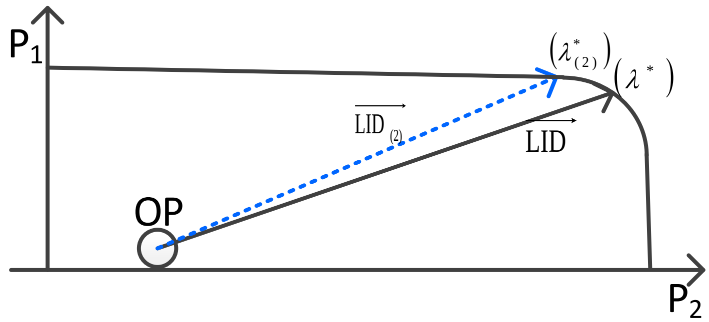

Figure 4.8: CPF scan - perturb along Bus 2

$\Delta\sum P^*_{(1)}$. They are, respectively, the change of the maximum loading factor and the change of the maximum total real power between the perturbed LID along Bus 1, $\overrightarrow{\mathbf{LID}}_{(1)}$, and unperturbed LID, $\overrightarrow{\mathbf{LID}}$. Similar notations go to the perturbed LID along Bus 2. The weak bus is determined based on the change of maximum loading factor or based on the change of maximum total real power. Bus 1 is weaker if $|\Delta\lambda^*_{(1)}| \geq |\Delta\lambda^*_{(2)}|$ or $|\Delta\sum P^*_{(1)}| \geq |\Delta\sum P^*_{(2)}|$. In Section 4.4, we will show the condition under which $|\Delta\lambda^*_{(1)}| \geq |\Delta\lambda^*_{(2)}|$ implies $|\Delta\sum P^*_{(1)}| \geq |\Delta\sum P^*_{(2)}|$.

$$\Delta\lambda^*_{(1)} = \lambda^*_{(1)} - \lambda^* \tag{4.31}$$

$$\Delta\lambda^*_{(2)} = \lambda^*_{(2)} - \lambda^* \tag{4.32}$$

$$\Delta\sum P^*_{(1)} = \sum P^*_{(1)} - \sum P^* \tag{4.33}$$

$$\Delta\sum P^*_{(2)} = \sum P^*_{(2)} - \sum P^* \tag{4.34}$$

4.4 Properties of CPF scan method

For single-phase or three-phase CPF scan methods, there are three properties of CPF scan results worth discussion. In the following, we will explain with single-phase example and show the numerical results of three-phase example.

The first property is that the results of the CPF scan method are different for different LIDs. Suppose we have two different LIDs: $\overrightarrow{\mathbf{LID_1}}$ and $\overrightarrow{\mathbf{LID_2}}$, as shown in Fig.4.9. For $\overrightarrow{\mathbf{LID_1}}$, the corresponding maximum loading factor is λ_1^*. The CPF scan method perturbs $\overrightarrow{\mathbf{LID_1}}$ along Bus 1 and Bus 2 to get $\overrightarrow{\mathbf{LID_{1(1)}}}$ and $\overrightarrow{\mathbf{LID_{1(2)}}}$, respectively. The corresponding maximum loading factor is $\lambda_{1(1)}^*$ and $\lambda_{1(2)}^*$, respectively. Fig.4.9 shows that $\lambda_{1(1)}^* \geq \lambda_1^* \geq \lambda_{1(2)}^*$. Because the difference between $\lambda_{1(1)}^*$ and λ_1^* is greater than the difference between $\lambda_{1(2)}^*$ and λ_1^*, Bus 1 is the weaker bus than Bus 2.

On the other hand, for $\overrightarrow{\mathbf{LID_2}}$, the corresponding maximum loading factor is λ_2^*. The CPF scan method perturbs $\overrightarrow{\mathbf{LID_2}}$ along bus 1 and bus 2 to get $\overrightarrow{\mathbf{LID_{2(1)}}}$ and $\overrightarrow{\mathbf{LID_{2(2)}}}$, respectively. The corresponding maximum loading factor is $\lambda_{2(1)}^*$ and $\lambda_{2(2)}^*$, respectively. Fig.4.9 shows that $\lambda_{2(2)}^* \geq \lambda_2^* \geq \lambda_{2(1)}^*$. Because the difference between $\lambda_{2(2)}^*$ and λ_2^* is greater than the difference between $\lambda_{2(1)}^*$ and λ_2^*, Bus 2 is the weaker bus than Bus 1. We can see that different LIDs may have different weak buses results.

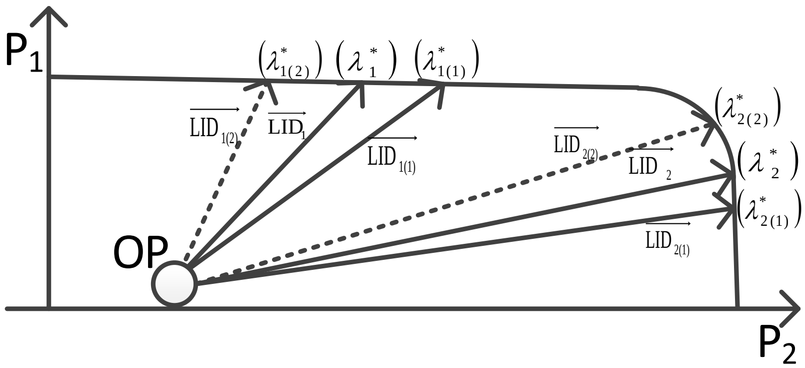

Figure 4.9: Weak bus that depends on LID

The second property is that the CPF scan method results vary for different loading factors. As shown in Fig.4.10, there are two operating points, $\mathrm{OP_A} = (P_{A1}, Q_{A1}, P_{A2}, Q_{A2})$ and $\mathrm{OP_B} = (P_{B1}, Q_{B1}, P_{B2}, Q_{B2})$. The relationship between $\mathrm{OP_A}$ and $\mathrm{OP_B}$ can be expressed as (4.35).

$$\begin{cases} P_{B1} = P_{A1} + \lambda \cdot \mathrm{PLID}(1) \\ Q_{B1} = Q_{A1} + \lambda \cdot \mathrm{QLID}(1) \\ P_{B2} = P_{A2} + \lambda \cdot \mathrm{PLID}(2) \\ Q_{B2} = Q_{A2} + \lambda \cdot \mathrm{QLID}(2) \end{cases} \tag{4.35}$$

We apply the CPF scan method on $\mathrm{OP_A}$ and the resulting maximum loading factor after LID perturbation along Bus 1 and Bus 2 are $\lambda^*_{A(1)}$ and $\lambda^*_{A(2)}$. Similarly, we apply the CPF scan method on $\mathrm{OP_B}$ and the resulting maximum loading factor after LID perturbation along Bus 1 and Bus 2 are $\lambda^*_{B(1)}$ and $\lambda^*_{B(2)}$. Depending on the shape of the SNB surface near λ^*, it is possible that $\lambda^*_{A(1)} \geq \lambda^*_{A(2)}$ while $\lambda^*_{B(1)} \leq \lambda^*_{B(2)}$. Therefore, for $\mathrm{OP_A}$, the weak bus is Bus 1. For $\mathrm{OP_B}$, the weak bus is Bus 2

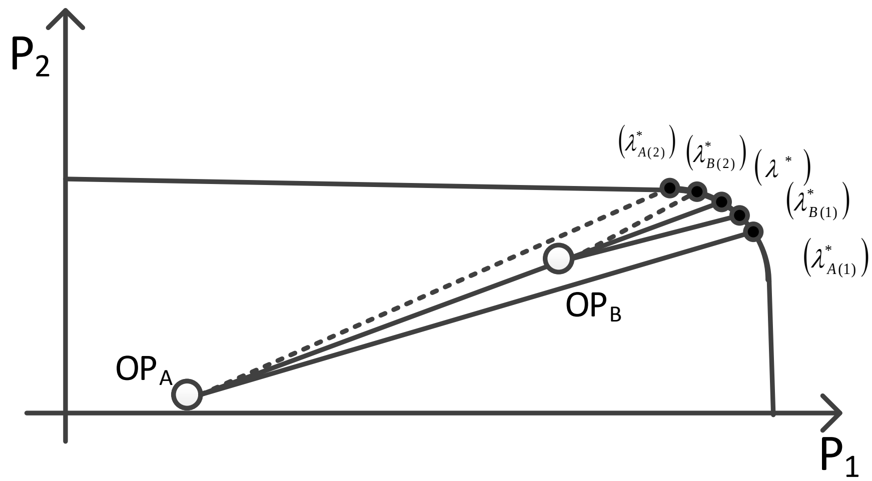

Figure 4.10: Weak bus change as the loading factor is changed

The third property is about the rankings of the CPF scan results. The CPF scan results include the loading factor sensitivity and the maximum total real power sensitivity. These two sensitivities can be used to rank the CPF scan results. However, these two rankings are different unless LID perturbation amount at each bus is the same. We will use a two-bus system to explain this property.

In a two-bus system, the real power on these two buses can be expressed as

$$P_1 = P_{\text{base},1} + \lambda \cdot \text{PLID}(1) \tag{4.36}$$

$$P_2 = P_{\text{base},2} + \lambda \cdot \text{PLID}(2) \tag{4.37}$$

Suppose λ^* is the maximum loading factor for this given LID. Then the maximum total real power is

$$\sum P^* = P_{\text{base},1} + P_{\text{base},2} + \lambda^* \cdot [\text{PLID}(1) + \text{PLID}(2))] \tag{4.38}$$

For the first case, the LID perturbations along Bus 1 and Bus 2 are different: $\Delta\text{PLID}(1) \neq$

$\Delta\text{PLID}(2)$. For the LID perturbation along Bus 1:

$$P_1 = P_{\text{base},1} + \lambda \cdot [\text{PLID}(1) - \Delta\text{PLID}(1)] \tag{4.39}$$

$$P_2 = P_{\text{base},2} + \lambda \cdot \text{PLID}(2) \tag{4.40}$$

If the corresponding maximum loading factor is $\lambda^*_{(1)}$, then the maximum total real power for the system is

$$\sum P^*_{(1)} = P_{\text{base},1} + P_{\text{base},2} + \lambda^*_{(1)} \cdot [\text{PLID}(1) + \text{PLID}(2))] - \lambda^*_{(1)} \cdot \Delta\text{PLID}(1) \tag{4.41}$$

For the LID perturbation along Bus 2:

$$P_1 = P_{\text{base},1} + \lambda \cdot \text{PLID}(1) \tag{4.42}$$

$$P_2 = P_{\text{base},2} + \lambda \cdot [\text{PLID}(2) - \Delta\text{PLID}(2))] \tag{4.43}$$

If the corresponding maximum loading factor is $\lambda^*_{(2)}$, then the maximum total real power for the system is

$$\sum P^*_{(2)} = P_{\text{base},1} + P_{\text{base},2} + \lambda^*_{(2)} \cdot [\text{PLID}(1) + \text{PLID}(2))] - \lambda^*_{(2)} \cdot \Delta\text{PLID}(2) \tag{4.44}$$

The changes of the maximum total real power from the base case to these two perturbed cases are:

$$\Delta \sum P^*_{(1)} = (\lambda^*_{(1)} - \lambda^*)(\text{PLID}(1) + \text{PLID}(2)) - \lambda^*_{(1)}\Delta\text{PLID}(1) \tag{4.45}$$

$$\Delta \sum P^*_{(2)} = (\lambda^*_{(2)} - \lambda^*)(\text{PLID}(1) + \text{PLID}(2)) - \lambda^*_{(2)}\Delta\text{PLID}(2) \tag{4.46}$$

(4.47)

Therefore,

$$\Delta\sum P^*_{(1)} - \Delta\sum P^*_{(2)} = (\lambda^*_{(1)} - \lambda^*_{(2)})\,[\mathrm{PLID}(1) + \mathrm{PLID}(2)]$$
$$- \lambda^*_{(1)}\Delta\mathrm{PLID}(1) + \lambda^*_{(2)}\Delta\mathrm{PLID}(2) \tag{4.48}$$

Even if $\lambda^*_{(1)}$ is greater than $\lambda^*_{(2)}$, it is not necessarily that $\Delta\sum P^*_{(1)}$ is greater than $\Delta\sum P^*_{(2)}$. It will depend on the value of $\lambda^*_{(1)}$, $\lambda^*_{(2)}$, $\mathrm{PLID}(1)$, $\mathrm{PLID}(2)$, $\Delta\mathrm{PLID}(1)$ and $\Delta\mathrm{PLID}(2)$. Therefore, the ranking based on loading factor is not necessarily the same as that based on the maximum total real power.

For the second case, however, the LID perturbations are the same for Bus 1 and Bus 2. That is, $\Delta\mathrm{PLID}(1) = \Delta\mathrm{PLID}(2) = \Delta\mathrm{PLID}$. Therefore, (4.48) can be expressed as:

$$\Delta\sum P^*_{(1)} - \Delta\sum P^*_{(2)} = (\lambda^*_{(1)} - \lambda^*_{(2)})\,[\mathrm{PLID}(1) + \mathrm{PLID}(2) - \Delta\mathrm{PLID}] \tag{4.49}$$

Because $\mathrm{PLID}(1)$ and $\mathrm{PLID}(2)$ are larger than $\Delta\mathrm{PLID}$ in the CPF scan method, $\lambda^*_{(1)} - \lambda^*_{(2)} \geq 0$ implies $\Delta\sum P^*_{(1)} - \Delta\sum P^*_{(2)} \geq 0$. Therefore, the ranking of maximum loading factor and of the total real power is the same when the perturbation, ΔPLID for each bus is the same.

In conclusion, the properties of the CPF scan method were discussed. The results of CPF scan method are different for different LIDs and different initial loading factor. Moreover, the ranking based on maximum loading factor and that based on the total real power is the same when the perturbation, ΔPLID, for each bus is the same.

4.5 Change LID by demand response

If the system is close to voltage collapse point, certain control actions should be taken such that the system can avoid voltage collapse problem. One of the applications of CPF scan method is to steer the system away from the voltage collapse point, or to increase the voltage stability margin. The CPF scan can find the best adjustment on how the load is increased so that the voltage stability margin can be increased. Therefore, how to adjust the way the loads are increased, that is, the load increase direction, LID, is vital for the CPF scan application in the area of increasing the voltage stability margin. In this section, how to change LID by using demand response is described.

The demand response can adjust the load at each time step [78]. The load can be increased by load shifting [79], that is, shifting the load from hour X to hour Y. The load can be increased or decrease by demand response. However, demand response is controlling the load at each time slot. How can demand response be used to change LID?

We use a simple example to illustrate the approach. Here we only consider real power loads for simplicity; demand response can also adjust reactive power loads. Suppose the loads of the buses at current time t_0 is $\mathbf{S}(t_0)$. $\mathbf{S}$ is a vector, whose elements are the real and reactive power loading at each bus. Suppose that according to the load forecast, the load at time T is $\mathbf{S}(T)$. Assuming the load is changed at the same rate from time t_0 to time T. Therefore, the LID can be calculated as

$$\mathbf{LID} = \frac{\mathbf{S}(T) - \mathbf{S}(t_0)}{T - t_0} \tag{4.50}$$

Therefore, the ith bus of **SLID** can be expressed as

$$\mathrm{LID}_i = \frac{S_i(T) - S_i(t_0)}{T - t_0} \tag{4.51}$$

The load at Bus i at time t, $t \in [t_0, T]$ is

$$S_i(t) = S_i(t_0) + [\text{LID}_i]\,(t - t_0) \tag{4.52}$$

Suppose that according to CPF scan, in order to the increase the voltage stability margin, the best direction to change LID is along bus i. Therefore, we would like to change **LID** along bus i by ΔLID, which has two elements: ΔPLID for real power and by ΔQLID for reactive power.

The load at Bus i at time t, $t \in [t_0, T]$ can be expressed as

$$S_i(t) = S_i(t_0) + [\text{LID}_i - \Delta\text{LID}]\,(t - t_0) \tag{4.53}$$

$$= S_i(t_0) + \text{LID}_i \times (t - t_0) - \Delta\text{LID} \times (t - t_0) \tag{4.54}$$

$$\begin{aligned} &= P_i(t_0) + \text{PLID}_i \times (t - t_0) - \Delta\text{PLID} \times (t - t_0) \\ &+ j\,[Q_i(t_0) + \text{QLID}_i \times (t - t_0) - \Delta\text{QLID} \times (t - t_0)] \end{aligned} \tag{4.55}$$

To change **LID** along bus i by ΔLID, at time t, demand response should adjust the load at bus i by

$$\text{DR}_{P,i}(t) = \Delta\text{PLID} \times (t - t_0) \tag{4.56}$$

$$\text{DR}_{Q,i}(t) = \Delta\text{QLID} \times (t - t_0) \tag{4.57}$$

while the demand response does not need to adjust the load at the other buses, that is

$$\text{DR}_{P,j}(t) = 0 \quad \text{for } j \neq i \tag{4.58}$$

$$\text{DR}_{Q,j}(t) = 0 \quad \text{for } j \neq i \tag{4.59}$$

4.6 Case studies

In the following case studies, the CPF scan method was applied first to an 8-bus distribution system, shown in Fig.4.11. The reason to use this simple 8-bus distribution system is to study the impact of different components in distribution systems. After that, the CPF scan method was applied to a more realistic distribution system, the modified IEEE 13-node test feeder with DG. Lastly, we demonstrated the application of the CPF scan method in the operation and planning of distribution systems.

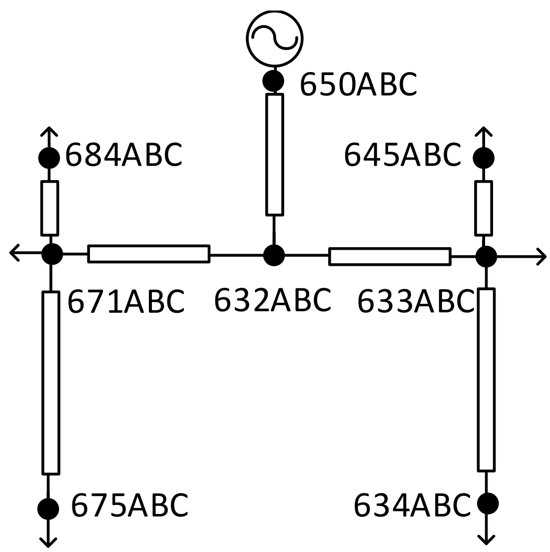

Figure 4.11: 8-bus system

4.6.1 8-bus case studies

The line impedance matrix for the lines in this 8-bus system is the same. The value of impedance matrix is:

$$\begin{bmatrix} 0.347+1.018i & 0.1560+0.502i & 0.1560+0.502i \\ 0.1560+0.502i & 0.347+1.018i & 0.1560+0.502i \\ 0.1560+0.502i & 0.1560+0.502i & 0.347+1.018i \end{bmatrix} \Omega/\text{mile} \qquad (4.60)$$

The length of each branch is summarized in Table 4.1 while the load at each bus is summarized in Table 4.2.

This system is perfectly balanced; all the lines are transposed and all the loads are balanced. The left side of the system is exactly the same as the right side, including the length of branches, the line impedance matrices, and the loadings. Therefore, this system has three pairs of two buses of the same characteristics. These three pairs are Bus 675 and

Table 4.1: Branch information of 8-bus system

Branch information		
Lines	length [ft]	Impedance matrix (4.60)
650-632	2000	type 609
632-633	2000	type 609
632-671	2000	type 609
633-645	1000	type 609
671-684	1000	type 609
633-634	3000	type 609
671-675	3000	type 609

Table 4.2: Load information of 8-bus system

Loads (constant power load)			
Bus	Phase A [kW,kVar]	Phase B [kW,kVar]	Phase C [kW,kVar]
633	120+90j	120+90j	120+90j
671	120+90j	120+90j	120+90j
675	120+90j	120+90j	120+90j
684	120+90j	120+90j	120+90j
645	120+90j	120+90j	120+90j
634	120+90j	120+90j	120+90j

Bus 634, Bus 684 and Bus 645, and Bus 671 and Bus 633.

In the following case studies, we made one change to this 8-bus system, such as adding untransposed line in one of the branches on the right side. By comparing the pair (Bus 684, Bus 645), (Bus 671, Bus 633), and (Bus 675, Bus 634), the impact on the weak buses of different components in the system can be investigated. Moreover, the ranking of CPF scan result was compared with the ranking of voltage magnitude at the maximum loading point, which was the proposed method in [53]. The pairwise ranking, the weakest bus and overall ranking of CPF scan and voltage were compared.

Base case

Table 4.3 shows the CPF scan result for the base case. The ranking is based on the absolute value of $\Delta\sum P^*$ of CPF scan result. The higher the absolute value, the weaker the bus. Because the system is perfectly balanced system, the CPF scan result is the same for all three phases. Also, the buses in each pair had the same CPF scan result, indicating that the left side and the right side of the system were exactly the same. Moreover, Bus 675 and Bus 634 were weaker than Bus 684 and Bus 645, while Bus 684 and Bus 645 were weaker than Bus 671 and Bus 633. The CPF scan results followed upstream/downstream relationship; the upstream node was stronger than the downstream node. Because the example system is radial, these results are as expected.

Table 4.4 shows the comparison of CPF scan result with voltage magnitude ranking as well as branch power flow. The first column shows the CPF scan result ($\Delta\sum P^*$), the second column shows the voltage magnitude for each bus and the third and forth columns

Table 4.3: CPF scan for the 8-bus base case

Phase A		Phase B		Phase C	
675A	-175.395	675B	-175.395	675C	-175.395
634A	-175.395	634B	-175.395	634C	-175.395
645A	-171.971	645B	-171.971	645C	-171.971
684A	-171.971	684B	-171.971	684C	-171.971
671A	-170.678	671B	-170.678	671C	-170.678
633A	-170.678	633B	-170.678	633C	-170.678
632A	-155.693	632B	-155.693	632C	-155.693

are real and reactive power flow for each branch. The overall ranking of CPF scan result is exactly the same as the voltage magnitude ranking. Moreover, the branch power flow matches the CPF scan result. For example, from the CPF scan result, Bus 634 is weaker than Bus 645; the real power flow and the reactive power flow on Branch 633-634 are higher than that on Branch 633-645. Note that to make the branch power flow comparison meaningful, the branches that are being compared should be at the same tier/level from the substation. For example, it is meaningful to compare the branch 633-645 with the branch 671-684 or with the branch 633-645. It is meaningless to compare the branch 632-671 with branch 633-634.

Table 4.4: Comparison for 8-bus base case

CPF scan		V		P		Q	
675A	-175.395	675A	0.487	650-632a	5.270	650-632a	7.012
634A	-175.395	634A	0.487	632-633a	2.153	632-633a	2.202
645A	-171.971	645A	0.539	632-671a	2.153	632-671a	2.202
684A	-171.971	684A	0.539	633-634a	0.664	633-634a	0.590
671A	-170.678	671A	0.561	671-675a	0.664	671-675a	0.590
633A	-170.678	633A	0.561	633-645a	0.630	633-645a	0.498
632A	-155.693	632A	0.702	671-684a	0.630	671-684a	0.498
		650A	1.000				

Doubled load

This case study investigated the impact of doubled loads. The load was doubled in every phase at one of the three buses on the right side, shown in Fig.4.12. For example, the load at Bus 634 was doubled. The CPF scan method was applied to these three cases. Table 4.5 shows the CPF scan results. The column whose heading is Base shows the CPF scan result for the case where all the loads are balanced. The column whose heading is Bus 634 shows the CPF scan result for the case where the load at Bus 634 is doubled in all of the three phases. Only phase A results are shown because the system was balanced, making the results for phase B and phase C exactly the same.

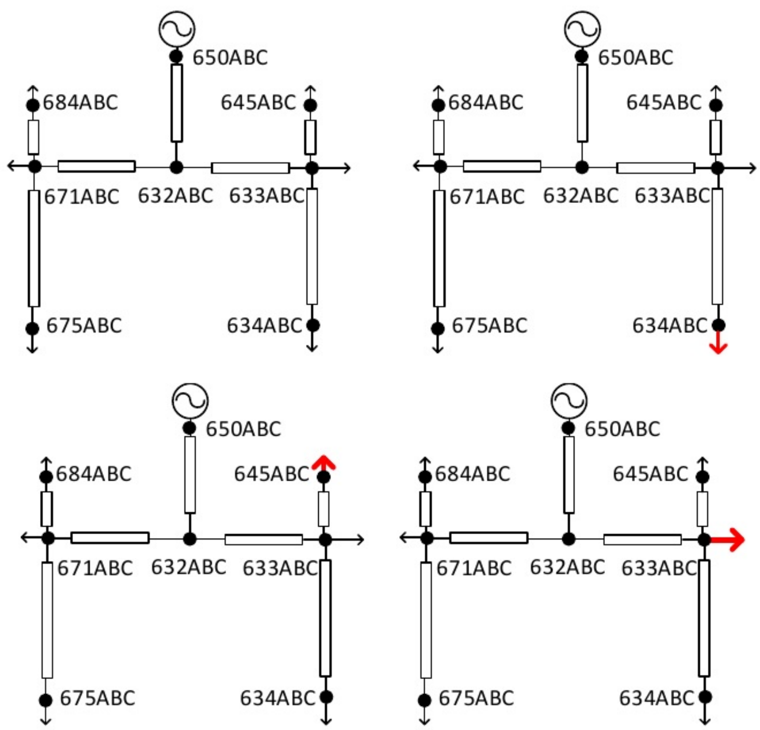

Figure 4.12: Load is doubled at different locations

The impact of the doubled load was investigated by the difference of the CPF scan results of the corresponding buses in the three pairs. For these three cases where the load was doubled, the right side was weaker than the left side in all phases: Bus 634 was weaker than Bus 675, Bus 633 was weaker than Bus 671 (with exception of small different for Bus 645 and Bus 633 case) and Bus 645 was weaker than Bus 684. Moreover, for one specific case where the load at Bus 634 was doubled, Bus 645 became weaker than Bus 675, even though the load at Bus 645 was the same as the load at Bus 675, and Bus 675 was farther away from the substation than Bus 645 based on the impedance value.

Table 4.5: CPF scan for different locations of doubled load

Base		Bus 634		Bus 645		Bus 633	
675A	-175.395	634A	-158.702	634A	-173.866	634A	-173.471
634A	-175.395	645A	-149.000	645A	-168.913	645A	-170.616
645A	-171.971	675A	-148.165	675A	-166.334	684A	-170.592
684A	-171.971	633A	-148.161	671A	-165.098	671A	-170.251
671A	-170.678	684A	-143.645	633A	-164.802	633A	-169.361
633A	-170.678	671A	-142.937	684A	-161.912	675A	-168.823
632A	-155.693	632A	-133.450	632A	-149.209	632A	-153.224

Table 4.6 shows the comparison of CPF scan results with voltage ranking as well as branch power flow. The pairwise ranking of CPF scan matched voltage; the weaker bus in the CPF scan ranking had the lower voltage at the maximum loading point. Also, the weakest bus identified from CPF scan was the same as the weakest bus identified from the voltage, which was Bus 634. Moreover, the overall ranking of CPF scan and the overall ranking of voltage magnitude were the same except the ranking of Bus 675 and Bus 633. The difference of CPF scan between Bus 675 and 633 was very small, 0.002%. Therefore, the overall ranking of CPF scan and the overall ranking of voltage magnitude were almost

the same.

Table 4.6: Comparison for 8-bus with load at Bus 634 doubled

CPF scan		V		P		Q	
634A	-158.702	634A	0.452	650-632a	4.728	650-632a	6.116
645A	-149.000	645A	0.564	632-633a	2.384	632-633a	2.637
675A	**-148.165**	**633A**	**0.580**	632-671a	1.595	632-671a	1.455
633A	**-148.161**	**675A**	**0.599**	633-634a	1.111	633-634a	1.100
684A	-143.645	684A	0.631	671-675a	0.507	671-675a	0.418
671A	-142.937	671A	0.646	633-645a	0.495	633-645a	0.385
632A	-133.450	632A	0.738	671-684a	0.493	671-684a	0.381
		650A	1.000	650-632b	4.728	650-632b	6.116

Capacitor bank

This case study investigates the impact of capacitor banks. A three-phase capacitor bank was installed at one of the three buses on the right, as shown in Fig. 4.13. The injected reactive power for each phase was 200 kVar.

Table 4.7 shows the CPF scan results. The column whose heading is Base shows the CPF scan result for the case where there was no capacitor banks connected. The column whose heading is Bus 634 shows the CPF scan result for the case where a three-phase capacitor bank was connected at Bus 634. Only phase A was shown because the system was balanced, making the results for phase B and phase C exactly the same.

The impact of the three-phase capacitor bank on the right can be investigated by the difference of the CPF scan results of the corresponding buses in the three pairs. The investigation reveals that the three-phase capacitor bank on the right made all of the buses on the right side stronger than the corresponding buses on the left side in all of the three pairs.

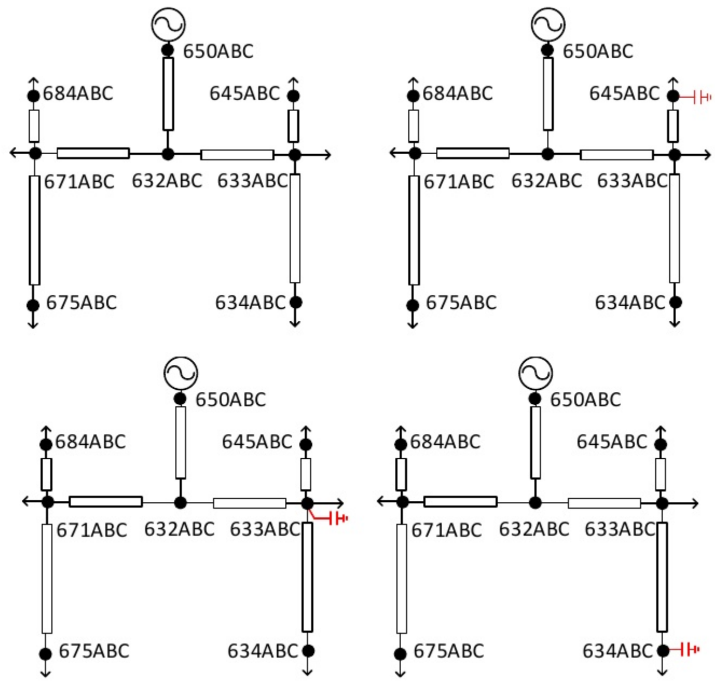

Figure 4.13: For capacitor case study

It is interesting to see that the CPF scan results were much smaller for the case where the three-phase capacitor was connected at Bus 634. The possible reason is that the three-phase capacitor changed the SNB surface tremendously so that the LID perturbation along different buses did not change the maximum total real power too much. This is only conjecture; more investigation is needed.

Table 4.7: CPF scan for different location of three-phase capacitor

Base		Bus 645		Bus 633		Bus 634	
675A	-175.395	684A	-177.628	675A	-177.564	675A	-5.191
634A	-175.395	675A	-177.160	634A	-176.647	634A	-5.097
645A	-171.971	634A	-176.434	684A	-173.884	684A	-4.836
684A	-171.971	645A	-172.648	645A	-172.881	645A	-4.773
671A	-170.678	671A	-172.145	671A	-172.082	671A	-4.688
633A	-170.678	633A	-171.494	633A	-171.530	633A	-4.637
632A	-155.693	632A	-156.870	632A	-156.740	632A	-2.415

Table 4.8 shows the comparison of CPF scan result with voltage ranking as well as branch power flow. It can be seen that the overall ranking of CPF scan result was exactly the same as the voltage magnitude overall ranking. Moreover, the branch power flow matched the CPF scan result. For example, from the CPF scan result, Bus 675 was weaker than Bus 634; the real power flow at Branch 671-675 was higher than that at Branch 633-634.

Table 4.8: Comparison for 8-bus with three-phase capacitor at Bus 634

CPF scan		V		P		Q	
675A	-5.191	675A	0.476	650-632a	5.371	650-632a	7.062
634A	-5.097	634A	0.498	632-671a	2.210	632-671a	2.291
684A	-4.836	684A	0.530	632-633a	2.174	632-633a	2.104
645A	-4.773	645A	0.541	671-675a	0.680	671-675a	0.610
671A	-4.688	671A	0.553	633-634a	0.669	671-684a	0.508
633A	-4.637	633A	0.563	671-684a	0.642	633-645a	0.507
632A	-2.415	632A	0.700	633-645a	0.642	633-634a	0.492

Unbalanced load

This case study investigates the impact of unbalanced loads. The balanced load at one of the three buses on the right side of the base case was changed into an unbalanced load, shown in Fig. 4.14. When the load at Bus 634 was made unbalanced, then the load at Bus 634A remained the same, the load at Bus 634B was increased by 50%, and the load at Bus 634C was decreased by 50%.

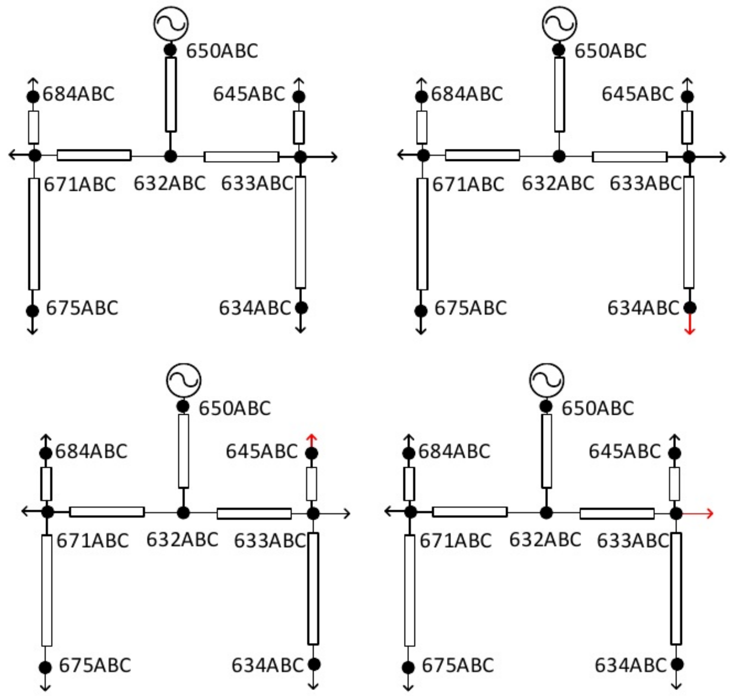

Figure 4.14: For unbalanced load

Table 4.9 shows CPF scan results for different cases. The column whose heading is Base shows the CPF scan result for the case where all the loads were balanced. The column whose heading is Bus 634 shows the CPF scan result for the case where the load at Bus 634A was changed to be unbalanced. The impact of the unbalanced load was investigated by the difference of the CPF scan results of the corresponding buses in the three pairs. The comparison shows two observations. First, the impact of unbalanced load at Bus 634 is bigger than that at Bus 633 and Bus 645 based on the CPF scan difference between Bus 634 and Bus 675. When unbalanced load was at Bus 634, the CPF scan difference between Bus 634 and Bus 675 was bigger than that where the unbalanced load was at Bus 633 or Bus 645. This is because Bus 634 was further away from the substation than Bus 633 and

Bus 645. Moreover, the unbalanced load, no matter whether it was at Bus 634, Bus 645 or Bus 633, made the right side in phase B weaker and the left side in phase C stronger in each of the three pairs. This is because the right side in phase B had higher loadings while that in phase C had lower loadings. However, there was not much difference in the CPF scan ranking between the left and the right in phase A in each of the three pairs. This is because the loadings at the both sides in these three pairs were the same. In summary, the unbalanced load that was far away from the substation had a bigger impact on the CPF scan result. Also, when the unbalanced load increased the loading in a particular phase, this phase on the side of the unbalanced load got weaker.

Table 4.9: CPF scan for different locations of unbalanced load

Base		Bus 634		Bus 645		Bus 633	
675A	-175.395	634A	-9.386	634A	-10.075	634A	-10.605
634A	-175.395	645A	-7.654	645A	-9.349	645A	-9.512
645A	-171.971	633A	-7.385	675A	-8.815	675A	-9.377
684A	-171.971	675A	-6.948	633A	-8.774	633A	-9.126
671A	-170.678	684A	-6.473	684A	-8.079	684A	-8.580
633A	-170.678	671A	-6.290	671A	-7.803	671A	-8.285
632A	-155.693	632A	-4.384	632A	-5.066	632A	-5.408
634B	-175.395	634B	16.435	634B	15.129	634B	16.378
675B	-175.395	645B	9.933	645B	12.933	645B	12.849
645B	-171.971	633B	9.054	633B	10.809	675B	11.941
684B	-171.971	675B	7.417	675B	10.478	633B	11.699
633B	-170.678	684B	6.238	684B	8.592	684B	9.750
671B	-170.678	671B	5.766	671B	7.890	671B	8.911
632B	-155.693	632B	-0.220	632B	-0.114	632B	0.175
634C	-175.395	675C	-2.789	675C	-3.035	675C	-3.143
675C	-175.395	684C	-2.713	684C	-2.938	684C	-3.035
684C	-171.971	671C	-2.671	634C	-2.893	671C	-2.979
645C	-171.971	645C	-2.593	671C	-2.888	634C	-2.972
633C	-170.678	633C	-2.543	645C	-2.780	645C	-2.898
671C	-170.678	634C	-2.515	633C	-2.768	633C	-2.851
632C	-155.693	632C	-1.373	632C	-1.468	632C	-1.375

Table 4.10 shows the comparison of CPF scan result with voltage ranking as well as branch power flow. For phase B and phase C, the ranking of CPF scan result was exactly the same as the voltage ranking. Moreover, the branch power flow matched the CPF scan result. For example, from the CPF scan result, Bus 634B was weaker than Bus 645B. In the branch flow, the real power flow at Branch 633-634B, was higher than that at Branch 633-645B.

However, for phase A, the ranking of CPF scan was different from the voltage ranking, including overall ranking, pairwise ranking and even the weakest bus. From the CPF scan ranking, the right side of each pair was weaker than the left side; however, the voltage ranking did not have the same pattern. The right side and left side in each pair had a very similar voltage magnitude. Similar observation can be made for branch power flow. This was because for phase A, the loadings at both side were very similar, making the voltage and branch flow similar. However, in the CPF scan, the SNB surface is was extremely complicated, even though the loadings at both sides were similar, the CPF scan result may be quite different.

Table 4.10: Comparison for 8-bus with unbalanced load at Bus 634

CPF scan		V		P		Q	
634A	-9.386	675A	0.811	650-632a	2.899	650-632a	2.319
645A	-7.654	634A	0.812	632-633a	1.336	632-671a	1.039
633A	-7.385	684A	0.829	632-671a	1.292	632-633a	0.977
675A	-6.948	645A	0.831	633-634a	0.432	671-675a	0.323
684A	-6.473	671A	0.838	671-675a	0.418	671-684a	0.312
671A	-6.290	633A	0.840	633-645a	0.412	633-645a	0.312
632A	-4.384	632A	0.892	671-684a	0.412	633-634a	0.305
		650A	1.000				
634B	16.435	634B	0.552	650-632b	3.370	650-632b	4.013
645B	9.933	645B	0.634	632-633b	1.620	632-633b	1.661
633B	9.054	633B	0.649	632-671b	1.323	632-671b	1.165
675B	7.417	675B	0.654	633-634b	0.656	633-634b	0.618
684B	6.238	684B	0.683	671-675b	0.423	671-675b	0.343
671B	5.766	671B	0.697	633-645b	0.414	633-645b	0.320
632B	-0.220	632B	0.778	671-684b	0.413	671-684b	0.318
		650B	1.000				
675C	-2.789	675C	0.877	650-632c	2.193	650-632c	2.177
684C	-2.713	684C	0.891	632-671c	1.248	632-671c	1.045
671C	-2.671	671C	0.899	632-633c	0.983	632-633c	0.828
645C	-2.593	645C	0.929	671-675c	0.412	671-675c	0.324
633C	-2.543	633C	0.935	671-684c	0.410	671-684c	0.312
634C	-2.515	632C	0.943	633-645c	0.410	633-645c	0.312
632C	-1.373	634C	0.963	633-634c	0.195	633-634c	0.154
		650C	1.000				

Untransposed line

In this case study, an untransposed line replaced one of the transposed line at different locations, shown in Fig. 4.15. The line impedance of the untransposed line is:

$$\begin{bmatrix} 0.3465+1.0179i & 0.1560+0.5017i & 0.158+0.4236i \\ 0.1560+0.5017i & 0.3375+1.0478i & 0.1535+0.3849i \\ 0.158+0.4236i & 0.1535+0.3849i & 0.3414+1.0348i \end{bmatrix} \Omega/\text{mile} \qquad (4.61)$$

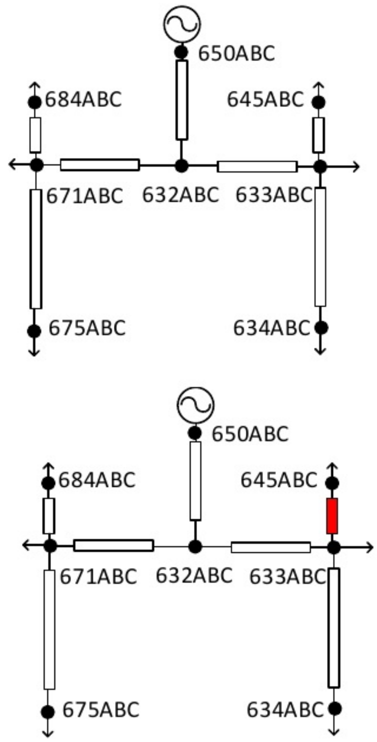

Figure 4.15: For untransposed line

Table 4.11 shows the CPF scan results. The column whose heading is Base shows the CPF scan results for the case where all the loads were balanced. The column whose heading is 633-634 shows the CPF scan results for the case where the line between Bus 633 and Bus 634 was replaced by an untransposed line.

Checking the difference of the CPF scan results between Bus 675 and Bus 634 in all three phases reveals that the impact of untransposed line was bigger if the untransposed line was at branch 632-633, which was upstream to branch 633-634 and branch 633-645. For example, when the untransposed line was at branch 633-634, the CPF scan difference between Bus 675A and Bus 634A was $|5.764 - 6.014| = 0.2500$. When the untransposed line was at branch 632-633, the CPF scan difference between Bus 675A and Bus 634A

Table 4.11: CPF scan for different locations of untransposed line

Base		633-634		633-645		632-633	
675A	-175.395	633A	-6.981	675A	-32.778	684A	46.922
634A	-175.395	671A	-6.840	634A	-32.777	645A	46.922
645A	-171.971	684A	6.014	633A	-30.445	634A	-10.951
684A	-171.971	645A	6.014	671A	-30.441	675A	-6.639
671A	-170.678	634A	6.014	684A	-29.316	633A	-4.479
633A	-170.678	675A	5.764	645A	-29.301	671A	-4.323
632A	-155.693	632A	-2.018	632A	-13.827	632A	0.565
634B	-175.395	671B	-13.893	684B	-38.099	634B	46.922
675B	-175.395	633B	-13.267	634B	-37.872	684B	46.922
645B	-171.971	632B	-8.414	675B	-37.750	645B	46.922
684B	-171.971	684B	6.014	645B	-34.354	633B	-24.281
633B	-170.678	645B	6.014	633B	-33.340	671B	-24.178
671B	-170.678	634B	6.014	671B	-33.319	675B	-22.091
632B	-155.693	675B	5.764	632B	-19.659	632B	-13.611
634C	-175.395	675C	32.983	675C	-37.719	634C	46.922
675C	-175.395	634C	32.667	634C	-34.909	684C	46.922
684C	-171.971	645C	25.510	645C	-31.304	645C	46.922
645C	-171.971	633C	23.632	684C	-31.254	675C	-17.419
633C	-170.678	671C	23.049	633C	-29.946	633C	-12.432
671C	-170.678	684C	18.505	671C	-29.897	671C	-12.168
632C	-155.693	632C	2.587	632C	-13.793	632C	4.821

is $|-6.639+10.951| = 4.3120$, which is larger than 0.25. Therefore, the impact of the untransposed line at branch 633-634 is smaller than that of the untransposed line at branch 632-633,

Moreover, also using the difference of the CPF scan results between Bus 675 and Bus 634, the impact of the untransposed line of branch 633-645 was smaller than that of branch 633-634. Even though these two branches were at the same tier, the length of branch 633-645 was shorter than the length of branch 633-634.

Surprisingly, regarding the comparison between the left side and the right side, there was no clear pattern, as shown in Table 4.12. In the table, ”R weaker” means that the bus on the right side in the same pair was weaker. ”Similar” means that the CPF scan value for the buses at both sides are very similar, almost the same. For example, for the case where untransposed line is at branch 633-634, comparison of Bus 675A and Bus 634A reveals that right side was weaker; however, comparison of Bus 675C and Bus 634C reveals that right side was stronger. Different phases had different results. Moreover, for the same phase, different pairs had different results. For example, when the untransposed line was at Branch 633-645, the right side was weaker for pair (Bus 675B vs Bus 634B); on the other hand, the right side was weaker for the pair (Bus 684B vs Bus 645B).

In summary, the length and the location of an untransposed line influenced the CPF scan results. When the untransposed line was longer or was at upstream location, its impact on the CPF scan results was larger. However, there was no pattern regarding whether an untransposed line weakened or strengthened the buses.

Table 4.12: Impact of untransposed line on the weakness of bus pairs

Comparison	633-634	633-645	632-633
Bus 675A vs Bus 634A	R weaker	R stronger	R weaker
Bus 675B vs Bus 634B	R weaker	R weaker	R weaker
Bus 675C vs Bus 634C	R stronger	R stronger	R weaker
Bus 684A vs Bus 645A	similar	similar	similar
Bus 684B vs Bus 645B	similar	R stronger	similar
Bus 684C vs Bus 645C	R weaker	similar	similar
Bus 671A vs Bus 633A	similar	similar	similar
Bus 671B vs Bus 633B	similar	similar	similar
Bus 671C vs Bus 633C	similar	similar	similar

Table 4.13 shows the comparison of CPF scan results with voltage ranking as well as branch power flow. The overall ranking, pairwise ranking and the weakest bus from CPF scan and that from the voltage magnitude did not match. Also for pairwise ranking, the CPF scan, voltage and branch power flow did not match either. For CPF scan ranking,

- A: $684 < 645$, $671 > 633$, $675 > 634$
- B: $684 < 645$, $671 < 633$, $\mathbf{675} > \mathbf{634}$
- C: $684 > 645$, $671 > 633$, $675 < 634$

For voltage ranking:

- A: $684 < 645$, $671 <= 633$, $675 > 634$
- B: $684 < 645$, $671 < 633$, $\mathbf{675} > \mathbf{634}$
- C: $684 > 645$, $671 > 633$, $675 >= 634$

Table 4.14 shows the branch flow comparison between branch 671-675 and branch 633-634 when the untransposed line was at branch 633-634. Before replacing one transposed line with an untransposed line, the branch power flows at both sides were

Table 4.13: Comparison for 8-bus with Branch 633-634 untransposed

CPF scan		V		P		Q	
684A	46.922	634A	0.698	650-632a	3.683	650-632a	4.031
645A	46.922	675A	0.705	632-633a	1.686	632-633a	1.510
634A	-10.951	684A	0.733	632-671a	1.684	632-671a	1.502
675A	-6.639	645A	0.733	633-634a	0.548	633-634a	0.447
633A	-4.479	671A	0.746	671-675a	0.543	671-675a	0.442
671A	-4.323	633A	0.746	671-684a	0.533	671-684a	0.410
632A	0.565	632A	0.828	633-645a	0.533	633-645a	0.410
		650A	1.000				
634B	46.922	675B	0.700	650-632b	3.805	650-632b	3.932
684B	46.922	634B	0.705	632-671b	1.709	632-633b	1.489
645B	46.922	684B	0.729	632-633b	1.699	632-671b	1.487
633B	-24.281	645B	0.730	671-675b	0.547	633-634b	0.446
671B	-24.178	671B	0.743	633-634b	0.536	671-675b	0.439
675B	-22.091	633B	0.744	671-684b	0.534	671-684b	0.410
632B	-13.611	632B	0.827	633-645b	0.534	633-645b	0.410
		650B	1.000				
634C	46.922	634C	0.633	650-632c	3.950	650-632c	4.392
684C	46.922	675C	0.647	632-633c	1.741	632-633c	1.590
645C	46.922	645C	0.679	632-671c	1.731	632-671c	1.566
675C	-17.419	684C	0.682	633-634c	0.555	633-634c	0.467
633C	-12.432	633C	0.695	671-675c	0.550	671-675c	0.452
671C	-12.168	671C	0.697	633-645c	0.535	633-645c	0.413
632C	4.821	632C	0.794	671-684c	0.535	671-684c	0.413
		650C	1.000				

exactly the same in all three phases. After the untransposed line was added, the branch power flow at the right side in phase A and C were higher while in phase B was lower. Moreover, for the same side, branch power flow in Phase C was higher than that in phase A, and branch power flow in phase A was higher than that in phase B.

Table 4.14: The branch flow comparison

	671-675		633-634
P in A	0.543 (2)	$<$	0.548 (2)
P in B	0.541 (3)	$>$	0.536 (3)
P in C	0.550 (1)	$<$	0.555 (1)
Q in A	0.442 (2)	$<$	0.447 (2)
Q in B	0.439 (3)	$<$	0.446 (3)
Q in C	0.452 (1)	$<$	0.467 (1)

The bus admittance matrix, the bus impedance matrix, the Jacobian matrix and the inverse of reduced Jacobian matrix were investigated. The difference of the above four matrices between the base case and the case where the untransposed line was at Branch 633-634 are shown in Table 4.15, Table 4.16, Table 4.17 and Table 4.18, respectively. This difference matrix only show which buses/phases were affected by the untransposed line; however, they did not provide information regarding the ranking of the CPF scan.

Table 4.15: Difference of bus admittance matrix wrt base case

	632A	632B	632C	633A	633B	633C	671A	671B	671C	675A	675B	675C	684A	684B	684C	645A	645B	645C	634A	634B	634C	650A	650B	650C
632A	0	0	0	0	0	0	0	0	0	0	0	0	0	0	0	0	0	0	0	0	0	0	0	0
632B	0	0	0	0	0	0	0	0	0	0	0	0	0	0	0	0	0	0	0	0	0	0	0	0
632C	0	0	0	0	0	0	0	0	0	0	0	0	0	0	0	0	0	0	0	0	0	0	0	0
633A	0	0	0	0.506232	0.492739	0.97014	0	0	0	0	0	0	0	0	0	0	0	0	0.506224	0.492741	0.970138	0	0	0
633B	0	0	0	0.492739	1.366194	1.954636	0	0	0	0	0	0	0	0	0	0	0	0	0.492741	1.366188	1.954635	0	0	0
633C	0	0	0	0.97014	1.954636	2.174732	0	0	0	0	0	0	0	0	0	0	0	0	0.970138	1.954635	2.174726	0	0	0
671A	0	0	0	0	0	0	0	0	0	0	0	0	0	0	0	0	0	0	0	0	0	0	0	0
671B	0	0	0	0	0	0	0	0	0	0	0	0	0	0	0	0	0	0	0	0	0	0	0	0
671C	0	0	0	0	0	0	0	0	0	0	0	0	0	0	0	0	0	0	0	0	0	0	0	0
675A	0	0	0	0	0	0	0	0	0	0	0	0	0	0	0	0	0	0	0	0	0	0	0	0
675B	0	0	0	0	0	0	0	0	0	0	0	0	0	0	0	0	0	0	0	0	0	0	0	0
675C	0	0	0	0	0	0	0	0	0	0	0	0	0	0	0	0	0	0	0	0	0	0	0	0
684A	0	0	0	0	0	0	0	0	0	0	0	0	0	0	0	0	0	0	0	0	0	0	0	0
684B	0	0	0	0	0	0	0	0	0	0	0	0	0	0	0	0	0	0	0	0	0	0	0	0
684C	0	0	0	0	0	0	0	0	0	0	0	0	0	0	0	0	0	0	0	0	0	0	0	0
645A	0	0	0	0	0	0	0	0	0	0	0	0	0	0	0	0	0	0	0	0	0	0	0	0
645B	0	0	0	0	0	0	0	0	0	0	0	0	0	0	0	0	0	0	0	0	0	0	0	0
645C	0	0	0	0	0	0	0	0	0	0	0	0	0	0	0	0	0	0	0	0	0	0	0	0
634A	0	0	0	0.506224	0.492741	0.970138	0	0	0	0	0	0	0	0	0	0	0	0	0.506232	0.492739	0.97014	0	0	0
634B	0	0	0	0.492741	1.366188	1.954635	0	0	0	0	0	0	0	0	0	0	0	0	0.492739	1.366194	1.954636	0	0	0
634C	0	0	0	0.970138	1.954635	2.174726	0	0	0	0	0	0	0	0	0	0	0	0	0.97014	1.954636	2.174732	0	0	0
650A	0	0	0	0	0	0	0	0	0	0	0	0	0	0	0	0	0	0	0	0	0	0	0	0
650B	0	0	0	0	0	0	0	0	0	0	0	0	0	0	0	0	0	0	0	0	0	0	0	0
650C	0	0	0	0	0	0	0	0	0	0	0	0	0	0	0	0	0	0	0	0	0	0	0	0

Table 4.16: Difference of bus impedance matrix wrt base case

	632A	632B	632C	633A	633B	633C	671A	671B	671C	675A	675B	675C	684A	684B	684C	645A	645B	645C	634A	634B	634C	650A	650B	650C
632A	4007.929	1858.509	1858.509	4007.933	1858.511	1858.511	4007.927	1858.509	1858.509	4007.926	1858.508	1858.508	4007.927	1858.508	1858.508	4007.933	1858.511	1858.511	4007.937	1858.513	1858.513	4007.929	1858.509	1858.509
632B	1858.509	4007.929	1858.509	1858.511	4007.933	1858.511	1858.509	4007.927	1858.508	1858.508	4007.926	1858.508	1858.508	4007.927	1858.508	1858.511	4007.933	1858.511	1858.513	4007.937	1858.513	1858.509	4007.929	1858.509
632C	1858.509	1858.509	4007.929	1858.511	1858.511	4007.933	1858.509	1858.509	4007.927	1858.508	1858.508	4007.926	1858.508	1858.508	4007.927	1858.511	1858.511	4007.933	1858.513	1858.513	4007.937	1858.509	1858.509	4007.929
633A	4007.933	1858.511	1858.511	4007.937	1858.513	1858.513	4007.931	1858.51	1858.51	4007.93	1858.51	1858.51	4007.931	1858.51	1858.51	4007.937	1858.513	1858.513	4007.941	1858.515	1858.515	4007.933	1858.511	1858.511
633B	1858.511	4007.933	1858.511	1858.513	4007.937	1858.513	1858.51	4007.931	1858.51	1858.51	4007.93	1858.51	1858.51	4007.931	1858.51	1858.513	4007.937	1858.513	1858.515	4007.941	1858.515	1858.511	4007.933	1858.511
633C	1858.511	1858.511	4007.933	1858.513	1858.513	4007.937	1858.51	1858.51	4007.931	1858.51	1858.51	4007.93	1858.51	1858.51	4007.931	1858.513	1858.513	4007.937	1858.515	1858.515	4007.941	1858.511	1858.511	4007.933
671A	4007.927	1858.509	1858.509	4007.931	1858.51	1858.51	4007.925	1858.508	1858.508	4007.924	1858.507	1858.507	4007.925	1858.507	1858.507	4007.931	1858.51	1858.51	4007.935	1858.512	1858.512	4007.926	1858.508	1858.508
671B	1858.509	4007.927	1858.508	1858.51	4007.931	1858.51	1858.508	4007.925	1858.508	1858.507	4007.924	1858.507	1858.507	4007.925	1858.507	1858.51	4007.931	1858.51	1858.512	4007.935	1858.512	1858.508	4007.926	1858.508
671C	1858.509	1858.509	4007.927	1858.51	1858.51	4007.931	1858.508	1858.508	4007.925	1858.507	1858.507	4007.924	1858.507	1858.507	4007.925	1858.51	1858.51	4007.931	1858.512	1858.512	4007.935	1858.508	1858.508	4007.926
675A	4007.926	1858.508	1858.508	4007.93	1858.51	1858.51	4007.924	1858.507	1858.507	4007.923	1858.507	1858.507	4007.924	1858.507	1858.507	4007.93	1858.51	1858.51	4007.934	1858.511	1858.511	4007.925	1858.508	1858.508
675B	1858.508	4007.926	1858.508	1858.51	4007.93	1858.51	1858.507	4007.924	1858.507	1858.507	4007.923	1858.507	1858.507	4007.924	1858.507	1858.51	4007.93	1858.51	1858.511	4007.934	1858.511	1858.508	4007.925	1858.508
675C	1858.508	1858.508	4007.926	1858.51	1858.51	4007.93	1858.507	1858.507	4007.924	1858.507	1858.507	4007.923	1858.507	1858.507	4007.924	1858.51	1858.51	4007.93	1858.511	1858.511	4007.934	1858.508	1858.508	4007.925
684A	4007.927	1858.508	1858.508	4007.931	1858.51	1858.51	4007.925	1858.507	1858.507	4007.924	1858.507	1858.507	4007.924	1858.507	1858.507	4007.931	1858.51	1858.51	4007.934	1858.512	1858.512	4007.926	1858.508	1858.508
684B	1858.508	4007.927	1858.508	1858.51	4007.931	1858.51	1858.507	4007.925	1858.507	1858.507	4007.924	1858.507	1858.507	4007.924	1858.507	1858.51	4007.931	1858.51	1858.512	4007.934	1858.512	1858.508	4007.926	1858.508
684C	1858.508	1858.508	4007.927	1858.51	1858.51	4007.931	1858.507	1858.507	4007.925	1858.507	1858.507	4007.924	1858.507	1858.507	4007.924	1858.51	1858.51	4007.931	1858.512	1858.512	4007.934	1858.508	1858.508	4007.926
645A	4007.933	1858.511	1858.511	4007.937	1858.513	1858.513	4007.931	1858.51	1858.51	4007.93	1858.51	1858.51	4007.931	1858.51	1858.51	4007.937	1858.513	1858.513	4007.941	1858.515	1858.515	4007.933	1858.511	1858.511
645B	1858.511	4007.933	1858.511	1858.513	4007.937	1858.513	1858.51	4007.931	1858.51	1858.51	4007.93	1858.51	1858.51	4007.931	1858.51	1858.513	4007.937	1858.513	1858.515	4007.941	1858.515	1858.511	4007.933	1858.511
645C	1858.511	1858.511	4007.933	1858.513	1858.513	4007.937	1858.51	1858.51	4007.931	1858.51	1858.51	4007.93	1858.51	1858.51	4007.931	1858.513	1858.513	4007.937	1858.515	1858.515	4007.941	1858.511	1858.511	4007.933
634A	4007.937	1858.513	1858.513	4007.941	1858.515	1858.515	4007.935	1858.512	1858.512	4007.934	1858.511	1858.511	4007.934	1858.512	1858.512	4007.941	1858.515	1858.515	4007.944	1858.516	1858.517	4007.936	1858.513	1858.513
634B	1858.513	4007.937	1858.513	1858.515	4007.941	1858.515	1858.512	4007.935	1858.512	1858.511	4007.934	1858.511	1858.512	4007.934	1858.512	1858.515	4007.941	1858.515	1858.516	4007.943	1858.516	1858.513	4007.936	1858.513
634C	1858.513	1858.513	4007.937	1858.515	1858.515	4007.941	1858.512	1858.512	4007.935	1858.511	1858.511	4007.934	1858.512	1858.512	4007.934	1858.515	1858.515	4007.941	1858.517	1858.516	4007.944	1858.513	1858.513	4007.936
650A	4007.929	1858.509	1858.509	4007.933	1858.511	1858.511	4007.926	1858.508	1858.508	4007.925	1858.508	1858.508	4007.926	1858.508	1858.508	4007.933	1858.511	1858.511	4007.936	1858.513	1858.513	4007.928	1858.509	1858.509
650B	1858.509	4007.929	1858.509	1858.511	4007.933	1858.511	1858.508	4007.926	1858.508	1858.508	4007.925	1858.508	1858.508	4007.926	1858.508	1858.511	4007.933	1858.511	1858.513	4007.936	1858.513	1858.509	4007.928	1858.509
650C	1858.509	1858.509	4007.929	1858.511	1858.511	4007.933	1858.508	1858.508	4007.926	1858.508	1858.508	4007.925	1858.508	1858.508	4007.926	1858.511	1858.511	4007.933	1858.513	1858.513	4007.936	1858.509	1858.509	4007.928

Table 4.17: Difference of Jacobian matrix wrt base case

	632A	632B	632C	633A	633B	633C	671A	671B	671C	675A	675B	675C	684A	684B	684C	645A	645B	645C	634A	634B	634C	632A	632B	632C	633A	633B	633C	671A	671B	671C	675A	675B	675C	684A	684B	684C	645A	645B	645C	634A	634B	634C
632A	0.00	0.00	0.00	0.00	0.00	0.00	0.00	0.00	0.00	0.00	0.00	0.00	0.00	0.00	0.00	0.00	0.00	0.00	0.00	0.00	0.00	0.00	0.00	0.00	0.00	0.00	0.00	0.00	0.00	0.00	0.00	0.00	0.00	0.00	0.00	0.00	0.00	0.00	0.00	0.00	0.00	0.00
632B	0.00	0.00	0.00	0.00	0.00	0.00	0.00	0.00	0.00	0.00	0.00	0.00	0.00	0.00	0.00	0.00	0.00	0.00	0.00	0.00	0.00	0.00	0.00	0.00	0.00	0.00	0.00	0.00	0.00	0.00	0.00	0.00	0.00	0.00	0.00	0.00	0.00	0.00	0.00	0.00	0.00	0.00
632C	0.00	0.00	0.00	0.00	0.00	0.00	0.00	0.00	0.00	0.00	0.00	0.00	0.00	0.00	0.00	0.00	0.00	0.00	0.00	0.00	0.00	0.00	0.00	0.00	0.00	0.00	0.00	0.00	0.00	0.00	0.00	0.00	0.00	0.00	0.00	0.00	0.00	0.00	0.00	0.00	0.00	0.00
633A	0.00	0.00	0.00	**-0.34**	**0.47**	**0.32**	0.00	0.00	0.00	0.00	0.00	0.00	0.00	0.00	0.00	0.00	0.00	0.00	**0.34**	**-0.47**	**-0.32**	0.00	0.00	0.00	**-0.32**	**0.02**	**-0.83**	0.00	0.00	0.00	0.00	0.00	0.00	0.00	0.00	0.00	0.00	0.00	0.00	**0.34**	**-0.03**	**0.83**
633B	0.00	0.00	0.00	**-0.26**	**-0.87**	**-1.86**	0.00	0.00	0.00	0.00	0.00	0.00	0.00	0.00	0.00	0.00	0.00	0.00	**0.26**	**0.89**	**1.86**	0.00	0.00	0.00	**0.38**	**-0.93**	**0.20**	0.00	0.00	0.00	0.00	0.00	0.00	0.00	0.00	0.00	0.00	0.00	0.00	**-0.37**	**0.92**	**-0.19**
633C	0.00	0.00	0.00	**-0.92**	**0.75**	**-1.30**	0.00	0.00	0.00	0.00	0.00	0.00	0.00	0.00	0.00	0.00	0.00	0.00	**0.92**	**-0.76**	**1.30**	0.00	0.00	0.00	**0.15**	**-1.64**	**-1.57**	0.00	0.00	0.00	0.00	0.00	0.00	0.00	0.00	0.00	0.00	0.00	0.00	**-0.14**	**1.62**	**1.57**
671A	0.00	0.00	0.00	0.00	0.00	0.00	0.00	0.00	0.00	0.00	0.00	0.00	0.00	0.00	0.00	0.00	0.00	0.00	0.00	0.00	0.00	0.00	0.00	0.00	0.00	0.00	0.00	0.00	0.00	0.00	0.00	0.00	0.00	0.00	0.00	0.00	0.00	0.00	0.00	0.00	0.00	0.00
671B	0.00	0.00	0.00	0.00	0.00	0.00	0.00	0.00	0.00	0.00	0.00	0.00	0.00	0.00	0.00	0.00	0.00	0.00	0.00	0.00	0.00	0.00	0.00	0.00	0.00	0.00	0.00	0.00	0.00	0.00	0.00	0.00	0.00	0.00	0.00	0.00	0.00	0.00	0.00	0.00	0.00	0.00
671C	0.00	0.00	0.00	0.00	0.00	0.00	0.00	0.00	0.00	0.00	0.00	0.00	0.00	0.00	0.00	0.00	0.00	0.00	0.00	0.00	0.00	0.00	0.00	0.00	0.00	0.00	0.00	0.00	0.00	0.00	0.00	0.00	0.00	0.00	0.00	0.00	0.00	0.00	0.00	0.00	0.00	0.00
675A	0.00	0.00	0.00	0.00	0.00	0.00	0.00	0.00	0.00	0.00	0.00	0.00	0.00	0.00	0.00	0.00	0.00	0.00	0.00	0.00	0.00	0.00	0.00	0.00	0.00	0.00	0.00	0.00	0.00	0.00	0.00	0.00	0.00	0.00	0.00	0.00	0.00	0.00	0.00	0.00	0.00	0.00
675B	0.00	0.00	0.00	0.00	0.00	0.00	0.00	0.00	0.00	0.00	0.00	0.00	0.00	0.00	0.00	0.00	0.00	0.00	0.00	0.00	0.00	0.00	0.00	0.00	0.00	0.00	0.00	0.00	0.00	0.00	0.00	0.00	0.00	0.00	0.00	0.00	0.00	0.00	0.00	0.00	0.00	0.00
675C	0.00	0.00	0.00	0.00	0.00	0.00	0.00	0.00	0.00	0.00	0.00	0.00	0.00	0.00	0.00	0.00	0.00	0.00	0.00	0.00	0.00	0.00	0.00	0.00	0.00	0.00	0.00	0.00	0.00	0.00	0.00	0.00	0.00	0.00	0.00	0.00	0.00	0.00	0.00	0.00	0.00	0.00
684A	0.00	0.00	0.00	0.00	0.00	0.00	0.00	0.00	0.00	0.00	0.00	0.00	0.00	0.00	0.00	0.00	0.00	0.00	0.00	0.00	0.00	0.00	0.00	0.00	0.00	0.00	0.00	0.00	0.00	0.00	0.00	0.00	0.00	0.00	0.00	0.00	0.00	0.00	0.00	0.00	0.00	0.00
684B	0.00	0.00	0.00	0.00	0.00	0.00	0.00	0.00	0.00	0.00	0.00	0.00	0.00	0.00	0.00	0.00	0.00	0.00	0.00	0.00	0.00	0.00	0.00	0.00	0.00	0.00	0.00	0.00	0.00	0.00	0.00	0.00	0.00	0.00	0.00	0.00	0.00	0.00	0.00	0.00	0.00	0.00
684C	0.00	0.00	0.00	0.00	0.00	0.00	0.00	0.00	0.00	0.00	0.00	0.00	0.00	0.00	0.00	0.00	0.00	0.00	0.00	0.00	0.00	0.00	0.00	0.00	0.00	0.00	0.00	0.00	0.00	0.00	0.00	0.00	0.00	0.00	0.00	0.00	0.00	0.00	0.00	0.00	0.00	0.00
645A	0.00	0.00	0.00	0.00	0.00	0.00	0.00	0.00	0.00	0.00	0.00	0.00	0.00	0.00	0.00	0.00	0.00	0.00	0.00	0.00	0.00	0.00	0.00	0.00	0.00	0.00	0.00	0.00	0.00	0.00	0.00	0.00	0.00	0.00	0.00	0.00	0.00	0.00	0.00	0.00	0.00	0.00
645B	0.00	0.00	0.00	0.00	0.00	0.00	0.00	0.00	0.00	0.00	0.00	0.00	0.00	0.00	0.00	0.00	0.00	0.00	0.00	0.00	0.00	0.00	0.00	0.00	0.00	0.00	0.00	0.00	0.00	0.00	0.00	0.00	0.00	0.00	0.00	0.00	0.00	0.00	0.00	0.00	0.00	0.00
645C	0.00	0.00	0.00	0.00	0.00	0.00	0.00	0.00	0.00	0.00	0.00	0.00	0.00	0.00	0.00	0.00	0.00	0.00	0.00	0.00	0.00	0.00	0.00	0.00	0.00	0.00	0.00	0.00	0.00	0.00	0.00	0.00	0.00	0.00	0.00	0.00	0.00	0.00	0.00	0.00	0.00	0.00
634A	0.00	0.00	0.00	**0.35**	**-0.46**	**-0.32**	0.00	0.00	0.00	0.00	0.00	0.00	0.00	0.00	0.00	0.00	0.00	0.00	**-0.35**	**0.46**	**0.32**	0.00	0.00	0.00	**0.34**	**-0.02**	**0.83**	0.00	0.00	0.00	0.00	0.00	0.00	0.00	0.00	0.00	0.00	0.00	0.00	**-0.35**	**0.03**	**-0.83**
634B	0.00	0.00	0.00	**0.24**	**0.84**	**1.84**	0.00	0.00	0.00	0.00	0.00	0.00	0.00	0.00	0.00	0.00	0.00	0.00	**-0.25**	**-0.86**	**-1.84**	0.00	0.00	0.00	**-0.39**	**0.93**	**-0.20**	0.00	0.00	0.00	0.00	0.00	0.00	0.00	0.00	0.00	0.00	0.00	0.00	**0.38**	**-0.91**	**0.19**
634C	0.00	0.00	0.00	**0.91**	**-0.74**	**1.29**	0.00	0.00	0.00	0.00	0.00	0.00	0.00	0.00	0.00	0.00	0.00	0.00	**-0.91**	**0.75**	**-1.29**	0.00	0.00	0.00	**-0.15**	**1.63**	**1.56**	0.00	0.00	0.00	0.00	0.00	0.00	0.00	0.00	0.00	0.00	0.00	0.00	**0.14**	**-1.62**	**-1.57**
632A	0.00	0.00	0.00	0.00	0.00	0.00	0.00	0.00	0.00	0.00	0.00	0.00	0.00	0.00	0.00	0.00	0.00	0.00	0.00	0.00	0.00	0.00	0.00	0.00	0.00	0.00	0.00	0.00	0.00	0.00	0.00	0.00	0.00	0.00	0.00	0.00	0.00	0.00	0.00	0.00	0.00	0.00
632B	0.00	0.00	0.00	0.00	0.00	0.00	0.00	0.00	0.00	0.00	0.00	0.00	0.00	0.00	0.00	0.00	0.00	0.00	0.00	0.00	0.00	0.00	0.00	0.00	0.00	0.00	0.00	0.00	0.00	0.00	0.00	0.00	0.00	0.00	0.00	0.00	0.00	0.00	0.00	0.00	0.00	0.00
632C	0.00	0.00	0.00	0.00	0.00	0.00	0.00	0.00	0.00	0.00	0.00	0.00	0.00	0.00	0.00	0.00	0.00	0.00	0.00	0.00	0.00	0.00	0.00	0.00	0.00	0.00	0.00	0.00	0.00	0.00	0.00	0.00	0.00	0.00	0.00	0.00	0.00	0.00	0.00	0.00	0.00	0.00
633A	0.00	0.00	0.00	**-0.34**	**0.02**	**-0.87**	0.00	0.00	0.00	0.00	0.00	0.00	0.00	0.00	0.00	0.00	0.00	0.00	**0.34**	**-0.03**	**0.87**	0.00	0.00	0.00	**0.33**	**-0.45**	**-0.31**	0.00	0.00	0.00	0.00	0.00	0.00	0.00	0.00	0.00	0.00	0.00	0.00	**-0.33**	**0.45**	**0.31**
633B	0.00	0.00	0.00	**0.40**	**-0.98**	**0.21**	0.00	0.00	0.00	0.00	0.00	0.00	0.00	0.00	0.00	0.00	0.00	0.00	**-0.40**	**0.97**	**-0.20**	0.00	0.00	0.00	**0.25**	**0.83**	**1.78**	0.00	0.00	0.00	0.00	0.00	0.00	0.00	0.00	0.00	0.00	0.00	0.00	**-0.24**	**-0.84**	**-1.77**
633C	0.00	0.00	0.00	**0.16**	**-1.71**	**-1.63**	0.00	0.00	0.00	0.00	0.00	0.00	0.00	0.00	0.00	0.00	0.00	0.00	**-0.15**	**1.71**	**1.63**	0.00	0.00	0.00	**0.88**	**-0.72**	**1.24**	0.00	0.00	0.00	0.00	0.00	0.00	0.00	0.00	0.00	0.00	0.00	0.00	**-0.87**	**0.72**	**-1.24**
671A	0.00	0.00	0.00	0.00	0.00	0.00	0.00	0.00	0.00	0.00	0.00	0.00	0.00	0.00	0.00	0.00	0.00	0.00	0.00	0.00	0.00	0.00	0.00	0.00	0.00	0.00	0.00	0.00	0.00	0.00	0.00	0.00	0.00	0.00	0.00	0.00	0.00	0.00	0.00	0.00	0.00	0.00
671B	0.00	0.00	0.00	0.00	0.00	0.00	0.00	0.00	0.00	0.00	0.00	0.00	0.00	0.00	0.00	0.00	0.00	0.00	0.00	0.00	0.00	0.00	0.00	0.00	0.00	0.00	0.00	0.00	0.00	0.00	0.00	0.00	0.00	0.00	0.00	0.00	0.00	0.00	0.00	0.00	0.00	0.00
671C	0.00	0.00	0.00	0.00	0.00	0.00	0.00	0.00	0.00	0.00	0.00	0.00	0.00	0.00	0.00	0.00	0.00	0.00	0.00	0.00	0.00	0.00	0.00	0.00	0.00	0.00	0.00	0.00	0.00	0.00	0.00	0.00	0.00	0.00	0.00	0.00	0.00	0.00	0.00	0.00	0.00	0.00
675A	0.00	0.00	0.00	0.00	0.00	0.00	0.00	0.00	0.00	0.00	0.00	0.00	0.00	0.00	0.00	0.00	0.00	0.00	0.00	0.00	0.00	0.00	0.00	0.00	0.00	0.00	0.00	0.00	0.00	0.00	0.00	0.00	0.00	0.00	0.00	0.00	0.00	0.00	0.00	0.00	0.00	0.00
675B	0.00	0.00	0.00	0.00	0.00	0.00	0.00	0.00	0.00	0.00	0.00	0.00	0.00	0.00	0.00	0.00	0.00	0.00	0.00	0.00	0.00	0.00	0.00	0.00	0.00	0.00	0.00	0.00	0.00	0.00	0.00	0.00	0.00	0.00	0.00	0.00	0.00	0.00	0.00	0.00	0.00	0.00
675C	0.00	0.00	0.00	0.00	0.00	0.00	0.00	0.00	0.00	0.00	0.00	0.00	0.00	0.00	0.00	0.00	0.00	0.00	0.00	0.00	0.00	0.00	0.00	0.00	0.00	0.00	0.00	0.00	0.00	0.00	0.00	0.00	0.00	0.00	0.00	0.00	0.00	0.00	0.00	0.00	0.00	0.00
684A	0.00	0.00	0.00	0.00	0.00	0.00	0.00	0.00	0.00	0.00	0.00	0.00	0.00	0.00	0.00	0.00	0.00	0.00	0.00	0.00	0.00	0.00	0.00	0.00	0.00	0.00	0.00	0.00	0.00	0.00	0.00	0.00	0.00	0.00	0.00	0.00	0.00	0.00	0.00	0.00	0.00	0.00
684B	0.00	0.00	0.00	0.00	0.00	0.00	0.00	0.00	0.00	0.00	0.00	0.00	0.00	0.00	0.00	0.00	0.00	0.00	0.00	0.00	0.00	0.00	0.00	0.00	0.00	0.00	0.00	0.00	0.00	0.00	0.00	0.00	0.00	0.00	0.00	0.00	0.00	0.00	0.00	0.00	0.00	0.00
684C	0.00	0.00	0.00	0.00	0.00	0.00	0.00	0.00	0.00	0.00	0.00	0.00	0.00	0.00	0.00	0.00	0.00	0.00	0.00	0.00	0.00	0.00	0.00	0.00	0.00	0.00	0.00	0.00	0.00	0.00	0.00	0.00	0.00	0.00	0.00	0.00	0.00	0.00	0.00	0.00	0.00	0.00
645A	0.00	0.00	0.00	0.00	0.00	0.00	0.00	0.00	0.00	0.00	0.00	0.00	0.00	0.00	0.00	0.00	0.00	0.00	0.00	0.00	0.00	0.00	0.00	0.00	0.00	0.00	0.00	0.00	0.00	0.00	0.00	0.00	0.00	0.00	0.00	0.00	0.00	0.00	0.00	0.00	0.00	0.00
645B	0.00	0.00	0.00	0.00	0.00	0.00	0.00	0.00	0.00	0.00	0.00	0.00	0.00	0.00	0.00	0.00	0.00	0.00	0.00	0.00	0.00	0.00	0.00	0.00	0.00	0.00	0.00	0.00	0.00	0.00	0.00	0.00	0.00	0.00	0.00	0.00	0.00	0.00	0.00	0.00	0.00	0.00
645C	0.00	0.00	0.00	0.00	0.00	0.00	0.00	0.00	0.00	0.00	0.00	0.00	0.00	0.00	0.00	0.00	0.00	0.00	0.00	0.00	0.00	0.00	0.00	0.00	0.00	0.00	0.00	0.00	0.00	0.00	0.00	0.00	0.00	0.00	0.00	0.00	0.00	0.00	0.00	0.00	0.00	0.00
634A	0.00	0.00	0.00	**0.35**	**-0.02**	**0.87**	0.00	0.00	0.00	0.00	0.00	0.00	0.00	0.00	0.00	0.00	0.00	0.00	**-0.35**	**0.03**	**-0.87**	0.00	0.00	0.00	**-0.33**	**0.44**	**0.31**	0.00	0.00	0.00	0.00	0.00	0.00	0.00	0.00	0.00	0.00	0.00	0.00	**0.33**	**-0.44**	**-0.31**
634B	0.00	0.00	0.00	**-0.40**	**0.97**	**-0.21**	0.00	0.00	0.00	0.00	0.00	0.00	0.00	0.00	0.00	0.00	0.00	0.00	**0.40**	**-0.96**	**0.20**	0.00	0.00	0.00	**-0.23**	**-0.80**	**-1.76**	0.00	0.00	0.00	0.00	0.00	0.00	0.00	0.00	0.00	0.00	0.00	0.00	**0.23**	**0.81**	**1.75**
634C	0.00	0.00	0.00	**-0.15**	**1.70**	**1.63**	0.00	0.00	0.00	0.00	0.00	0.00	0.00	0.00	0.00	0.00	0.00	0.00	**0.15**	**-1.70**	**-1.63**	0.00	0.00	0.00	**-0.87**	**0.71**	**-1.23**	0.00	0.00	0.00	0.00	0.00	0.00	0.00	0.00	0.00	0.00	0.00	0.00	**0.87**	**-0.71**	**1.23**

Table 4.18: Difference of inverse reduced Jacobian wrt base case

	632A	632B	632C	633A	633B	633C	671A	671B	671C	675A	675B	675C	684A	684B	684C	645A	645B	645C	634A	634B	634C
632A	0.0000	0.0000	0.0000	0.0000	0.0000	0.0000	0.0000	0.0000	0.0000	0.0000	0.0000	0.0000	0.0000	0.0000	0.0000	0.0000	0.0000	0.0000	**0.0001**	**-0.0001**	0.0000
632B	0.0000	0.0000	0.0000	0.0000	0.0000	0.0000	0.0000	0.0000	0.0000	0.0000	0.0000	0.0000	0.0000	0.0000	0.0000	0.0000	0.0000	0.0000	-0.0001	0.0000	0.0000
632C	0.0000	0.0000	0.0000	0.0000	0.0000	0.0000	0.0000	0.0000	0.0000	0.0000	0.0000	0.0000	0.0000	0.0000	0.0000	0.0000	0.0000	0.0000	0.0000	0.0001	**0.0001**
633A	0.0000	0.0000	0.0000	0.0000	0.0000	0.0000	0.0000	0.0000	0.0000	0.0000	0.0000	0.0000	0.0000	0.0000	0.0000	0.0000	0.0000	0.0000	**0.0002**	**-0.0002**	-0.0001
633B	0.0000	0.0000	0.0000	0.0000	0.0000	0.0000	0.0000	0.0000	0.0000	0.0000	0.0000	0.0000	0.0000	0.0000	0.0000	0.0000	0.0000	0.0000	**-0.0001**	0.0000	0.0000
633C	0.0000	0.0000	0.0000	0.0000	0.0000	0.0000	0.0000	0.0000	0.0000	0.0000	0.0000	0.0000	0.0000	0.0000	0.0000	0.0000	0.0000	0.0000	0.0001	**0.0001**	**0.0003**
671A	0.0000	0.0000	0.0000	0.0000	0.0000	0.0000	0.0000	0.0000	0.0000	0.0000	0.0000	0.0000	0.0000	0.0000	0.0000	0.0000	0.0000	0.0000	**0.0001**	**-0.0001**	0.0000
671B	0.0000	0.0000	0.0000	0.0000	0.0000	0.0000	0.0000	0.0000	0.0000	0.0000	0.0000	0.0000	0.0000	0.0000	0.0000	0.0000	0.0000	0.0000	-0.0001	0.0000	0.0000
671C	0.0000	0.0000	0.0000	0.0000	0.0000	0.0000	0.0000	0.0000	0.0000	0.0000	0.0000	0.0000	0.0000	0.0000	0.0000	0.0000	0.0000	0.0000	0.0000	0.0001	**0.0002**
675A	0.0000	0.0000	0.0000	0.0000	0.0000	0.0000	0.0000	0.0000	0.0000	0.0000	0.0000	0.0000	0.0000	0.0000	0.0000	0.0000	0.0000	0.0000	**0.0001**	**-0.0001**	0.0000
675B	0.0000	0.0000	0.0000	0.0000	0.0000	0.0000	0.0000	0.0000	0.0000	0.0000	0.0000	0.0000	0.0000	0.0000	0.0000	0.0000	0.0000	0.0000	-0.0001	0.0000	0.0000
675C	0.0000	0.0000	0.0000	0.0000	0.0000	0.0000	0.0000	0.0000	0.0000	0.0000	0.0000	0.0000	0.0000	0.0000	0.0000	0.0000	0.0000	0.0000	0.0001	0.0001	**0.0002**
684A	0.0000	0.0000	0.0000	0.0000	0.0000	0.0000	0.0000	0.0000	0.0000	0.0000	0.0000	0.0000	0.0000	0.0000	0.0000	0.0000	0.0000	0.0000	**0.0001**	**-0.0001**	0.0000
684B	0.0000	0.0000	0.0000	0.0000	0.0000	0.0000	0.0000	0.0000	0.0000	0.0000	0.0000	0.0000	0.0000	0.0000	0.0000	0.0000	0.0000	0.0000	-0.0001	0.0000	0.0000
684C	0.0000	0.0000	0.0000	0.0000	0.0000	0.0000	0.0000	0.0000	0.0000	0.0000	0.0000	0.0000	0.0000	0.0000	0.0000	0.0000	0.0000	0.0000	0.0000	0.0001	**0.0002**
645A	0.0000	0.0000	0.0000	0.0000	0.0000	0.0000	0.0000	0.0000	0.0000	0.0000	0.0000	0.0000	0.0000	0.0000	0.0000	0.0000	0.0000	0.0000	**0.0002**	**-0.0002**	-0.0001
645B	0.0000	0.0000	0.0000	0.0000	0.0000	0.0000	0.0000	0.0000	0.0000	0.0000	0.0000	0.0000	0.0000	0.0000	0.0000	0.0000	0.0000	0.0000	**-0.0001**	0.0000	0.0000
645C	0.0000	0.0000	0.0000	0.0000	0.0000	0.0000	0.0000	0.0000	0.0000	0.0000	0.0000	0.0000	0.0000	0.0000	0.0000	0.0000	0.0000	0.0000	0.0001	**0.0001**	**0.0003**
634A	0.0000	0.0000	0.0001	-0.0001	-0.0001	**0.0002**	0.0000	0.0000	**0.0001**	0.0000	0.0000	**0.0001**	0.0000	0.0000	**0.0001**	-0.0001	-0.0001	**0.0002**	**0.0002**	**-0.0004**	**0.0045**
634B	-0.0001	**0.0001**	0.0000	**-0.0002**	**0.0002**	**-0.0001**	-0.0001	**0.0001**	0.0000	-0.0001	**0.0001**	0.0000	-0.0001	**0.0001**	0.0000	**-0.0002**	**0.0002**	**-0.0001**	**-0.0005**	**0.0035**	**0.0062**
634C	-0.0001	**0.0001**	0.0000	**-0.0002**	**0.0002**	0.0001	-0.0001	**0.0001**	0.0000	-0.0001	**0.0001**	0.0000	-0.0001	**0.0001**	0.0000	**-0.0002**	**0.0002**	0.0001	**0.0038**	**0.0064**	**0.0024**

DG in PQ mode

In the following three case studies, DG in PQ mode was connected at Bus 634, Bus645 and Bus 634, respectively, as shown in Fig. 4.16. In each case study, the output of DG had different level: 0%, 30%, 70% and 130% of the local loading. Only results for phase A was shown because the system was balanced, making the results for phase B and phase C exactly the same.

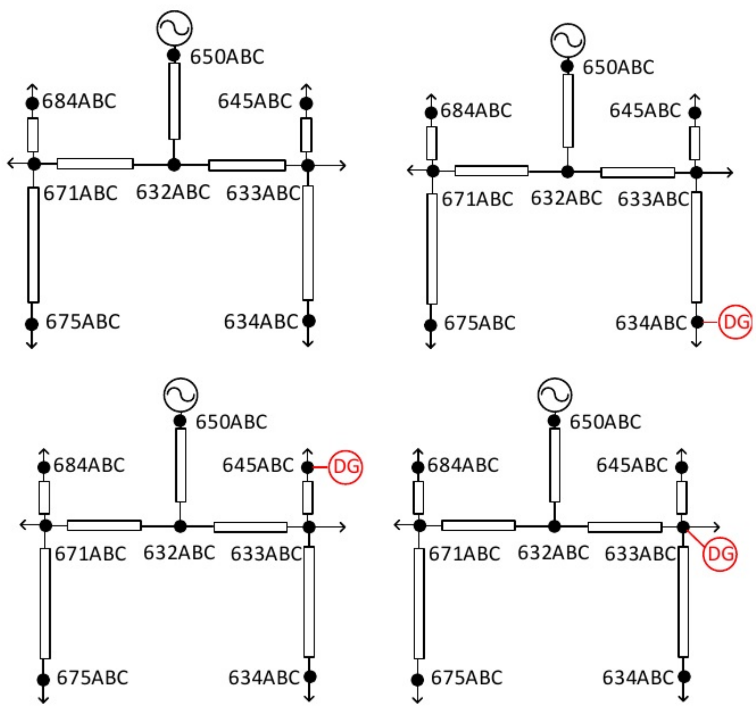

Figure 4.16: For DG case study

Table 4.19 shows the CPF scan results when DG in PQ mode was connected at Bus 634. The results reveal that by adding DG to Bus 645 on the right, the buses on the right side got stronger than the corresponding buses on the left in the same pair. For phase A, B and C, Bus 634 was stronger than Bus 675, Bus 645 was stronger than Bus 684, and

Bus 633 was stronger than Bus 671. Moreover, to our surprise, with higher DG output the difference of CPF scan results of the left and right buses was not necessarily higher. Between Bus 675 and Bus 634, the CPF scan difference were around 1.2, 6, and 0.8 for 30%, 70% and 130%, respectively. This suggests that higher amount of DG output did not necessarily strengthen the bus more. Similar observation can be made for DG in PQ mode connected at Bus 645 and Bus 633, as seen from Table 4.20 and Table 4.21.

Table 4.19: CPF scan for DG in PQ mode at Bus 634

0%		30%		70%		130%	
675A	-175.395	675A	-176.424	675A	-181.472	675A	-179.455
634A	-175.395	634A	-175.228	634A	-174.983	684A	-178.947
645A	-171.971	671A	-174.478	684A	-173.810	634A	-178.698
684A	-171.971	633A	-174.236	645A	-172.410	671A	-173.772
671A	-170.678	684A	-172.822	671A	-172.381	633A	-173.485
633A	-170.678	645A	-172.281	633A	-171.251	645A	-172.819
632A	-155.693	632A	-155.762	632A	-156.178	632A	-157.089

Table 4.20: CPF scan for DG in PQ mode at Bus 645

0%		30%		70%		130%	
675A	-175.395	675A	-176.133	675A	-176.908	675A	-178.196
634A	-175.395	634A	-175.538	684A	-176.180	684A	-177.695
645A	-171.971	684A	-172.440	634A	-175.733	634A	-176.124
684A	-171.971	645A	-171.920	645A	-175.660	671A	-172.908
671A	-170.678	671A	-171.190	671A	-175.590	645A	-172.016
633A	-170.678	633A	-170.719	633A	-170.865	633A	-171.091
632A	-155.693	632A	-155.686	632A	-156.009	632A	-156.717

Table 4.22 shows the comparison of CPF scan results with voltage ranking as well as branch power flow when DG in PQ is connected at Bus 634, outputting 70% of local load. It can be found that the ranking of CPF scan results was exactly the same as the voltage ranking. Moreover, the branch power flow matched the CPF scan results.

Table 4.21: CPF scan for DG in PQ mode at Bus 633

0%		30%		70%		130%	
675A	-175.395	675A	-179.006	675A	-181.286	675A	-177.953
634A	-175.395	671A	-177.244	634A	-175.775	634A	-176.085
645A	-171.971	634A	-175.553	633A	-174.041	671A	-175.130
684A	-171.971	684A	-172.443	684A	-173.062	645A	-175.051
671A	-170.678	645A	-172.048	645A	-172.261	633A	-174.446
633A	-170.678	633A	-170.771	671A	-171.754	684A	-174.013
632A	-155.693	632A	-155.809	632A	-158.245	632A	-156.231

Table 4.22: Comparison for 8-bus with DG in PQ at Bus 634, 70% output

CPF scan		V		P		Q	
675A	-181.472	675A	0.470	650-632a	5.314	650-632a	7.106
634A	-174.983	634A	0.498	632-671a	2.235	632-671a	2.331
684A	-173.810	684A	0.526	632-633a	2.091	632-633a	2.107
645A	-172.410	645A	0.540	671-675a	0.687	671-675a	0.619
671A	-172.381	671A	0.549	671-684a	0.647	671-684a	0.513
633A	-171.251	633A	0.562	633-645a	0.647	633-645a	0.511
632A	-156.178	632A	0.699	633-634a	0.585	633-634a	0.508

Table 4.23 shows the comparison of CPF scan results with voltage ranking as well as branch power flow when DG in PQ was connected at Bus 634, outputting 130% of local load. It can be found that the weakest bus and the pairwise ranking were the same for the CPF scan results and the voltage ranking. The overall ranking was roughly the same, except the small difference of 684, 634 and 633, 645.

Table 4.23: Comparison for 8-bus with DG in PQ at Bus 634, 130% output

CPF scan		V		P		Q	
675A	-179.455	675A	0.468	650-632a	5.284	650-632a	7.017
684A	**-178.947**	**634A**	**0.517**	632-671a	2.288	632-671a	2.400
634A	**-178.698**	**684A**	**0.526**	632-633a	2.028	632-633a	2.002
671A	-173.772	671A	0.549	671-675a	0.702	671-675a	0.635
633A	**-173.485**	**645A**	**0.550**	671-684a	0.661	671-684a	0.524
645A	**-172.819**	**633A**	**0.572**	633-645a	0.659	633-645a	0.521
632A	-157.089	632A	0.702	633-634a	0.516	633-634a	0.439

However, if the DG in PQ mode supplied X% of local load and the output was increased with loading factor λ, that is,

$$P^s_{\mathrm{DG},k} = (1+\lambda)(X\%)P^s_{\mathrm{load},k} \tag{4.62}$$

the CPF scan ranking were different, as shown in Table 4.24, Table 4.25, and Table 4.26. It can be found that the larger the DG output, the stronger the corresponding and the nearby buses. For DG at Bus 634, Bus 634 was getting stronger in the ranking as output power was increasing. Bus 634 was even stronger than 645 when DG at Bus 634 supplied 70% and 130% of the local load.

For DG at Bus 645, Bus 645 was getting stronger in the ranking. When DG at Bus 645 supplied 130% of the local load, Bus 645 was even stronger than Bus 633. Moreover, Bus 634 was getting stronger than Bus 684 and Bus 671.

For DG at Bus 633, Bus 633 ranking was the same; its ranking was the second strongest. As DG power was increased, Bus 634 was getting stronger, even stronger than Bus 684 and Bus 671 when DG at Bus 633 supplied 130% of the local load.

Table 4.24: CPF scan for DG in PQ mode at Bus 634 with output increasing with λ

0%		30%		70%		130%	
675A	-175.395	675A	-179.346	675A	-179.687	675A	-175.090
634A	-175.395	684A	-178.230	684A	-174.801	684A	-169.427
645A	-171.971	671A	-174.418	671A	-173.022	671A	-167.568
684A	-171.971	**634A**	-174.321	645A	-168.954	645A	-159.569
671A	-170.678	645A	-172.512	**634A**	-168.682	633A	-158.168
633A	-170.678	633A	-171.077	633A	-167.292	**634A**	-156.994
632A	-155.693	632A	-156.939	632A	-154.231	632A	-147.472

Table 4.25: CPF scan for DG in PQ mode at Bus 645 with output increasing with λ

CPF scan							
0%		30%		70%		130%	
675A	-175.395	675A	-176.865	675A	-176.952	675A	-172.746
634A	-175.395	671A	-174.931	634A	-173.286	684A	-167.440
645A	-171.971	634A	-174.612	684A	-172.232	671A	-165.779
684A	-171.971	684A	-172.987	671A	-170.620	634A	-162.690
671A	-170.678	**645A**	-170.656	**645A**	-166.653	633A	-158.011
633A	-170.678	633A	-169.738	633A	-166.355	**645A**	-157.703
632A	-155.693	632A	-155.349	632A	-153.190	632A	-146.375

Table 4.26: CPF scan for DG in PQ mode at Bus 633 with output increasing with λ

0%		30%		70%		130%	
675A	-175.395	675A	-176.193	675A	-175.670	675A	-171.710
634A	-175.395	634A	-174.166	684A	-174.262	684A	-166.868
645A	-171.971	684A	-172.425	634A	-170.783	671A	-164.947
684A	-171.971	671A	-170.893	671A	-169.885	634A	-163.885
671A	-170.678	645A	-170.657	645A	-167.198	645A	-159.144
633A	-170.678	**633A**	-169.323	**633A**	-165.865	**633A**	-157.774
632A	-155.693	632A	-154.786	632A	-152.318	632A	-146.140

Table 4.27 and Table 4.28 show the comparison of CPF scan results with voltage ranking as well as branch power flow when DG in PQ connected at Bus 634 supplied 70% and 130% of the local load, respectivey. It can be found that CPF scan ranking was exactly the same as the voltage ranking. Moreover, the CPF scan pairwise ranking matched the branch power flow.

Table 4.27: DG at Bus 634, 70%

CPF scan		V		P		Q	
675A	-179.687	675A	0.457	650-632a	5.148	650-632a	6.744
684A	-174.801	684A	0.520	632-671a	2.494	632-671a	2.683
671A	-173.022	671A	0.546	632-633a	1.751	632-633a	1.622
645A	-168.954	645A	0.584	671-675a	0.760	671-675a	0.702
634A	-168.682	634A	0.587	671-684a	0.710	671-684a	0.566
633A	-167.292	633A	0.607	633-645a	0.706	633-645a	0.557
632A	-154.231	632A	0.713	633-634a	0.211	633-634a	0.166

Table 4.28: DG at Bus 634, 130%

CPF scan		V		P		Q	
675A	-175.090	675A	0.459	650-632a	4.845	650-632a	6.271
684A	-169.427	684A	0.527	632-671a	2.700	632-671a	2.942
671A	-167.568	671A	0.554	632-633a	1.357	632-633a	1.201
645A	-159.569	645A	0.632	671-675a	0.820	671-675a	0.766
633A	-158.168	633A	0.654	671-684a	0.763	671-684a	0.610
634A	-156.994	634A	0.673	633-645a	0.757	633-645a	0.594
632A	-147.472	632A	0.732	633-634a	-0.220	633-634a	-0.159

DG in PV mode

In this case study, DG in PV mode was connected at different locations: Bus 634, Bus 633 and Bus 645. Table 4.29 shows the CPF scan results. The results show that by adding DG in PV to one of the three buses on the right, the bus on the right was stronger than the corresponding bus on the left, meaning that for phase A, B and C, Bus 634 was stronger than Bus 675, Bus 645 was stronger than Bus 684, and Bus 633 was stronger than Bus 671. Moreover, Bus 632 was no longer the strongest bus. Because of DG in PV mode, the distribution system had two sources: one was substation, the other was the DG in PV mode.

Table 4.29: CPF scan for DG in PV mode at different locations

No DG		Bus 634		Bus 633		Bus 645	
675A	-175.395	675A	-179.455	675A	-338.416	675A	-295.531
634A	-175.395	684A	-178.947	684A	-323.101	684A	-283.367
645A	-171.971	634A	-178.698	671A	-318.214	671A	-279.277
684A	-171.971	671A	-173.772	632A	-272.023	634A	-247.718
671A	-170.678	633A	-173.485	634A	-266.641	633A	-242.438
633A	-170.678	645A	-172.819	645A	-262.742	632A	-240.053
632A	-155.693	632A	-157.089	633A	-260.798	645A	-234.390
634B	-175.395	675B	-179.455	675B	-338.416	675B	-295.531
675B	-175.395	684B	-178.947	684B	-323.101	684B	-283.367
645B	-171.971	634B	-178.698	671B	-318.214	671B	-279.277
684B	-171.971	671B	-173.772	632B	-272.023	634B	-247.718
633B	-170.678	633B	-173.485	634B	-266.641	633B	-242.438
671B	-170.678	645B	-172.819	645B	-262.742	632B	-240.053
632B	-155.693	632B	-157.089	633B	-260.798	645B	-234.390
634C	-175.395	675C	-179.455	675C	-338.416	675C	-295.531
675C	-175.395	684C	-178.947	684C	-323.101	684C	-283.367
684C	-171.971	634C	-178.698	671C	-318.214	671C	-279.277
645C	-171.971	671C	-173.772	632C	-272.023	634C	-247.718
633C	-170.678	633C	-173.485	634C	-266.641	633C	-242.438
671C	-170.678	645C	-172.819	645C	-262.742	632C	-240.053
632C	-155.693	632C	-157.089	633C	-260.798	645C	-234.390

Another observation is that even though the ranking of buses on the left side followed the upstream/downstream pattern, the ranking of buses on the right did not. For DG at Bus 634, Bus 633 was stronger than Bus 632 because Bus 633 was closer to the source. For DG at Bus 633, Bus 634, Bus 645 and Bus 633 were stronger than Bus 632, because these three buses were closer to the source than Bus 632. For DG at Bus 645, Bus 645 was stronger than Bus 632. This DG strengthened Bus 634 and Bus 633 such that Bus 634 was even stronger than Bus 671.

Moreover, the results show that DG at Bus 633 and Bus 645 made Bus 633 and Bus 645 strongest among the buses, respectively. To our surprise, DG at Bus 634 was the exception. Even though DG at Bus 634 strengthened Bus 634, Bus 634 was not the strongest among the buses.

In conclusion, DG in PV mode made the buses on the same side stronger. Sometimes DG also made the bus at which the DG was connected strongest. Also, DG caused the ranking of buses not consistent with upstream/downstream relationship because DG introduced another source into the system.

Table 4.30 shows the comparison of CPF scan results with voltage ranking as well as branch power flow when DG in PV was connected at Bus 634. It can be found that the weakest bus and the pairwise ranking were the same for the CPF scan results and the voltage ranking. The overall ranking of CPF scan was not the same as that of voltage.

Table 4.30: Comparison for 8-bus with DG in PV at Bus 634

CPF scan		V		P		Q	
675A	-179.455	675A	0.466	650-632a	7.317	650-632a	4.669
684A	-178.947	684A	0.544	**632-633a**	3.220	632-671a	3.517
634A	-178.698	671A	0.574	**632-671a**	3.152	671-675a	0.907
671A	-173.772	632A	0.774	**633-634a**	1.242	671-684a	0.706
633A	-173.485	645A	0.779	**671-675a**	0.953	633-645a	0.672
645A	-172.819	633A	0.800	671-684a	0.878	**632-633a**	-1.400
632A	-157.089	**634A**	1.000	633-645a	0.866	**633-634a**	-3.411
		650A	1.000				

Summary

Table 4.31 summarized the case studies for 8-bus system. The pair ranking column means that whether the pair ranking matches the network characteristics. For example, if more load is connected on the right side, the buses on the right side should be weaker than that on the left side for each pair. For pair ranking perspective, CPF scan results matched the network characteristics except for the unbalanced load and the untransposed line. For these two cases, the impact of these two elements cannot be determined due to the coupling among phases. Therefore, we cannot determine whether the CPF scan results matched the network characteristics. In the comparison between CPF scan ranking and voltage ranking, the weakest bus and the pairwise ranking were the same for all the cases except for the unbalanced load and the untransposed line. The overall rankings were not the same for most of the cases.

Table 4.31: Summary of 8-Bus CPF scan case studies

Case	Pair ranking	CPF scan vs V		
		Weakest	Pair ranking	Overall
Base	V	V	V	V
Doubled	V	V	V	X
3P Cap	V	V	V	V
Unbalanced load	V(BC), ?(A)	V(BC), ?(A)	V(BC), ?(A)	X
Untran. line	??	X	X	X
DG at 70%	V	V	V	V
DG at 130%	V	V	V	X
DG at 70% increasing with λ	V	V	V	V
DG at 130% increasing with λ	V	V	V	V
DG in PV	V	V	V	X

V: consistent, X: not consistent, ??: cannot be determined, V(BC): consistent in phase B and C, ?(A): cannot be determined in phase A

4.6.2 13-node test feeder case studies

This section shows the results of applying CPF scan method to the modified IEEE 13-node test feeder with DG, shown in Fig. 4.17, as the example to show the CPF scan results for a complex three-phase unbalanced distribution system. In this modified IEEE 13-node test feeder with DG, each branch has different line configurations, each bus can be single, two or three phase, and the load at each bus/phase can be balanced or unbalanced. The detailed information of this test feeder can be found in [73].

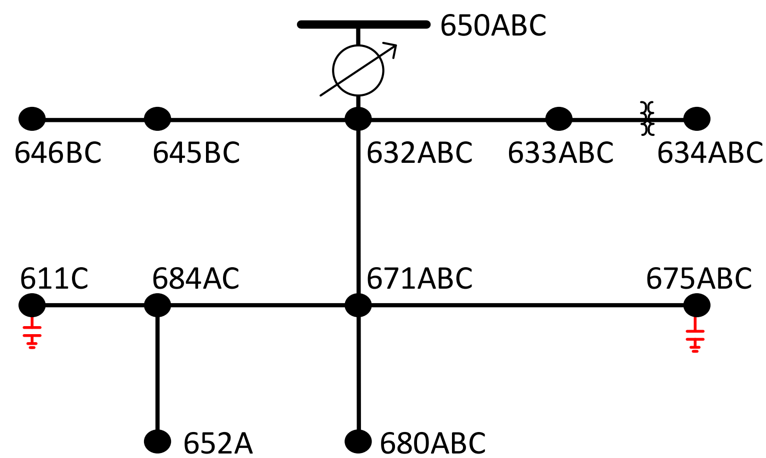

Figure 4.17: IEEE 13-node test feeder

This section first investigates the base case, then the impact of capacitors and, lastly, DG in PQ and PV mode. After that, this section demonstrates how to use CPF scan for the distribution system operation and planning.

Base case

Table 4.32 shows the CPF scan results, voltage and branch flow of IEEE 13-node test feeder. Because this 13-node test feeder is a complicated network, we cannot do the same thing as 8-Bus system, such as compare the pair ranking. In this base case, the CPF scan results did not follow upstream/downstream relationship. For example, Bus 632C was weaker than Bus 645C. Also, the overall ranking of CPF scan was not the same as the overall ranking of voltage, even the weakest bus for each phase was different. Note that the voltage ranking did not follow the upstream/downstream either. The branch power flow, on the other hand, followed the upstream/downstream.

Table 4.32: Comparison of CPF scan with V and branch power flow for 13-node test feeder

CPF scan		V		P		Q	
632A	0.247	632A	0.837	650-632A	3.228	650-632A	3.103
633A	0.339	633A	0.828	632-671A	2.493	632-671A	2.132
634A	3.595	634A	0.759	671-675A	1.093	671-675A	0.444
684A	4.060	671A	0.712	632-633A	0.374	632-633A	0.283
675A	7.336	684A	0.706	633-634A	0.371	633-634A	0.278
671A	7.666	680A	0.704	671-684A	0.290	671-680A	0.223
652A	8.847	652A	0.688	684-652A	0.289	671-684A	0.194
680A	11.040	675A	0.688	671-680A	0.220	684-652A	0.191
632B	-0.774	675B	0.870	650-632B	3.571	650-632B	3.388
633B	-0.794	671B	0.866	632-645B	1.963	632-645B	1.327
671B	-1.610	680B	0.862	632-671B	1.160	632-671B	0.835
646B	-1.646	632B	0.843	645-646B	1.041	645-646B	0.610
645B	-1.845	633B	0.838	632-633B	0.275	671-680B	0.221
634B	-1.893	634B	0.785	633-634B	0.274	632-633B	0.220
675B	-2.468	645B	0.757	671-680B	0.219	633-634B	0.218
680B	-2.491	646B	0.728	671-675B	0.147	671-675B	0.131
645C	-2.535	646C	0.842	650-632C	3.338	650-632C	3.278
632C	-2.566	645C	0.840	632-671C	2.575	632-671C	2.054
633C	-2.606	632C	0.828	671-675C	0.651	671-675C	0.468
646C	-2.764	633C	0.820	671-684C	0.385	671-680C	0.224
634C	-3.401	634C	0.766	684-611C	0.378	632-633C	0.221
684C	-4.405	671C	0.629	632-633C	0.277	633-634C	0.219
611C	-5.139	680C	0.618	633-634C	0.275	671-684C	0.186
671C	-5.156	684C	0.617	671-680C	0.221	684-611C	0.181
675C	-5.383	675C	0.616	645-646C	0.218	632-645C	0.091
680C	-5.854	611C	0.605	632-645C	0.213	645-646C	0.089

With and without capacitor

In this case study, we investigated the impact of capacitors on the CPF scan results. As shown in Fig. 4.17, a single phase capacitor and a three-phase capacitor were connected at Bus 611 and Bus 675, respectively. Table 4.33 shows the CPF scan results for different cases. The column whose heading is No C shows the CPF scan results for the case where no capacitor was connected in the system. The column whose heading is Bus 611(1P) shows the CPF scan results for the case where a single-phase capacitor was connected at Bus 611. The column whose heading is Bus 611(1P)+Bus 675(3P) shows the CPF scan results for the case where a single-phase capacitor was connected at Bus 611 and a three-phase capacitor was connected at Bus 675.. The rating of the single phase capacitor was 100 kVAr, while that of the three-phase capacitor was 200 kVAr for each of the three phases.

First, we compared 611(1P)+675(3P) column with 675(3P) column, which shows the impact of disconnecting the single-phase capacitor at Bus 611C. The results show that Bus 611C was getting weaker. Originally in 611(1P)+675(3P), Bus 611C was stronger than Bus 671C. After the single-phase capacitor was removed, Bus 611C was weaker than Bus 671C. Moreover, the rankings in Phase A and Phase B are different from these two cases. In phase A, Bus 652A was getting stronger and Bus 675A was the weakest bus. In phase B, Bus 646B became the weakest. More investigation needs to be done to explain the ranking change in phase A and phase B.

Secondly, we compared 611(1P)+675(3P) with 611(1P), which shows the impact of disconnecting the three-phase capacitor at Bus 675. To our surprise, the rankings in all

Table 4.33: CPF scan result for 13-node test feeder with/without capacitor

611(1P)+675(3P)		675(3P)		611(1P)		No C	
632A	0.247	632A	0.663	632A	0.183	632A	-1.900
633A	0.339	633A	0.796	633A	0.270	684A	-3.841
634A	3.595	652A	1.374	634A	3.558	634A	-4.374
684A	4.060	680A	3.882	684A	3.929	675A	-5.995
675A	7.336	634A	6.242	675A	7.395	671A	-6.466
671A	7.666	684A	6.552	671A	7.773	652A	-7.116
652A	8.847	671A	7.523	652A	9.008	633A	-7.588
680A	11.040	675A	8.297	680A	11.571	680A	-8.333
632B	-0.774	633B	-0.574	632B	-0.788	634B	-2.206
633B	-0.794	632B	-0.576	633B	-0.790	645B	-2.388
671B	-1.610	671B	-1.275	671B	-1.470	632B	-2.642
646B	-1.646	645B	-1.704	646B	-1.473	633B	-2.660
645B	-1.845	634B	-1.849	645B	-1.655	680B	-2.705
634B	-1.893	675B	-2.361	634B	-1.747	671B	-3.256
675B	-2.468	680B	-2.509	675B	-2.285	646B	-7.836
680B	-2.491	646B	-7.476	680B	-2.449	675B	-7.895
645C	-2.535	645C	-3.334	645C	-2.498	634C	-0.702
632C	-2.566	632C	-3.355	632C	-2.526	646C	2.073
633C	-2.606	633C	-3.432	633C	-2.568	632C	2.488
646C	-2.764	646C	-3.827	646C	-2.964	645C	2.516
634C	-3.401	634C	-4.856	634C	-3.581	633C	2.647
684C	-4.405	684C	-6.322	684C	-4.569	684C	-3.343
611C	-5.139	671C	-7.632	611C	-5.471	671C	-5.784
671C	-5.156	611C	-7.648	671C	-5.482	611C	-6.001
675C	-5.383	675C	-8.121	675C	-5.785	675C	-6.684
680C	-5.854	680C	-8.886	680C	-6.226	680C	-7.793

of the three phases were exactly the same. We expect that the impact of disconnecting a three-phase capacitor would be larger than disconnecting a sing-phase capacitor. If we take a close look at the CPF scan results, the difference between Bus 675 and 671 in phase A increased from 0.33 to 0.378, that in phase B decreased from 0.858 to 0.815, and that in phase C increased from 0.227 to 0.303. The difference showed that by removing the three-phase capacitor at Bus 675, even though the ranking was the same, Bus 675A became weaker, Bus 675B became stronger, and Bus 675C became weaker. More investigation needs to be done to explain why Bus 675B got stronger when the three-phase capacitor at Bus 675 was removed.

We can also investigate the impact of disconnecting the three-phase capacitor at Bus 675 by comparing 675(3P) with No C. Unlike the previous comparison, the ranking in all of the phases experienced changes. In phase A, both Bus 675A and Bus 684A became stronger while Bus 633 became weaker. In phase B, Bus 675B became weaker while Bus 634B became the strongest bus. In phase C, the ranking of Bus 675C was the same while Bus 634C became the strongest bus. More investigation needs to be done to explain these observed phenomena.

Lastly, we can investigate the impact of disconnecting the single-phase capacitor at Bus 611C by comparing 611(1P) with No C. As expected, 611C became weaker, CPF scan results in phase A, B and C had some changes. For phase A, Bus 633A had the biggest change and 633A became weaker. For phase B, the biggest change was Bus 634B; it became the strongest bus. For phase C, the biggest change was Bus 634C; it became the strongest bus, too.

By comparing the CPF scan results in different cases, the impact of capacitors can be investigated. However, the results did not have clear pattern and some did not match the network characteristics. The possible reason is that the CPF scan method is a highly nonlinear investigation and depends on so many factors, such as unbalanced load, untransposed line, base operating point and LID. The observation we made from the 8-bus balanced case cannot be directly applied to the 13-node test feeder. This is the reason why CPF scan method is an important tool. The ranking of CPF scan results cannot be easily inferred from the the network characteristics.

DG in PQ and PV mode

In this 13-node test feeder, we connected a DG at two possible locations: Bus 671 or Bus 675. The CPF scan method was applied to these two cases and the impact of DG was investigated.

In the first case study, a DG was connected at Bus 671, as shown in Fig.4.18. The DG could be in PQ mode or in PV mode. For DG in PQ mode, the DG supplied X% of local load. For DG in PV mode, the reactive power limit was big enough so that even at the maximum loading point, the DG was still in PV mode, not hitting its reactive power limit. Table 4.34 shows the CPF scan results for DG in PQ mode outputting different amounts of power and for DG in PV mode.

To our surprise, the results show that for DG in PQ mode, Bus 671A, Bus 671B and Bus 671C remained relatively the same. Moreover, as the DG output was increased, the

Figure 4.18: IEEE 13-node test feeder with DG at Bus 671

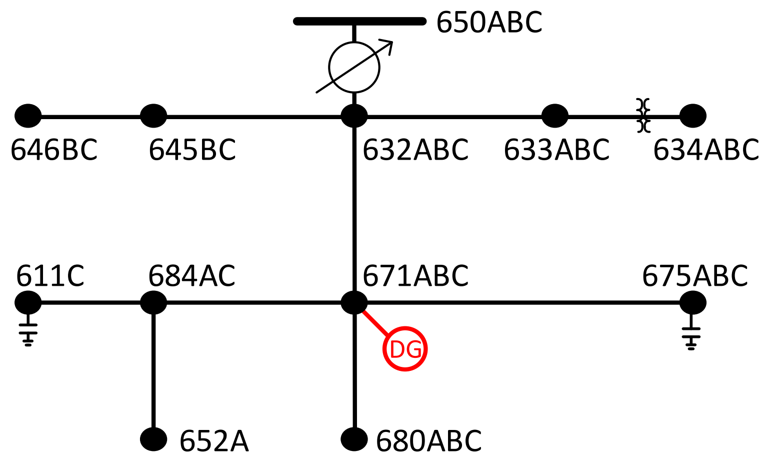

ranking in phase A and phase B did not change, while the ranking in phase C had different ranking results. For example, Bus 632C was not the strongest bus. It ranked at 2nd, 4th and 2nd for DG output was 30%, 70% and 130%, respectively. Bus 645C and Bus 633C had the similar changes. However, the differences of the CPF scan results of different buses of Bus 632C, Bus 633C and Bus 645C and Bus646C were small.

By comparing the CPF scan results for 0% and PV, the impact of the DG in PV mode can be found. Bus 671A and Bus 671C became stronger with higher ranking. Even though the ranking of Bus 671B is the same, the CPF scan value was smaller, which means that 671B became stronger. Furthermore, we can see from the ranking that Bus 684A, Bus 652A, Bus 675A, Bus 680B, Bus 675B, Bus 680C, Bus 611C, and Bus 684C became stronger.

Table 4.34: CPF scan for DG in PQ/PV mode at Bus 671

0%		30%		70%		130%		PV	
632A	0.247	632A	0.148	632A	0.236	632A	0.243	684A	-3.517
633A	0.339	633A	0.247	633A	0.319	633A	0.380	652A	-3.520
634A	3.595	634A	3.552	634A	4.193	634A	4.812	680A	-3.562
684A	4.060	684A	4.085	684A	4.500	684A	4.911	675A	-3.578
675A	7.336	675A	7.563	675A	8.099	675A	9.081	671A	-4.084
671A	7.666	671A	7.873	671A	8.351	671A	9.398	632A	-4.325
652A	8.847	652A	9.216	652A	9.750	652A	11.138	633A	-4.419
680A	11.040	680A	11.529	680A	12.295	680A	13.780	634A	-5.560
632B	-0.774	632B	-0.978	632B	-1.107	632B	-1.306	632B	-0.069
633B	-0.794	633B	-0.981	633B	-1.113	633B	-1.316	633B	0.140
671B	-1.610	671B	-1.745	671B	-1.936	671B	-2.306	680B	-1.105
646B	-1.646	646B	-1.793	646B	-2.000	646B	-2.485	671B	-1.115
645B	-1.845	645B	-1.938	645B	-2.201	645B	-2.703	675B	-1.116
634B	-1.893	634B	-2.062	634B	-2.342	634B	-2.861	634B	6.406
675B	-2.468	675B	-2.632	675B	-2.908	675B	-3.419	645B	10.117
680B	-2.491	680B	-2.842	680B	-3.071	680B	-3.604	646B	12.064
645C	-2.535	645C	-2.723	633C	-3.019	645C	-3.251	645C	-2.105
632C	-2.566	632C	-2.757	645C	-3.063	632C	-3.295	633C	-2.337
633C	-2.606	633C	-2.826	646C	-3.099	633C	-3.359	632C	-2.377
646C	-2.764	646C	-2.951	632C	-3.101	646C	-3.469	646C	-2.643
634C	-3.401	634C	-3.553	634C	-3.722	634C	-4.123	680C	-3.079
684C	-4.405	684C	-4.718	684C	-5.069	684C	-5.501	611C	-3.089
611C	-5.139	671C	-5.421	671C	-5.695	671C	-6.346	671C	-3.101
671C	-5.156	611C	-5.436	611C	-5.725	611C	-6.404	684C	-3.101
675C	-5.383	675C	-5.730	675C	-5.964	675C	-6.616	675C	-3.106
680C	-5.854	680C	-6.227	680C	-6.462	680C	-7.159	634C	-3.169

In the second case study related to DG, a DG was connected at Bus 675, as shown in Fig. 4.19. The same setup as the previous case study was applied. Table 4.35 shows the CPF scan results for DG in PQ mode outputting different amounts of power and for DG in PV mode.

For DG in PQ mode, there was no clear pattern for Bus 675A, Bus 675B and Bus 675C. Bus 675A and Bus 675B got stronger at 70% while got weaker at 130%, while Bus

Figure 4.19: IEEE 13-node test feeder with DG at Bus 675

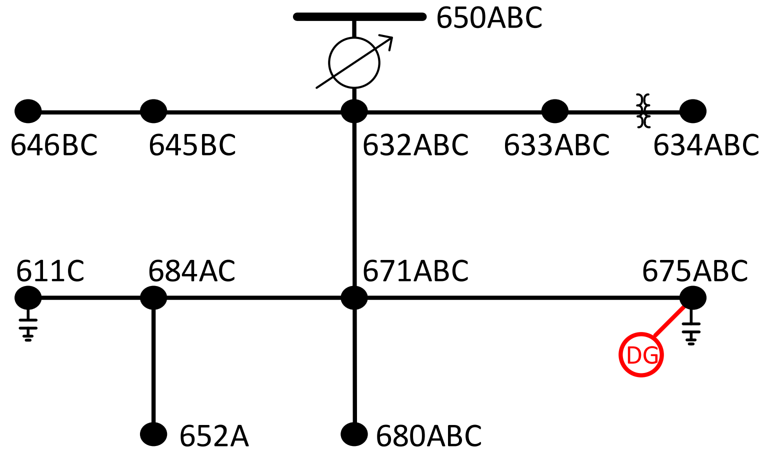

675C got weaker at 70% and relatively the same at 30% and 130%. Moreover, as the DG output was increased, the ranking in all of the three phase changed. No pattern were found in these changes.

By comparing the CPF scan results for 0% and PV, the impact of the DG in PV mode can be found. Bus 675A, Bus 675B, and Bus 675C were all getting stronger. Moreover, we can see from the ranking that Bus 684A, Bus 652A, Bus 671A, Bus 680B, Bus 671B, Bus 680C became stronger.

The results show that for DG in PQ mode, Bus 671C was getting stronger as the DG output was increased; however, Bus 671A and Bus 671B remained relatively the same. Moreover, as the DG output was increased, the ranking in phase A and phase B did not change, while the ranking in phase C were changed. For example, Bus 632C was not the strongest bus. It ranked at 2nd, 4th and 2nd when DG output was 30%, 70% and 130%, respectively. Bus 645C and Bus 633C had the similar change. However, the difference of the CPF scan results of different buses of Bus 632C, Bus 633C and Bus 645C and Bus646C

Table 4.35: CPF scan for DG in PQ and PV mode at Bus 675

0%		30%		70%		130%		PV	
632A	0.247	632A	0.611	632A	-2.017	632A	-3.283	**675A**	-4.154
633A	0.339	633A	0.727	684A	-3.467	633A	-3.346	671A	-4.194
634A	3.595	634A	5.452	634A	-4.282	634A	-4.261	684A	-4.197
684A	4.060	684A	5.789	**675A**	-5.278	684A	-4.273	652A	-4.211
675A	7.336	**675A**	10.422	671A	-5.737	**675A**	-4.708	680A	-4.243
671A	7.666	671A	11.021	652A	-6.277	671A	-4.818	632A	-4.783
652A	8.847	652A	12.935	680A	-7.652	652A	-5.004	633A	-4.882
680A	11.040	680A	16.847	633A	-13.079	680A	-5.387	634A	-6.112
632B	-0.774	632B	-0.985	634B	-2.705	632B	0.855	632B	0.033
633B	-0.794	633B	-0.991	645B	-2.821	633B	0.999	680B	-0.231
671B	-1.610	671B	-2.060	646B	-2.930	671B	5.326	633B	0.236
646B	-1.646	646B	-2.168	632B	-3.028	634B	5.676	671B	-0.454
645B	-1.845	645B	-2.343	633B	-3.061	645B	6.130	**675B**	-1.184
634B	-1.893	634B	-2.448	**675B**	-3.195	646B	6.237	634B	6.296
675B	-2.468	**675B**	-3.162	680B	-3.237	**675B**	6.675	645B	9.081
680B	-2.491	680B	-3.388	671B	-13.399	680B	7.867	646B	11.258
645C	-2.535	645C	-3.118	632C	1.220	645C	-1.283	645C	-1.998
632C	-2.566	632C	-3.156	645C	1.243	633C	-1.313	633C	-2.195
633C	-2.606	633C	-3.219	646C	2.856	632C	-1.327	632C	-2.232
646C	-2.764	646C	-3.462	634C	-3.365	684C	-1.530	646C	-2.519
634C	-3.401	634C	-4.294	633C	-5.662	646C	-1.836	**675C**	-2.759
684C	-4.405	684C	-5.783	684C	8.372	634C	-2.408	684C	-2.833
611C	-5.139	671C	-6.762	680C	11.928	611C	-2.471	611C	-2.920
671C	-5.156	611C	-6.791	611C	12.186	671C	-2.608	671C	-2.949
675C	-5.383	**675C**	-7.129	671C	14.414	**675C**	-2.931	680C	-3.020
680C	-5.854	680C	-7.804	**675C**	15.575	680C	-3.505	634C	-3.021

remained small.

By comparing the CPF scan results of 0% and PV, the impact of the DG in PV mode can be found. Bus 671A and Bus 671C was getting stronger with higher ranking. Even though the ranking of Bus 671B was the same, the CPF scan value was smaller, which means that 671B got stronger. Furthermore, we can see from the ranking that Bus 684A, Bus 652A, Bus 675A, Bus 680B, Bus 675B, Bus 680C, Bus 611C, and Bus 684C became stronger.

4.6.3 Application of CPF scan results in distribution system operation

In the distribution system operation, it is desirable to know along which direction and how much to change LID so that the desired maximum total real power can be achieved. This is an important information because this information can be used to increase the voltage stability margin of the system. In the following, a hypothetical example was used to illustrate the application of CPF scan results to increase the voltage stability margin of the system.

The system was the IEEE 13-node test feeder. Suppose at the current time, t_0 min, the load of the system was S_{base}, which was a vector and was specified in [73]. S_{base} has two components: real power load, P_{base} and reactive power load, Q_{base}. Assume that the load forecast was that at $t = T$ min, the load of the system was $S_{\text{base}} + 1.34 S_{\text{base}} = 2.34 S_{\text{base}}$. Assume that from $t = t_0$ to $t = T$, the load was changed at the same rate. Therefore, the load increase direction is

$$\text{LID} = \frac{1.34}{T - t_0} S_{\text{base}} \quad [\text{kW, kVar}]/\text{min} \tag{4.63}$$

With the base operating point, S_{base} and LID, the CPF method can be use to find the maximum loading factor and the total real power. It turns out that along this particular LID, the maximum loading factor is 1.3318. Therefore, when $t = T$, the system would experience voltage collapse, because 1.34 is greater than 1.3318. The stability margin based on total real power is -0.031 MW.

To avoid the voltage collapse at $t = T$, LID was changed. From the Table 4.32, the change along 680A was most effective because it was the largest value. The PLID and QLID were changed along 680A by 5kW and 1kVar, respectively. With the base operating point, S_{base} and the changed LID, the CPF method found the maximum loading factor and the total real power. Along this changed LID, the maximum loading factor was 1.3484. Therefore, when $t = T$, the system would not experience voltage collapse because 1.34 was smaller than 1.3484. The stability margin based on total real power was 0.0317 MW.

If the PLID and QLID were changed along 652A by 5kW and 1kVar respectively, along this changed LID, the maximum loading factor was 1.3431. Therefore, when $t = T$, the system would not experience voltage collapse because 1.34 was smaller than 1.3431. The stability margin based on total real power was 0.0117 MW. Therefore, the perturbation along 680A was more effective than the perturbation along 652A.

To implement the PLID perturbation along 680A by 5kW, and the QLID perturbation along 680A by 1kVar, according to (4.56), the demand response had to reduce the real power load and reactive power load at 680A at time t by

$$DR_{P,680A}(t) = 5(t - t_0) \quad \text{kW} \tag{4.64}$$

$$DR_{Q,680A}(t) = 1(t - t_0) \quad \text{kVar} \tag{4.65}$$

, while the demand response program did not change the load at the other buses.

4.6.4 Application of CPF scan results in planning

In the following, the IEEE 13-node test feeder was used as the example. In the planning problem, the best location of reactive power support should be determined. To determine the best location, different objectives can be used. In this example, the objective of the planning is to place a three-phase SVC so that the maximum loadability of the system is the highest. SVC is a device that can adjust its reactive power output so that its terminal voltage can be regulated.

To achieve the planning purpose, the CPF scan method results may be useful in this application. However, because CPF scan results only give the ranking for each buses/phases, for three-phase buses, their CPF scan ranking for each three phase may be different. Therefore, we proposed a method to determine the weakness of buses that are three-phase. The proposed method is based on the summation of CPF scan results of each of the three phases.

Table 4.36 shows the CPF scan results of the base case where there was no SVC connected. Only the CPF scan results of the three-phase buses are shown. This CPF scan value was exact the same as the one shown in Table 4.32. For each phase shown in the first three columns, the CPF scan results were ranked by the absolute value. For the last column, the value was the summation of the CPF scan result of Phase A, Phase B and Phase C. The last column was also ranked by the absolute value.

Table 4.36: CPF scan result for each phase and total impact

Phase A		Phase B		Phase C		Total	
632A	0.247	632B	-0.774	632C	-2.566	675	-0.516
633A	0.339	633B	-0.794	633C	-2.606	671	0.900
634A	3.595	671B	-1.610	634C	-3.401	634	-1.699
675A	7.336	634B	-1.893	671C	-5.156	680	2.694
671A	7.666	675B	-2.468	675C	-5.383	633	-3.061
680A	11.040	680B	-2.491	680C	-5.854	632	-3.093

In the following case study, a three-phase SVC was placed at different three-phase buses. Table 4.37 shows the maximum total real power, maximum loading factor, the generated reactive power from the substation and the generated reactive power from the SVC. Bus 632 was the most effective location to connected three-phase SVC because the corresponding maximum total real power, $\sum P^*$, was the largest. The ranking $\sum P^*$ was the same as the ranking of Q_{gtotal}, total generated reactive power. Moreover, for the case where SVC was connected at Bus 632, the generated reactive power from the substation was negative. However, it can be found that the ranking in Table 4.37 was not exactly the same as the last column of Table 4.36.

Table 4.37: Three-phase SVC at different three-phase buses

Bus #	$\sum \mathbf{P}^*$	$Q_{g,sub}^{total}$	$Q_{g,sub}^{a}$	$Q_{g,sub}^{b}$	$Q_{g,sub}^{c}$	$Q_{g,SVC}^{a}$	$Q_{g,SVC}^{b}$	$Q_{g,SVC}^{c}$	$Q_{g,SVC}^{total}$	$\mathbf{Q_g^{total}}$
632	15.630	-3.183	-1.237	-1.123	-0.824	7.502	7.059	8.740	23.301	20.118
671	14.935	2.590	-0.714	3.491	-0.187	6.040	5.775	5.214	17.030	19.619
675	14.361	3.191	-0.537	3.706	0.022	5.889	5.211	4.920	16.020	19.212
680	14.177	5.061	0.459	4.060	0.542	4.738	4.238	4.279	13.255	18.316
633	13.343	0.892	0.131	0.261	0.499	5.110	4.786	5.703	15.600	16.491
634	10.390	6.977	2.429	2.507	2.041	1.884	1.350	1.468	4.701	11.678

Table 4.38 shows the SVC impact on the CPF scan ranking. Each column represents the CPF scan when the SVC was connected at different locations. By comparing the different columns with the first column,□the impact of 3-phase SVC was investigated. It can be seen that for SVC connected at 671, 675, 680, and 634, the buses where the SVC was connected became stronger as well as the neighboring buses. However, for SVC connected at 632, and 633 the buses where the SVC was connected did not necessarily become stronger. For example, for SVC connected at 632, 632B and 632C became weaker. For SVC connected at 633, 633C became weaker.

Table 4.38: The CPF scan result for different 3-phase SVC locations

No SVC		632		671		675		680		633		634	
632A	0.247	632A	-4.346	684A	-3.517	**675A**	-4.154	**680A**	-3.848	632A	-3.542	671A	0.025
633A	0.339	633A	-4.356	652A	-3.520	671A	-4.194	684A	-4.364	**633A**	-3.731	675A	0.455
634A	3.595	634A	-4.614	680A	-3.562	684A	-4.197	671A	-4.516	634A	-3.903	**634A**	-0.474
684A	4.060	684A	-5.070	675A	-3.578	652A	-4.211	675A	-4.583	684A	-5.129	633A	0.779
675A	7.336	675A	-7.697	**671A**	-4.084	680A	-4.243	652A	-4.599	675A	-7.837	632A	0.854
671A	7.666	671A	-7.779	632A	-4.325	632A	-4.783	632A	-4.731	671A	-8.044	652A	-0.977
652A	8.847	652A	-8.637	633A	-4.419	633A	-4.882	633A	-4.844	652A	-8.865	680A	-2.905
680A	11.040	680A	-10.201	634A	-5.560	634A	-6.112	634A	-6.291	680A	-10.446	684A	4.373
632B	-0.774	646B	-2.688	632B	-0.069	632B	0.033	632B	0.179	634B	-2.570	671B	0.146
633B	-0.794	645B	-2.754	633B	0.140	680B	-0.231	671B	0.273	**633B**	-2.587	632B	-0.212
671B	-1.610	634B	-2.902	680B	-1.105	633B	0.236	633B	0.389	645B	-3.070	**634B**	0.317
646B	-1.646	632B	-2.913	**671B**	-1.115	671B	-0.454	675B	0.637	646B	-3.075	633B	-0.358
645B	-1.845	633B	-2.925	675B	-1.116	**675B**	-1.184	**680B**	-0.656	632B	-3.111	646B	-0.753
634B	-1.893	675B	-5.875	634B	6.406	634B	6.296	634B	6.449	675B	-5.210	645B	-0.990
675B	-2.468	671B	-6.088	645B	10.117	645B	9.081	645B	9.657	680B	-5.562	675B	-1.592
680B	-2.491	680B	-6.312	646B	12.064	646B	11.258	646B	11.536	671B	-5.593	680B	-6.559
645C	-2.535	634C	-1.403	645C	-2.105	645C	-1.998	645C	-2.021	645C	-0.021	**634C**	-4.131
632C	-2.566	633C	-1.631	633C	-2.337	633C	-2.195	633C	-2.190	632C	-0.022	633C	-4.562
633C	-2.606	645C	-1.658	632C	-2.377	632C	-2.232	632C	-2.229	646C	0.653	645C	-4.749
646C	-2.764	632C	-1.658	646C	-2.643	646C	-2.519	646C	-2.586	634C	-0.819	632C	-4.791
634C	-3.401	646C	-1.661	680C	-3.079	**675C**	-2.759	684C	-2.886	**633C**	-0.978	646C	-5.548
684C	-4.405	684C	10.022	611C	-3.089	684C	-2.833	611C	-3.081	684C	10.486	684C	-10.029
611C	-5.139	671C	15.626	**671C**	-3.101	611C	-2.920	671C	-3.118	671C	17.234	671C	-12.110
671C	-5.156	611C	17.480	684C	-3.101	671C	-2.949	634C	-3.137	611C	18.422	611C	-12.121
675C	-5.383	675C	19.847	675C	-3.106	680C	-3.020	**680C**	-3.188	675C	21.196	675C	-12.793
680C	-5.854	680C	23.855	634C	-3.169	634C	-3.021	675C	-3.201	680C	25.816	680C	-13.961

Table 4.39 shows the SVC impact on the voltage ranking. Each column represents the voltage ranking when the SVC was connected at different locations. By comparing the different column with the first column, the impact of 3-phase SVC on the voltage can be investigated. It can be seen that SVC successfully regulated its terminal voltage at 1 pu. The neighboring buses voltage were increased. Sometimes, the voltage at certain buses was even higher than 1 pu.

Table 4.39: Voltage ranking for different 3-phase SVC locations

No SVC		632		671		675		680		633		634	
632A	0.797	**632A**	1.000	**671A**	1.000	**675A**	1.000	**680A**	1.000	**633A**	1.000	**634A**	1.000
633A	0.787	633A	0.985	684A	0.992	671A	0.993	632A	0.929	632A	0.941	633A	0.850
634A	0.708	634A	0.870	680A	0.989	684A	0.985	633A	0.916	634A	0.905	632A	0.837
671A	0.639	671A	0.777	632A	0.974	680A	0.982	671A	0.914	671A	0.737	671A	0.651
684A	0.634	684A	0.769	675A	0.970	632A	0.968	684A	0.906	684A	0.729	684A	0.645
680A	0.628	680A	0.763	652A	0.969	652A	0.963	652A	0.883	680A	0.724	680A	0.639
652A	0.618	652A	0.741	633A	0.961	633A	0.955	675A	0.883	652A	0.705	652A	0.626
675A	0.613	675A	0.736	634A	0.847	634A	0.846	634A	0.803	675A	0.700	675A	0.621
675B	0.910	675B	1.099	675B	1.005	**675B**	1.000	**680B**	1.000	675B	1.028	**634B**	1.000
671B	0.905	671B	1.090	**671B**	1.000	671B	0.959	675B	0.926	671B	1.021	675B	0.939
680B	0.901	680B	1.087	680B	0.991	680B	0.949	671B	0.921	680B	1.016	671B	0.934
632B	0.869	**632B**	1.000	632B	0.746	632B	0.738	632B	0.735	**633B**	1.000	680B	0.929
633B	0.863	633B	0.992	633B	0.730	633B	0.723	633B	0.721	632B	0.954	633B	0.900
634B	0.809	634B	0.905	634B	0.605	634B	0.601	634B	0.603	634B	0.928	632B	0.890
645B	0.790	645B	0.863	645B	0.540	645B	0.541	645B	0.548	645B	0.834	645B	0.797
646B	0.766	646B	0.818	646B	0.474	646B	0.479	646B	0.489	646B	0.795	646B	0.768
646C	0.897	646C	1.026	646C	1.068	646C	1.052	646C	1.030	**633C**	1.000	**634C**	1.000
645C	0.895	645C	1.022	645C	1.060	645C	1.044	645C	1.023	646C	0.959	646C	0.905
632C	0.885	**632C**	1.000	632C	1.027	632C	1.013	**680C**	1.000	645C	0.956	645C	0.903
633C	0.877	633C	0.987	633C	1.016	633C	1.002	632C	0.992	632C	0.938	633C	0.894
634C	0.824	634C	0.900	**671C**	1.000	**675C**	1.000	633C	0.982	634C	0.928	632C	0.890
671C	0.744	671C	0.609	680C	0.989	671C	0.976	671C	0.935	671C	0.634	671C	0.712
675C	0.737	684C	0.588	675C	0.989	680C	0.965	675C	0.924	684C	0.618	675C	0.703
684C	0.736	675C	0.586	684C	0.988	684C	0.964	684C	0.923	675C	0.617	684C	0.702
680C	0.735	680C	0.585	611C	0.976	611C	0.952	611C	0.911	680C	0.616	680C	0.701
611C	0.728	611C	0.568	634C	0.935	634C	0.924	634C	0.903	611C	0.602	611C	0.692

4.7 Discussions and limitations

From the case studies on 8-bus system, it can be seen that the CPF scan results follow the physics of the network characteristics for the following cases: doubled loads, three-phase capacitors, unbalanced loads. On the other hand, it is diffucult to determine if the CPF scan results follow the physics of the network characteristics of the more complex components: untransposed lines, DG in PQ mode and DG in PV mode. The possible reason is that the CPF scan method considers three factors simultaneously: network characteristics, base operating point, and load increase direction. The CPF scan results highly depend on the shape of SNB surface. The shape of SNB surface is extremely complicated [77]. Therefore, it s difficult to know a prior what the expected CPF scan results will be for a more complex distribution systems.

From the case studies on the IEEE-13 test feeder, it can be seen that based on the CPF scan results, the impact of capacitors on the weak buses were not as expected. For example, removing the three-phase capacitor bank, the corresponding bus in a certain phase became stronger in the ranking of the CPF scan results. For DG in PQ, according to the CPF scan ranking results, the connected buses may get stronger or weaker, depending on the output of the DG. For DG in PV, according to the CPF scan ranking result, the connected buses did get stronger. Also the neighboring buses also got stronger.

For the application of CPF scan on operation, the demand response program was used to determine how to adjust the load at each time step so that the perturbed LID can be achieved. The direction of perturbation that achieved the highest increase of stability margin can be found based on the CPF scan results. For the application of CPF scan on planning, the best location to place the three-phase SVC did not match the CPF scan result ranking.

The advantage of CPF scan method is that the three factors are considered simultaneously: the network characteristics, the base operating point, and the load increase direction (LID). Because CPF scan method uses CPF method, CPF scan method can avoid the singularity issues that arise when the system is close to the maximum loading point. However, there are several drawbacks of the CPF scan method. First, it is computationally intensive. The CPF method is executed for each possible bus/phase. If the number of the buses and phases in the system is large, it will take lots of time to perform the CPF scan method. Secondly, the CPF scan method requires load increase direction information. However, currently there is no such information in distribution systems. There are only aggregated load forecasts. Lastly, it is challenging to verify whether the CPF scan results are accurate. There are several other methods that determine the weak buses; however, different methods determine the weak buses from different perspectives. Due to the complicated nature of distribution systems, it is challenging to see the relationship between different components and the CPF scan results.

4.8 Summary

In this section, a new voltage stability analysis method for three-phase unbalanced distribution system was proposed. This method considers the three factors that impact the location of weak buses: network characteristics, base operation point and load increase direction. The properties of the CPF scan method were investigated. The proposed CPF scan method was applied to the 8-bus system to investigate the te impacts of different components common to distribution systems. Moreover, the proposed CPF scan method was applied to the modified IEEE 13-node test feeder with DG. The impact of capacitor banks, DG in PQ and DG in PV mode were investigated. Lastly, the CPF scan results were applied to the operation and planning of distribution systems.

5 VOLTAGE STABILITY INDEX FOR THREE-PHASE UNBALANCED DISTRIBUTION SYSTEMS WITH DGS

5.1 Introduction

In distribution system operations, monitoring the system is one of important tasks. One example of monitoring the system is to determine whether the system is close to the voltage collapse point. If the system is close to this point, even a small disturbance would cause the system to experience voltage collapse problem and blackout will occur. Therefore, to ensure distribution systems have a robust operation, monitoring whether the system is close to voltage collapse point is important.

To monitoring the system to avoid voltage collapse problem, voltage stability index (VSI) is wide used. In addition to determining whether the system is close to voltage collapse point, VSI can be used to create control actions so that the system is steered away from the voltage collapse point. There are two kinds of VSI. One is for the overall system; it determines whether the system is close to voltage collapse point. Based on this value, the safety margin of the current operating point can be found. Another type of index is for each individual bus; it determines the buses that cause the system to experience voltage collapse. This index can identify the weak buses and the effective buses to apply the control actions, such as load shedding and reactive power injection.

Most of the voltage stability indices proposed in the literature are for single-phase transmission systems. The eigenvalue [XX] and the singular value [xx] of the Jacobian matrix are used for VSI. The disadvantage of these methods is that for large power systems, calculation of eigenvalue and singular value is time consuming. Another method is based on the condition of real value solution of power flow [58] and [59]. Also, the fact that at voltage collapse point the determinant of the Jacobian matrix is zero is used in [56] and [57]. All the literature mentioned above is for single-phase transmission systems.

To the author's knowledge, no truly three-phase voltage stability index is proposed in the literature for three-phase unbalanced distribution systems. Juanuwattanakul and Masoum proposed VSI for distribution systems using the ratio of positive sequence voltage between the base and the maximum loading point [52]. However, there are two disadvantages. First, this method is only based on voltage magnitudes; no other factors are considered. This results from this method will be inaccurate, especially in a highly reactive power compensated system. This is because voltage magnitude alone is not a good indicator for voltage stability problem [7]. Another disadvantage is that this method is not truly for three-phase systems. This method only considers positive sequence voltages; it does not consider negative and zero sequence voltages. As a result, the answer from this method meaningful only in a system with balanced operating conditions and with all buses being three phase. For a general three-phase distribution system, where the operating condition is not balanced and buses are three-, two- or single-phases, the result from this method is not meaningful.

Another method, CPF scan, which is discussed in the previous section, can provide an index for different buses/phases. However, this method is time consuming, because

CPF method needs to be executed for different buses/phases. Moreover, CPF scan only provides the individual index for different buses/phases; it does not provide the overall index for the system.

This section will propose a new VSI for three-phase unbalanced distribution systems. The proposed VSI has some advantages. First, this proposed VSI is for unbalanced three-phase distribution systems. It considers the coupling among phases, considers the case where the buses are three-, two-, or single-phase, and considers the impact of positive, negative and zero sequence voltage at the same time. No simplifications or assumptions are made in this method. Second, the proposed VSI only needs the measurements and system topology information. No other information is needed, such as the load increase direction, as required in the CPF scan method. Furthermore, the proposed VSI provides both individual and system-wide indices. Each phases (phase A, B or C, depending on the phases a bus has) of every bus has its corresponding individual index. These individual indices can identify the weak buses of the system. On the other hand, the system-wide index can determine whether the system is close to the voltage collapse point. Last advantage is that the proposed VSI is time efficient. Unlike other methods discussed previously, the propose method is only based on the current operating point. It does not need to use CPF method to find the maximum loading point. Also, it does not need to perform complicated mathematical calculation, such as eigenvalue decomposition. It only requires simple algebraic calculations.

The organization of this section is as follows. First, the proposed VSI with a two-bus single-phase example is derived. After that, the extension into a N-bus single-phase and N-bus three-phase examples are made. Once the proposed VSI is derived, the trend of the proposed VSI is investigated. In the end, several case studies are presented, and some insights from the numerical results are discussed.

5.2 Derivation of VSI

To derive the proposed VSI for three-phase unbalanced distribution system, we will derive the VSI for single-phase 2-bus system first. Then we will extend the result into single-phase N-bus system. Lastly, we will extend the result into a three-phase N-bus system.

5.2.1 Derivation for single-phase 2-bus system

Fig.5.1 shows the one line diagram of a two-bus system. The series admittance of the line is $\vec{Y}_L$ while the sunt admittance of the line is $\vec{Y}_S$. The complex power injection at Bus 2 is $\vec{S}_s$.

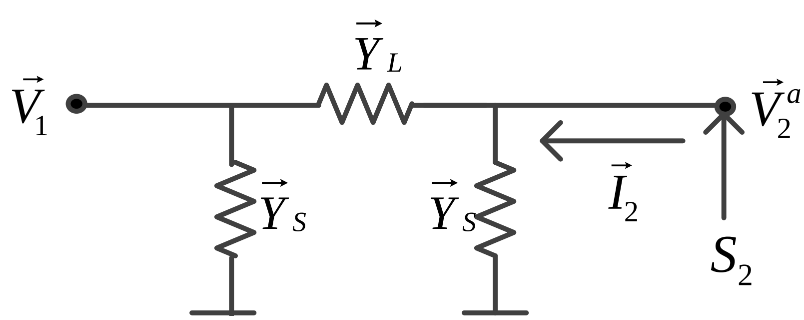

Figure 5.1: 2-bus example for VSI derivation

Based on the KCL, the current $\vec{I}_2$ can be expressed as

$$\vec{I}_2 = \vec{V}_2\vec{Y}_S + (\vec{V}_2 - \vec{V}_1)\vec{Y}_L = (\frac{\vec{S}_2}{\vec{V}_2})^*. \tag{5.1}$$

Multiply both side of (5.1) with $\vec{V}_2^{\ *}$,

$$=> V_2^2\vec{Y}_S + V_2^2\vec{Y}_L - \vec{V}_1\vec{V}_2^*\vec{Y}_L = V_2^2\vec{Y}_{22} + \vec{V}_0\vec{V}_2^*\vec{Y}_{22} = \vec{S}_2^* \tag{5.2}$$

where

$$\vec{Y}_{22} = \vec{Y}_S + \vec{Y}_L \tag{5.3}$$

$$\vec{V}_0 = -(\frac{\vec{Y}_L}{\vec{Y}_S + \vec{Y}_L})\vec{V}_1 \tag{5.4}$$

With simple substitutions, (5.2) can be expressed as:

$$V_2^2 + \vec{V}_0\vec{V}_2^* = \frac{\vec{S}_2^*}{\vec{Y}_{22}} = a + jb \tag{5.5}$$

There are two equations for real and imaginary part in (5.5):

$$f(V_2, \delta) = V_0V_2\cos\delta + V_2^2 = a \tag{5.6}$$

$$g(V_2, \delta) = V_0V_2\sin\delta = b \tag{5.7}$$

By squaring both sides of (5.6) and (5.7)), we can solve for $|V_2|$:

$$(V_2^2 - a)^2 = (-V_0V_2\cos\delta)^2 \tag{5.8}$$

$$b^2 = (V_0V_2\sin\delta)^2. \tag{5.9}$$

By summing the above two equations, we can solve the following equation to get V_2:

$$V_2^4 - 2aV_2^2 + a^2 + b^2 = V_0^2V_2^2$$

$$=> V_2^4 + (-2a - V_0^2)V_2^2 + (a^2 + b^2) = 0 \tag{5.10}$$

To make sure V_2 is a real number, the following condition should be satisfied:

$$\mathrm{VSI} = (-2a - V_0^2)^2 - 4(a^2 + b^2) \geq 0 \tag{5.11}$$

When the system is close to voltage collapse point, VSI will be very close to zero.

5.2.2 Derivation for single-phase N-bus system

For N-bus single-phase system, the concept is similar to two-bus single-phase system. For a load bus j, by using the network equations we transform the rest parts of the network into another bus $0j$ and find its voltage $\vec{V}_{0j}$. By using the similar concept as two-bus case, VSI for N-bus single-phase system can be found. The following are the detailed derivation.

The relationship between the injected currents and the bus voltages can be expressed as:

$$\begin{bmatrix} \vec{\mathbf{I}}_L \\ \vec{\mathbf{I}}_G \end{bmatrix} = \begin{bmatrix} \vec{\mathbf{Y}}_{LL} & \vec{\mathbf{Y}}_{LG} \\ \vec{\mathbf{Y}}_{GL} & \vec{\mathbf{Y}}_{GG} \end{bmatrix} \begin{bmatrix} \vec{\mathbf{V}}_L \\ \vec{\mathbf{V}}_G \end{bmatrix}. \tag{5.12}$$

$\vec{\mathbf{I}}_L$ and $\vec{\mathbf{I}}_G$ are the injected current for load buses and generator buses, respectively. $\vec{\mathbf{V}}_L$ and $\vec{\mathbf{V}}_G$ are the voltage for load buses and generator buses, respectively.

After some mathematical manipulations, $\vec{\mathbf{V}}_L$ can be expressed as (5.13).

$$\vec{\mathbf{V}}_L = \vec{\mathbf{Y}}_{LL}^{-1}\vec{\mathbf{I}}_L - \vec{\mathbf{Y}}_{LL}^{-1}\vec{\mathbf{Y}}_{LG}\vec{\mathbf{V}}_G \tag{5.13}$$

From (5.13), the voltage at the load bus j, which is the jth element of $\vec{\mathbf{V}}_L$, can be expressed as:

$$\vec{V}_j = \sum_{i \in L} \vec{\mathbf{Y}}_{LL}^{-1}(j,i)\vec{I}_i - \sum_{k \in G} \vec{\mathbf{Y}}_{LL}^{-1}\vec{\mathbf{Y}}_{LG}(j,k)\vec{V}_k \tag{5.14}$$

Multiply both sides of (5.14) with $\vec{V}_j^*$:

$$V_j^2 = \sum_{i \in L} \vec{\mathbf{Y}}_{LL}^{-1}(j,i)\vec{I}_i\vec{V}_j^* - \sum_{k \in G} \vec{\mathbf{Y}}_{LL}^{-1}\vec{\mathbf{Y}}_{LG}(j,k)\vec{V}_k\vec{V}_j^*$$

$$=> V_j^2 + \left[\sum_{k \in G} \vec{\mathbf{Y}}_{LL}^{-1}\vec{\mathbf{Y}}_{LG}(j,k)\vec{V}_k - \sum_{i \in L, i \neq j} \vec{\mathbf{Y}}_{LL}^{-1}(j,i)\vec{I}_i\right]\vec{V}_j^* = \vec{\mathbf{Y}}_{LL}^{-1}(j,j)\vec{I}_j\vec{V}_j^* \tag{5.15}$$

Because

$$\vec{I}_j = -\frac{\vec{S}_j^*}{\vec{V}_j^*} \tag{5.16}$$

(5.15) can be expressed as:

$$V_j^2 + \left[\sum_{k \in G} \vec{\mathbf{Y}}_{LL}^{-1}\vec{\mathbf{Y}}_{LG}(j,k)\vec{V}_k + \sum_{i \in L, i \neq j} \vec{\mathbf{Y}}_{LL}^{-1}(j,i)\frac{\vec{S}_i^*}{\vec{V}_i^*}\right]\vec{V}_j^* = -\vec{\mathbf{Y}}_{LL}^{-1}(j,j)\vec{S}_j^* = a + jb \tag{5.17}$$

Define $\vec{V}_{0j}$ as

$$\vec{V}_{0j} = \sum_{k \in G} \vec{\mathbf{Y}}_{LL}^{-1}\vec{\mathbf{Y}}_{LG}(j,k)\vec{V}_k + \sum_{i \in L, i \neq j} \vec{\mathbf{Y}}_{LL}^{-1}(j,i)\frac{\vec{S}_i^*}{\vec{V}_i^*} \tag{5.18}$$

(5.17) can be written as:

$$V_j^2 + \vec{V}_{0j}\vec{V}_j^* = a + jb \tag{5.19}$$

By separating the equation into real and imaginary part, we have two equations:

$$a = V_j^2 + V_{0j}V_j\cos\delta \tag{5.20}$$

$$b = V_{0j}V_j\sin\delta \tag{5.21}$$

where δ is the angle difference between $\vec{V}_j$ and $\vec{V}_{0j}$.

By squaring both sides of (5.20) and (5.21)), we can solve for V_j:

$$(V_j^2 - a)^2 = (-V_{0j}V_j\cos\delta)^2 \tag{5.22}$$

$$b^2 = (V_{0j}V_j\sin\delta)^2 \tag{5.23}$$

By summing the above two equations, we can solve the following equation to get V_j:

$$\begin{aligned} & V_j^4 - 2aV_j^2 + a^2 + b^2 = V_{0j}^2 V_j^2 \\ & => V_j^4 + (-2a - V_{0j}^2)V_j^2 + (a^2 + b^2) = 0 \end{aligned} \tag{5.24}$$

To make sure V_j is a real number, the following condition should be satisfied:

$$\mathrm{VSI}_j = (-2a - V_{0j}^2)^2 - 4(a^2 + b^2) \geq 0 \tag{5.25}$$

When the system is close to voltage collapse point, VSI_j of one of the buses will be very close to zero.

5.2.3 Derivation for three-phase N-bus system

For N-bus three-phase system, the concept is similar to N-bus single-phase system. For a load bus j in phase s, by using the network equations we transform the rest parts of the network into another bus $0j^s$ and find its voltage $\vec{V}_{0j}^s$. By using the similar concept as two-bus case, VSI for N-bus three-phase system can be found. The following are the detailed derivation.

The relationship between three-phase injected currents and three-phase bus voltages can be expressed as:

$$\begin{bmatrix} \vec{\mathbf{I}}_L \\ \vec{\mathbf{I}}_G \end{bmatrix} = \begin{bmatrix} \vec{\mathbf{Y}}_{LL} & \vec{\mathbf{Y}}_{LG} \\ \vec{\mathbf{Y}}_{GL} & \vec{\mathbf{Y}}_{GG} \end{bmatrix} \begin{bmatrix} \vec{\mathbf{V}}_L \\ \vec{\mathbf{V}}_G \end{bmatrix} \tag{5.26}$$

$\vec{\mathbf{I}}_L$ and $\vec{\mathbf{I}}_G$ are the three-phase injected current for load buses and generator buses, respectively. $\vec{\mathbf{V}}_L$ and $\vec{\mathbf{V}}_G$ are the three-phase voltage for load buses and generator buses, respectively.

After some mathematical operations, $\vec{\mathbf{V}}_L$ can be expressed as:

$$\vec{\mathbf{V}}_L = \vec{\mathbf{Y}}_{LL}^{-1}\vec{\mathbf{I}}_L - \vec{\mathbf{Y}}_{LL}^{-1}\vec{\mathbf{Y}}_{LG}\vec{\mathbf{V}}_G \tag{5.27}$$

From (5.27) the voltage at the load bus j in phase s, which is the element of $\vec{\mathbf{V}}_L$ in (5.27), can be expressed as

$$\vec{V}_j^s = \sum_{i\in L}\sum_{t\in a,b,c}(\vec{\mathbf{Y}}_{LL}^{-1})_{(j,i)}^{(s,t)}\vec{I}_i^t - \sum_{k\in G}(\vec{\mathbf{Y}}_{LL}^{-1}\vec{\mathbf{Y}}_{LG})_{(j,k)}^{(s,t)}\vec{V}_k^t \tag{5.28}$$

By multiply both sides of (5.28) with $\vec{V}_j^{s*}$, we can get

$$(V_j^s)^2 = \sum_{i\in L}\sum_{t\in a,b,c}(\vec{\mathbf{Y}}_{LL}^{-1})_{(j,i)}^{(s,t)}\vec{I}_i^t\vec{V}_j^{s*} - \sum_{k\in G}\sum_{t\in a,b,c}(\vec{\mathbf{Y}}_{LL}^{-1}\vec{\mathbf{Y}}_{LG})_{(j,k)}^{(s,t)}\vec{V}_k^t\vec{V}_j^{s*} \tag{5.29}$$

$$=> (V_j^s)^2 + \left[\sum_{k\in G}\sum_{t\in a,b,c}(\vec{\mathbf{Y}}_{LL}^{-1}\vec{\mathbf{Y}}_{LG})_{(j,k)}^{(s,t)}\vec{V}_k^t - \sum_{i\in L}\sum_{t\in a,b,c}(\vec{\mathbf{Y}}_{LL}^{-1})_{(j,i)}^{(s,t)}\vec{I}_i^t + (\vec{\mathbf{Y}}_{LL}^{-1})_{(j,j)}^{(s,s)}\vec{I}_i^s\right]\vec{V}_j^{s*}$$

$$= (\vec{\mathbf{Y}}_{LL}^{-1})_{(j,j)}^{(s,s)}\vec{I}_j^s\vec{V}_j^{s*} \tag{5.30}$$

Because

$$\vec{I}_i^s = -\frac{\vec{S}_i^{s*}}{\vec{V}_i^{s*}} \tag{5.31}$$

(5.30) can be expressed as:

$$(V_j^s)^2 + \left[\sum_{k\in G}\sum_{t\in a,b,c}(\vec{\mathbf{Y}}_{LL}^{-1}\vec{\mathbf{Y}}_{LG})_{(j,k)}^{(s,t)}\vec{V}_k^t + \sum_{i\in L}\sum_{t\in a,b,c}(\vec{\mathbf{Y}}_{LL}^{-1})_{(j,i)}^{(s,t)}\frac{\vec{S}_i^{t*}}{\vec{V}_i^{t*}} - (\vec{\mathbf{Y}}_{LL}^{-1})_{(j,j)}^{(s,s)}\frac{\vec{S}_j^{s*}}{\vec{V}_j^{s*}}\right]\vec{V}_j^{s*}$$

$$= -(\vec{\mathbf{Y}}_{LL}^{-1})_{(j,j)}^{(s,s)}\vec{S}_j^{s*} = a + jb \tag{5.32}$$

Define $\vec{V}_{0j}^s$ as

$$\vec{V}_{0j}^s = \sum_{k\in G}\sum_{t\in a,b,c}(\vec{\mathbf{Y}}_{LL}^{-1}\vec{\mathbf{Y}}_{LG})_{(j,k)}^{(s,t)}\vec{V}_k^t + \sum_{i\in L}\sum_{t\in a,b,c}(\vec{\mathbf{Y}}_{LL}^{-1})_{(j,i)}^{(s,t)}\frac{\vec{S}_i^{t*}}{\vec{V}_i^{t*}} - (\vec{\mathbf{Y}}_{LL}^{-1})_{(j,j)}^{(s,s)}\frac{\vec{S}_j^{s*}}{\vec{V}_j^{s*}}. \tag{5.33}$$

(5.32) can be written as:

$$(V_j^s)^2 + \left[\vec{V}_{0j}^s\right]\vec{V}_j^{s*} = a + jb. \tag{5.34}$$

By separating into real and imaginary, we have two equations:

$$a = (V_j^s)^2 + V_{0j}^s V_j^s \cos\delta \tag{5.35}$$

$$b = V_{0j}^s V_j^s \sin\delta \tag{5.36}$$

where δ is the angle difference between $\vec{V}_j^s$ and $\vec{V}_{0j}^s$.

By Squaring both sides of (5.35) and (5.36), we can solve for V_j^s:

$$\left[(V_j^s)^2 - a\right]^2 = (-V_{0j}^s V_j^s \cos\delta)^2 \tag{5.37}$$

$$b^2 = (V_{0j}^s V_j^s \sin\delta)^2 \tag{5.38}$$

By summing the above two equations, we can solve the following equation to get V_j^s:

$$(V_j^s)^4 - 2a(V_j^s)^2 + a^2 + b^2 = (V_{0j}^s)^2 (V_j^s)^2 \tag{5.39}$$

$$=> (V_j^s)^4 + \left[-2a - (V_{0j}^s)^2\right](V_j^s)^2 + (a^2 + b^2) = 0 \tag{5.40}$$

To make sure V_j^s is a real number, not imaginary one, the condition is (5.41).

$$\mathrm{VSI}_j^s = \left[-2a - (V_{0j}^s)^2\right]^2 - 4(a^2 + b^2) \geq 0 \tag{5.41}$$

When the system is close to voltage collapse point, $\mathrm{VSI_j^s}$ of one of the buses will be very close to zero. Notice that not all VSI of each bus/phase will be close to zero when voltage collapse occurs. Only one of them will be close to zero.

The minimum value of $\mathrm{VSI_j^s}$ of all buses/phases, as shown in (5.42) can be used as the system-wide VSI. This system-wide VSI provides information regarding whether the system is close to voltage collapse point. Based on this information, the appropriate control action can be taken to steer the system away from the voltage collapse point.

$$\mathrm{VSI_{sys}} = \mathrm{Min}\left\{\mathrm{VSI}_j^s, \quad \forall j, \forall s\right\} \tag{5.42}$$

5.3 Monotonic property of VSI

After deriving the VSI for three-phase unbalanced distribution systems, this section investigates the trend of the proposed VSI. This section analytically show that in most of the distribution systems, for any given bus i and phase s, the corresponding VSI will decrease when the loading factor of the system increases.

To show this monotonic decrease property of VSI, there are two steps. The first step is to show that VSI is a continuous function of the loading factor λ. Because $\vec{S}_j^s$ is a continuous function of λ, as seen from (5.32), a and b are continuous in λ. Therefore, from (5.41), VSI is also a continuous function of λ. The second step is to show that the derivative of $\mathrm{VSI}_\mathrm{j}^\mathrm{s}$ with respect to λ is negative. The derivative of $\mathrm{VSI}_\mathrm{j}^\mathrm{s}$ with respect to λ can be decomposed into two components:

$$\begin{aligned}\frac{\partial \mathrm{VSI}_\mathrm{j}^\mathrm{s}}{\partial \lambda} &= \frac{\partial \mathrm{VSI}_\mathrm{j}^\mathrm{s}}{\partial a}\frac{\partial a}{\partial \lambda} + \frac{\partial \mathrm{VSI}_\mathrm{j}^\mathrm{s}}{\partial b}\frac{\partial b}{\partial \lambda} = 2\left[-2a-(V_{0j}^s)^2\right](-2)\frac{\partial a}{\partial \lambda} - 8a\frac{\partial a}{\partial \lambda} - 8b\frac{\partial b}{\partial \lambda} \\ &= 4(V_{0j}^s)^2\frac{\partial a}{\partial \lambda} - 8b\frac{\partial b}{\partial \lambda} \qquad (5.43)\end{aligned}$$

Assume that $\vec{\mathbf{Y}}_{LL(j,j)}^{-1(s,s)} = A + jB$ and $\vec{S}_j^s = P(\lambda) + jQ(\lambda)$, from (5.32) a and b can be expressed as:

$$a = -AP(\lambda) - BQ(\lambda) \qquad (5.44)$$

$$b = AQ(\lambda) - BP(\lambda). \qquad (5.45)$$

Because in the distribution systems the loads usually are inductive with normal power factor and the lines are inductive, A, B, $P(\lambda)$, and $Q(\lambda)$ are positive. Moreover, A is smaller than B and $P(\lambda)$ is greater than $Q(\lambda)$. With these relationships, both a and b are negative.

Assuming that $P(\lambda)$ and $Q(\lambda)$ can be expressed as $P(\lambda) = \lambda P_0$ and $Q(\lambda) = \lambda Q_0$. The derivative of a and b with respect to λ can be found as:

$$\frac{\partial a}{\partial \lambda} = -AP_0 - BQ_0 \leq 0 \tag{5.46}$$

$$\frac{\partial b}{\partial \lambda} = AQ_0 - BP_0 \leq 0 \tag{5.47}$$

From (5.43), (5.46) and (5.47), it can be found that:

$$\frac{\partial \mathrm{VSI}_{\mathrm{j}}^{\mathrm{s}}}{\partial \lambda} = = 4(V_{0j}^{s})^2 \frac{\partial a}{\partial \lambda} - 8b\frac{\partial b}{\partial \lambda} \leq 0 \tag{5.48}$$

which proves that the proposed VSI decreases when the loading factor is increasing, as shown in Fig. 5.2.

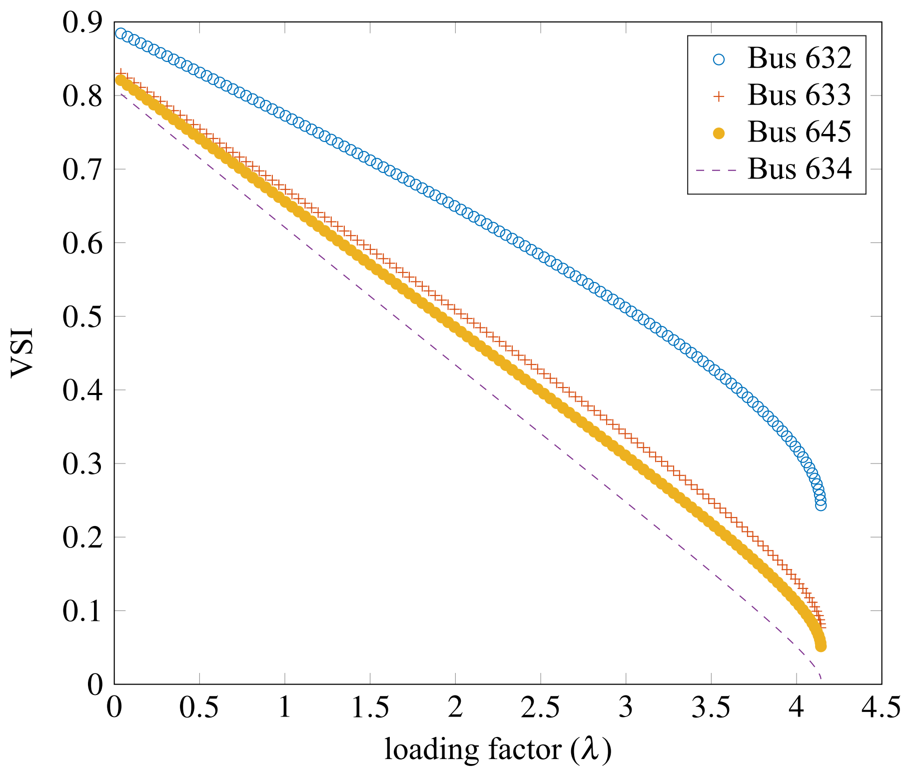

Figure 5.2: Voltage stability index for 8-bus example

5.4 Case studies

In the following case studies, the proposed VSI will be found in the 8-bus system and the modified IEEE 13-node test feeder with DG. The reason to use the 8-bus system as an example is to find the impacts of different factors on the proposed VSI. Once the impacts are found, we use the IEEE 13-node test feeder as the example to see whether these observed impacts are still applicable in the more complicated and complete distribution system.

5.4.1 8-bus VSI case study

There are many factors that can influence the CPF scan results. To be able to see the impact of different factors, an 8-bus example with some features was used. This system was perfectly balanced; all the lines were transposed and all the loads were balanced. The left side of the system was exactly the same as the right side, including the length of branch, the line impedance matrix, and the loading. Therefore, this system had three pairs of two buses of the same characteristics. These three pairs were Bus 675 and Bus 634, Bus 684 and Bus 645, and Bus 671 and Bus 633.

Table 5.1 shows the VSI result for the base case. The results shows that the buses in each pair had the same VSI, indicating that the left side and the right side of the system were exactly the same. Moreover, based on these VSI, Bus 675 and Bus 634 were weaker than Bus 684 and Bus 645, while Bus 684 and Bus 645 were weaker than Bus 671 and Bus 633. This matched the fact that compared with other buses, Bus 675 and Bus 634 had the longest electrical distance from the substation.

This 8-bus was used as the base system. To investigate different factors that impact

Table 5.1: VSI for the 8-bus base case

Phase A		Phase B		Phase C	
634A	0.007	634B	0.007	634B	0.007
675A	0.007	675B	0.007	675B	0.007
645A	0.052	645B	0.052	645B	0.052
684A	0.052	684B	0.052	684B	0.052
671A	0.077	671B	0.077	671B	0.077
633A	0.077	633B	0.077	633B	0.077
632A	0.243	632B	0.243	632B	0.243

VSI, this base case system was modified according to the factor being investigated. For example, if we would like to see the impact of untransposed line, one of the branch in the base case was replaced by an untransposed line. The VSI of the modified case would be different from that of the base case. By comparing these two cases, we can determine the impact of the untransposed line.

In the following case studies, the network of the base case was modified, such as adding capacitors, replacing one branch with untransposed line, making the load unbalanced, doubling the load, and connecting DG. These case studies focused on the change of VSI of each bus in each pair. The change of VSI showed the impact of the factors that is being investigated.

Doubled load

In this case study, the balanced load was doubled load at one of the three buses on the right. Table 5.2 shows the VSI at the maximum loading point, which was found by CPF method with LID equal to the base loading point. Base case means that all the loads were balanced, while Bus 634 means that the load at Bus 634 was doubled in all of the three phases. The VSI at each bus/phase was shown in this table and the ranking was based on the magnitude of VSI. Only phase A was shown because the system was balanced, making the result for phase B and phase C exactly the same.

Table 5.2: VSI for different locations of doubled load

Base		Bus 634		Bus 645		Bus 633	
634A	0.007	634A	0.057	645A	0.002	634A	0.009
675A	0.007	645A	0.079	634A	0.013	633A	0.025
645A	0.052	675A	0.088	675A	0.045	675A	0.034
684A	0.052	633A	0.099	633A	0.071	645A	0.044
633A	0.077	684A	0.137	684A	0.092	684A	0.080
671A	0.077	671A	0.160	671A	0.115	671A	0.103
632A	0.243	632A	0.297	632A	0.254	632A	0.242

The impact of the doubled load can be investigated by the VSI difference of the corresponding buses on the left and right side: the pair of Bus 675 and Bus 634, the pair of Bus 684 and Bus 645 and the pair of Bus 671 and Bus 633. It can be found that the doubled load made the right side weaker than the left side. Moreover, the doubled load at Bus 645 made Bus 645 weaker than Bus 634, even though Bus 634 was farther away from the substation. Lastly, the doubled load at Bus 633 made Bus 633 weaker than Bus 645, which was downstream to Bus 633. Therefore, the resulting ranking did not follow upstream/downstream relationship.

Table 5.3 shows the comparison of VSI, CPF scan and voltage. The overall ranking of VSI was exactly the same as CPF scan and roughly the same as voltage except for Bus 633 and Bus 675.

Table 5.3: Comparison of VSI and CPF scan for 8-bus with doubled load at Bus 634

VSI		CPF scan		V	
634A	0.057	634A	-158.702	634A	0.452
645A	0.079	645A	-149.000	645A	0.564
675A	0.088	675A	-148.165	633A	0.580
633A	0.099	633A	-148.161	675A	0.599
684A	0.137	684A	-143.645	684A	0.631
671A	0.160	671A	-142.937	671A	0.646
632A	0.297	632A	-133.450	632A	0.738
				650A	1.000

Capacitor impact

In this case study, a three-phase capacitor was installed at one of the three buses on the right. The injected reactive power for each phase was 90 kVar. Table 5.4 shows the VSI at the maximum loading point, which was found by CPF method with LID equal to the base loading point. Base case means that there was no capacitor connected, while Bus 634 means that a three-phase capacitor was connected at Bus 634. The VSI at each bus/phase was shown in this table and the ranking was based on the magnitude of VSI. Only phase A was shown because the system was balanced, making the results for phase B and phase C exactly the same.

The impact of the capacitor can be investigated by the VSI difference of the corresponding buses on the left and right side: the pair of Bus 675 and Bus 634, the pair of Bus 684 and Bus 645 and the pair of Bus 671 and Bus 633. It can be found that the three-phase capacitor on the right made the bus on the right side stronger than the corresponding bus on the left side.

Table 5.5 shows the comparison of VSI, CPF scan and voltage. The overall ranking

Table 5.4: VSI for different location of three-phase capacitor

Base		Bus 645		Bus 633		Bus 634	
634A	0.007	675A	0.005	675A	0.005	675A	0.004
675A	0.007	634A	0.008	634A	0.008	634A	0.013
645A	0.052	684A	0.049	684A	0.049	684A	0.045
684A	0.052	645A	0.060	645A	0.054	645A	0.051
633A	0.077	671A	0.075	671A	0.075	671A	0.071
671A	0.077	633A	0.081	633A	0.083	633A	0.077
632A	0.243	632A	0.245	632A	0.244	632A	0.240

of VSI was exactly the same as CPF scan and voltage.

Table 5.5: Comparison of VSI and CPF scan for 8-bus with a 3P capacitor at Bus 634

VSI		CPF scan		V	
675A	0.004	675A	-5.191	675A	0.476
634A	0.013	634A	-5.097	634A	0.498
684A	0.045	684A	-4.836	684A	0.530
645A	0.051	645A	-4.773	645A	0.541
671A	0.071	671A	-4.688	671A	0.553
633A	0.077	633A	-4.637	633A	0.563
632A	0.240	632A	-2.415	632A	0.700

Unbalanced load

In this case study, the balanced load was changed into unbalanced load at one of the three buses on the right. Table 5.6 shows the VSI at the maximum loading point, which was found by CPF method with LID equal to the base loading point. Base case means that all the loads were balanced, while Bus 634 means that the load in phase A was the same, the load in phase B was increased by 50%, and the load in phase C was decreased by 50%. The VSI at each bus/phase is shown in this table and the ranking was based on the magnitude of VSI.

The impact of the unbalanced load can be investigated by the VSI difference of the

Table 5.6: VSI for different locations of unbalanced load

Base		Bus 634		Bus 645		Bus 633	
634A	0.007	675A	0.400	675A	0.400	634A	0.350
675A	0.007	634A	0.403	634A	0.403	675A	0.352
645A	0.052	684A	0.456	684A	0.456	645A	0.403
684A	0.052	645A	0.461	645A	0.461	684A	0.409
633A	0.077	671A	0.482	671A	0.482	633A	0.430
671A	0.077	633A	0.487	633A	0.487	671A	0.437
632A	0.243	632A	0.634	632A	0.634	632A	0.593
634B	0.007	634B	0.035	634B	0.035	634B	0.082
675B	0.007	645B	0.146	645B	0.146	675B	0.119
645B	0.052	675B	0.153	675B	0.153	645B	0.131
684B	0.052	633B	0.167	633B	0.167	633B	0.139
671B	0.077	684B	0.202	684B	0.202	684B	0.170
633B	0.077	671B	0.225	671B	0.225	671B	0.194
632B	0.243	632B	0.367	632B	0.367	632B	0.345
634B	0.007	675C	0.560	675C	0.560	675C	0.529
675B	0.007	684C	0.615	684C	0.615	684C	0.586
645B	0.052	671C	0.642	671C	0.642	671C	0.614
684B	0.052	645C	0.728	645C	0.728	634C	0.635
671B	0.077	633C	0.754	633C	0.754	645C	0.692
633B	0.077	632C	0.790	632C	0.790	633C	0.728
632B	0.243	634C	0.851	634C	0.851	632C	0.768

corresponding buses on the left and right side: the pair of Bus 675 and Bus 634, the pair of Bus 684 and Bus 645 and the pair of Bus 671 and Bus 633. It can be found that the impact of unbalanced load at Bus 634 was bigger than the unbalanced load at Bus 645 and Bus 633. Moreover, the unbalanced load made right side in phase B weaker and left side in phase C stronger. This is because the right side in phase B had higher loading while that in phase C had lower loading. There was not much difference between the left and the right in phase A because the loadings at both side were the same.

Table 5.7 shows the comparison of VSI, CPF scan and voltage. The pairwise ranking of VSI and CPF scan were the same in phase B and phase C. However, in phase A, the right side was stronger from VSI while weaker from CPF scan. The overall ranking of VSI was not the same as CPF scan and voltage.

Table 5.7: Comparison of VSI and CPF scan for 8-bus with unbalanced load at Bus 634

VSI		CPF scan		V	
675A	0.400	634A	-9.386	675A	0.811
634A	0.403	645A	-7.654	634A	0.812
684A	0.456	633A	-7.385	684A	0.829
645A	0.461	675A	-6.948	645A	0.831
671A	0.482	684A	-6.473	671A	0.838
633A	0.487	671A	-6.290	633A	0.840
632A	0.634	632A	-4.384	632A	0.892
				650A	1.000
634B	0.035	634B	16.435	634B	0.552
645B	0.146	645B	9.933	645B	0.634
675B	0.153	633B	9.054	**633B**	0.649
633B	0.167	675B	7.417	**675B**	0.654
684B	0.202	684B	6.238	684B	0.683
671B	0.225	671B	5.766	671B	0.697
632B	0.367	632B	-0.220	632B	0.778
				650B	1.000
675C	0.560	675C	-2.789	675C	0.877
684C	0.615	684C	-2.713	684C	0.891
671C	0.642	671C	-2.671	671C	0.899
645C	0.728	645C	-2.593	645C	0.929
633C	0.754	633C	-2.543	633C	0.935
632C	0.790	634C	-2.515	632C	0.943
634C	0.851	632C	-1.373	634C	0.963
				650C	1.000

Untransposed line

In this case study, the untransposed line replaced one of the transposed line at different locations. Table 5.8 shows the VSI at the maximum loading point, which was found by CPF method with LID equal to the base loading point. Base case means that all the lines were transposed line, while 633-634 means that the line between Bus 633 and Bus 634 was replaced by an untransposed line. The VSI at each bus/phase is shown in this table and the ranking was based on the magnitude of VSI.

The impact of the untransposed lie can be investigated by the VSI difference of the corresponding buses on the left and right side: the pair of Bus 675 and Bus 634, the pair of Bus 684 and Bus 645 and the pair of Bus 671 and Bus 633. It can be found that the impact of untransposed line was bigger if the untransposed line was at the 632-633, which was upstream to the line of 633-634. Moreover, the impact of the untransposed line of 633-645 was smaller than 633-634 because of the shorter length. Lastly, untransposed line made the right side in phase C weaker while made the right side in phase B stronger. There was no clear pattern for phase A.

Table 5.9 shows the comparison of VSI, CPF scan and voltage. Even though there was no clear pattern of CPF scan regarding the pairwise ranking, as shown in Table 4.12, there was a pattern of VSI in phase B and C: right side was stronger in phase B and weaker in phase C. The overall ranking of VSI was not the same as CPF scan and voltage.

Table 5.8: VSI for different locations of untransposed line

Base		633-634		633-645		632-633	
634A	0.007	634A	0.187	675A	0.172	634A	0.237
675A	0.007	675A	0.196	634A	0.172	675A	0.256
645A	0.052	684A	0.262	645A	0.235	645A	0.297
684A	0.052	645A	0.262	684A	0.238	684A	0.319
633A	0.077	671A	0.292	671A	0.269	633A	0.325
671A	0.077	633A	0.293	633A	0.269	671A	0.349
632A	0.243	632A	0.470	632A	0.449	632A	0.520
634B	0.007	675B	0.190	675B	0.163	675B	0.254
675B	0.007	634B	0.195	634B	0.163	634B	0.269
645B	0.052	684B	0.256	684B	0.229	684B	0.319
684B	0.052	645B	0.257	645B	0.231	645B	0.333
671B	0.077	671B	0.287	671B	0.260	671B	0.350
633B	0.077	633B	0.288	633B	0.260	633B	0.364
632B	0.243	632B	0.467	632B	0.441	632B	0.526
634B	0.007	634C	0.111	634C	0.128	634C	0.092
675B	0.007	675C	0.126	675C	0.129	675C	0.123
645B	0.052	645C	0.186	645C	0.188	645C	0.151
684B	0.052	684C	0.189	684C	0.193	633C	0.179
671B	0.077	633C	0.216	633C	0.222	684C	0.183
633B	0.077	671C	0.219	671C	0.223	671C	0.211
632B	0.243	632C	0.398	632C	0.404	632C	0.383

Table 5.9: Comparison of VSI and CPF scan for 8-bus with untransposed line at Branch 633-634

VSI		CPF scan		V	
634A	0.187	684A	46.922	634A	0.698
675A	0.196	645A	46.922	675A	0.705
684A	0.262	634A	-10.951	684A	0.733
645A	0.262	675A	-6.639	645A	0.733
671A	0.292	633A	-4.479	671A	0.746
633A	0.293	671A	-4.323	633A	0.746
632A	0.470	632A	0.565	632A	0.828
				650A	1.000
675B	0.190	634B	46.922	675B	0.700
634B	0.195	684B	46.922	634B	0.705
684B	0.256	645B	46.922	684B	0.729
645B	0.257	633B	-24.281	645B	0.730
671B	0.287	671B	-24.178	671B	0.743
633B	0.288	675B	-22.091	633B	0.744
632B	0.467	632B	-13.611	632B	0.827
				650B	1.000
634C	0.111	634C	46.922	634C	0.633
675C	0.126	684C	46.922	675C	0.647
645C	0.186	645C	46.922	645C	0.679
684C	0.189	675C	-17.419	684C	0.682
633C	0.216	633C	-12.432	633C	0.695
671C	0.219	671C	-12.168	671C	0.697
632C	0.398	632C	4.821	632C	0.794
				650C	1.000

DG in PQ mode

In this case study, DG in PQ mode was connected at Bus 633. Table 5.10 shows the VSI at the maximum loading point, which was found by CPF method with LID equal to the base loading point. Only phase A was shown because the system is balanced, making the result for phase B and phase C exactly the same. The percentage in this table is the DG output: the percentage of the original load of Bus 633. The VSI at each bus/phase is shown in this table and the ranking was based on the magnitude of VSI.

It can be found that by adding DG to Bus 633, the bus on the right was stronger than the corresponding bus on the left, meaning that for A,B,C phase, Bus 634 was stronger than Bus 675, Bus 645 was stronger than Bus 684, and Bus 633 was stronger than Bus 671. Moreover, with higher DG output the difference of VSI between left and right buses was higher. For example, between Bus 675 and Bus 634, the VSI difference was 0.001, 0.002 and 0,005 for 30%, 70% and 130%, respectively. Similar trend can be observed for the pair of Bus 645 and Bus 684 and the pair of Bus 633 and Bus 671.

Table 5.10: VSI for DG in PQ mode at Bus 633

0%		30%		70%		130%	
634A	0.007	675A	0.006	675A	0.004	675A	0.002
675A	0.007	634A	0.007	634A	0.006	634A	0.007
645A	0.052	684A	0.050	684A	0.046	684A	0.044
684A	0.052	645A	0.053	645A	0.051	645A	0.054
633A	0.077	671A	0.076	671A	0.071	671A	0.069
671A	0.077	633A	0.081	633A	0.083	633A	0.091
632A	0.243	632A	0.244	632A	0.241	632A	0.243

In the similar setting, DG in PQ mode was connected at Bus 645 and Bus 634, and Table 5.11 and Table 5.12 shows the VSI at the maximum loading point. Similar observation can be made as DG in PQ mode connected at Bus 633. The bus on the right was stronger than the corresponding bus on the left. Moreover, with higher DG output, the difference of VSI between left and right buses were higher. When DG in PQ mode connected at Bus 645 supplied 130% of its local load, Bus 645 became stronger than not only 684 but also 671.

Table 5.11: VSI for DG in PQ mode at Bus 645

0%		30%		70%		130%	
634A	0.007	675A	0.006	675A	0.004	675A	0.003
675A	0.007	634A	0.008	634A	0.007	634A	0.008
645A	0.052	684A	0.051	684A	0.046	684A	0.044
684A	0.052	645A	0.057	645A	0.062	671A	0.070
633A	0.077	671A	0.076	671A	0.072	**645A**	0.073
671A	0.077	633A	0.079	633A	0.079	633A	0.083
632A	0.243	632A	0.245	632A	0.242	632A	0.245

Table 5.12: VSI for DG in PQ mode at Bus 634

0%		30%		70%		130%	
634A	0.007	675A	0.004	675A	0.002	675A	0.001
675A	0.007	634A	0.010	634A	0.017	634A	0.033
645A	0.052	684A	0.046	684A	0.043	684A	0.041
684A	0.052	645A	0.050	645A	0.050	645A	0.055
633A	0.077	671A	0.072	671A	0.068	671A	0.067
671A	0.077	633A	0.075	633A	0.077	633A	0.083
632A	0.243	632A	0.239	632A	0.238	632A	0.243

Table 5.13 and Table 5.14 show the comparison of VSI, CPF scan and voltage. For DG in PQ mode supplying 70%, the overall ranking of VSI, CPF scan and voltage were exactly the same. However, for DG in PQ mode supplying 130%, the pairwise ranking

of VSI, CPF scan and voltage were exactly the same, but the overall ranking of VSI, CPF scan and voltage were not.

Table 5.13: Comparison of VSI/CPF scan for 8-bus with DG in PQ at Bus 634, 70% power

VSI		CPF scan		V	
675A	0.002	675A	-181.472	675A	0.470
634A	0.017	634A	-174.983	634A	0.498
684A	0.043	684A	-173.810	684A	0.526
645A	0.050	645A	-172.410	645A	0.540
671A	0.068	671A	-172.381	671A	0.549
633A	0.077	633A	-171.251	633A	0.562
632A	0.238	632A	-156.178	632A	0.699

Table 5.14: Comparison of VSI/CPF scan for 8-bus with DG in PQ at Bus 634, 130% power

VSI		CPF scan		V	
675A	0.001	675A	-179.455	675A	0.468
634A	0.033	684A	-178.947	634A	0.517
684A	0.041	634A	-178.698	684A	0.526
645A	0.055	671A	-173.772	671A	0.549
671A	0.067	633A	-173.485	645A	0.550
633A	0.083	645A	-172.819	633A	0.572
632A	0.243	632A	-157.089	632A	0.702

DG in PV mode

In this case study, DG in PV mode was connected at different locations: Bus 634, Bus 633 and Bus 645. Table 5.15 shows the VSI at the maximum loading point, which was found by CPF method with LID equal to the base loading point. The VSI at each bus/phase is shown in this table and the ranking was based on the magnitude of VSI.

It can be found that by adding DG in PV to one of the three buses on the right, the bus on the right was stronger than the corresponding bus on the left, meaning that for A,B,C phase, Bus 634 was stronger than Bus 675, Bus 645 was stronger than Bus 684, and Bus 633 was stronger than Bus 671. Moreover, Bus 632 was no longer the strongest bus. Because of DG in PV mode, there were two sources: one was substation, the other was DG in PV mode. The ranking of buses on the left side followed the upstream/downstream pattern. However, the ranking of buses on the right depended on the location of DG in PV mode. For DG in PV mode at Bus 634, Bus 633 was stronger than Bus 632 because Bus 633 was closer to the source. For DG in PV mode at Bus 633, Bus 634 and Bus 645 were stronger than Bus 632, because Bus 634 and Bus 645 were closer to the source. For DG in PV mode at Bus 645, Bus 633 was stronger than Bus 632, and Bus 632 was stronger than 634 for the similar reason. Note that even though the ranking of VSI in each phase was not the same, the ranking, however, was the same in each phase.

Table 5.16 shows the comparison of VSI, CPF scan and voltage. The pairwise ranking of VSI, CPF scan and voltage are exactly the same, while The overall ranking are not the same.

Table 5.15: VSI for DG in PV mode at different locations

No DG		Bus 634		Bus 633		Bus 645	
634A	0.007	675A	0.265	675A	0.244	675A	0.256
675A	0.007	684A	0.347	684A	0.351	684A	0.349
645A	0.052	671A	0.387	671A	0.402	671A	0.394
684A	0.052	645A	0.591	632A	0.735	634A	0.610
633A	0.077	632A	0.632	634A	0.775	632A	0.679
671A	0.077	633A	0.640	645A	0.928	633A	0.796
632A	0.243						
634B	0.007	675B	0.502	675B	0.521	675B	0.520
675B	0.007	684B	0.570	684B	0.604	684B	0.593
645B	0.052	671B	0.604	671B	0.646	671B	0.631
684B	0.052	645B	0.744	632B	0.855	634B	0.763
671B	0.077	632B	0.777	634B	0.863	632B	0.817
633B	0.077	633B	0.779	645B	0.958	633B	0.884
632B	0.243						
634B	0.007	675C	0.040	675C	0.037	675C	0.033
675B	0.007	684C	0.115	684C	0.134	684C	0.117
645B	0.052	671C	0.151	671C	0.182	671C	0.158
684B	0.052	645C	0.423	632C	0.570	632C	0.491
671B	0.077	632C	0.432	634C	0.771	634C	0.509
633B	0.077	633C	0.471	645C	0.928	633C	0.697
632B	0.243						

Table 5.16: Comparison of VSI/CPF scan for 8-bus with DG in PV at Bus 634

VSI		CPF scan		V	
675A	0.265	675A	-179.455	675A	0.466
684A	0.347	684A	-178.947	684A	0.544
671A	0.387	634A	-178.698	671A	0.574
645A	0.591	671A	-173.772	632A	0.774
632A	0.632	633A	-173.485	645A	0.779
633A	0.640	645A	-172.819	633A	0.800
		632A	-157.089	634A	1.000
				650A	1.000

Summary

The pair ranking column means that whether the pair ranking matches the network characteristics. For example, if more load is connected on the right side, the buses on the right side should be weaker than that on the left side for each pair. For pair ranking perspective, VSI results matched the network characteristics except for the unbalanced load and the untransposed line. For these two cases, the impact of these two elements cannot be determined by the network characteristics due to the coupling among phases. Therefore, we cannot determine whether the VSI results matched the network characteristics, similar argument as CPF scan. In the comparison among VSI, CPF scan ranking and voltage ranking, the weakest bus and the pairwise ranking were the same for all the cases except for the unbalanced load and the untransposed line. The overall rankings were not the same for the most of the cases.

Table 5.17: Summary of 8-Bus VSI case studies

Case	Pair ranking	VSI vs CPF scan			VSI vs V		
		Weakest	PR	Overall	Weakest	PR	Overall
Base	V	V	V	V	V	V	V
Doubled	V	V	V	V	V	V	X
3P Cap	V	V	V	V	V	V	X
Unbalanced load	V(BC), ?(A)	V(BC), ?(A)	X	X	X	X	X
Untran. line	??	X	X	X	V	X	X
DG at 70%	V	V	V	V	V	V	V
DG at 130%	V	V	V	X	V	V	X
DG in PV	V	V	V	X	V	V	X

V: consistent, X: not consistent, ??: cannot be determined, V(BC): consistent in phase B and C, ?(A): cannot be determined in phase A

5.4.2 13-node test feeder VSI Case study

In the following case studies of the modified IEEE 13-node test feeder with DG, the impacts of different operating points on VSI were investigated. Moreover, the impacts of capacitors, DG in PQ mode and DG in PV mode on VSI were investigated.

Different operating points

We performed a case study on the IEEE 13-node test feeder. The VSI at different operating points was found. CPF method with LID equal to the base loading point was used to find the corresponding operating point. Table 5.18 shows the VSI at different operating points. For the base, the mid and the max, the loading factor λ were 0.034, 0.762 and 1.332, respectively.

The rankings at different operating point were not exactly the same. Moreover, the rankings did not exactly follow the upstream/downstream relationship. For phase B and phase C, Bus 632 was not the strongest; in phase B the strongest was Bus 675 while in phase C, the strongest was Bus 646.

Table 5.18: VSI at different operating points

Base		Mid		Max	
675A	0.674	675A	0.391	675A	0.092
652A	0.684	652A	0.425	671A	0.134
680A	0.696	671A	0.433	652A	0.148
671A	0.699	680A	0.440	680A	0.156
684A	0.701	684A	0.450	684A	0.168
634A	0.720	634A	0.492	634A	0.234
633A	0.812	633A	0.635	633A	0.389
632A	0.823	632A	0.654	632A	0.410
646B	0.672	646B	0.445	646B	0.311
645B	0.701	645B	0.489	645B	0.366
634B	0.723	634B	0.523	634B	0.411
633B	0.794	633B	0.634	633B	0.551
632B	0.802	632B	0.646	632B	0.565
680B	0.817	671B	0.657	671B	0.621
671B	0.817	680B	0.666	680B	0.645
675B	0.834	675B	0.692	675B	0.678
611C	0.709	611C	0.429	671C	0.243
680C	0.712	675C	0.430	675C	0.248
675C	0.712	671C	0.431	611C	0.253
671C	0.715	680C	0.438	680C	0.264
684C	0.717	684C	0.444	684C	0.273
634C	0.789	634C	0.584	634C	0.432
633C	0.862	633C	0.700	633C	0.574
632C	0.873	632C	0.716	632C	0.594
645C	0.887	645C	0.741	645C	0.624
646C	0.889	646C	0.743	646C	0.627

With and without capacitor

In this case study, we connected the single phase capacitor and three-phase capacitor at Bus 611 and Bus 675, respectively The VSI at different operating points was found. CPF method with LID equal to the base loading point was used to find the corresponding operating point. Table 5.19 shows the VSI for different cases.

By comparing No C and 611(1P), even though the ranking in phase C was the same for No C and 611(1P), 652A was getting stronger than 671A. By comparing No C and 675(3P), the VSI difference between 675A and 671A was getting smaller and 675C was getting stronger than 671C. By comparing No C and 611(1P)+675(3P), the VSI difference between 675A and 671A was getting smaller and 675C was getting stronger than 671C.

Table 5.19: VSI for different capacitor locations

No C		611(1P)		675(3P)		611(1P)+675(3P)	
675A	0.167	675A	0.080	675A	0.102	675A	0.092
652A	0.216	671A	0.126	671A	0.146	671A	0.134
671A	0.221	652A	0.139	652A	0.160	652A	0.148
680A	0.239	680A	0.146	680A	0.169	680A	0.156
684A	0.249	684A	0.158	684A	0.182	684A	0.168
634A	0.314	634A	0.236	634A	0.240	634A	0.234
633A	0.471	633A	0.383	633A	0.400	633A	0.389
632A	0.491	632A	0.402	632A	0.420	632A	0.410
646B	0.244	646B	0.325	646B	0.306	646B	0.311
645B	0.311	645B	0.377	645B	0.362	645B	0.366
634B	0.368	634B	0.420	634B	0.408	634B	0.411
633B	0.492	633B	0.554	633B	0.549	633B	0.551
632B	0.505	632B	0.567	632B	0.563	632B	0.565
671B	0.524	671B	0.603	671B	0.622	671B	0.621
680B	0.545	680B	0.625	680B	0.647	680B	0.645
675B	0.572	675B	0.651	675B	0.681	675B	0.678
675C	0.116	675C	0.218	671C	0.173	671C	0.243
671C	0.120	671C	0.222	675C	0.179	675C	0.248
611C	0.123	611C	0.232	611C	0.183	611C	0.253
680C	0.139	680C	0.242	680C	0.196	680C	0.264
684C	0.145	684C	0.250	684C	0.204	684C	0.273
634C	0.333	634C	0.419	634C	0.373	634C	0.432
633C	0.452	633C	0.553	633C	0.509	633C	0.574
632C	0.469	632C	0.572	632C	0.529	632C	0.594
645C	0.498	645C	0.599	645C	0.557	645C	0.624
646C	0.502	646C	0.601	646C	0.559	646C	0.627

DG in PV and PQ mode

In this case study, we connected a DG at Bus 671. The DG can be in PQ mode or in PV mode. For DG in PQ mode, the DG supplied X% of local load. For DG in PV mode, the reactive power limit was large enough so that even at the maximum loading point, the DG was still in PV mode. CPF method with LID equal to the base loading point was used to find the maximum operating point and the VSI was calculated. Table 5.20 shows the VSI for DG in PQ mode outputting different amounts of power and for DG in PV mode.

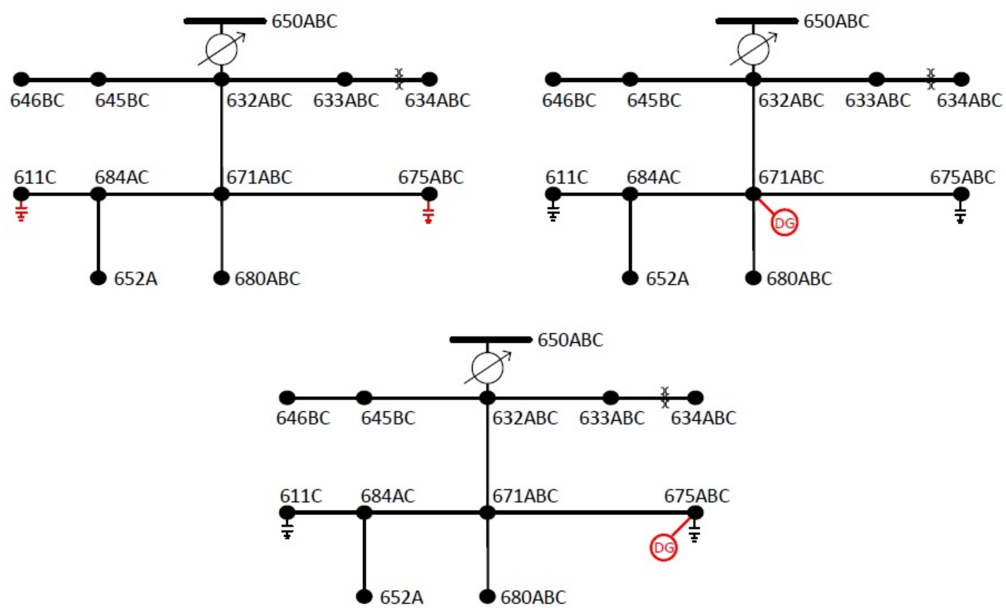

Figure 5.3: 13-node test feeder with DGs

For DG in PQ mode, Bus 671A and Bus 671C were getting weaker as the DG output was increased while 671B remained relatively the same. This phenomenon was quite unexpected. For DG in PV mode, 671 had no VSI because the proposed VSI was only defined for the load buses. From the table, we can see from the ranking that Bus 675A, Bus 680A, Bus 684A and Bus 675C were getting stronger. Even though the rankings of 684C and 680C were similar to No DG case, the VSI differences between 680C/684C and 633C were smaller, which means that 680C and 684C were getting stronger as well.

Table 5.20: VSI for DG in PQ/PV mode at Bus 671

0%		30%		70%		130%		PV	
675A	0.167	675A	0.062	675A	0.011	**671A**	0.021	634A	0.473
652A	0.216	**671A**	0.118	**671A**	0.071	675A	0.048	633A	0.857
671A	0.221	652A	0.142	652A	0.110	652A	0.082	**675A**	0.879
680A	0.239	680A	0.162	680A	0.130	680A	0.103	652A	0.880
684A	0.249	684A	0.167	684A	0.138	684A	0.116	632A	0.905
634A	0.314	634A	0.219	634A	0.181	634A	0.141	**680A**	0.968
633A	0.471	633A	0.384	633A	0.351	633A	0.321	**684A**	0.969
632A	0.491	632A	0.406	632A	0.372	632A	0.343		
646B	0.244	646B	0.268	646B	0.235	646B	0.180	646B	0.019
645B	0.311	645B	0.324	645B	0.292	645B	0.237	645B	0.063
634B	0.368	634B	0.371	634B	0.341	634B	0.289	634B	0.109
633B	0.492	633B	0.515	633B	0.490	633B	0.443	633B	0.287
632B	0.505	632B	0.529	632B	0.505	632B	0.458	632B	0.313
671B	0.524	**671B**	0.565	**671B**	0.532	**671B**	0.461	680B	0.972
680B	0.545	680B	0.608	680B	0.587	680B	0.535	**675B**	1.017
675B	0.572	675B	0.628	675B	0.607	**675B**	0.557		
675C	0.116	675C	0.128	**671C**	0.113	**671C**	0.072	634C	0.740
671C	0.120	**671C**	0.129	675C	0.115	675C	0.080	611C	0.895
611C	0.123	611C	0.149	611C	0.143	611C	0.120	**675C**	0.946
680C	0.139	680C	0.173	680C	0.171	680C	0.152	**684C**	0.947
684C	0.145	684C	0.173	684C	0.174	684C	0.159	**680C**	0.966
634C	0.333	634C	0.340	634C	0.334	634C	0.311	633C	1.068
633C	0.452	633C	0.480	633C	0.484	633C	0.472	632C	1.114
632C	0.469	632C	0.500	632C	0.504	632C	0.494	645C	1.267
645C	0.498	645C	0.529	645C	0.536	646C	0.529	646C	1.303
646C	0.502	646C	0.531	646C	0.537	645C	0.529		

In this case study, we connected a DG at Bus 675. The exactly the same setup as the previous case was applied. Table 5.21 shows the VSI for DG in PQ mode generating different amount of power and for DG in PV mode.

Table 5.21: VSI for DG in PQ/PV mode at Bus 675

0%		30%		70%		130%		PV	
675A	0.167	**675A**	0.138	**675A**	0.121	**675A**	0.179	634A	0.475
652A	0.216	671A	0.208	671A	0.207	671A	0.282	633A	0.842
671A	0.221	652A	0.228	652A	0.241	652A	0.325	652A	0.860
680A	0.239	680A	0.255	680A	0.274	634A	0.369	632A	0.887
684A	0.249	684A	0.261	684A	0.283	680A	0.369	**680A**	0.945
634A	0.314	634A	0.286	634A	0.285	684A	0.381	**684A**	0.946
633A	0.471	633A	0.468	633A	0.484	633A	0.592	**671A**	0.974
632A	0.491	632A	0.490	632A	0.508	632A	0.616		
646B	0.244	646B	0.249	646B	0.184	646B	0.070	646B	0.021
645B	0.311	645B	0.301	645B	0.231	645B	0.098	645B	0.064
634B	0.368	634B	0.345	634B	0.271	634B	0.123	634B	0.107
633B	0.492	633B	0.484	633B	0.407	671B	0.182	633B	0.276
632B	0.505	632B	0.499	632B	0.423	680B	0.200	632B	0.300
671B	0.524	671B	0.523	671B	0.429	**675B**	0.213	680B	0.825
680B	0.545	680B	0.555	680B	0.457	633B	0.227	**671B**	0.850
675B	0.572	**675B**	0.576	**675B**	0.478	632B	0.241		
675C	0.116	**675C**	0.056	671C	0.008	671C	0.100	634C	0.705
671C	0.120	671C	0.056	**675C**	0.012	**675C**	0.100	611C	0.812
611C	0.123	611C	0.083	611C	0.053	611C	0.144	**684C**	0.861
680C	0.139	680C	0.102	680C	0.073	680C	0.178	**680C**	0.879
684C	0.145	684C	0.104	684C	0.079	684C	0.184	**671C**	0.908
634C	0.333	634C	0.265	634C	0.226	634C	0.353	633C	1.013
633C	0.452	633C	0.394	633C	0.360	633C	0.513	632C	1.056
632C	0.469	632C	0.412	632C	0.378	632C	0.534	645C	1.195
645C	0.498	645C	0.439	645C	0.408	645C	0.583	646C	1.227
646C	0.502	646C	0.440	646C	0.408	646C	0.586		

For DG in PQ mode, by calculating the difference of VSI between 675A and 671A, Bus 675A was found to be weaker as the DG output is increased. For phase B and phase C, Bus 675 was getting stronger but not so clearly. This phenomenon was quite unexpected. For DG in PV mode, 675 had no VSI because the proposed VSI was only defined for the load buses. From the table, we can see from the ranking that Bus 671A, Bus 684A, Bus 680A ,Bus 671B, Bus 680B and Bus 671C were getting stronger. Even though the rankings of 684C, 680C were similar to No DG case, the VSI differences between 680C/684C and 633C were getting smaller, which means that 680C and 684C were getting stronger as well.

5.5 Discussions and limitations

From the case studies in the 8-bus system, for the impact of unbalanced load, doubled load and three-phase capacitor, the rankings of the VSI matched the network characteristics. Moreover, the pair-wise ranking based on VSI was exactly the same as that based on CPF scan method. However, for complicated network characteristics, such as untransposed line, DG in PQ, and DG in PV mode, it is difficult to determine if the rankings of VSI were correct. The pair-wise ranking based on VSI was not exactly the same as that based on CPF scan method. In the 13-node test feeder, VSI was used to rank the weakness of the buses/phases. The VSI ranking did not follow the upstream/down relationship. Because VSI is also related to saddle node bifurcation, the shape of saddle node bifurcation surface affects the VSI. Therefore, not only is the VSI ranking related to upstream/downstream relationship, it is also related to the SNB surface.

There are some limitations of this proposed methods. Firstly, this method requires an accurate model of the system. That is, the information of the line impedance. In most of the distribution systems, the line impedance information is not accurate. Secondly, this method requires the phasor information for all of the nodes. This means that lots of PMU need to be installed in the system, which is not practical for distribution systems. Thirdly, even though the proposed method can be used to determine the weak buses of the system, the threshold value below which the voltage collapse is near will depends on the system. Sometimes, the VSI is close to zero with small value, such as 0.001, but sometimes, VSI is close to 0.1 when the loading point is close to knee point. Lastly, the propose method requires all information sent to a central controller, which requires high communication bandwidth. However, in distribution system, this type of communication requirement is not economical.

5.6 Conclusions

A new voltage stability index for three-phase unbalanced distribution systems with DG was proposed in this section. This new index only requires the network information and the load information. It is measurement based; not complicated calculation is needed. It is based on the real number solution of power flow solution. It not only provides the system wide information but also the individual bus information. The derivation of the proposed voltage stability index were derived with 2-bus single phase, N-bus single phase and N-bus three phase network. The monotonic property of the index was investigated in the case where the loading factor of the system was increased. Similar to CPF scan method, an 8-bus and the IEEE 13-node test feeder were used as the examples. Different factors that influences this index were investigated. Similar to CPF scan result, for the impact of unbalanced load, doubled load and three-phase capacitor, the rankings of the VSI matched the network characteristics. Moreover, the pair-wise ranking based on VSI was exactly the same as that based on CPF scan method. However, for complicated network characteristics, such as untransposed line, DG in PQ, and DG in PV mode, it is difficult to determine if the rankings of VSI were correct. The pair-wise ranking based on VSI was not exactly the same as that based on CPF scan method. In the 13-node test feeder, VSI was used to rank the weakness of the buses/phases. The VSI ranking was not exactly the same as that based on CPF scan method.

6 CONCLUSIONS AND FUTURE WORK

6.1 Summary and conclusions

In this work, the voltage stability problems of three-phase unbalanced distribution systems with DG were investigated. Several methods were proposed and utilized to investigate the voltage stability problem.

Firstly, a three-phase CPF method was improved and implemented so that the maximum loading factor of the distribution system can be found accurately. The improved CPF method allows faster and more robust computations, due to the arc parameterization approach and the step size control. The improved CPF method models various components in distribution systems such as different phase and connection of loads, voltage regulator control, and DG in PQ mode and PV mode with reactive power limit.

The results of the improved CPF method were verified with OpenDSS and Matpower software. The results were fairly consistent with these two programs. Some case studies were performed to investigate the impact of different factors on the maximum loading factor. It was found that different load modeling had different impact on the maximum loading. The constant power load model had the lowest maximum loadability. Also, when the DG in PQ mode generated more power, the maximum loading factor was increased. When the DG in PV mode had higher reactive power limit, the maximum loading factor was increased. Lastly, the step size used in the CPF prediction stage should be within a given range. If the step size was too small or too big, the CPF method cannot trace the whole PV curve.

Secondly, a new voltage stability analysis method, the CPF scan method, was proposed. The CPF scan method perturbs the load increase direction (LID) along different buses/phases to identify which buses/phases have the highest impact on the maximum loading factor and the maximum total real power. The CPF scan method utilizes the modified CPF method. It simultaneously considers three factors that impact the weak bus locations: the network characteristics, the base operating point, the load increase direction. The CPF scan provides the weak bus ranking for all of the buses/phases of a system. Some properties of the CPF scan results were investigated. For example, the CPF scan results varies for different LID and different initial loading points. The condition was found so that the weakness ranking of buses based on loading factor and on maximum total real power are the same.

To evaluate the CPF scan method, it was applied to an 8-bus system and the IEEE 13-node test feeder with DG. The weakness ranking results were compared with the ranking based on the voltage magnitude at the maximum loading factor. Comparisons were made regarding the overall ranking, pairwise ranking and the weakest bus for the 8-bus system. For the 8-bus system, the impact of different components on the weak bus ranking were examined, such as untransposed lines, unbalanced loads, doubled loads, three-phase capacitor banks. Moreover, the impact of DG in PQ mode with different output power and the impact of DG in PV mode were investigated, too. The results shows that for simple components, such as doubled loads and three-phase capacitor banks, the ranking of the

CPF scan results matched the ranking of voltage magnitude. However, for complicated components, such as unbalanced loads, untransposed lines, and DG in PV mode, the results did not match the ranking of voltage magnitude. This is because of the complicated shape of SNB surface. In addition, the application of CPF scan method to operation and planning of distribution systems scenarios were demonstrated. The application to operation of distribution system identified the direction and the amount of the LID perturbation to increase the voltage stability margin. In the study of CPF scan method for the planning, the most effective location to place reactive power compensation by SVC did not follow the ranking of the CPF scan results.

Lastly, a new voltage stability index for three-phase unbalanced distribution systems with DGs was proposed. It can determine the weak buses of the system and determine whether the system is close to voltage collapse point. This new index only requires the network information and the load information. It is measurement based; complicated calculation is not needed. It not only provides the system wide information but also the individual bus information. The derivation of the proposed voltage stability index were derived and the monotonic property of the index was investigated.

Similar to the CPF scan method, to evaluate the proposed voltage stability index, an 8-bus system and the modified IEEE 13-node test feeder with DG were used as examples. The proposed VSI successfully detected the occurrence of voltage collapse. The ranking results were compared with the ranking based on the CPF scan method and with the ranking based on the voltage magnitude at the maximum loading factor. The comparisons were made regarding the overall ranking, pairwise ranking and the weakest bus for the 8-bus system. For the 8-bus system, the impact of different components on the weak bus ranking were examined, such as untransposed lines, unbalanced loads, doubled loads, three-phase capacitor banks. Moreover, the impact of DG in PQ mode with different output power and the impact of DG in PV mode were investigated, too. The results shows that for simple components, such as doubled loads and three-phase capacitor banks, the overall ranking of the VSI results matched the ranking of the CPF scan method. Moreover, the pair-wise rankings based on VSI were exactly the same as that based on voltage magnitude. However, for complicated components, such as unbalanced loads, untransposed lines, and DG in PV mode, the results did not match the ranking of voltage magnitude. The ranking of VSI did not exactly match the CPF scan results, either. In the modified IEEE 13-node test feeder with DG, VSI was used to rank the weakness of the buses/phases. The ranking based on VSI did not follow the upstream/down relationships. However, the VSI successfully identified the impact of DGs in PQ mode and PV mode.

6.2 Future work

Several future work can be performed for the CPF scan method. One of the future work is related to how to verify the CPF scan results. As seen from the case studies in CPF scan section, in some cases where the network characteristics were complicated, such as untransposed lines, DGs in PQ and PV mode, it was very hard to verify the CPF scan results. The major part of the work was doing exhaustive simulation to investigate these effects. More investigation on the complicated network characteristics is needed. For example, for untransposed lines, the degree of untransposed lines needs to be defined. Then, by sweeping the different degree of untransposed lines, it may be possible to find the impact of untransposed lines. Secondly, the combination of LID perturbation (via demand response) and base operating point perturbation (via load shedding) can be made to increase the maximum total real power or maximum loading factor of the system. Furthermore, because the loads in the system are constantly changing and the DG output is constantly changing, some stochastic feature can be incorporated in the LID. The resulting weak buses rankings can be related to these stochastic features. Lastly, because the CPF scan method is computationally intensive, to reduce the time requirement, CPF scan method may be combined with linear approximation, such as the one proposed in [55].

Several future work can be performed for the proposed VSI. The proposed VSI needs the overall system information such as voltage measurement and network parameters. Moreover, all the information would be collected at a central center to calculate the proposed VSI. However, in distribution systems it is impossible to have overall and accurate information of the system. The load information from all the nodes are not available to send to the control center. Therefore, new ways of calculating the proposed VSI are needed. Firstly, the network topology of distribution systems, the upstream/downstream relationship, may be used to reduce the requirement of measurement information. Secondly, the system parameter identification may be performed by taking advantage of the data from smart meters across the distribution system. Some state estimation techniques may be included to identify system parameters or load estimation. Thirdly, a distributed algorithm for VSI and a distributed communication scheme could be designed. In this way, a central controller and a centralized communication scheme can be avoided, which is more practical to the application of distribution systems.

REFERENCES

[1] "Smart grid system report," tech. rep., Energy, U.S. Department of, 2009.

[2] E. Marris, "Energy: Upgrading the grid," *Nature News*, vol. 454, pp. 570–573, July 2008.

[3] A. G. Phadke, "Synchronized phasor measurements in power systems," *IEEE Comput. Appl. Power*, vol. 6, no. 2, pp. 10–15, 1993.

[4] V. Terzija, G. Valverde, C. Deyu, P. Regulski, V. Madani, J. Fitch, S. Skok, M. M. Begovic, and A. Phadke, "Wide-area monitoring, protection, and control of future electric power networks," *Proc. IEEE*, vol. 99, no. 1, pp. 80–93, 2011.

[5] W. H. Kersting, *Distribution System Modeling and Analysis*. CRC Press, 2 ed., 2006.

[6] R. C. Dugan and M. McGranaghan, "Sim city," *Power and Energy Magazine, IEEE*, vol. 9, no. 5, pp. 74–81, 2011.

[7] C. V. Thierry van Cutsem, *Voltage Stability of Electric Power Systems*. Springer, 2007.

[8] P. Kundur, *Power System Stability and Control*. McGraw-Hill Professional, 1994.

[9] A. Augugliaro, L. Dusonchet, and S. Mangione, "Voltage collapse proximity indicators for radial distribution networks," in *Proc. 9th International Conference on Electrical Power Quality and Utilisation*, pp. 1–6, 2007.

[10] M. Moghavvemi and M. O. Faruque, “Technique for assessment of voltage stability in ill-conditioned radial distribution network,” *IEEE Power Eng. Rev.*, vol. 21, no. 1, pp. 58–60, 2001. BD1.

[11] M. Chakravorty and D. Das, “Voltage stability analysis of radial distribution networks,” *International Journal of Electrical Power and Energy Systems*, vol. 23, no. 2, pp. 129–135, 2001.

[12] M. M. Hamada, M. A. A. Wahab, and N. G. A. Hemdan, “Simple and efficient method for steady-state voltage stability assessment of radial distribution systems,” *Electric Power Systems Research*, vol. 80, no. 2, pp. 152–160, 2010.

[13] V. Ajjarapu and B. Lee, “Bibliography on voltage stability,” *IEEE Trans. Power Syst.*, vol. 13, no. 1, pp. 115–125, 1998.

[14] R. B. Prada and L. J. Souza, “Voltage stability and thermal limit: constraints on the maximum loading of electrical energy distribution feeders,” *IEE Proc. Generation, Transmission and Distribution*, vol. 145, no. 5, pp. 573–577, 1998.

[15] G. Brownell and H. Clark, “Analysis and solutions for bulk system voltage instability,” *IEEE Comput. Appl. Power*, vol. 2, no. 3, pp. 31–35, 1989.

[16] P. P. Barker and R. W. De Mello, “Determining the impact of distributed generation on power systems Part I: Radial distribution systems,” in *Power Engineering Society Summer Meeting, IEEE*, vol. 3, 2000.

[17] T. Basso and R. DeBlasio, "IEEE 1547 series of standards: interconnection issues," *IEEE Transactions on Power Electronics*, vol. 19, pp. 1159–1162, Sept. 2004.

[18] R. B. Vu Van Thong, Johan Driesen, "Power quality and voltage stability of distribution system with dirstributed energy resources," *International Journal of Distributed energy Resources*, vol. 1, 2005.

[19] A. P. S. Meliopoulos, "Distributed energy sources: needs for analysis and design tools," in *Power Engineering Society Summer Meeting, 2001*, vol. 1, pp. 548–550 vol.1, 2001.

[20] A. Girgis and S. Brahma, "Effect of distributed generation on protective device coordination in distribution system," in *Power Engineering, 2001. LESCOPE '01. 2001 Large Engineering Systems Conference on*, pp. 115–119.

[21] S. M. Brahma and A. A. Girgis, "Development of adaptive protection scheme for distribution systems with high penetration of distributed generation," *IEEE Trans. Power Del.*, vol. 19, no. 1, pp. 56–63, 2004.

[22] N. G. A. Hemdan and M. Kurrat, "Distributed generation location and capacity effect on voltage stability of distribution networks," in *Student Paper, 2008 Annual IEEE Conference*, pp. 1–5.

[23] A. D. T. Le, M. A. Kashem, M. Negnevitsky, and G. Ledwich, "Control strategy of distributed generation for voltage support in distribution systems," in *Power*

Electronics, Drives and Energy Systems, 2006. PEDES '06. International Conference on, pp. 1–6.

[24] N. C. Scott, D. J. Atkinson, and J. E. Morrell, "Use of load control to regulate voltage on distribution networks with embedded generation," *IEEE Trans. Power Syst.*, vol. 17, no. 2, pp. 510–515, 2002.

[25] P. Kundur, J. Paserba, V. Ajjarapu, G. Andersson, A. Bose, C. Canizares, N. Hatziargyriou, D. Hill, A. Stankovic, C. Taylor, T. V. Cutsem, and V. Vittal, "Definition and classification of power system stability IEEE/CIGRE joint task force on stability terms and definitions," *IEEE Trans. on Power Syst.*, vol. 19, pp. 1387–1401, Aug. 2004.

[26] C. A. Canizares *et al.*, "Voltage stability assessment: concepts, practices and tools," *Power System Stability Subcommittee Special Publication IEEE/PES, Final Document*, 2002.

[27] I. Dobson, H.-D. Chiang, J. Thorp, and L. Fekih-Ahmed, "A model of voltage collapse in electric power systems," in *, Proceedings of the 27th IEEE Conference on Decision and Control, 1988*, pp. 2104–2109 vol.3, 1988.

[28] I. Dobson and H.-D. Chiang, "Towards a theory of voltage collapse in electric power systems," *Systems & Control Letters*, vol. 13, pp. 253–262, Sept. 1989.

[29] I. Dobson, "Observations on the geometry of saddle node bifurcation and voltage collapse in electrical power systems," *IEEE Transactions on Circuits and Systems I: Fundamental Theory and Applications*, vol. 39, no. 3, pp. 240–243, 1992.

[30] V. Ajjarapu and C. Christy, "The continuation power flow: a tool for steady state voltage stability analysis," *IEEE Trans. on Power Syst.*, vol. 7, no. 1, pp. 416–423, 1992.

[31] C. Rajagopalan, B. Lesieutre, P. Saucer, and M. Pai, "Dynamic aspects of voltage/power characteristics," *IEEE Trans. on Power Syst.*, vol. 7, 1992.

[32] B. Gao, G. K. Morison, and P. Kundur, "Voltage stability evaluation using modal analysis," *IEEE Trans on Power Syst.*, vol. 7, no. 4, pp. 1529–1542, 1992.

[33] V. Venkatasubramanian, H. Schattler, and J. Zaborszky, "Voltage dynamics: study of a generator with voltage control, transmission, and matched mw load," *IEEE Transactions on Automatic Control*, vol. 37, no. 11, pp. 1717–1733, 1992. 5.

[34] E. H. Abed, A. M. A. Hamdan, H. C. Lee, and A. G. Parlos, "On bifurcations in power system models and voltage collapse," in *Decision and Control, 1990., Proceedings of the 29th IEEE Conference on*, pp. 3014–3015 vol.6.

[35] G. K. Morison, B. Gao, and P. Kundur, "Voltage stability analysis using static and dynamic approaches," *IEEE Trans. on Power Syst.*, vol. 8, no. 3, pp. 1159–1171, 1993. 2.

[36] R. C. Dugan, R. F. Arritt, T. E. McDermott, S. M. Brahma, and K. Schneider, “Distribution system analysis to support the smart grid,” in *Power and Energy Society General Meeting, 2010 IEEE*, pp. 1–8.

[37] X.-P. Zhang, “Continuation power flow in distribution system analysis,” in *Proc. IEEE PES Power Systems Conference and Exposition*, pp. 613–617, 2006.

[38] F. Gubina and B. Strmcnik, “A simple approach to voltage stability assessment in radial networks,” *IEEE Trans. on Power Syst.*, vol. 12, no. 3, pp. 1121–1128, 1997.

[39] R. B. Vu Van Thong, Johan Driesen, “Power quality and voltage stability of distribution system with dirstributed energy resources,” *International Journal of Distributed energy Resources*, vol. 1, 2005.

[40] S. Gunalan, A. K. Ramasamy, and R. Verayiah, “Impact of static load on voltage stability of an unbalanced distribution system,” in *Power and Energy (PECon), 2010 IEEE International Conference on*, pp. 288–293.

[41] X. P. Zhang, P. Ju, and E. Handschin, “Continuation three-phase power flow: A tool for voltage stability analysis of unbalanced three-phase power systems,” *Power Systems, IEEE Transactions on*, vol. 20, no. 3, pp. 1320–1329, 2005.

[42] M. Abdel-Akher, M. E. Ahmad, R. N. Mahanty, and K. M. Nor, “An approach to determine a pair of power-flow solutions related to the voltage stability of unbalanced three-phase networks,” *IEEE Trans. on Power Syst.*, vol. 23, no. 3, pp. 1249–1257, 2008.

[43] M. Abdel-Akher, A. Bedawy, and M. M. Aly, “Application of bifurcation analysis on active unbalanced distribution system,” in *Renewable Power Generation (RPG 2011), IET Conference on*, pp. 1–7.

[44] G. Carpinelli, D. Lauria, and P. Varilone, “Voltage stability analysis in unbalanced power systems by optimal power flow,” *Generation, Transmission and Distribution, IEE Proceedings-*, vol. 153, no. 3, pp. 261–268, 2006.

[45] K. N. Miu and C. Hsiao-Dong, “Existence, uniqueness, and monotonic properties of the feasible power flow solution for radial three-phase distribution networks,” *IEEE Transactions on Circuits and Systems I: Fundamental Theory and Applications*, vol. 47, no. 10, pp. 1502–1514, 2000.

[46] T. J. O. J. Duncan Glover, Mulukutla S. Sarma, *Power system analysis and design*. CL Engineering, 4 ed., 2007.

[47] O. O. Obadina and G. Berg, “Identifying electrically weak and strong segments of a power system from a voltage stability viewpoint,” *Generation, Transmission and Distribution, IEE Proceedings C*, vol. 137, no. 3, pp. 205–212, 1990.

[48] M. Esmaili, E. C. Firozjaee, and H. A. Shayanfar, “Optimal placement of distributed generations considering voltage stability and power losses with observing voltage-related constraints,” *Applied Energy*, vol. 113, pp. 1252–1260, Jan. 2014.

[49] A. de Souza, C. Canizares, and V. Quintana, "New techniques to speed up voltage collapse computations using tangent vectors," *IEEE Trans. on Power Syst.*, vol. 12, no. 3, pp. 1380–1387.

[50] Y.-L. Chen, C.-W. Chang, and C.-C. Liu, "Efficient methods for identifying weak nodes in electrical power networks," *Generation, Transmission and Distribution, IEE Proceedings-*, vol. 142, pp. 317–322, May 1995.

[51] P. Juanuwattanakul and M. A. S. Masoum, "Voltage stability enhancement for unbalanced multiphase distribution networks," in *Power and Energy Society General Meeting, 2011 IEEE*, pp. 1–6.

[52] P. Juanuwattanakul and M. Masoum, "Increasing distributed generation penetration in multiphase distribution networks considering grid losses, maximum loading factor and bus voltage limits," *IET Generation, Transmission Distribution*, vol. 6, pp. 1262–1271, Dec. 2012.

[53] H. Sheng and H.-D. Chiang, "CDFLOW: a practical tool for tracing stationary behaviors of general distribution networks," *IEEE Trans. on Power Syst.*, vol. 29, pp. 1365–1371, May 2014.

[54] N. Flatabo, R. Ognedal, and T. Carlsen, "Voltage stability condition in a power transmission system calculated by sensitivity methods," *IEEE Trans. on Power Syst.*, vol. 5, pp. 1286–1293, Nov. 1990.

[55] S. Greene, I. Dobson, and F. Alvarado, “Sensitivity of the loading margin to voltage collapse with respect to arbitrary parameters,” *IEEE Trans. on Power Syst.*, vol. 12, no. 1, pp. 262–272, 1997.

[56] P. Kessel and H. Glavitsch, “Estimating the voltage stability of a power system,” *IEEE Trans. on Power Del.*, vol. 1, pp. 346–354, July 1986.

[57] G. M. Huang and L. Zhao, “Measurement based voltage stability monitoring of power system,” *Power Systems Engineering Research Center, University of Wisconsin, Madison, WI*, 2001.

[58] N. Ismail, A. Zin, A. Khairuddin, and S. Khokhar, “A comparison of voltage stability indices,” in *Power Engineering and Optimization Conference (PEOCO), 2014 IEEE 8th International*, pp. 30–34, Mar. 2014.

[59] C. Reis and F. Barbosa, “A comparison of voltage stability indices,” in *Electrotechnical Conference, 2006. MELECON 2006. IEEE Mediterranean*, pp. 1007–1010, May 2006.

[60] B. Venkatesh, R. Ranjan, and H. Gooi, “Optimal reconfiguration of radial distribution systems to maximize loadability,” *IEEE Transactions on Power Systems*, vol. 19, pp. 260–266, Feb. 2004.

[61] M. Chakravorty and D. Das, “Voltage stability analysis of radial distribution networks,” *International Journal of Electrical Power and Energy Systems*, vol. 23, no. 2, pp. 129–135, 2001.

[62] T. Van Cutsem, "An approach to corrective control of voltage instability using simulation and sensitivity," *IEEE Trans. on Power Syst.*, vol. 10, pp. 616–622, May 1995.

[63] R. Avalos, C. Canizares, F. Milano, and A. Conejo, "Equivalency of continuation and optimization methods to determine saddle-node and limit-induced bifurcations in power systems," *IEEE Transactions on Circuits and Systems I: Regular Papers*, vol. 56, no. 1, pp. 210–223, 2009.

[64] C. Vournas, M. Karystianos, and N. Maratos, "Bifurcation points and loadability limits as solutions of constrained optimization problems," in *IEEE Power Engineering Society Summer Meeting, 2000*, vol. 3, pp. 1883–1888 vol. 3, 2000.

[65] R. Zimmerman, C. Murillo-Sánchez, and R. Thomas, "MATPOWER: Steady-State Operations, Planning, and Analysis Tools for Power Systems Research and Education," *IEEE Trans. on Power Syst.*, vol. 26, pp. 12–19, Feb. 2011.

[66] H.-M. Chou and K. Butler-Purry, "Investigation of voltage stability in unbalanced distribution systems with DG using three-phase current injection based CPF," in *2014 IEEE PES General Meeting*, pp. 1–5, July 2014.

[67] V. V. AR Bergen, *Power Systems Analysis*. Prentice Hall, 2 ed., 1999.

[68] G. W. . E.-A. Stagg, A. H., *Computer methods in power system analysis*. New Delhi: McGraw-Hill, 1st ed. edition ed., 1968.

[69] R. C. Dugan, “Reference guide: the open distribution system simulator (opendss),” *Electric Power Research Institute, Inc*, 2012.

[70] M. Shin, C. Park, J. Jung, K. Kim, and S. So, “Nodal admittance modeling of three-phase step-voltage regulators and their applications,” in *2013 International Conference on Electrical Machines and Systems (ICEMS)*, pp. 362–367, Oct. 2013.

[71] P. Garcia, J. Pereira, and J. Carneiro, S., “Voltage control devices models for distribution power flow analysis,” *IEEE Transactions on Power Systems*, vol. 16, pp. 586–594, Nov. 2001.

[72] H.-D. Chiang, A. Flueck, K. Shah, and N. Balu, “CPFLOW: a practical tool for tracing power system steady-state stationary behavior due to load and generation variations,” *IEEE Trans. on Power Syst.*, vol. 10, pp. 623–634, May 1995.

[73] W. H. Kersting, “Radial distribution test feeders,” in *Proceedings of 2001 IEEE PES Winter Meeting*, vol. 2, pp. 908–912 vol.2.

[74] A. Wiszniewski, “New Criteria of Voltage Stability Margin for the Purpose of Load Shedding,” *IEEE Trans. Power Del.*, vol. 22, pp. 1367–1371, July 2007.

[75] X. Wang, G. C. Ejebe, J. Tong, and J. G. Waight, “Preventive/corrective control for voltage stability using direct interior point method,” *IEEE Trans. on Power Systs.*, vol. 13, pp. 878–883, Aug. 1998.

[76] I. Dobson and L. Lu, “New methods for computing a closest saddle node bifurcation and worst case load power margin for voltage collapse,” *IEEE Trans. on Power Syst.*, vol. 8, pp. 905–913, Aug. 1993.

[77] I. Hiskens and R. Davy, “Exploring the power flow solution space boundary,” *IEEE Trans. on Power Syst.*, vol. 16, pp. 389–395, Aug. 2001.

[78] A. J. Conejo, J. M. Morales, and L. Baringo, “Real-Time Demand Response Model,” *IEEE Transactions on Smart Grid*, vol. 1, pp. 236–242, Dec. 2010.

[79] P. Palensky and D. Dietrich, “Demand Side Management: Demand Response, Intelligent Energy Systems, and Smart Loads,” *IEEE Transactions on Industrial Informatics*, vol. 7, pp. 381–388, Aug. 2011.